Geotechnical characterization of sediments from the Rockall Bank Slide Complex

By

D. van Opdurp

Geotechnical characterization of sediments from the Rockall Bank Slide Complex

By

D. van Opdurp

in partial fulfilment of the requirements for the degree of

Master of Science

in

Applied Earth Sciences

at the Delft University of Technology,

to be defended publicly on Thursday March 5, 2020 at 15:00 PM.

Thesis committee:

Prof. dr. Ir. Gavin, K.G. (Chair)	Delft University of Technology
Dr. Ir. Broere, W.	Delft University of Technology
Dr. Ir. Ngan-Tillard, D.J.M.	Delft University of Technology
Dr. Ir. Lanzafame, R	Delft University of Technology

Department of Geoscience & Engineering
Delft University of Technology

Abstract

The main reason for this research is the possibility of landslides that could trigger a tsunami together with general interest from the oil and gas industry. The goal of this thesis is to find out what the geotechnical properties are of the 7 different locations at the eastern flank of the Rockall bank which is located to the west of Ireland and to the south of Iceland in the Atlantic Ocean. The possible effects of these properties on slope stability are then discussed. This will be done by geotechnically testing the sediments in a laboratory. All standards used during testing can be seen in chapter 3.1.1.

The gravity cores used for this research were found to contain parts of sediment that were quite intact together with other more disturbed parts of sediment.

The sediments that were found could be classified as silty SAND, clayey SILTS and silty CLAYS which are calcareous to very higly calcareous,from medium to very high plasticity, low to medium-organic and have extremely low to very low undrained shear strengths. Grain size distribtions were found to be gap-graded and well graded and the the sediments were found to be inactive to normal soil based on the Atterberg limits.

Geotechnical properties such as gravimetric water contents are found to range from 0.20 to 1.18, the volumetric water contents range from 0.50 to 0.80, a liquidity index from 0 to 3, specific gravities from 2.72 to 2.79, void ratios from 1 to 3, bulk volumetric weights from 14 kN/m^3 to 18 kN/m^3, dry volumetric weights from 7 kN/m^3 to 13 kN/m^3, clay contents from 10% to 60%, a silt content of 15% to 60%, a sand content from 8% to 70%, calcite contents from 17.3% to 57.4%, organic matter contents from 2.6% to 9.0%, liquid limits from 0.40 to 0.82 and plastic limits from 0.23 to 0.49.

The undrained shear strength for the original and remoulded sediments from the UU DS tests is found to range from 2 kPa to 8 kPa and from 0 kPa to 4 kPa. The undrained shear strengths from original and remoulded sediments from the fall cone test range from 4 kPa to 33 kPa and from 0 kPa to 4 kPa. The undrained shear strengths from the original pocket vane tests range from 5 kPa to 22 kPa. The sensitivities of the sediments measured by the fall cone tests are found to range from 2 to 28 and the sensitivities obtained by direct shear testing are found to range from 0.5 to 4.

Based on these undrained shear strengths a failure mechanism similar to that of a direct shear test is found to be more likely on the undisturbed sediments and a failure mechanism like that of a fall cone test is found to be more likely for the remoulded sediments.

The non-phyllosilicate minerals that are present are Smectite, Illite, Muscovite, Chlorite and Kaolinite. The phyllosilicate minerals that are present are Quartz, Alkali feldspar, Plagioclase, Calcite, Ankerite, Siderite, Anatase, Rutile, Hematite, Pyrite, Halite and Apatite. This mineral composition can be logically explained by their possible weathering paths and indicates that the possible parent material is Monzogranite type 2 also called Muscovite-metagranite. Magnetic particles are found to be present in all sediments in small amounts that are not quantified.

Similar sediments are found to be present from the research of (Georgiopoulou, Krastel et al., 2019). This confirms the presence of turbidty deposits. These turbidity deposits are indicated to be present at all sites based on the fininng-upward sequences found. Also the presence of lighter interglacial and darker glacial sediments is found. It was also found that the likley reasons for slope instability on the eastern side of the Rockall Bank are the much higher water contents and clay contents of the sediments present compared to the sediments found on eastern side of the Rockall through.

The risk of liquefaction upon distrubance is found at sites 1736, 1672, 1988, 1959 and 1604. No risk of liquefaction upon disturbance is found at site 688.

The organic matter content is considered to not have an effect on strenght parameters of the sediments present whereas an increase in the amount of foraminifera shells could increase stability of the sediments. Only differential compaction is not found to be a probable factor in lanslide initiation. A long term instability could arise from weathering of Smectite minerals. Erosion could cause slope instability due to sediments with widely varying grain size distributions. The high water content sediments that are present are prone to liquefaction due a disturbance possibly from seismic activity.

It is recommended that in future studies a quantification of the marine shell fraction is made. Also a microscope spectrometry is recommended to be done on the sand fraction together with an X-ray diffraction on the <63µm fraction. The most important recommendation is to do a slope stability analysis on the RBSC using the geotechnical properties presented in this thesis.

Preface

I would like to thank Ing. Wim Verwaal for his advice and help in the laboratory, Qminerals for doing an X-ray diffraction at a reduced cost and Jolanda van Haagen for helping me with the chemical tests done in the lab. My thanks also go to Ir. Maaike van Tooren for giving me advice on the mineralogy of the sediments. I would like to thank the whole committee consisting out of Prof. Dr. Ir. Ken Gavin, Dr. Ir. Wout Broere, Dr. Ir. Dominique Ngan-Tillard, Dr. Ir. Robert Lanzafame for giving their advice on my research. I also would like to thank my friends and family.

Nomenclature

Abbreviation	Explanation
SOC	soil organic carbon
SOM	soil organic matter
Ψ	dilation angle
γ_{bulk}	bulk volumetric weight
γ_{dry}	dry volumetric weight
UU	unconsolidated undrained
DS	direct sheartest
S_u	undrained shear strength
S_d	drained shear strength
$S_{u,pocket}$	pocket vane undrained shear strength
θ_g	gravimetric water content
θ_v	volumetric water content
ε_h	horizontal strain
°	degrees
A_c	activity based on atterberg limits
PL	plastic limit
LL	liquid limit
PI	plasticity index
LOI	loss on iginition
ρ_{grain}	average particle density
S	saturation
e	void ratio
D_{10}	particle size where 10% of soil passes through
D_{30}	particle size where 30% of soil passes through
D_{50}	particle size where 50% of soil passes through
D_{60}	particle size where 60% of soil passes through
C_u	uniformity coefficient
C_c	coefficient of curvature
M_z	average cumulative % passing of the sand fraction
S_t	sensitivity
σ_{nf}'	normal effective stress
original	refers to the original soil as it was found in the gravity cores
remoulded	refers to the remoulded soil
%P	Planktonic foraminifera

List of Figures

List of Tables

List of Equations

Table of contents

1 Introduction

In this chapter the motiavtion for doing research on the Rockall Bank slide complex that is located to the west of Ireland in the Atlantic Ocean will be given. The sediments investigated in this report are assumed to be normally consolidated. Sediments that are tested without remoulding are referred to as original and sediments that have been remoulded are referred to as remoulded. All undrained shear strenghts names in this report are estimates of the true undrained shear strength.

1.1 Motivation

This research is done in order to allow further research into the slope stability of the eastern flank of the Rockall Bank also called the Rockall Bank slide complex (RBSC). This is located to the west of Ireland and to the south of Iceland in the North Atlantic Ocean. This slide complex has been subjected to several landslides. The initiation mechanisms for these landslides that are discussed in previous literature will be supported by test results from this report if possible. This may give a clear picture of what is most likely the cause of these landslides. These landslides could cause a tsunami that could reach the Mullet Peninsula, the Inishkea islands and the Achill island in less than 1 hour (Salmanidou, Georgiopoulou, et al., 2018). These isles are all located on the west coast of Ireland. A further slope stability analysis could also give more insight into the magnitude of a possible future landslide which determines the magnitude of the tsunami. There is also a long on-going interest in the Rockall Bank area for oil and gas exploration. This industry could benefit from a further slope stability analysis done based on this work and could use some of the data to aid in calculating bearing resistances for their oil rig structures.

1.2 Research questions

1. What are the geotechnical properties of the landslide deposits on the eastern slope of the Rockall Bank and what is their full geotechnical classification?
2. What are the mineralogical properties of the sediments present and what could be their parent material?
3. How do these geotechnical properties compare to geotechnical properties from the same or similar areas obtained in previous research.
4. How could all of these properties affect the strength parameters of the shallow marine sediments deposited on the eastern slope of the Rockall Bank?

These research questions will be answered based on the results from the geotechnical characterization and testing done in this thesis. The actual slope stability analysis itself is outside the scope of this thesis.

2 Literature research

In this chapter information about the Rockall bank slide complex will be given. The possible origin of this slide complex will be discussed together with possible initiation mechanisms for slope failure. Then a classification scheme for the sediments from the 7 different locations is given. Here all relevant and classifiable properties will be given a classification sheme according to ISO, NEN or ASTM or other standards. At last the testing procedures will be discussed. A brief discussion about the function of each test is given together with their reference to an ISO, NEN, ASTM or other standard if applicable.

2.1 The Rockall Bank

The Rockall bank is an isolated continental shelf present on the Rockall Plateau (see Figure 1) which has subsided and was formed due to seafloor spreading in the North Atlantic Ocean (Roberts, 1975). This Rockall Plateau is a micro continent (Roberts, 1975) and is located to the northwest of Ireland and to the south of Iceland in the Atlantic Ocean. The Rockall Bank is located in between the Rockall through and the Hatton Rockall Basin indicated by the blue arrow in Figure 1. In other words the Rockall Bank is located below seawater level in the Atlantic Ocean to the west of Ireland.

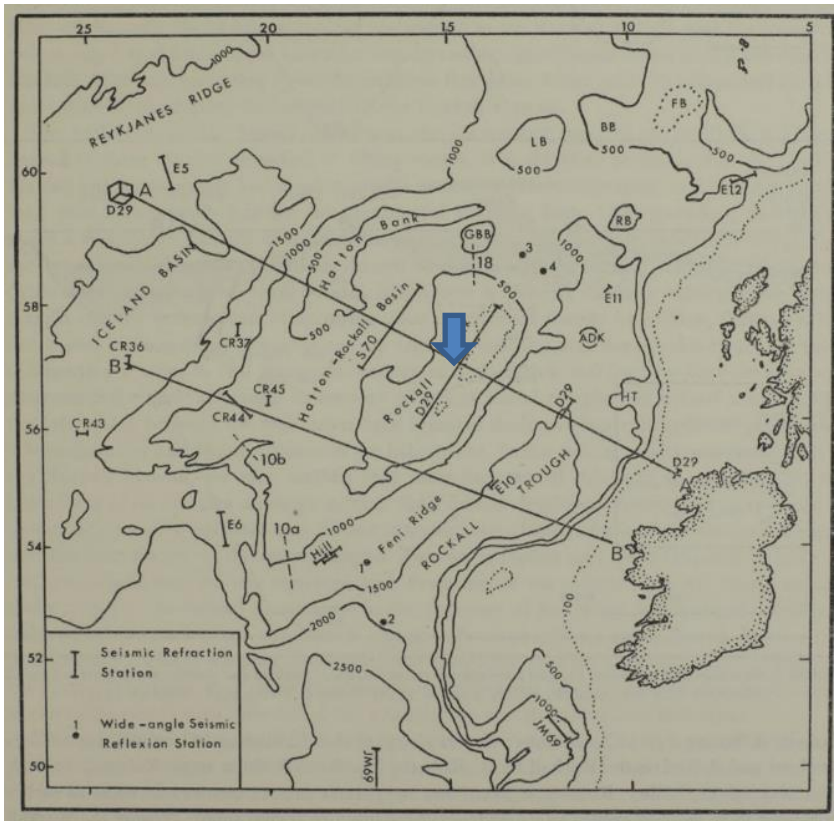

Figure 1: Generalized bathymetry of the Rockall Plateau with the latitude on the vertical axis and the longitude on the horizontal axis from (Roberts, 1975).

The Rockall through is thought to have been developed on continental crust including oceanic crust that is generated in the Late Jurassic and the Early Cretaceous (Roberts, 1975). Rockall Island which is the highest point of the Rockall Plateau is composed of 43-61 Ma year old Aegirine granite (Roberts, 1975).

On the eastern side of the Rockall Bank between 15'000 and 16'000 years ago debris flows and turbidity currents occurred which were caused by slumping (Flood, Hollister and Lonsdale, 1979). Slumping is movement of a mass of sediments that is slowly moving along the slope.

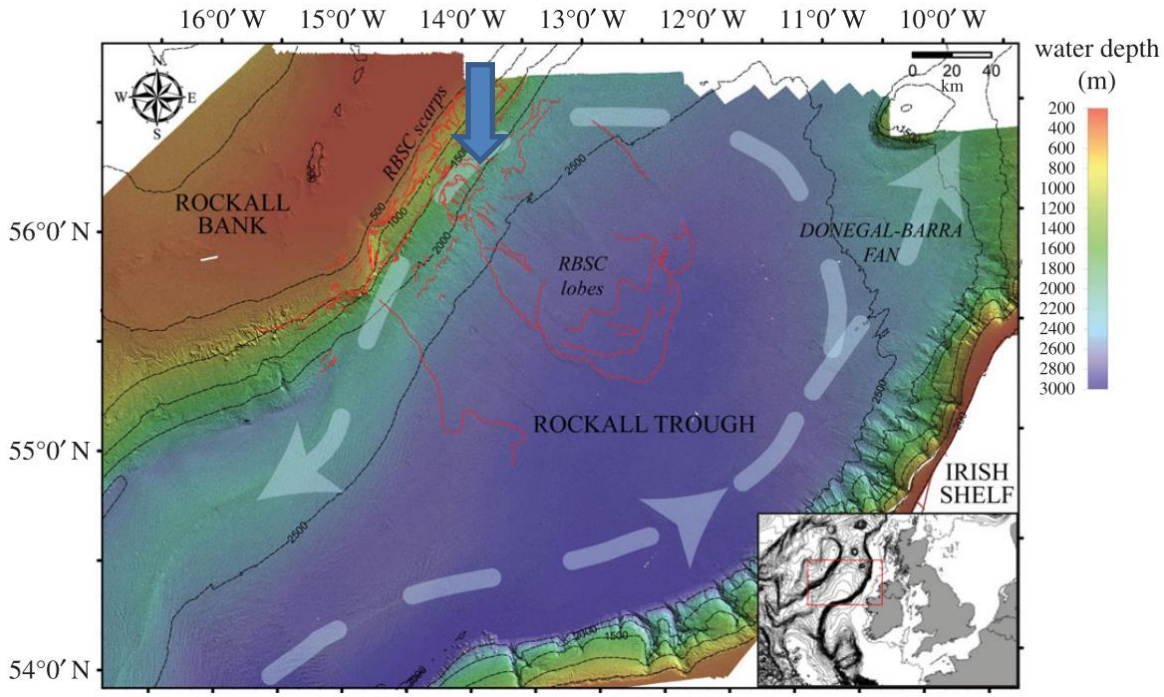

Figure 2: Multibeam bathyrmetry map of the Rockall Trough based on the Irish National Seabed Survey (INSS) dataset. The RBSC scarps and lobe limits are indicated with red lines. Arrows show the general oceanographic circulation. Bathymetric contours are shown with thin black lines. The map on the right-bottom corner shows the position of the RBSC with respect to Ireland and the UK. Adapted from (Georgiopoulou, Shannon, 2013).

The landslides that originated and formed the Rockall Bank Slide Complex (RBSC) blocked the Feni drift which is a major sedimentary drift alongside the eastern side of the Rockall Bank and can be seen in Figure 3 indicated by the blue arrow. This Feni drift transports sediment in a northwards direction along eastern side of the Rockall Bank.

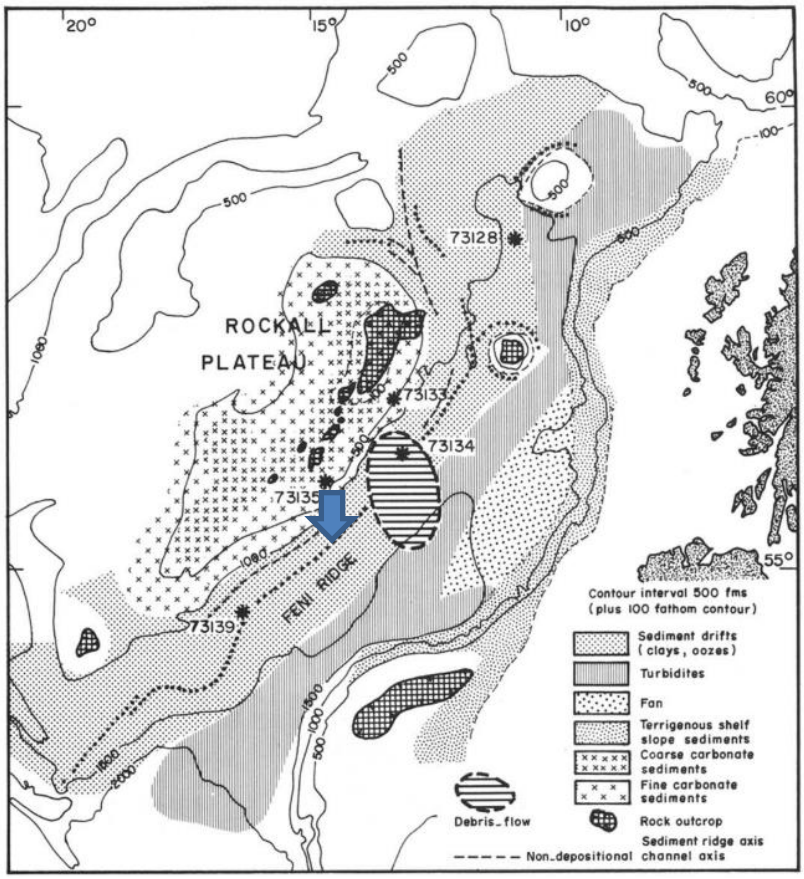

Figure 3: Rockall Plateau and basin from (Faugeres, Gauthier et al., 1981).

The landslides took place in the late Pleistocene in the Tarantian. An influx of glacial sediment may have caused the landslides to occur. This influx could have overloaded the sediment slopes. The Rockall through which lies at the foot of the Rockall Bank is about 250 km wide and is filled with sediment with a thickness of several kilometres (Georgiopoulou, Krastel et al., 2019). This through is approximately 1000km long and has slopes of 2-20 degrees. The Rockall Bank Slide Complex (RBSC) (see Figure 2) area where the landslide deposits are located has a length to width ratio of 150km by 120km (Elliot, Shannon et al. 2010). The 7 gravity coring locations are located in between 55.5° to 56° latitude and in between the 14.1° to 14.4° longitude (see Figure 4).

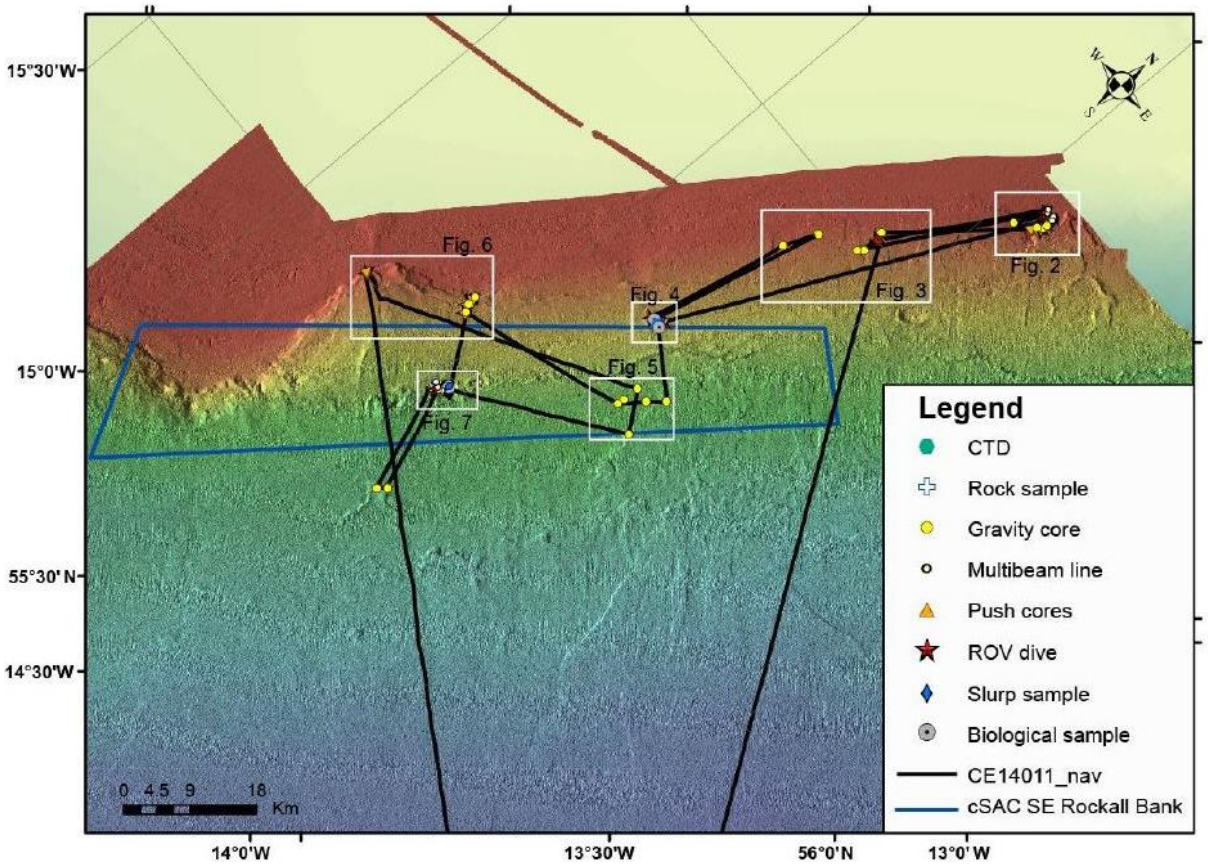

Figure 4: Map of the general study area showing the track of the ship that was used to collect all the gravity cores (Figure 1 from the CE14011 cruise report from the Marine institute Foras na Mara).

Figure 5 shows the locations of the gravity cores 1,2 as GRC06B, core 8 as GRC07, cores 3,11 as GRC13 and cores 4,5 as GRC8A. The yellow dots under each blue arrow represents the exact gravity coring location.

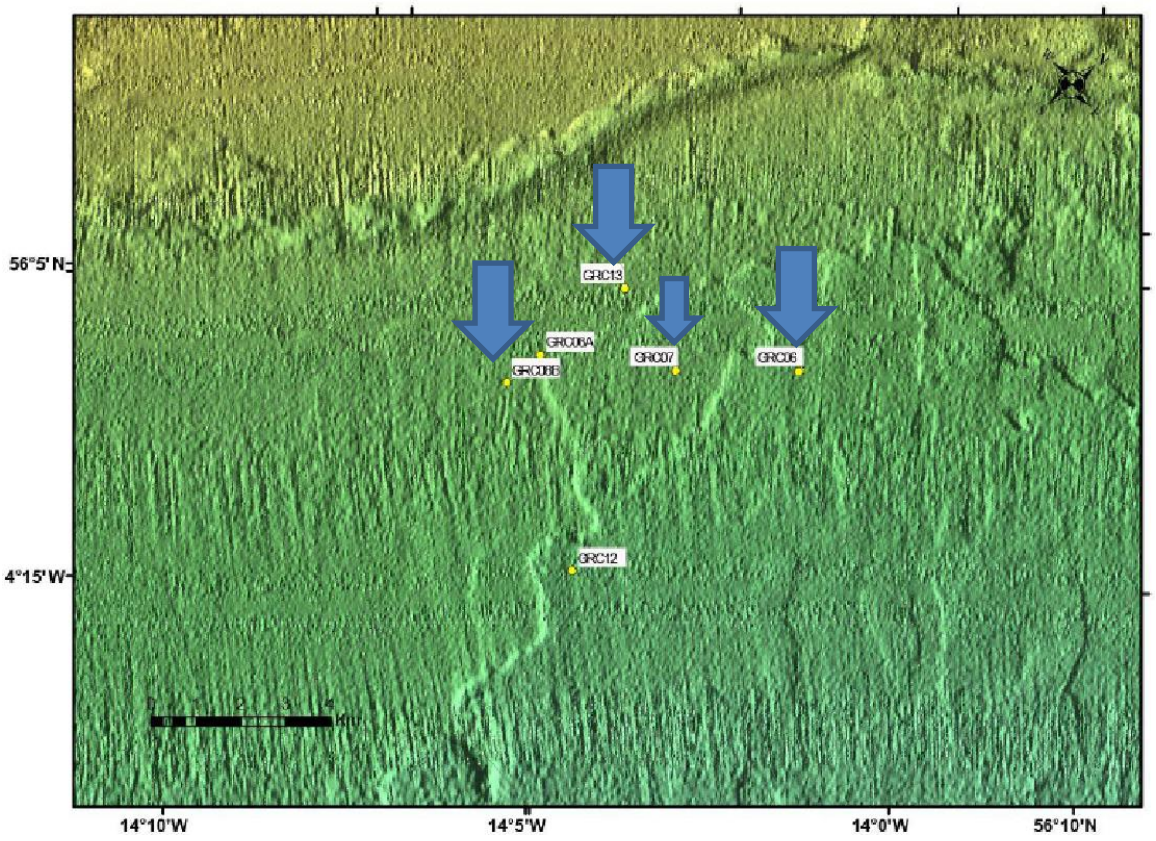

Figure 5: Gravity coring locations from deeper water area, see Figure 4 for a wider overview (Figure 5 from the CE14011 cruise report from the Marine institute Foras na Mara).

Figure 6 shows the location of the gravity core 6 as GRC01 indicated by the yellow dot under the blue arrow. No visual areas of cores 9, 10 and 7 from sites 1959 and 1988 are available.

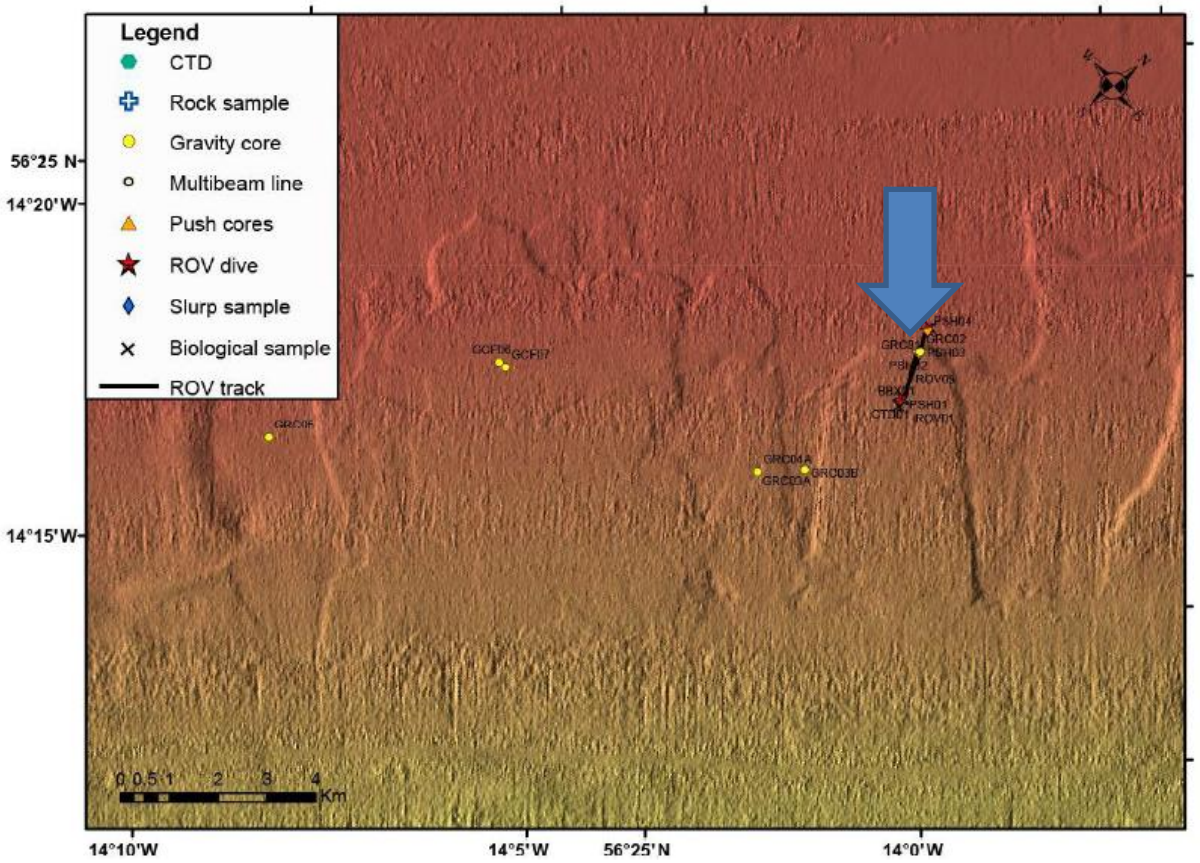

Figure 6: Gravity coring locations with yellow dots in the Centrul upper slope area (Figure 3 from the CE14011 cruise report from the Marine institute Foras na Mara).

The top 1m to 2m of deposits coming from these debris flows and turbidity currents is what will be investigated at depths of 688m and 1988m below sea level. Gravity cores have been drilled on several locations in the RBSC and these cores will be tested in the laboratory.

Two slope failure mechanisms that are at least partially responsible for slope failures occurring are bottom current activity and contourite deposits (Elliot, Shannon et al., 2010). The slope could be eroded downslope when the slope is covered in less stable high water content sediments. Rapid sedimentation on the upper slope could have enhanced the difference in slope steepness already caused by high bottom current velocities eroding the lower part of the slope and could have caused slope failure (Salmanidou, Guillas, et al., 2017). These contourite deposits are sediments that are reworked by bottom currents. This reworking causes loss of structure for the top of the sediments. They are also high water content and well sorted due to reworking already existing sediments.

The Rockall bank landslide deposits have formed as the result of three major landslide phases (see Figure 7). These phases took place during the last glacial minimum. According to calculations these three landslides have displaced a volume of 725 km^3 (Salmanidou, Georgiopoulou, et al., 2018). This comes close to the 765km^3 which is a maximum estimate (Georgiopoulou, Shannon, et al., 2013).

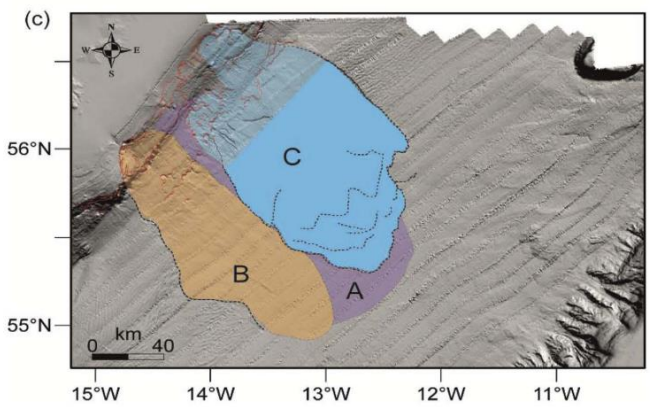

Figure 7: Three landslide scenarios that could have happened from (Salmanidou, Georgiopoulou, et al., 2018).

In these estimates the sediment accumulation since the slope collapses is found to be negligible. An investigation into the seismic facies indicates that the failed sediments and the slope almost completely consist out of contourites that are prone to failure, because of their high water content and well sorted character. “Focused fluid flow along basement-bounding faults, and/or differential compaction across the scarps, are considered to have had an important role in slope failure” (Georgiopoulou, Shannon, 2013). The reason for believing that there may be multiple slope failures instead of one big failure could be explained by the intensification of bottom current velocities that are eroding the lower part of the slope. These near bottom velocities are caused by the steep contour-swept slopes that are present. Due to these high bottom current velocities of seawater eroding the lower slope, the slope gradients remain steep and unstable. The Rockall Bank is a steep and high plateau that forms the western margin of the Rockall through. The Rockall through is an elongate deep water-basin that is sediment-starved (Georgiopoulou, Shannon, 2013). The basement of the Rockall through consists out of Precambrian deposits that are covered with a thin layer of Paleogene lavas (Georgiopoulou, Shannon, 2013).

Landslide C which is dated as an event 22 thousand years ago was probably activated by seismic activity that is not related to the isostatic rebound. Climate conditions were also not thought to be the cause of this landslide (Georgiopoulou, Krastel et al. 2019). So seismic activity definitely has to be considered for the more recent landslides.

The Rockall bank slide complex has the Feni drift right alongside it. The slide complex comprises out of a 6100km^2 area of slope failure scarps situated on the eastern slope of the Rockall Bank above the mass flow lobes which lay more downslope. These lobes cover 18000km^2 and cover the lower part of the slope and cover part of the Rockall through. Initial failure could have occurred along coherent layer parallel detachment surfaces with depths of up to a 100m. This would have caused downslope block sliding that generated debris flows. Factors like thermohaline currents modifying the mass flow that causes deep erosional moats and differential sedimentation may have been factors for slope failure. After the main landslide occurred small-volume turbidity deposits formed on the mass flow lobes. The trigger event for the smaller landslides that caused these turbidity deposits is uncertain, but may be attributed to earthquake events (Elliot, Shannon et al., 2010).

Also high sedimentation rate events have been attributed to causing slope failures (Evans, Harrison et al., 2005). The event that triggered the slope failures is not known, but an idea about the long-term failure mechanism is present. “The long-term instability control is suggested to be differential sedimentation and erosion on the slope associated with contourite drift development (Elliot, Shannon et al., 2010).

As a result of this an erosional moat system along the middle slope is produced. This eroded moat is the reason the upper slope is more prone to failure. The activation mechanism of the slope failure in this situation can be the localised accretion and redistribution of sediment over the upper slope (Elliot, Shannon et al., 2010).

2.2 Disturbance of the sediments

In this chapter the disturbance of the sediments will be discussed in a qualitative manner. Most of the cores showed forms of disturbance, but none of this has been quantified.

Gravity coring can cause some disturbance to the cored sediments. The cores went in between 40m/s and 60m/s. The impact of this could alter the structure of the soil. The gravity core can also bounce of the seafloor after already having penetrated into the soil, this can in some cases cause two intervals of the same sediment interval to be present. Another effect is the sleeving of sediments (see Figure 8) from other intervals along the inside walls of the gravity core. This creates a thin layer of sediments from other intervals around the cored sediments.

Figure 8: Sample taken from core 3 (50mm in diameter) showing the sleeving effect of a darker sediment surrounding the lighter sediment from that interval.

Drag effects (see Figure 9) were also present, but could only be seen in the cores that split open when opening the core due to a lack of cohesion. This occurred in core 5 and 11 with a high sand content.

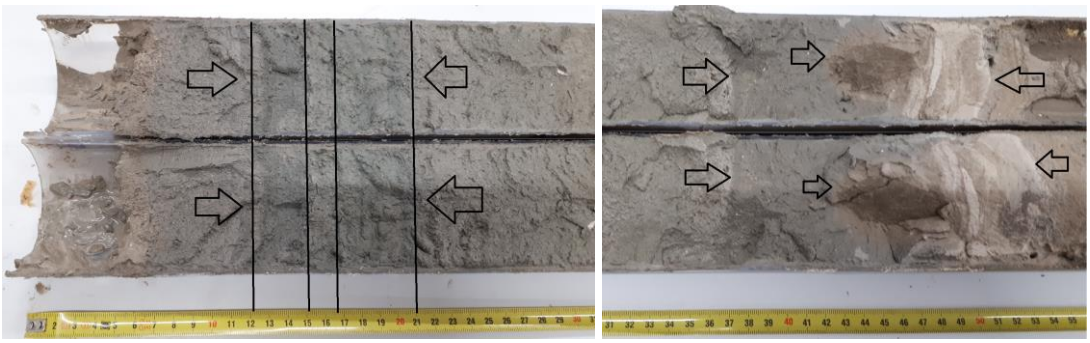

Figure 9: Core 5 which split partly open when opening the cylinder showing a clear drag effect causing the sediment intervals to be curved.

Parts of the gravity cores were also clearly distrubed (see Figure 10) by showing partial recovery of the sediment in that particular interval. These intervals are not used for strength testing.

Figure 10: Core 4 showing a partially recovered sediment interval.

The cores with ‘intact’ intervals (see Figure 11) were used for original strength tests and the determination of the saturation along the length of the gravity core. The diameter of the sediment in the gravity cores was of varying with diameters in between 63mm and 55mm. Only the intervals that had a big enough diameter were used for original (as found in core) direct shear testing and fall cone testing. These intervals are referred to as the original samples, because the terminology undisturbed would not be correct.

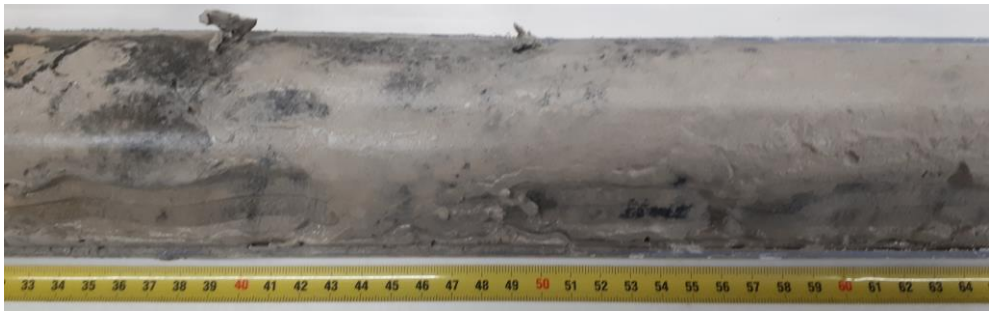

Figure 11: Example of an intact piece of core.

These gravity cores have been transported to the TU Delft and have been stored in wax sealed cylinders in the basement at a temperature of about 22 degrees for about 5 years untill Februari 2019. These gravity cores were drilled in July of 2014. In the meantime ageing took place causing the sediments to gain in strength and to give opportunity for the organic matter to oxidate. The cores were all found to have some seawater In them that was kept inside by the wax seal. All samples have also been checked for saturation and they showed values of saturation close to 1 (see Figure 12).

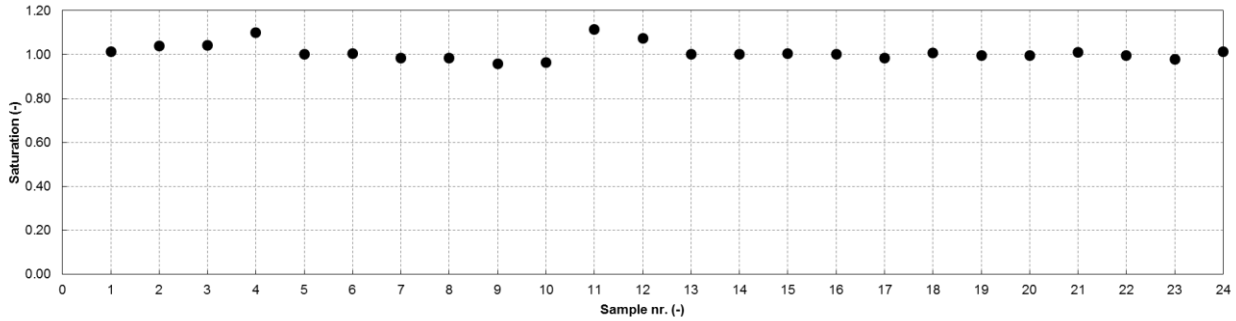

Figure 12: Saturation estimates made based on measured saturation values around these intervals. The sediments intervals presented here were stored in the fridge and used for fruther strength testing.

Tree outliers can be detected in samples 4, 11 and 12 which show saturation values higher than 1. This could be due to overfilling of the sampler ring even though they were all trimmed using a wire. The volume of void was determined each time by subtracting the volume of the solids from the volume inside the sampler ring. Overfilling would have caused a larger volume of water and solids to be present. This causes the volume of voids to become smaller and the volume of the water to become higher. Lower saturation values are due to the samples not being fully saturated.

Sampler rings of 37-55mm in diameter and 19-21 mm in height were used for determining the saturation. This made sure that a full intact sample could be taken. Only in a few cases of lack of equimpent the 19-21mm samplers were used. Mostly the samplers around 55mm were used.

Table 1 shows information about the site, sample name, depth and saturation estimates used for constructing Figure 12.

Table 1: Values of the saturation esitimates interpolated from all saturation measurements done.

Sample nr.	Site	Sample name	Depth (cm)	Saturation estimate (-)
1	1736	Core 1 sandy dark(F)	-17	1.01
2	1736	Core 1 dark (F)	-38	1.04
3	1736	Core 1 grey (F)	-56	1.04
4	1736	Core 1 grey (F)	-75	1.10
5	1736	Core 2 orange (F)	-114	1.00
6	1736	Core 2 black (F)	-148	1.01
7	1672	Core 4 dark(F)	-10	0.98
8	1672	Core 4 light(F)	-28	0.99
9	1672	Core 5 beige(F)	-138	0.96
10	1672	Core5 beige(F)	-157	0.96
11	688	Core 6 sandy clay(F)	-16	1.11
12	688	Core 6 clayey clay(F)	-47	1.07
13	1988	Core 7 dark(F)	-17	1.00
14	1988	Core 7 dark(F)	-28	1.00
15	1988	Core 7 light(F)	-57	1.00
16	1695	Core 8 dark(F)	-20	1.00
17	1695	Core 8 light(F)	-55	0.98
18	1959	Core 10 dark(F)	-39	1.01
19	1959	Core 10 light(F)	-61	1.00
20	1959	Core 10 light(F)	-71	1.00
21	1959	Core 10 light(F)	-89	1.01
22	1604	Core 3 dark grey(F)	-15	0.99
23	1604	Core 11 clayey clay(F)	-87	0.98
24	1604	Core 11 sandy clay 2(F)	-113	1.01

All the sediments were tested in their original state, because this could only be done once. In order to take away the uncertainty from disurbance and ageing the sediments are also tested in a remoulded state. This state is reached by creating a uniform paste from sediments using spatulas. This Remoulding method has the same degree of remoulding that is used to determine the liquid limit using the fall cone test. These remoulded sediments are then tested in direct shear tests and fall cone tests in order to obtain the remoulded shear strengths.

3 Methodology

In this chapter an overview is given of what standards are used for executing all the tests and in what manner they have been executed. Also an overview of all standards used is given with some elaboration on each step of the methodology. Due to copyright reasons not all classification tables are displayed. It is advised to look up the corresponding standard if this is the case.

3.1 Classifying the soil

In this chapter the classification schemes for classifying the soil will be given. Only certain classification tables will be shown due to cpyright reasons.

3.1.1 Overview of all standards used

All the standards that have been used in different tests can be seen in Table 2

Table 2: A summary of all the standards used.

Method	Standard name/ literary reference
Soil fraction classification	ISO 14688-1 (Table 2)
Activity determination	Skempton, 1953 (Table 3)
Estimating mineralogy	Skempton, 1953 (Table 1)
Organic matter content classification	ISO 14688-2 (Table 3)
Calcite classification	ISO 14688-2 (Table 4)
Plasticity classification	ISO 14688-2 (Figure 1)
Undrained shear strength classification	ISO-14688-2 (Table 6)
Sensitivity classification	ISO 14688-2 (Table 7)
Grain size distribution curve classification	ISO 14688-2 (Table 2)
Pocket vane test execution	Eijkelkamp manual
Water content determination	ISO 17892-1
Volumetric water content determination	ISO 17892-2
Loss on ignition determination	NEN-EN 15935
Organic matter content determination	NEN 5754
Inorganic matter content determination	ISO 14688-2
Wet sieving method	ISO 17892-4
Hydrometer test	ISO 17892-4
Deriving SOC from LOI and clay content	Common, 2018 (Equation 3)
Deriving % Clay underestimated	Jensen et al. 2017 (Equation 2)
Methylene blue test	ASTM C837
Fall cone test for undrained shear strength determination	ISO 17892-6
Fall cone test for liquid limit determination	ISO 17892-12
Direct shear testing	ISO 17892-10
Strain rate correction	Kulhawy and Main 1990 EPRI manual

3.1.2 The fraction of sediments that is separated out and not considered

All sediments are tested based on their fraction that is smaller than 425µm. The percentage of sediments separated out of each sample is shown in Figure 13. The direct shear testing is however done on the unsieved sediments.

Sample name	>425 µm fraction
Core 1 grey	0.1
Core 1 dark	1.4
Core 2 dark	0.0
Core 2 orange	0.0
Core 3	0.1
Core 4 dark	0.4
Core 4 light	0.1
Core 5 beige	0.4
Core 6 sandy clay	0.7
Core 6 clayey clay	0.5
Core 7 dark	0.4
Core 7 light	0.2
Core 8 dark	0.3
Core 8 light	0.6
Core 9	5.5
Core 10 dark	0.4
Core 10 light	0.2
Core 11 clayey clay	0.4
Core 11 sandy clay	2.0
Core 11 sandy clay 2	0.2

Figure 13: The percentage of soil fractions that is separated out.

3.1.3 Gravity coring locations and names

Table 3 shows the names given to each of the 7 locations where gravity coring has taken place. Information like the depth of coring below sea level, the coordinates and how much of the gravity core was successfully retrieved are also given. Each location is given a site name in this report which refers back to the tube numbers which are the original names of the gravity cores.

Table 3: Information about the 7 locations where gravity coring has taken place.

Site name	Tube number (-)	Core number (-)	Depth from sea level to seabed (m)	Latitude(°)	Longitude(°)	Retrieval of sediment (m)
Site 1736	06-B	1,2	1736	56.1802	-14.1394	1.79
Site 1672	08-A	4,5	1672	56.1428	-14.2033	1.68
Site 688	1	6	688	56.5108	14.1201	0.81
Site 1988	09-B	7	1988	55.8434	-14.3971	0.95
Site 1695	07-B	8	1695	56.1615	-14.1679	0.74
Site 1959	10	9,10	1959	55.8541	-14.3838	1.25
Site 1604	13B	3,11	1604	56.1642	-14.2021	1.38

The pallet containing all 11 cores from 7 locations is shown in Figure 13. The arrows point to the top to the soil present nearest to the seabed. This means that the depth of the sediments increase with the opposite direction of the arrow. Parts 1/2 and 2/2 refer to the top and bottom part of the core. It also occurs that only 1 core is available for 1 site. This is indicated

by 1/1. The cores visible in Figure 14 are not necessarily placed in order, but they are placed close to each other if possible so that they optimally fit the pallet.

Figure 14: Pallet containing all 11 cores tested.

3.1.4 Soil fraction classification

The soil fraction names that are used in this report are from Table 1 from ISO standard 14688-1 (see Table 4).

Table 4: Soil fraction classification from ISO-14688-1.

Soil fraction	Grain size(µm)
Pebbles	>2000
Coarse sand	> 630 to ≤ 2000
Medium coarse sand	> 200 to ≤ 630
Fine sand	> 63 to ≤ 200
Coarse silt	> 20 to ≤ 63
Medium coarse silt	> 6.3 tot ≤ 20
Fine silt	> 2 tot ≤ 6.3
Clay	≤ 2

3.1.5 Determination of Activity of the soil

The activity of the soil is classified according to (Skempton, 1953) and is calculated using Equation 1 and classified according to Table 3.

Equation 1: Calculating the activity based on the plasticity index and the clay content (Skempton, 1953).

$$Ac = \frac{PI}{clay\ content} \quad (1)$$

Where PI means plasticity index, Ac means activity.

Table 5: Activity classification from (Skempton, 1953).

Class	A_c(-)
1. Inactive soil	< 0.75
2. Normal soil	0.75 - 1.25
3. Active soil	> 1.25

3.1.6 Calcite content classification

The calcite content is classified according to Table 4 from ISO 14688-2.

3.1.7 Organic matter content classification

The organic matter content (SOM) has been classified according to Table 3 from ISO 14688-2.

3.1.8 Estimating the mineralogy

An estimate of the mineralogy (see Table 6) was made using the classification from Table 1 from (Skempton, 1953).

Table 6: Mineral estimate based on Atterberg limits from (Table 1 of Skempton, 1953).

Clay mineral	A_c(-)
Kaolinite	0.33-0.46
Illite	0.9
Ca-montmorillonite	1.5
Na-montmorillonite	7.2

3.1.9 Plasticity classification

A classification about the type of soil present was made based on the liquid limit and the plastic limit according to Figure 1 from ISO standard 14688-2 (see Table 7). This plasticity classification is based on Atterberg limits obtained from ISO standard 17892-12.

Table 7: Plasticity classification from ISO 14688-2.

L	Low
M	Medium
H	High
V	Very high
O	Organic

3.1.10 Undrianed shear strength classification

The undrained shear strenght of the soil is classified accoring to Table 6 from ISO standard 14688-2.

3.1.11 Sensitivity classification

The sensitivity of the soil is classified according to Table 7 from ISO standard 14688-2.

3.1.12 Grain size distribution classification

The grain size distribution has been taken over the clay, silt and sand fraction. This is then classified according to Table 2 from ISO 14688-2.

Description	C_u(-)	C_c(-)
Uniformly graded	<3	<1
Poorly graded	3 to 6	<1
Medium graded	6 to 15	<1
Well graded	>15	1 to 3
Gap graded	>15	<0.5

3.1.13 Visual description of the cores

A visual description of the colour of all the soil samples is given after opening the cores. For this no standard was used. In order to leave the soil as intact as possible for further testing, no more visual or on the spot descriptions were done, because these would disturb the sample or would be rendered useless due to further testing of the soil samples.

3.2 Testing procesdures

In this chapter the testing procedures that have been used are discussed. All soil has been tested on the soil fraction <425µm which contains 99% to 100% of the tested samples. This is required by ISO standards.

3.2.1 Soil testing immediately after openig the cores.

The opening of the cores was done using an electric metal saw that could cut the top off the plastic cylinder. This way minimal disturbance was caused and the metal saw only penetrated a bit into the soil along the side of the cylinder where the plastic was being cut. Figure 15 shows an example of how all the cylinders were cut.

Figure 15: Core 3 opened (45 cm in length)

3.2.2 Pocket vane test

Figure 16 shows the pocket vane test used and the imprint of the pocket vane into the soil. The pocket vane was put straight into the soil and turned at a constant speed until failure occurred. The pocket vane test CL 100 and CL 101 from the Eijkelkamp manual was used.

Figure 16: Pocket vane test on the left and tested soil sample on the right with a 55 mm imprint.

3.2.3 Volumetric water content and volumetric weight determination

The volumetric water content and volumetric weight are determined by using a steel cylinder of about 50mm (see Figure 17) which is pressed gently into the soil, then trimmed and then dried according to ISO 17892-2. In this manner the saturation was also determined. Gravimetric water content is determined using only the wet soil and a petri dish.

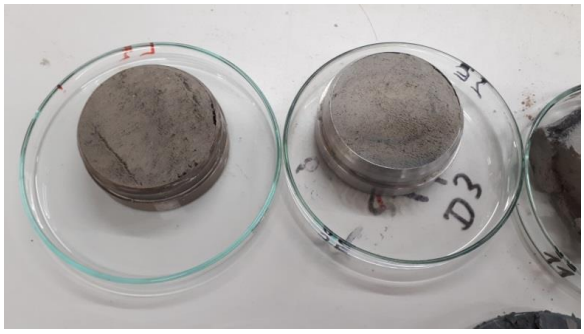

Figure 17: Full sampler rings (50mm in diameter) after pressing them into the soil core.

3.2.4 Pycnometer test

All the samples have been tested for their average particle density. This has been done using the pycnometer test. This is a machine that adds helium gas to the dried particles that are entrapped in an enclosed chamber of a known volume. The mass of the dry particles inside is also known and thus after 10 iterations an average particle density is determined based on the average of the last three readings. There is an ISO standard for this, but this was not available at NEN. Thus instructions were followed from the lab supervisor. The machine that was used is called an ultrapycnometer 1000 from the brand Quantachrome Instruments.

3.2.5 Organic and inorganic content determination

The organic matter content together with the calcite content of the soil is estimated using the loss on ignition method. The soil is dried in powder form after which it is heated up to 550° Celsius over 1 hour after which it is left in the oven for 3 hours. After this is finished the sample is reheated to 950° Celsius over the course of 1 hour after which the sample is left in the oven for 3 more hours. After each heating step the mass is weighed to determine the loss on ignition. This loss on ignition can then be used to obtain an estimate of the organic matter content and the inorganic matter content which is assumed to be 100% calcite. The LOI for both tests are determined using NEN-EN 15935. For determining the organic matter content

the NEN5754 has been used and for determining the inorganic content ISO standard 14688-2 has been used. Classification of the organic and the calcite content of the soils was done using Table 3 and 4 from ISO 14688-2.

3.2.6 Wet sieving

In order to determine the distribution of the sand fraction a wet sieving was used due to the presence of clay. The sieve sizes (see Figure 18) 63µm, 125µm, 210µm, 300µm, 425µm, 600µm, 1mm and 2mm were used on all soil samples. Only demineralized water was used in this process to preserve the <63um fraction for further hydrometer testing. All wet sievings are done according to ISO standard 17892-4. Each sieve contains a mesh grid.

Figure 18: Sieving tower used for wet sieving.

3.2.7 Hydrometer tests

A hydrometer test was carried out to determine the grain size distribution of the soil fraction smaller than 63µm. This is done using demineralized water and a dispersant. The dispersant was added to the <63µm fraction 18 hours before testing started. Before adding the slurry to the cylinders 20 minutes of mixing was done. The dispersant consists out of 33 g/L sodiumhexametaphosphate and 29 g/L sodium carbonate. This test was done according to ISO standard 17892-4 using sedimentation cylinders (see Figure 19).

Figure 19: Hydrometer setup on the left and a cylinder full of silt and clay particles on the right

Hydrometer tests require organic matter to be removed before testing. This was not done since time and budget did not allow this. Instead a correction was used on the amount of clay measured since organic matter could clump together with clay particles and thereby cause

the clay particles to fall at a faster velocity which would cause those clay particles to be classified as silt. This correction is found to be highly necessary (Jensen, Christensen et al., 2018).

First the soil organic carbon (SOC) was determined using the loss ignition at 550° Celsius (see Equation 2).

Equation 2: Calculating the SOC value based on the LOI_{550} value and the clay content (Jensen, Christensen et al. 2018).

$$\%\,SOC = 0.513 \times \%\,LOI - (0.047 \times (\%Clay) - 0.00025 \times (\%Clay)^2 \quad (2)$$

Where SOC is the percentage of soil organic carbon which is about half the organic matter content. The LOI is the loss on ignition.

Then the amount of clay that was underestimated due to the presence of the SOM was corrected using Equation 3. The experiments from which this equation was formulated are done on the same type of clay minerals that are present in the gravity cores investigated in this report.

Equation 3: Calculating the percentage of clay content that is underestimated by the hydrometer test using the SOC (Jensen, Schjønning et al., 2017).

$$\%\,Clay\ underestimated = -0.78 + 0.66 \times \%\,SOC + 5.22 \times (\%\,SOC - 2.27) \quad (3)$$

SOC is the soil organic carbon. The maximum increase in clay content was calculated to be 8.3%. Then the decision was made to decrease the amount of silt present with the same magnitude. All this is necessary since the presence of organic matter increases clumping of particles which then causes the clay fraction to be underestimated and the silt fraction to be overestimated. The increase in clay content values is shown in Figure 20.

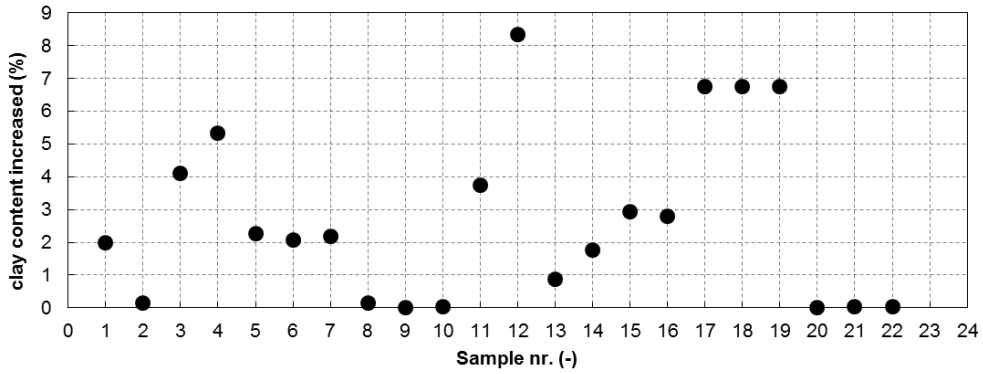

Figure 20: The clay content increase displayed for each sample.

Table 8 shows the values that are displayed in Figure 20. Here also the samples names are given corresponding to the numbers in Figure 20.

Table 8: Clay content correction per sample.

Sample nr. (-)	Sample name	clay content increased (%)
1	core 1 grey	2.0
2	core 1 dark	0.1
3	core 2 dark (37.5-54)	4.1
4	core 2 orange (4.5-20.5)	5.3
5	core 3	2.3
6	core 4 dark (5-15.5)	2.1
7	core 4 light (21-32)	2.2
8	core 5 beige(63.5-75)	0.1
9	core 6 sandy clay (8.5-24)	0.0
10	core 6 clayey clay (38-55.5)	0.0
11	core 7 dark(22.5-34)	3.8
12	core 7 light	8.3
13	core 8 dark	0.9
14	core 8 light	1.8
15	core 9	2.9
16	core 10 dark (6-22)	2.8
17	core 10 light (31-41)	6.8
18	core 10 light (41-51)	6.8
19	core 10 light(57-71)	6.8
20	core 11 clayey clay(42-52.5)	0.0
21	core 11 sandy clay	0.0
22	core 11 sandy clay 2	0.0

3.2.8 Methylene blue test

The methylene blue test was done on all soil samples in order to get an estimate of the activity of the soil. This test requires 2 grams of dried soil which is mixed with 300 ml of demineralized water after which methylene blue is added until a certain visual change in colour is observed in the drop on the filter paper (see Figure 21).

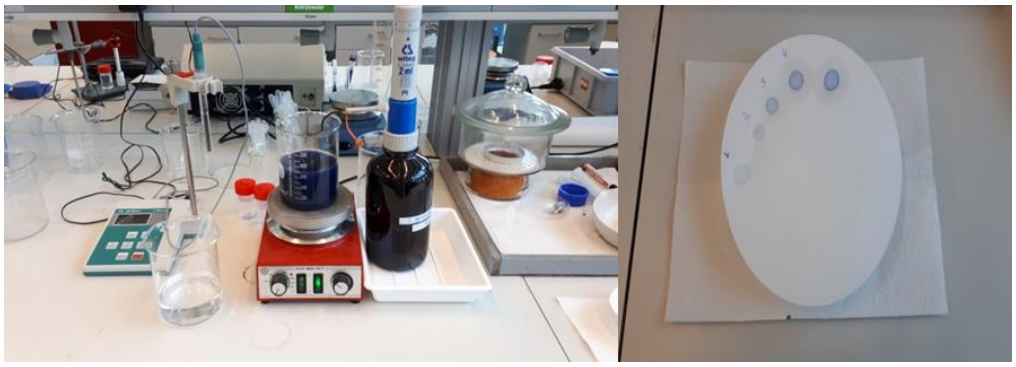

Figure 21: Methylene blue setup on the left and the results of the methylene blue drop test on the right.

Each time 1ml methylene blue was added after which 2 minutes of stirring occurred. Then a drop was taken and put on a filter paper to see whether the required change in corona of the drop had been reached. This change in corona colour occurs when all cations of the soil are exchanged. This is called the blue drop method and this test was done according to the ASTM C837 standard. It has to be said that the soil from all samples was very basic with a pH around 9.5. The required pH for testing in this ASTM standard is 2.5 to 3.8. A decrease in pH was attempted using sulphuric acid, but too much calcium carbonate was present to achieve this. The calcium carbonate started to act as a buffer around a pH of 5-6 and no

further decrease in pH could be reached. This means that only a general conclusion will be drawn from this test. No exact activity values will be obtained or estimates of mineralogy. The results from this test will be used to make the assumption that all soils tested are either similar or dissimilar.

3.2.9 Fall cone tests and determination of Atterberg limits

Fall cone tests (see Figure 22) were used in order to determine the liquid limits of all the soil samples, but also to obtain estimates of the original and remoulded undrained shear strengths. For the determination of the liquid limit and the remoulded undrained shear strength the 60g 60° fall cone was used and for the determination of the original undrained shear strength the 80g 30° cone was used. All these tests are done according to ISO standards 17892-6 and 17892-12 using semi-rough cones. The remoulded undrained shear strength values obtained were also fitted with an exponential fit (see Appendix C) so that comparisons at the same water content could be made by interpolating the results. Plastic limits were determined using the rolling technique where 8 threads of soil were rolled to 3mm after which crumbling of the thread into multiple pieces occurred. The thread was rolled until the thread was replaced by smaller pieces of soil around 1-2 cm. These pieces were put into 2 petri dishes. These petri dished were covered during the rolling of the threads so no or minimal water could escape the already stored pieces of thread. Each petri dish contains the pieces from 4 rolled threads. The results were then compared to check that the water content was within the limits of ISO 17892-12. This method proved to give very similar water content results between the two petri dished indicating a reliable test even though this test is user-dependent. Based on the Atterberg limits and the natural water also a liquidity index will be determined.

All the fall cone tests for liquid limit determination were checked for deviation from the linear fit and all the tests are within the 5% deviation from this linear fit that is used to determine the liquid limit.

Some soil samples only have a liquid limits reported, because the sand content is too high for some samples to allow for plastic limit determination.

Figure 22: Fall cone test setup with the 60° cone.

3.2.10 Direct shear tests

Direct shear testing is apart from two drained direct shear tests in this report only used to estimate the undrained shear strength. From these direct shear tests also estimates of oedometer stiffness are obtained. The direct shear tests itself cannot be used for doing a valid consolidation test, but can be used to obtain an estimate of the stiffness under a certain loading stress. All direct shear tests have been done according to ISO standard 17892-10. For all the undrained unconsolidated direct shear tests and some of consolidated shear tests the direct shearbox in the climate room of 17 degrees has been used. Some of the consolidated sheartests are done using the direct shearbox the main laboratory where the temperature is 23 degrees Celsius. Both shearboxes apply the load on the soil specimen using only one contact point. The results from the direct shear test in the main laboratory can be distinguished by their much smoother lines due to this test sensor being less sensitive.

The direct shearbox in the climate room uses a cylindrical mold that is 59.6 mm in diameter and 24.9 mm in height. The direct shearbox in the main laboratory uses a cylindrical mold that is 63.1 mm in diameter and 21.0 mm in height.

3.2.11 Construction of the remoulded samples

In order to create a remoulded sample for a direct shear test, the sample that is sheared initially is taken out and remoulded thoroughly with two spatulas. Then the remoulded soil is put into the sampler ring and smoothed out so that the full sampler ring is filled. Then the sampler ring is cleaned weighed and put on the cylindrical mould in which it is pushed with a stamper. The advantage is that one can say that the sample in this manner resembles soil that has fallen from the slope and is therefore disturbed in a similar manner. The soil can also obtain a different water content due to the change in void ratio caused by the remoulding. This method of remoulding is the same as the one used for determining the Atterberg limits and the remoulded undrained shear strengths using the fall cone tests. This remoulding method is consistent so that comparing the sensitivity values of both tests is possible even though this is not done, because the two tests have different failure mechanisms. Based on the mostly decrease in strength after remoulding, but sometimes also a decrease was observed. The sensitivity is then determined based on the strength obtained from the original sample divided by the remoulded sample. The sensitivity is not determined based upon the softening behaviour during shear testing since no softening behaviour was observed outside of the 0.3 kPa variation present in the direct shear tests.

3.2.12 Friction profiles of the direct shearbox in the climate room

The shearbox in the climate room requires a correction for friction, this base friction has been determined by shearing only the mould in wet and dry conditions without any applied load. These friction profiles are used to correct the force in Newton that is read from the force measurements during actual testing. Figure 23 shows the dry and wet friction profile. The wet friction profile which has been obtained by filling the shearbox with demineralized water. From both the dry and wet friction tests the average friction profile is used as a zero reading of shear force.

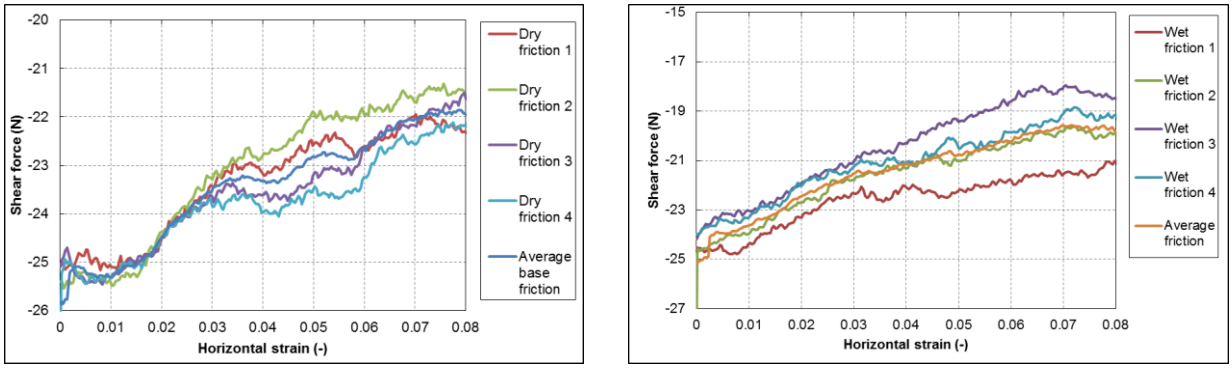

Figure 23: Shear force measured during shearing in dry and wet conditions respectively.

The maximum deviation from the average base friction lines for the dry and the wet friction profiles is displayed in Figure 24. This maximum deviation is determined using the highest and lowest friction values from the tests.

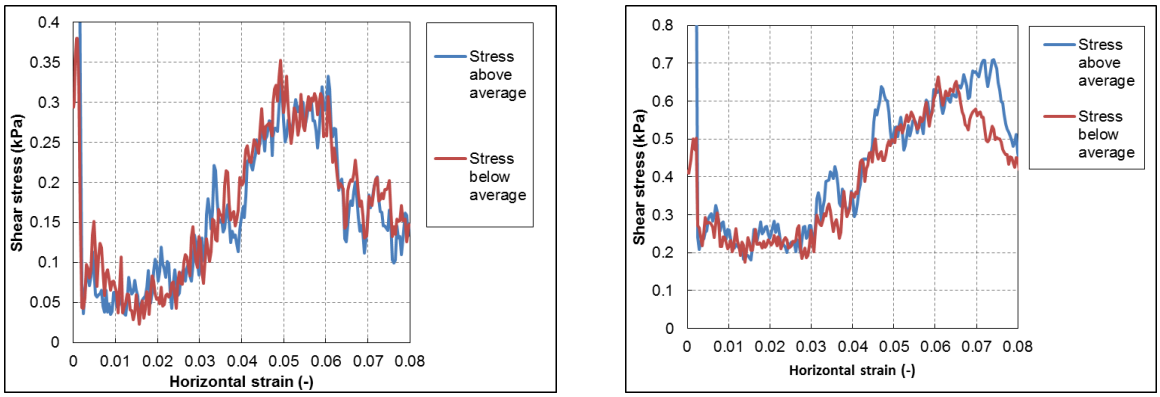

Figure 24: Deviation from the average friction measured when shearing in dry and wet conditions respectively.

This shows that the dry friction profile has a maximum deviation of 0.3 kPa and the wet friction profile shows a maximum deviation of 0.7 kPa. These deviations should be taken into account when looking at the results from the direct shear tests, but are fine for the purpose of estimating the undrained shear strengths. This partially explains why the shear test profiles are jumping up and down with small values. This behaviour prevents there from being a perfectly straight line. The other explanation is the sensitive measuring equipment which detects small changes in shear stress. The force sensor is also sensitive to temperature variations. This may affect drained direct shear tests which have to shear for longer periods of time. Based on this argumentation the dry shearbox test was chosen for all the unconsolidated undrained direct shear tests and the wet shearbox test was chosen for all the consolidated direct sheartests so that no drying out of the sample would occur. Due to the presence of low values of undrained shear strength any unnecessary variation in shear stress is to be prevented. Also since the shearing only takes 6 minutes in a room of 17 degrees (see Figure 25) and a relative humidity of around 80%, drying out of the samples is assumed not to happen in those 6 minutes.

Figure 25: The direct sheartest in the climate room shown with a consolidated sample in a wet condition.

The argument that added water could further saturate the soil samples and could provide a more undrained response is rejected here by arguing that the samples are already estimated to be near 100% saturation and added water will not make the direct shear test more undrained since water will have the chance to dissipate further into the sample when it is sheared over the middle. The results are treated as estimates of the true undrained shear

strength values since some volumetric strain always occurs. Figure 26 shows a sample that has been sheared in a wet condition.

Figure 26: A sheared sample (60mm in diameter) of the direct sheartest from the climate room.

3.2.13 Friction of the shearbox in the main laboratory

The shearbox in the main laboratory (see Figure 27) did not require any friction correction since a frictionless cylindrical mould of 63.1 mm was used. This mould was tested and found to have zero detectable friction. The sensitivity of this shear test is not known, but is found based on visual observation to be less than the sensitivity from the shearbox in the climate room. This is however also found to be adequate enough for the determination of the estimates of undrained shear strength.

Figure 27: The direct shearbox in the main laboratory.

3.2.14 Strain rate correction

In order to compare all the results that give undrained shear strengths or estimates thereof, a strain rate correction is used (see Equation 4). The strain rate is corrected to a strain rate of 1 %/hour according the method of Kullhawy and Mayne (Kulhawy, Mayne, 1990). Only the direct shear tests are required to be corrected since the fall cone tests already have a cone factor which corrects for their higher strain rate to a strain rate of 1 %/hour. The pocket vane test results are not corrected for strain rate. This strain rate correction is only used when results from the same tests are compared. Other than this comparison the direct shear test results are not corrected for strain rate. So results shown in the mandatory reporting contain the uncorrected values. In practice the shear strengths from the direct shear tests at 1.2mm/min are reduced by 16% to correct them to 1%/hour.

Equation 4: Correcting the undrained shear strenght obtained from direct shear testing for strain rate.

$$Su^{1\%} = \frac{Su}{(1.00 + 0.10 \times \log(\dot{\varepsilon}))} \tag{4}$$

Where $Su^{1\%}$ is the shear strenght corrected to a strain rate of 1%/hour, Su is the undrained shear strength obtained from direct shear test and $\dot{\varepsilon}$ is the strain rate used in the direct shear test.

3.3 The execution of all tests and all steps taken to characterize the sediments

This chapter gives an overview of all the steps taken to answer the reaserch questions.

3.3.1 Flow chart

A quick overview of the main phases of this project is given in Figure 28.

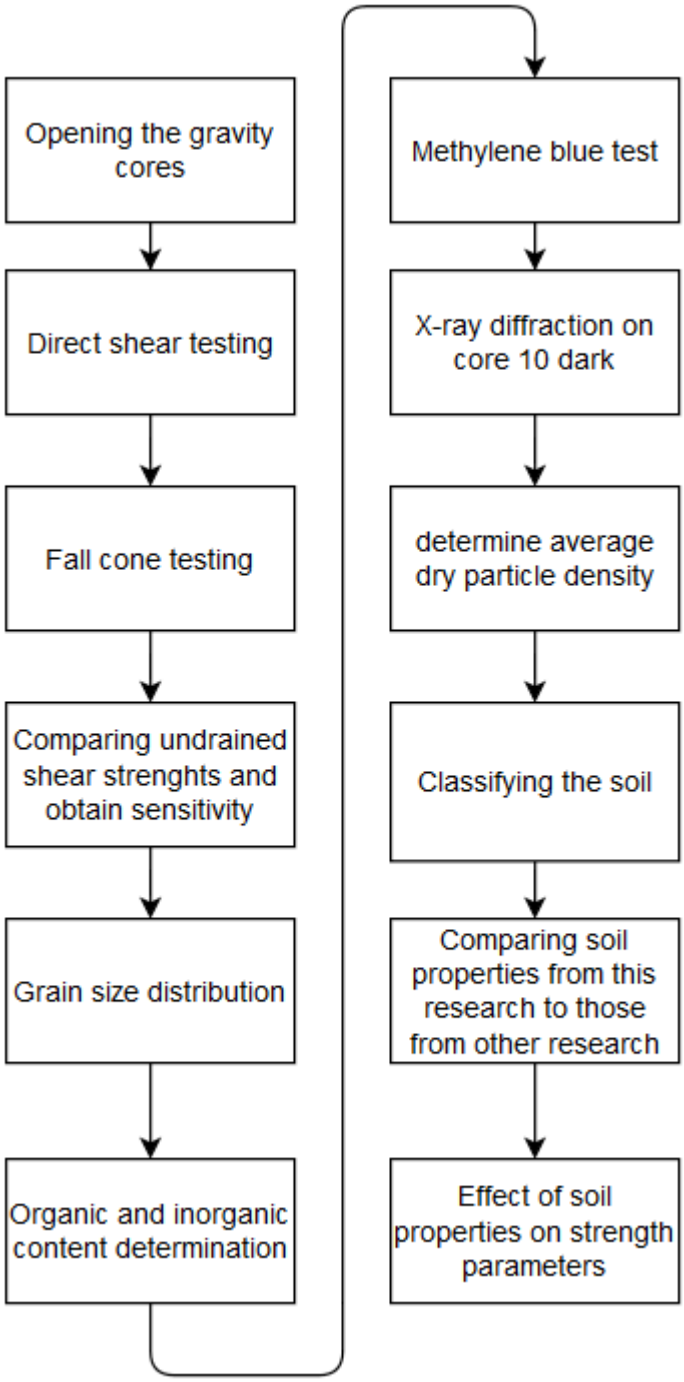

Figure 28: Flowhcart of the general phases in this project.

3.3.2 Opening of the cores

The cores will be opened(see Figure 29) and inspected for length of the sample, the full length of the core and the estimated length of the core that fills the core with the full diameter. The length of the soil present in the gravity cores will be taken as the total depth of the sediments.

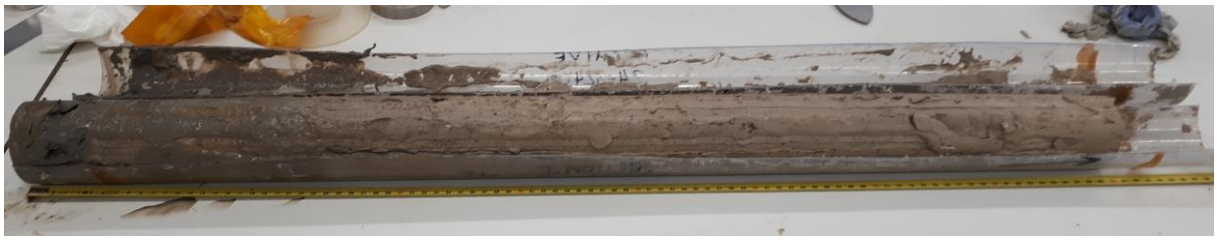

Figure 29: Example of a gravity core 10 opened with the top of the pastic cylinder cut off.

Photos will be taken and the best part of the cores will be stored in the fridge for further testing. The rest of the soil will be tested for volumetric water content , gravimetric water content and undrained shear strength by the pokcet vane testing. From this more soil properties like bulk and dry volumetric weight, void ratio and saturation will also be derived.

3.3.3 Direct shear testing

The soil will be tested in the direct shear test in a consolidated drained, a consolidated undrained and an unconsolidated undrained fashion.

From all tests the dilation angle, the bulk and dry volumetric weight, the undrained or drained shear strenghts will be determined and if the test is consolidated also an estimate of the oedometer stiffness is given. Since no triaxial testing was done, but direct shear testing was done the soil behaviour can never be truly undrained since always a change in volume in the form of dilation or contraction occurs that is larger than the 0.05% volume change allowed in triaxial testing. The tests that are done at a relatively fast speed of 1.2mm/min are thought to give an estimate of this undrained shear strength. The water content after consolidation will be used to deterime these properties and if no consolidation takes place the water content before consolidation will be used. With all shear tests the vertical displacement is measured so that the dilation angle can be determined together with the volumetric strain.

The consolidated drained tests are done only on core 8 dark at speeds of 0.024 mm/min and 0.0048 mm/min. These tests will give an idea about the peak and residual friction angle based on the peak and residual shear strenghts. These tests are done in a wet environment.

The consolidated undrained direct shear tests are done at 1.2mm/min so that an undrained shear strength estimate at a certain normal stress and water content can be determined. These tests are done in a wet environment and on some samples where enough good quality intact soil was availble.

The unconsolidated undrained shear tests are done at 1.2mm/min in order to obtain estimates of the undrained shear strenghts of the samples with their original water content. Due to the high water content of many of the samples a lot of volumetric strain took place when doing a consolidated direct shear test. This caused the water content and thus also the void ratio of the samples to go down. These tests would prevent this and are also faster in execution. This way many of these tests could be executed at original water contents. These test are all executed at a normal stress of 1.84 kPa which is not enough to initiate

consolidation. This normal stress is only present due to the mass of the equipment that is applied on top of the sample. All UU DS tests were done under 1.84 kPa.

The normal stresses that will be applied on the consolidated direct shear tests are 3 kPa, 6kPa, 9 kPa, 10kPa, 15 kPa, 20 kPa, 30 kPa and 45 kPa. This is based on the low dry volumetric weights found ranging from 7 kN/m^3 to 13 kN/m^3 and the fact that the sediments found could represent sediments up to 3m of depth. The main interest in this thesis is to obtain shear strenghts from shallow sediments with the interest of investigating the possibility of shallow failure in sediments of up to 3m depth.

3.3.4 Fall cone testing

The fall cone tests will be done in order to obtain original and remoulded undrained shear strenght estimates and the Atterberg limits.

3.3.5 Organic and inorganic content determination.

The loss on ignition method at 550° Celsius and 950° Celsius will be used on all samples in order to obtain estimates of the organic matter content and the calcite content. About 5 grams of dried powder dried at least 18 hours at 105° Celsius was supplied for this test. This test is done on all samples.

3.3.6 Grain size distribution

A grain size distribution of the soil will be created by means of a wet sieving and a hydrometer test. This will give an indication about the sand, silt and clay content of the soil samples.

3.3.7 Determining several soil properties

The soil will be tested for average dry particle density. An X-ray diffraction test will be done by a company on core 10 dark in order to determine the mineralogy and the methylene blue test will be done on all of the samples in order to obtain the activity of the soil and make a mineralogy estimate for all of the tested samples.

3.3.8 Comparing the undrained shear strengths

The undrained shear strengths of the original and remoulded unconsolidated undrained direct shear tests will be compared. This will give an idea about the sensitivity of the different samples at different water contents. The same will be done for the original and remoulded fall cone tests. Due to remoulding the remoulded samples may have a slightly different water content than the original sample. To solve this the average water content of the original and the remoulded samples was used to plot the sensitivity values (see Appendix E for all values). No comparisons of the consolidated shear tetsts will be made since these have all been done on orignal samples with different water content, soil compositions and different normal stresses applied.

3.3.9 Classifying the soil

Based on all the obtained soil properties the soil will be classified in the based on the classification scheme of Chapter 3.1.

3.3.10 Comparing soil properties to each other and to outside literature

Soil properties from this research will be compared to each other and to outside literature.

3.3.11 Effects of soil properties on strenght parameters

The effects of the obtained soil properties on strength parameters will be discussed based on the soil properties found in this research.

4 Results and discussion

In this chapter the results from all of the labortory tests done on all cores from the 7 gravity coring locations will be presented and discussed. This will involve the mineralogy, fossil content , activity, gravimetric water content, volumetric water content, bulk volumetric weight, dry volumetric weight, undrained shear strength from the pocket vane testing, grain size distribution, sand content, silt content, clay content, Atterberg limits, SOM content, SOC content, caclite content, undrained shear strenght from the direct shear tests, undrained shear strenght from the fall cone test and the sensitivity. All corresponding values to the Figures shown can be found in Appendices A to F.

Table 9 gives an overview of all the tests done on each soil interval

Table 9: Summary of what types of tests were used on certain intervals in different core at different sites.

Site	Sample name	UU Direct shear test	CU Direct shear test	CD Direct shear test	Fall cone test	Plastic limit test	pycnometer test	Methylene blue test	hydrometer test	wet sieving	organic matter test	inorganic matter test	Microscope study	X-ray diffraction
1736	Core 1 sandy dark	X	NA	NA	X	X	NA	X	NA	NA	NA	NA	X	NA
1736	Core 1 dark	NA	NA	NA	X	X	X	X	X	X	X	X	X	NA
1736	Core 1 grey	NA	NA	NA	X	X	X	X	X	X	X	X	X	NA
1736	Core 2 orange	X	X	NA	X	X	X	X	X	X	X	X	X	NA
1736	Core 2 dark	X	X	NA	X	X	X	X	X	X	X	X	X	NA
1672	Core 4 dark (5-15.5)	X	NA	NA	X	X	X	X	X	X	X	X	NA	NA
1672	Core 4 light (21-32)	X	NA	NA	X	X	X	X	X	X	X	X	NA	NA
1672	Core 5 beige clay 2 (12-22)	NA	NA	NA	NA	NA	NA	X	NA	NA	NA	NA	X	NA
1672	Core 5 (22-37)	NA	X	NA	X	X	X	X	NA	NA	NA	NA	NA	NA
1672	Core 5 (37-47.5)	NA	X	NA	NA	NA	NA	X	NA	NA	NA	NA	NA	NA
1672	Core 5 very light (44-56)	NA	NA	NA	NA	NA	X	X	NA	NA	NA	NA	X	NA
1672	Core 5 beige (63.5-75)	X	NA	NA	X	X	X	X	X	X	X	X	X	NA
688	Core 6 sandy clay (8.5-24)	X	NA	NA	X	NA	X	X	X	X	X	X	X	NA
688	Core 6 clayey clay (38-55.5)	X	NA	NA	X	X	X	X	X	X	X	X	X	NA
1988	Core 7 dark (10.5-22.5)	X	NA	NA	X	X	NA	X	NA	NA	NA	NA	NA	NA
1988	Core 7 dark(22.5-34)	X	NA	NA	X	X	X	X	X	X	X	X	X	NA
1988	Core 7 light	X	X	NA	X	X	X	X	X	X	X	X	NA	NA
1695	Core 8 dark	NA	NA	X	NA	NA	X	X	X	X	X	X	X	NA
1695	Core 8 light	NA	X	X	NA	NA	X	X	X	X	X	X	X	NA
1959	Core 9	NA	NA	NA	NA	NA	X	X	X	X	X	X	NA	NA
1959	Core 10 dark (6-22)	X	X	NA	X	X	X	X	X	X	X	X	NA	X
1959	Core 10 light (31-41)	X	NA	NA	X	X	NA	X	NA	NA	NA	NA	NA	NA
1959	Core 10 light (41-51)	X	NA	NA	X	X	X	X	X	X	X	X	NA	NA
1959	Core 10 light(57-71)	X	NA	NA	X	X	NA	X	NA	NA	NA	NA	NA	NA
1604	Core 3	X	NA	NA	X	X	X	X	X	X	X	X	X	NA
1604	Core 11 clayey clay(31-42)	X	NA	NA	X	X	NA	X	NA	NA	NA	NA	NA	NA
1604	Core 11 clayey clay(42-52.5)	NA	NA	NA	X	X	X	X	NA	X	X	X	X	NA
1604	Core 11 sandy clay	X	NA	NA	NA	NA	X	X	X	X	X	X	X	NA
1604	Core 11 sandy clay 2	NA	NA	NA	NA	NA	X	X	X	X	X	X	NA	NA

4.1 Mineralogy

In order to determine the mineralogy of the soil that is present on the eastern slope of the Rockall bank an X-ray diffraction has been executed by Qminerals on a soil sample from site 1959 called core 10 dark. Core 10 dark is classified as a silty CLAY and is chosen, because of its high clay content of 51%. The clay content plays a major role in soil behaviour. The mineralogy from this soil sample is assumed to be representative of the mineralogy of the soil on the RBSC based on the results of the methylene blue test. The amounts of the respective minerals present are assumed to change with location since it was found that there is a lot of variation in sand, silt and clay content. An indication of the parent materials will be given together with their possible weathering paths and weathering products.

4.1.1 Mineralogy of the sand fraction

All the non-clay minerals are displayed in Table 10. This table will be used for all the explanations of the mineralogy in chapter 4.1.

Table 10: Overview of all the non-phyllosilicates present in core 10 dark obtained from an XRD-diffraction test.

Mineral group	Mineral name	Theoretical formula	Presence (%)
Silicates	Quartz	SiO_2	14
Silicates	Alkali feldspar	$(K,Na)AlSi_3O_8$	6.7
Silicates	Plagioclase	$(Na,Ca)AlSi_3O_8$	6.8
Carbonates	Calcite	$CaCO_3$	26.5
Carbonates	Ankerite	$(Fe,Ca,Mg,Mn)CO_3$	1.6
Carbonates	Siderite	$FeCO_3$	0.2
Oxides	Anatase	TiO_2	0.3
Oxides	Rutile	TiO_2	0.2
Oxides	Hematite	Fe_2CO_3	0.5
Sulfides	Pyrite	FeS_2	0.1
Halites	Halite	NaCl	2
Phosphates	Apatite	$Ca_5(PO_4)_3$	0.1

The formation of pyrite (see Figure 30) could have occurred by reducing organic matter. Reducing environments are possible to be present due to the organic matter itself.

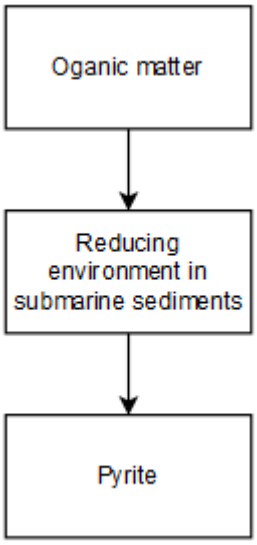

Figure 30: Flow chart of the formation of Pyrite.

The formation of hematite (see Figure 31) could have occurred via iron present in the seawater reacting with oxygen. This mineral is present in small quantities so this seems plausible.

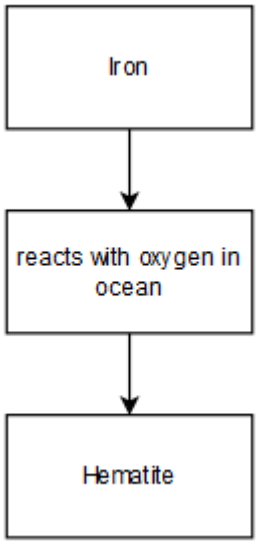

Figure 31: Flow chart of the formation of Hematite.

The carbonate fraction (see Figure 32) can be explained by the presence of mainly planktonic Foraminifera fossils which mainly consist out of calcite. These fossils have been detected in all of the samples. The marine life skeletons further can form siderite and ankerite via diagenesis. The marine skeletons are assumed to contain mostly calcite since this was found to be present the most of the carbonates. Ankertite could also have been formed by hydrothermal alteration of seawater.

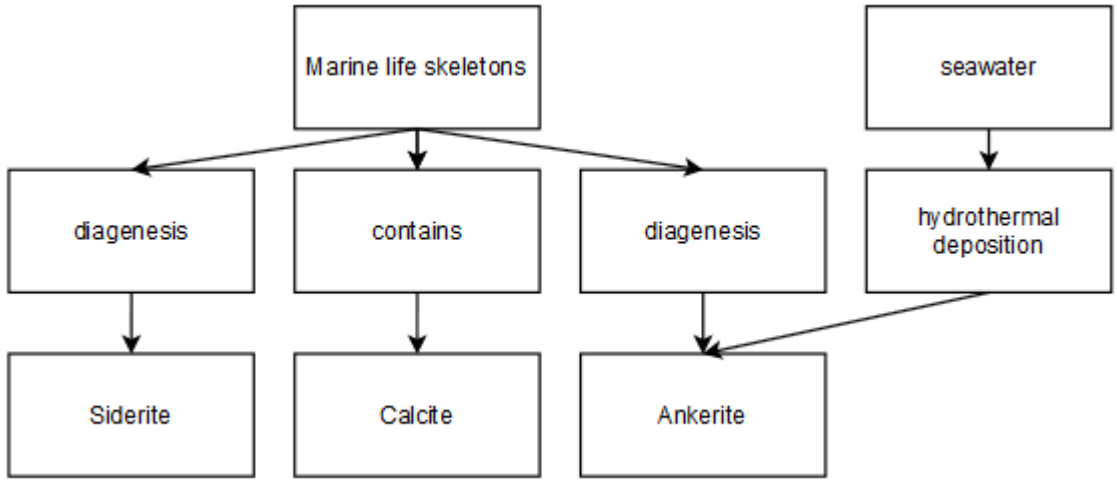

Figure 32: Flow chart of the formation of siderite, calcite, ankerite from marine life skeletons and seawater.

The mineral halite (see Figure 33) can be explained by the sodium chloride that is naturally present in the sea which has the ability to from the mineral halite by precipitation.

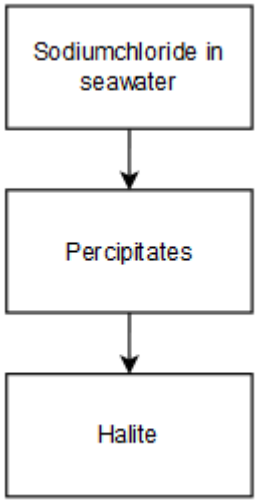

Figure 33: Flow chart of the formation of Halite.

The possible parent material can be determined by looking at the Quartz, Alkali feldspar and Plagioclase fraction. These quantities obtained from the X-ray diffraction normalized and in the QAPF diagram. This is a diagram used for classifying either intrusive rock that crystallizes slowly below surface to from clearly visible crystals. It can also be used to classify extrusive rocks that crystallized very fast on the surface itself. This causes the formation of crystals that are too small to see. In the case of an intrusive rock the parent material is called a Monzogranite. In the case of extrusive rock this would be called a Rhyolite. The assumption is made that the parent material is intrusive based on the Aegirine granite found to be present in Rockall Island (see Figure 34). It must be clarified that the mineral Aegirine was not found in the X-ray diffraction of core 10 dark.

Figure 34: A photo of an aegirine granite piece of rock found at Rockall island obtaine from the www.virtualmicroscope.org with thanks to the Sedswick museum. This image is under Creative Commons Attribution-NonCommercial_ShareAlike .20 License.

The Monzogranite (see Figure 35) is assumed to further contain muscovite in its original composition, so not as a weathering product. This makes the exact name of the rock a Monzogranite type 2 called muscovite-metagranite. Apatite together with the titanium oxide Anatase is also thought to be present in the original composition of the rock. Apatite and Anatase two minerals are present in very small quantities.

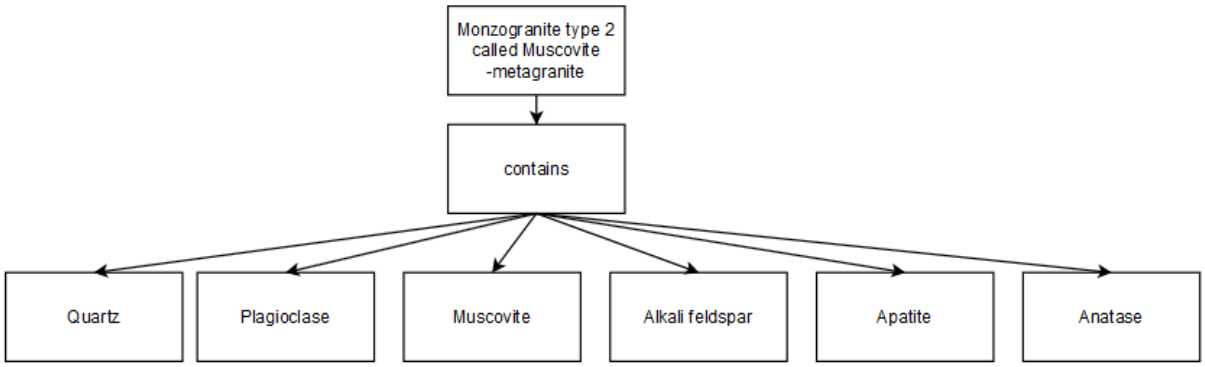

Figure 35: Flow chart of the possible contents of a Monzogranite type 2.

4.1.2 Mineralogy of the sand fraction

The clay fraction (see Table 11) which is important for determining the soil behaviour contains an Illite/muscovite fraction, an interstratified Illite/Smectite fraction, Kaolinite and Chlorite.

Table 11: Overview of all the clay minerals present in core 10 dark obtained from an XRD-diffraction test.

2:1 Clay minerals* $K(Al,Mg,Fe)_2(Si,Al)_4O_{10}[(OH)_2,(H_2O)]K(Al,Mg,Fe)_2(Si,Al)_4O_{10}[(OH)_2,(H_2O)]$	Presence (%)
Illite and muscovite (estimated)	19.1
Smectite and illite/smectite (estimated)	16.1
Kaolinite $Al_2Si_2O_5(OH)_4$	2.7
Chlorite $Mg_3Si_4O_{10}(OH)_2$	3.2
*consists out of illite, interstratified illite/smectite, smectite and muscovite	-

This specific composition of clay minerals is indicative of a process in which illitization of the Smectite minerals takes place. This Illitization is a weathering process whereby Smectite minerals transform to Illite minerals via an Illite/Smectite interstratified structure. This process takes place during burial diagenesis and is authigenic. The systemic presence of Illte, Chlorite, Kaolinite and Smectite minerals are found when the illitization process is occurring (Lanson, Sakharov, 2019).

The presence of interstratified Illite/Smectite can also have the implication that swelling due to the presence of Smectite minerals does not necessarily need to happen on the same magnitude everywhere since different stages of illitization are present (Lanson et al. 2009).

Figure 36 shows all the possible paths of weathering that are found to be a reasonable assumptions. The arrows in this flowchart point to the possible weathering products. The arrow starts from the parent mineral or parent material. Here the Plagioclase can weather to calcite or to chlorite through contact metamorphism or due to hydrothermal alteration. Chlorite itself can weather further to Smectite or directly to Kaolnite. The Quartz will not weather any further. The Muscovite and the Alkali feldspar could both weather to Smectite minerals or to Kaolinite. The Smectite minerals could then weather to Kaolinite or to Illite via a process called illitization. The Apatite will not weather any further and Anatase will weather to Rutile which is a different titanium oxide. All the minerals used in Figure 36 are found to be present in the soil from core 10 dark analysed by X-ray diffraction. The arrows point towards the possible weathering products.

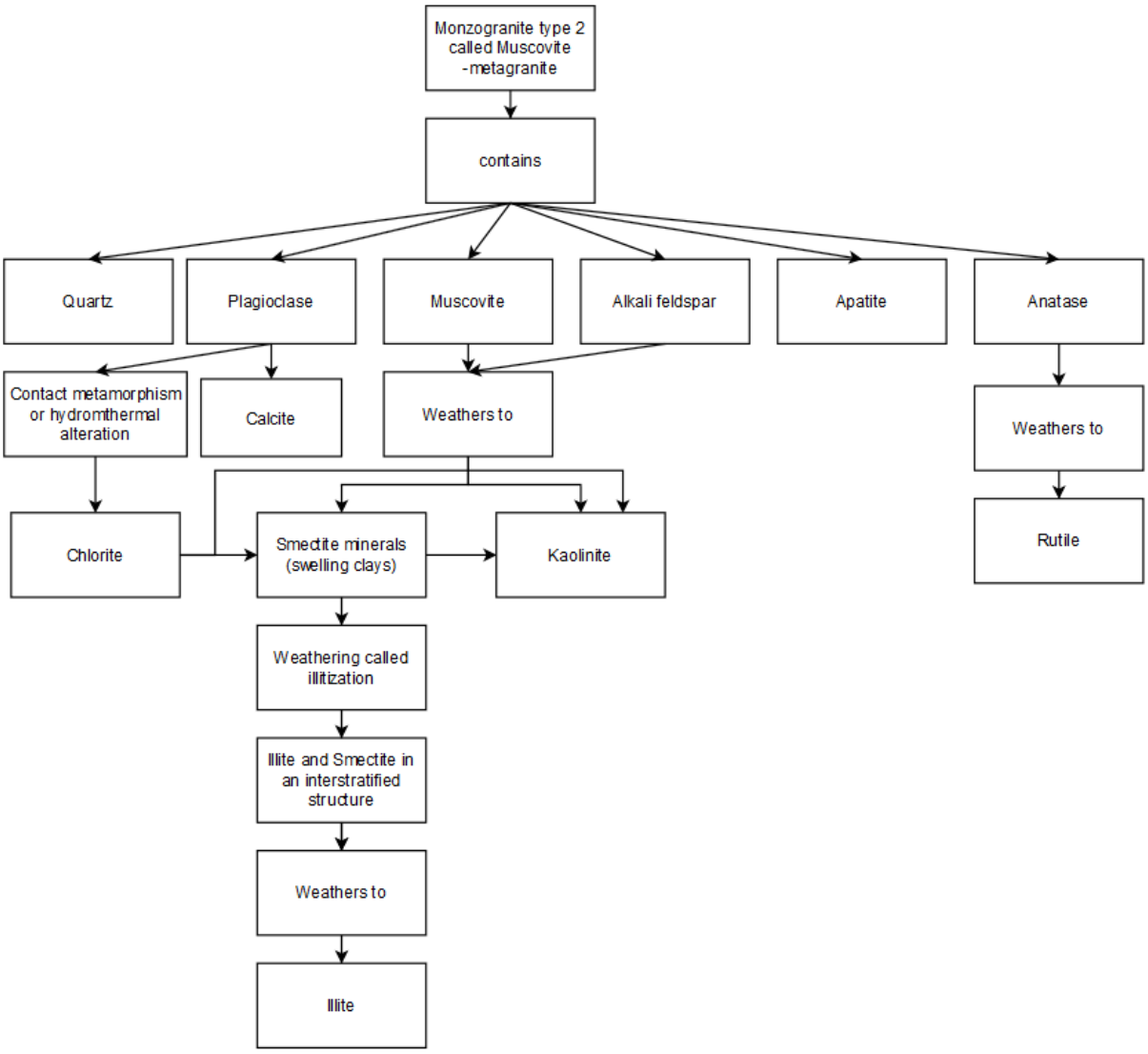

Figure 36: Flow chart showing the possible wheatering paths taken by the minelas found to be present in core 10 dark.

After drying some of the soil samples from site 1695 and site 1959, a sharp decrease in liquid limit was observed. The soil samples that originally had a water content of 100%, could only hold a water content of 40% before acting as a liquid after the soil had been dried in the oven at 105° Celsius for at least 18 hours. A sharp decrease in liquid limit was found compared to the non-dried materials of the same intervals.

This decrease in the liquid limit after over drying is attributed to the destruction of the soil structure which could contain calcite cement. This soil cementation may have been broken by drying and rewetting the soil sample. This drying and rewetting of the soil involves remoulding the soil and thus destroying the original structure or void ratio. Many of the non-dried remoulded samples have also been found to show a decrease in liquid limit. This is ascribed to the destruction of the original void ratio.

Another reason could be dehydration of intermolecular water molecules. This could be the case if Halloysite or Allophane were present. These clay minerals were not detected so this is not assumed to be the reason for the decrease in liquid limit.

The reason that the dehyroxylization is not found to be the reason is as follows. Any significant of transformation from hydroxide to water vapour occurs only after 550° Celsius. The organic matter content degradation can't be attributed to the decrease in liquid limit since only fresh non-oven dried soil was used for the determination of the liquid limit.

4.2 Microscopy study

The microscope study that was done used a binoculair microscope with falling light onto the sand fraction. This study resulted in the identification of all the visibly present marine life skeletons from which an estimate could be made about the depth of deposition. Only rough conclusions will be drawn about this estimated depth since the amount of planktonic foraminifera were found to be in the clear majority in all cases. This microscope study is only used to identify the marine life skeletons that are present in the 63µm to 2mm sand fraction that are clearly visible. Photos of the individual foraminifera shells are present in Appendix G and a general overview of all photos is present in Appendix H.

All the visibly present marine life skeletons are named and classified as planktonic or benthic foraminifera if this determination could be made. Otherwise only the name is given. Determinations are based on visual comparisons to formininfera specimens from the works of (Hinsbergen, Kouwenhoven, van der Zwaan, 2005) and (van Gorsel, 2018). Errors may be present in the interpretation of the name of these fossils since it was not done by an expert. However the most occurring marine shells in Figures 37 and 38 could be clearly identified. Based on these marine shells a depth estimate is made.

It is estimated that for all of the studied samples 90% to a 100% of the fossils present consists out of planktonic foraminifera. This gives according to Equation 5 a depositional depth between 869 metres deep for the fossil fraction with 90% planktonic foraminifera and a depositional depth of 1238 metres deep for the fossil fraction with 100% planktonic foraminifera. The conclusion that can be drawn from this is that the sediments from all of the sites except site 688 show sediment transport to deeper areas on the slope. This could also give an estimate about distance of sediment transportation along the slope. This could be used to verify the sediment transport distance simulated by flow models used to simulate landslides of the Rockall Bank slide complex.

Equation 5: Calculating the depositional depth of the fossils according to (Hinsbergen, Kouwenhoven, van der Zwaan 2005).

$$Depth(m) = e^{3.59+(0.0353\times\%P)} \quad (5)$$

%P in Equation 5 stands for the percentage of planktonic foraminifera in the part of the sand fraction that consists out of marine shells.

The fossils in Figures 37 and 38 were found to make up the majority of all of the marine life shells visibly found. Other fossils and rock fragments that have been found can be seen in Appendix G.

Figure 37: Images of Neogloboquadrina dutertrei of the planktonic formininfera (100µm to 300µm).

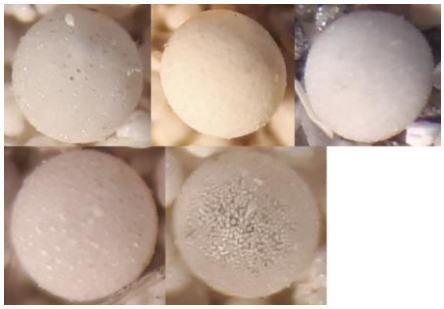

Figure 38: Images of Orbulina universa of the planktonic foraminifera (100µm to 300µm).

4.3 Methylene blue test results

All samples that were tested gave similar results. They all required 3 to 4 drops of the methylene blue solution to have exchanged all available cations. This indicates that the soil from all sites has similar activity. This activity in methylene blue tests is attributed to the clay fraction. The pH for all samples was around 9.5. This high pH enables in general a greater exchange of protons which leads to a higher measured activity. Even though some minerals can show higher activity at certain pH levels it is assumed here that the obtained activity values will not be higher if the pH was lower. The pH found was higher than allowed in the ASTM C837 standard so only the conclusion will be drawn that in all samples clays of similar activity are present. This is used to say that the mineralogy found in core 10 dark is representative of the types of minerals found at all sites.

4.4 Overview of all gravity cores

Here an overview of all the closed gravity cores is given in Figure 39. All the depth values used in this report are based on the average position of the soil samples present at a certain location in the gravity core. Depth values become more negative with increasing depth and start counting from the first piece of intact/disturbed sediment. So the full depth discussed will be the length that is equal to the total core recovery length found at each site. If water content is used then always the gravimetric water content is meant unless it is specifically stated that the volumetric water content is used. The water density used for calculations is 998 kg/m^3.

Figure 39: Overview of all the unopened gravity cores (core 11 is 1m).

4.5 All test results from site 1736

Here all the test result from site 1736 will be presented.

4.5.1 Opening of core 1 and 2 from site 1736

The opened cores 1 and 2 are displayed below in Figure 40 where core 2 is closest to the seabed. Core 1 increases with depth from right to left. The colour of the core 1 sediments becomes darker with depth from a lighter grey to a dark grey. Core 2 increases with depth from right to left and has a light grey colour without showing a clear change in colour with depth. Both cores have orange spots on them which is expected to be from the presence of iron oxide.

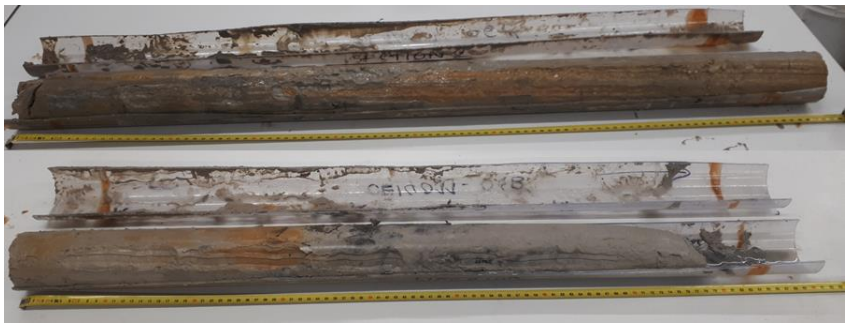

Figure 40: Core 1 above core 2.

Tables 12 to 14 give an overview of the amount of cores opened for one site and the total and full core recovery. The total core recovery includes also the broken/disturbed parts of the core whereas the full core recovery includes only parts of the core where the whole diameter is intact.

Table 12: Core 1 core recovery information

Core 1	
Mass of closed core (kg)	6.109
Mass of empty core (kg)	0.71
Lenght of cylinder section (cm)	102
Total core recovery (cm)	97
Full core recovery (cm)	95

Table 13: Core 2 core recovery information

Core 2	
Mass of closed core (kg)	4.139
Mass of empty core (kg)	0.734
Lenght of cylinder section (cm)	92
Total core recovery (cm)	78
Full core recovery (cm)	59

Table 14: Site 1736 core recovery information

Site 1736	
Penetration depth (cm)	NA
Total core recovery (cm)	175
Full core recovery (cm)	154
Recovery ratio (-)	NA
Pull out force (kg)	2000

Figure 41 shows the gravimetric water content decreasing from 0.98 to 0.40 with depth. The volumetric weight remains stables around 0.72 until a depth of 60 cm after which it starts to decline to a value of 0.55. The bulk volumetric weight shows an increase from 15 kN/m^3 to 17.5 kN/m$^{3.}$ The dry volumetric weight also shows an increasing trend. The saturation remains close 1 along the entire length of the core. The void ratio decreases from 2.7 to 1.2 and the liquidity index fluctuates between 0.75 and 2.1 showing a general increase in fluctuation with depth. The undrained shear strength values from the pocket vane test fluctuate between 7 kPa and 14 kPa.

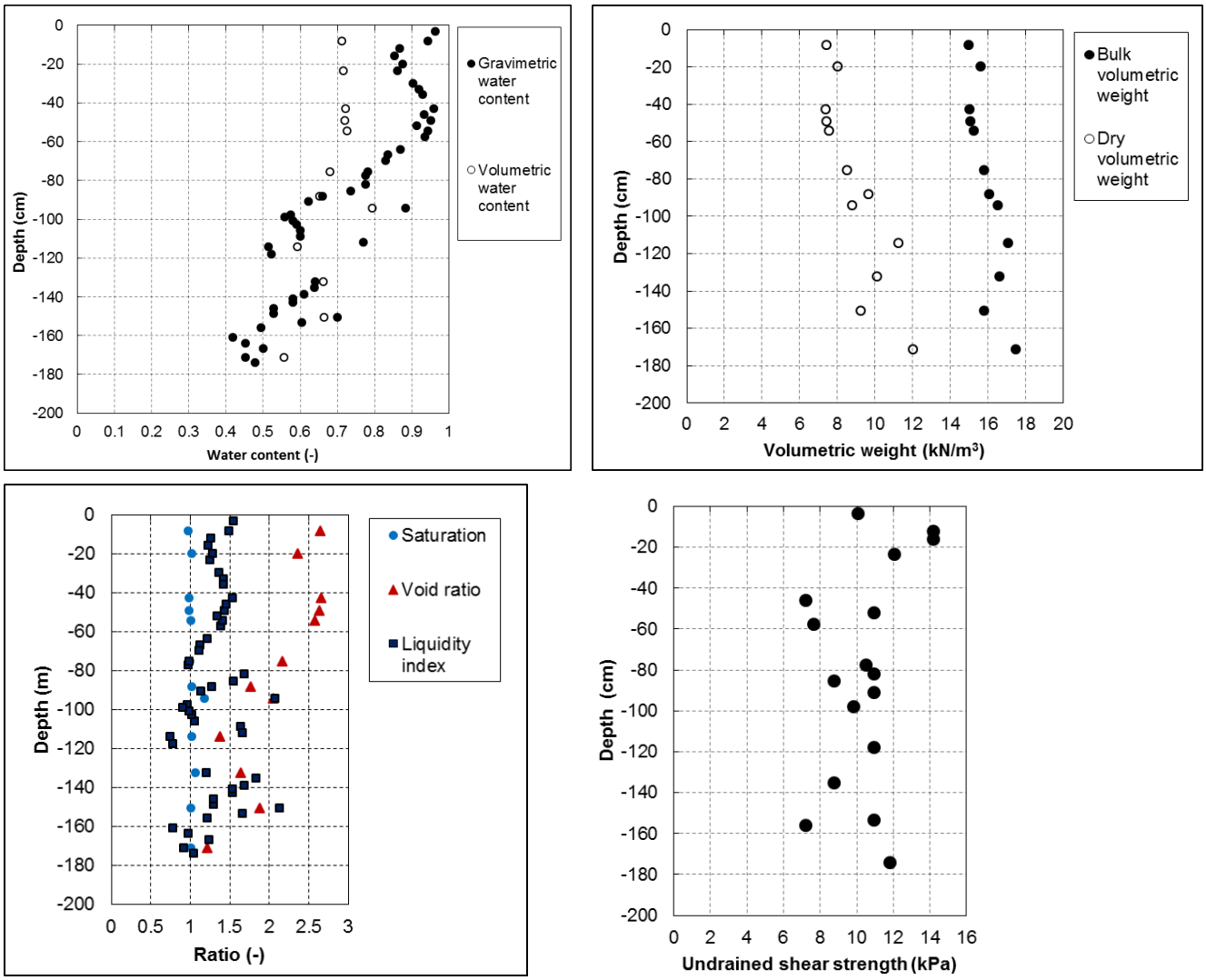

Figure 41: From left to right and top to bottom the water content, volumetric weight, saturation and void ratio and the undrained shear strength from the pocket vane with depth at site 1736.

4.5.2 Grain size distribution at site 1736

Figure 42 shows the grain size distribution of site 1736. This shows first an increase in clay content followed by a decrease in clay content. The silt and sand content increase in the top 70cm whereas they decrease below that depth. The fact that not all clay content values show a fining-upward trend may be the cause of multiple fining-upward sequences being present. This could not be seen since the resolution of this geotechnical research is less than that of stratigraphic research. One fining-upward and one coarsening-upward sequence is found.

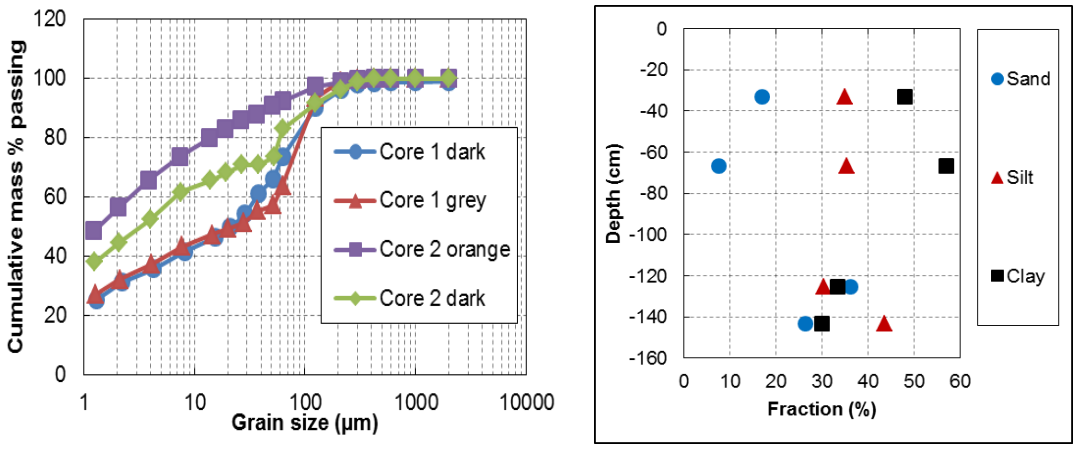

Figure 42: The grain size distribution and the soil fractions with depth from left to right at site 1736.

4.5.3 Atterberg limits and loss on ignition results at 550° and 950° Celsius at site 1736.

Figure 43 shows the plastic limit decreasing with depth from 0.43 to 0.28 and shows the liquid limit decreasing from 0.78 to 0.47. It also shows that the liquid limit is always below the natural water content. This indicates a risk of liquefaction if disturbance of the sediments occurs. The calcite content shows a decrease from 48% to 23% together with the organic matter content which shows a decrease from 7.3% to 3.9%.

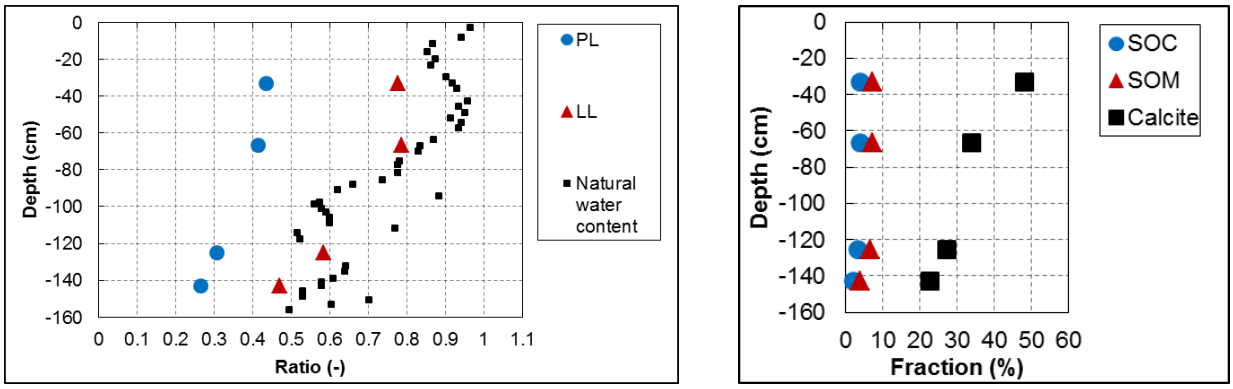

Figure 43: Atterberg limits with depth on the left and their corresponding fall cone test results on the right at site 1736.

Table 15 shows the classification results of site 1736. These sediments can be classified as clayey SILT and silty CLAY. This soil has a low to medium organic content is calcareous to highly calcareous. This soil is found to be inactive to normal.

Table 15: Classification of the soil from site 1736.

Sample name	Soil type	Plasticity	SOM classification	Calcite classification	Activity classification
Core 1 sandy dark	NA	medium	NA	NA	NA
Core 1 dark	clayey SILT	medium	low-organic	calcareous	inactive soil
Core 1 grey	silty CLAY	high	medium-organic	highly calcareous	normal soil
Core 2 orange	silty CLAY	very high	medium-organic	highly calcareous	inactive soil
Core 2 dark	silty CLAY	very high	medium-organic	highly calcareous	inactive soil

4.5.4 Unconsolidated undrained direct shear tests at site 1736

Figure 44 shows the results of the unconsolidated undrained direct shear test. Only core 1 sandy dark shows dilation, even when the sample is remoulded. All the other samples show contraction during shearing. The results show undrained shear strengths between 1.1 kPa and 5.3 kPa.

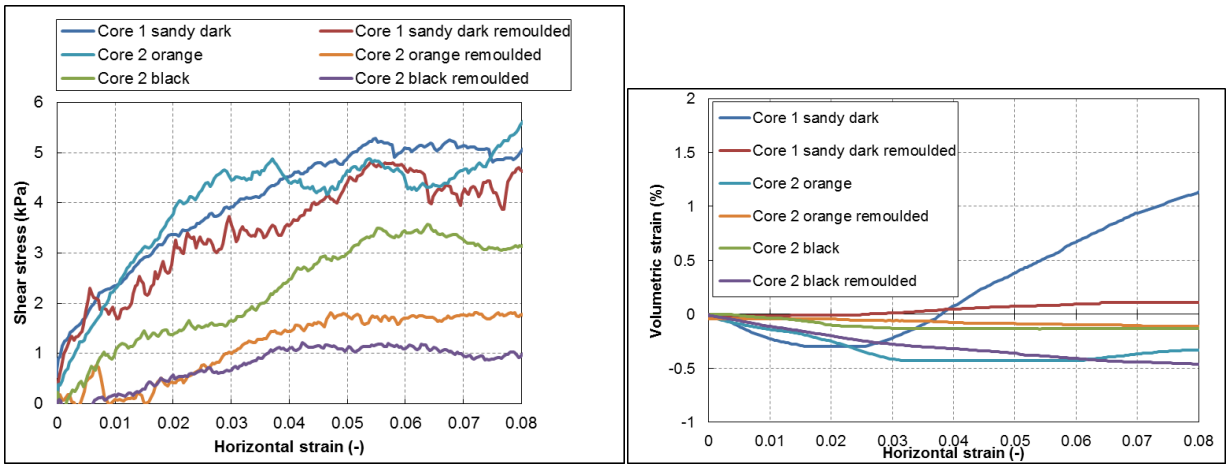

Figure 44: Unconsolidated undrained direct shear test results from site 1736.

Table 16 shows the mandary reporting results of the unconsolidated undrained direct shear test at site 1736.

Table 16: All unconsolidated undrained direct shear test results from site 1736.

Sample name	Ψ(°)	θ_{before} (-)	γ_{bulk}(kN/m^3)	γ_{dry} (kN/m^3)	ρ_{grain}(kg/m^3)	s_u(kPa)	determined at ε_h(%)
Core 1 sandy dark	7.3	0.42	16.7	11.8	2739	5.3	5.5
Core 1 sandy dark remoulded	0.3	0.43	17.2	12.0	2739	4.9	5.4
Core 2 orange	-1.5	0.87	14.6	7.8	2765	4.6	2.9
Core 2 orange remoulded	-0.2	0.91	14.6	7.6	2765	1.7	4.7
Core 2 dark	0.0	0.92	13.7	7.1	2765	3.5	5.5
Core 2 dark remoulded	-0.3	0.94	NA	NA	2765	1.1	3.8

4.5.5 Consolidated undrained direct shear test of core 1 dark at 1.2mm/min at site 1736

Figure 45 shows the results from the consolidated undrained direct shear test of core 1 dark. The soil is in all consolidated cases cases contractive during shearing. The soil however dilates when it is sheared without any considerable normal stress. The undrained shear strengths obtained are 4.1 kPa to 30.1 kPa at normal stresses from 0 kPa to 45 kPa. The stiffness of the deposits is found to increase with normal stress. The anomaly of the shear test at 0 kPa can be explained by equipment failure due to the vertical displacement sensor not remaining in place.

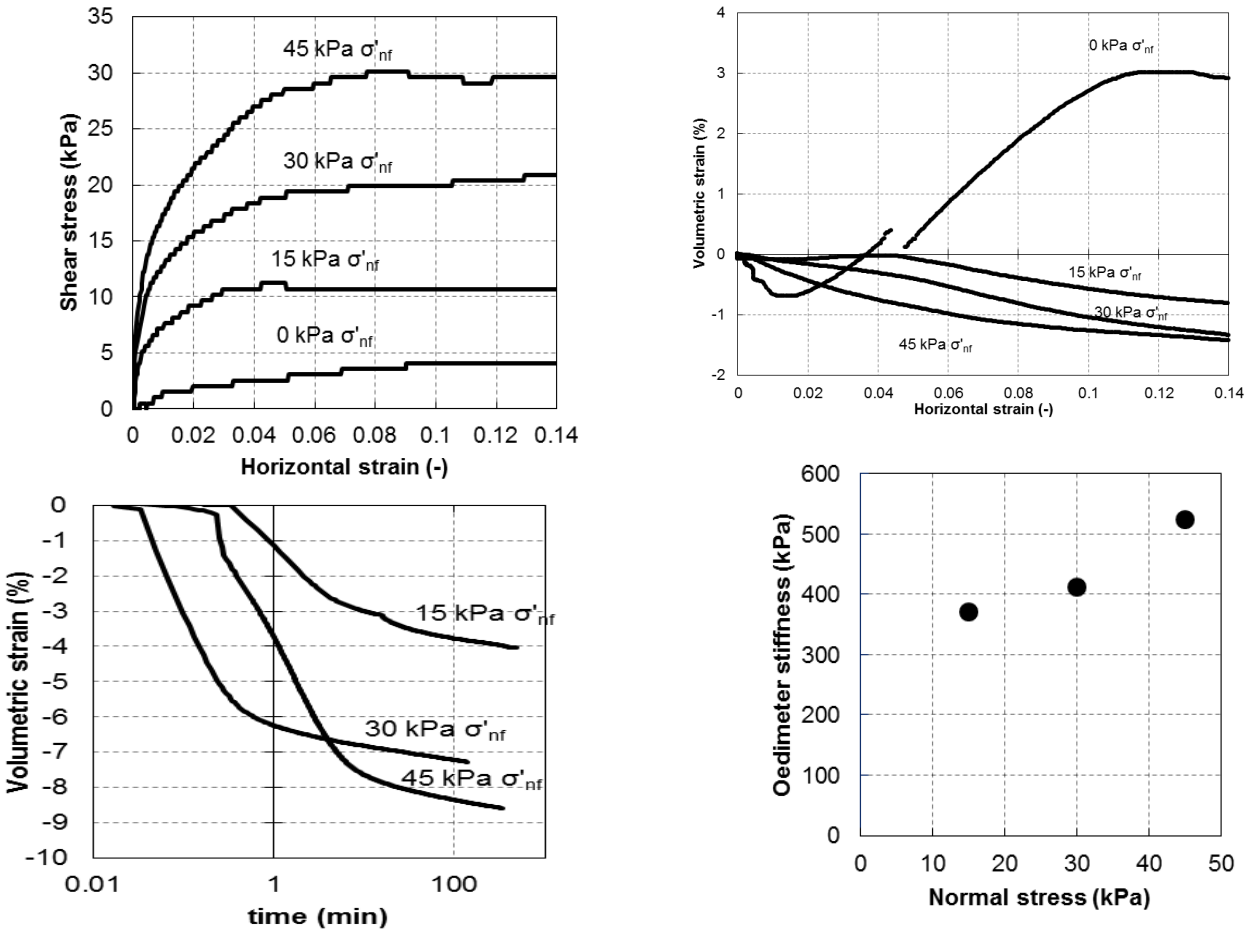

Figure 45: Results from the consolidated undrained direct shear test on core 1 dark.

Table 17 shows the mandatory reporting for the consolidated undrained direct shear test of core 1 dark.

Table 17: Mandatory reporting on the consolidated undrained direct shear test on core 1 dark.

Sample name	Ψ(°)	θ_{before} (-)	θ_{after} (-)	γ_{bulk}(kN/m^3)	γ_{dry} (kN/m^3)	ρ_{grain}(kg/m^3)	s_u(kPa)	determined at ε_h(%)	E_{oed} (kPa)
Core 1 dark UU test	13.0	0.53	0.55	16.6	10.7	2739	4.1	9.1	NA
Core 1 dark 15 kPa	-3.6	0.61	NA	16.3	10.1	2739	10.7	7.9	371
Core 1 dark 30 kPa	-4.6	0.58	0.48	16.6	11.2	2739	19.9	8.2	412
Core 1 dark 45 kPa	-3.5	0.58	0.41	17.4	12.3	2739	30.1	8.0	523

4.5.6 Consolidated undrained remoulded shear strength of core 1 dark at site 1736

Figure 46 shows the results from the consolidated undrained direct shear test of core 1 dark remoulded. The soil acts in all cases contractive during shearing, but the test at 30 kPa normal stress shows a strong dilatory behaviour during shearing. This can be explained by a possible higher sand content than the other samples. The undrained shear strengths range from 9.2 kPa to 24.5 kPa over normal stresses from 15 kPa to 45 kPa. An increase in stiffness if found with an increase in normal stress.

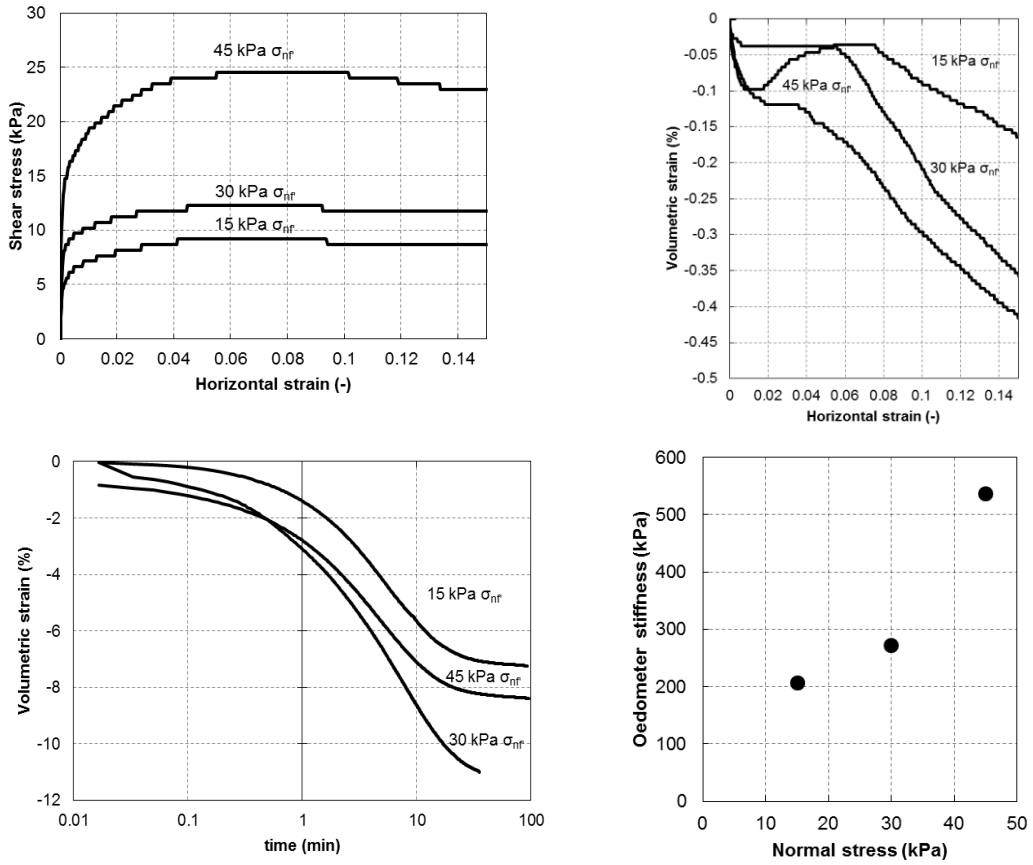

Figure 46: Results from the remoulded consolidated undrained direct shear test of core 1 dark

Table 18 shows the mandatory reporting for the consolidated undrained direct shear test of core 1 dark.

Table 18: Results from the remoulded consolidated undrained direct shear test of core 1 dark

Sample name	Ψ(°)	θ_{before} (-)	θ_{after} (-)	γ_{bulk}(kN/m3)	γ_{dry} (kN/m3)	ρ_{grain}(kg/m3)	s_u(kPa)	determined at ε_h(%)	E_{oed} (kPa)
Core 1 dark remoulded 15 kPa	-0.5	0.48	0.42	16.8	11.9	2739	9.2	4.3	207
Core 1 dark remoulded 30 kPa	-1.1	0.53	0.43	16.8	11.8	2739	12.3	4.3	273
Core 1 dark remoulded 45 kPa	-0.8	0.40	0.36	17.7	13.1	2739	24.5	5.6	537

The sensitivities for this tests are also determined in Table 19. This shows low sensitivity values ranging from 1.2 to 1.6. This is an indication that remoulded sediments can still retain a considerable portion of their original strength if they are reconsolidated at their respective normal stresses.

Table 19: Comparing the original and remoulded CU DS test in order to obtain sensititivty values.

normal stress (kPa)	S_u(kPa) of original CU DS test	S_u(kPa) of remoulded CU DS test	St(-)
15	10.7	9.2	1.2
30	19.9	12.3	1.6
45	30.1	24.5	1.2

4.5.7 Consolidated undrained direct shear tests of core 1 grey at site 1736

Figure 47 shows the consolidated undrained direct shear test of core 1 grey original. This shows that the soil acts in all cases contractive during shearing except for the test at 100 kPa which first shows some dilation at the start of shearing apart the shear test at 100 kPa. This shows dilation in the first 2% of strain. This is logical since the sample could have been

consolidated into a dense state under this high normal stress. This tests was done because more material was available and does not represent the in-situ normal stresses for these deposits. Undrained shear strengths from 5.3 kPa to 31 kPa are found over normal stresses from 5 kPa to 100kPa. The oedometer stiffness increases with increasing confining stress. An increase in stiffness is found with an increase in normal stress.

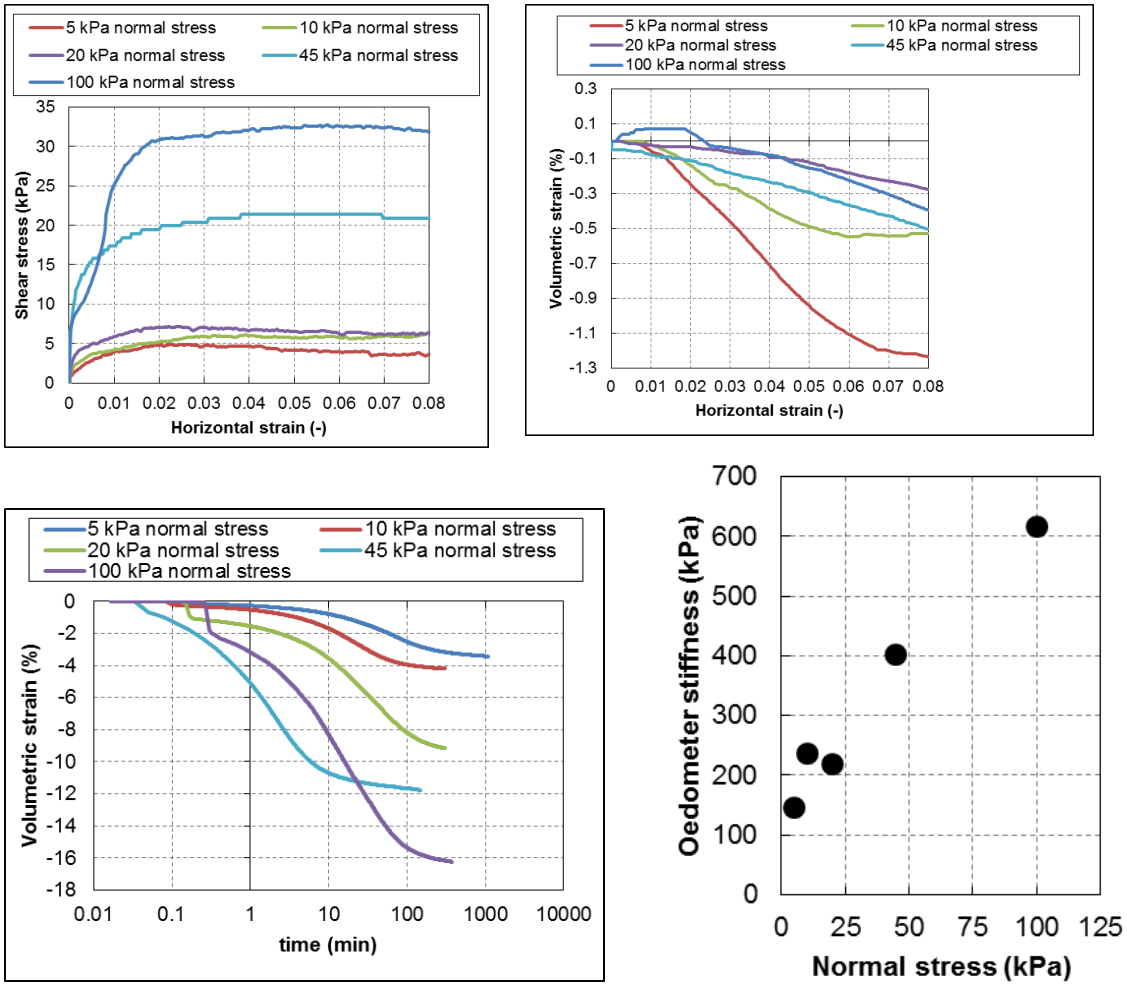

Figure 47: Results from the consolidated undrained direct sheartes of core 1 grey.

Table 20 shows all the mandatory reporting for the consolidated undrained direct shear test of core 1 grey original.

Table 20: Results from the consolidated undrained direct sheartes of core 1 grey.

Sample name	Ψ(°)	θ_{before} (-)	θ_{after} (-)	γ_{bulk}(kN/m^3)	γ_{dry} (kN/m^3)	ρ_{grain}(kg/m^3)	s_u(kPa)	determined at ε(%)	E_{oed} (kPa)
Core 1 grey 5 kPa*	-7.6	0.60	NA	16.4	10.3	2741	5.3	2.2	146
Core 1 grey 10 kPa	-3.8	0.59	0.49	17.1	11.5	2741	5.8	2.9	237
Core 1 grey 20 kPa	-0.9	0.77	0.54	16.4	10.6	2741	7.1	2.1	218
Core 1 grey 45 kPa	-1.1	0.58	0.48	15.9	10.7	2741	21.4	4.2	402
Core 1 grey 100 kPa	-2.5	0.56	0.47	16.3	11.1	2741	31.0	2.1	616
* volumetric weight determined based on water content before consolidation									

4.5.8 Comparing all undrained shear strengths from original and remoulded fall cone and direct shear tests from site 1736

Figure 48 shows a comparison of undrained shear strengths obtained from the unconsolidated undrained direct shear tests and the fall cone tests done on the original and remoulded soil. The direct shear test results show values for undrained shear strength around 3 kPa to 4.5 kPa for the original soil and 0.5 kPa to 2.5 kPa for the remoulded soil. The fall cone test shows values of 6 kPa to 14 kPa for the original soil and 0.5 kPa to 2kPa for the remoulded soil. The pocket vane test shows values of 7 kPa to 14 kPa for the original soil. The undrained shear strength here is classified as extremely low to very low.

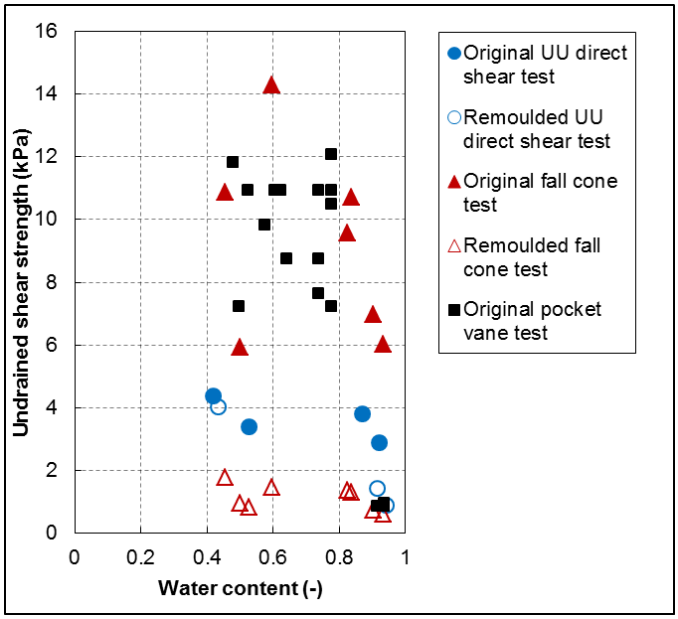

Figure 48: Comparing the undrained shear strenght results from the unconsolidated undrained shear test, fall cone tests and the pocket van tests.

4.5.9 Comparing all sensitivity result from the original and remoulded fall cone and direct shear tests from site 1736

Figure 49 shows the sensitivity values obtained from the direct shear tests and the fall cone tests done on the soil from site 1736. This shows that sensitivities obtained from fall cone testing are much higher than the sensitivities obtained from direct shear testing. Also a trend of increasing sensitivity with increased water content is detected. This is logical. The direct shear test has sensitivity values between 1 and 4 whereas the fall cone test has sensitivity values between 6 and 10. The sensitivity here is classified as low to medium.

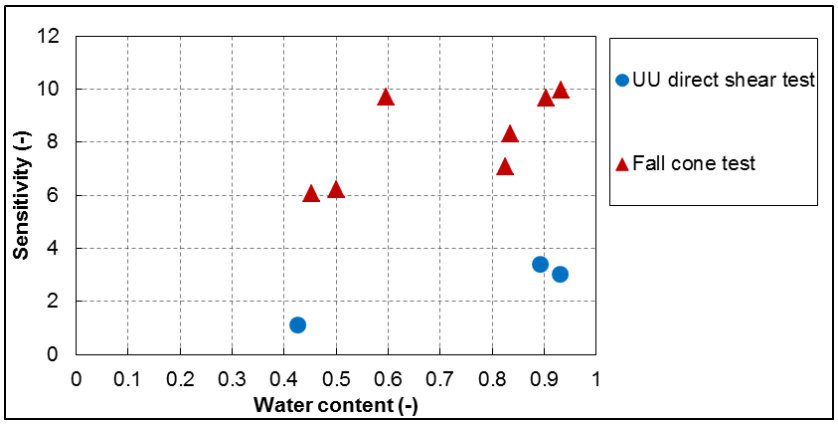

Figure 49: Comparing the sensitivity values from the unconsolidated undrained direct shear tests and the fall cone tests.

4.6 All test results from site 1672

Here all the test result from site 1672 will be presented.

4.6.1 Opening of core 4 and 5 at from site 1672

The opened cores 4 and 5 are displayed in Figure 28 where core 4 is closest to the seabed. Core 4 increase with depth from right to left and has a light grey colour with some black oxidation at the bottom of the core (left side). It also has some orange iron oxide spots. Core 5 which increases with depth from right to left has a beige brown colour followed a more clayey sediment which has a mainly white colour mixed with some beige colours. This is followed by sands of a dark grey, grey-greenish and dark grey colour. From visual it becomes clear that core 4 has less sand and core 5 is much more sandy. The most interesting sediment would here be the very light clay present at a depth of 127 cm since this is found by visual analysis to be much more clayey than the surrounding sandy parts.

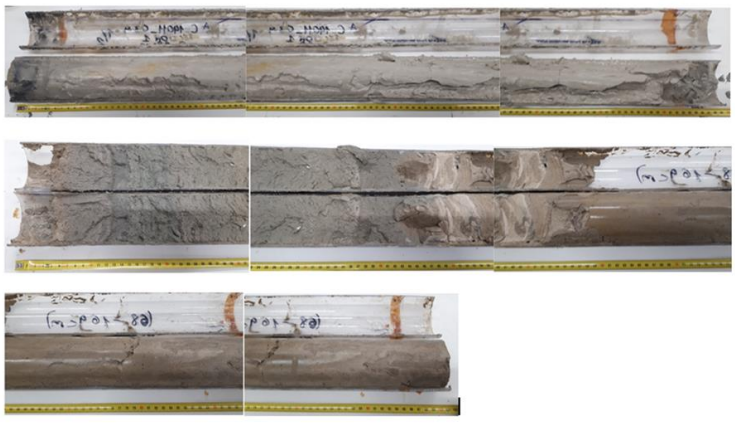

Figure 50: Core 4 above the two parts of core 5.

Tables 21 to 23 give an overview of the amount of cores opened for one site and the total and full core recovery. The total core recovery includes also the broken/disturbed parts of the core whereas the full core recovery includes only parts of the core where the whole diameter is intact.

Table 21: Core 4 core recovery information.

Core 4	
Mass of closed core (kg)	3.493
Mass of empty core (kg)	0.647
Lenght of cylinder section (cm)	70
Total core recovery (cm)	64
Full core recovery (cm)	35

Table 22: Core 5 core recovery information.

Core 5	
Mass of closed core (kg)	6.242
Mass of empty core (kg)	0.920
Lenght of cylinder section (cm)	101
Total core recovery (cm)	94
Full core recovery (cm)	94

Table 23: Site 1672 core recovery information.

Site 1672	
Penetration depth (cm)	NA
Total core recovery (cm)	158
Full core recovery (cm)	129
Recovery ratio (-)	NA
Pull out force (kg)	1700

Figure 51 shows a decreasing gravimetric water content with depth from 1 to 0.5. The volumetric water content decreases from 0.7 to 0.6 where it remains stable. The bulk volumetric weight increase from 14 kN/m^3 to 17 kN/m^3 with depth and the dry volumetric weight follows the same trend. The saturation remains stable around 1 along the entire depth. The void ratio decreases from 1.5 to 1.5 with depth and the liquidity index decreases from 2 to 1.2 with some cases showing a liquidity index lower than 1. This is the case in the sediments with a higher sand content. The undrained shear strength values from the pocket vane test show a general increasing trend with depth from 6 kPa to 20 kPa.

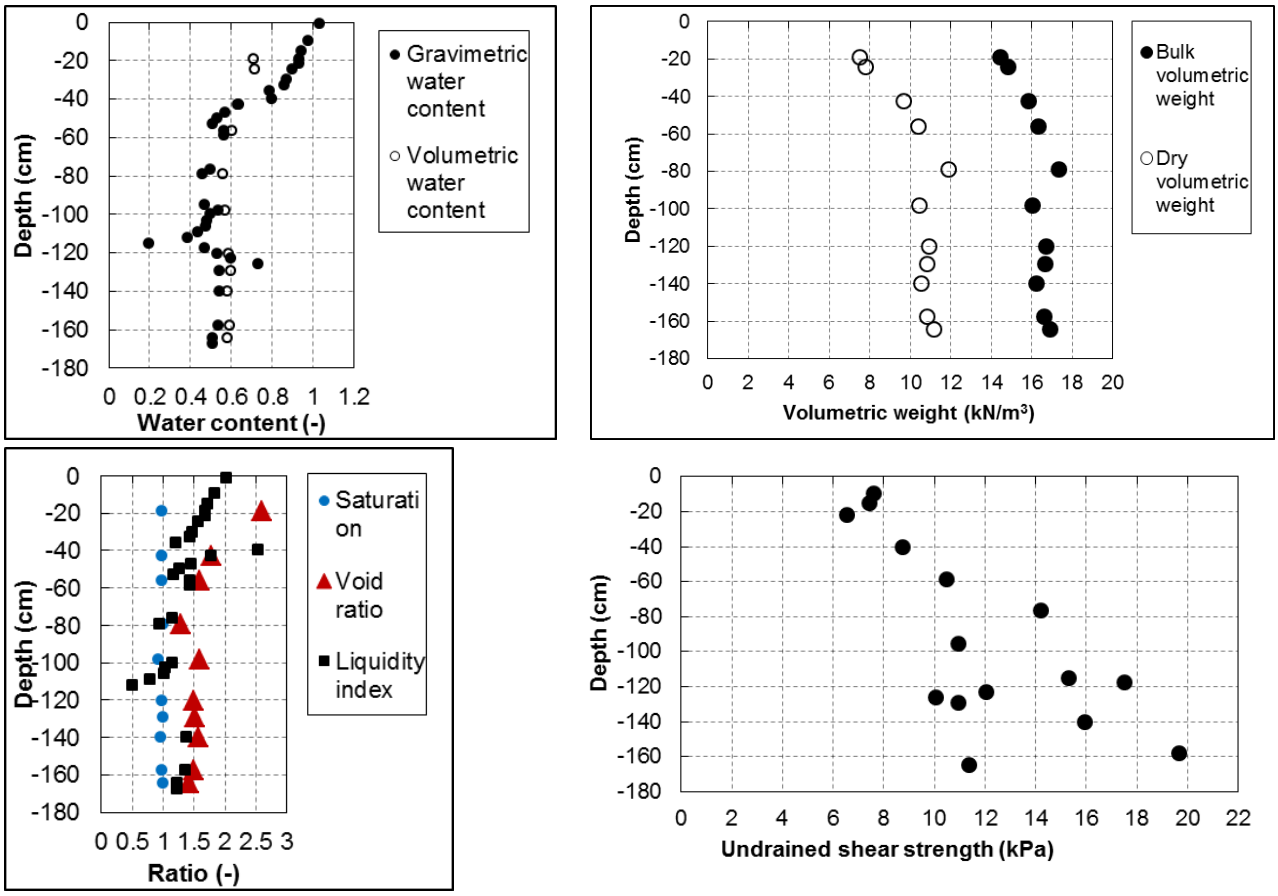

Figure 51: From left to right and top to bottom the water content, volumetric weight, saturation and void ratio and the undrained shear strength from the pocket vane with depth at site 1672.

4.6.2 Grain size distribution at site 1672

Figure 52 shows the grain size distribution of site 1672 which shows a decrease in clay content with depth and an increase in sand content with depth and a silt content which fluctuates between 30% and 40%. A fining-upward sequence is found.

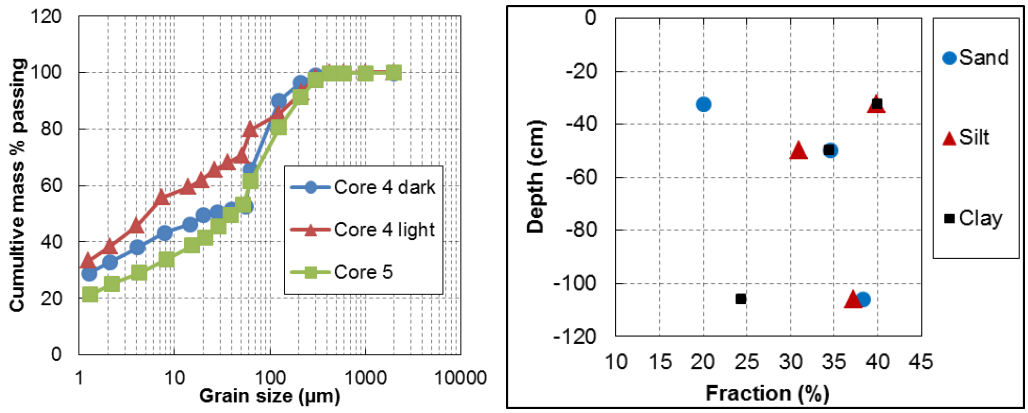

Figure 52: Grain size distribution on the left and the soil fractions with depth on the right at site 1672.

4.6.3 Atterberg limits and derived remoulded undrained shear strength at site 1672

Figure 53 shows a decrease in liquid limit from 0.73 to 0.47 where it remains stable with depth. The plastic limit shows the same pattern from 0.43 to 0.27. The liquid limit is in 3 cases below the natural water content. This indicates a risk of liquefaction upon disturbance. In 1 case the natural water content is at or below the liquid limit. Here the soil has less risk of failure upon disturbance. The organic matter content shows a decreasing trend with depth from 6.5% to 4.3% and the calcite content shows a general decreasing trend with depth from 55% to 23%.

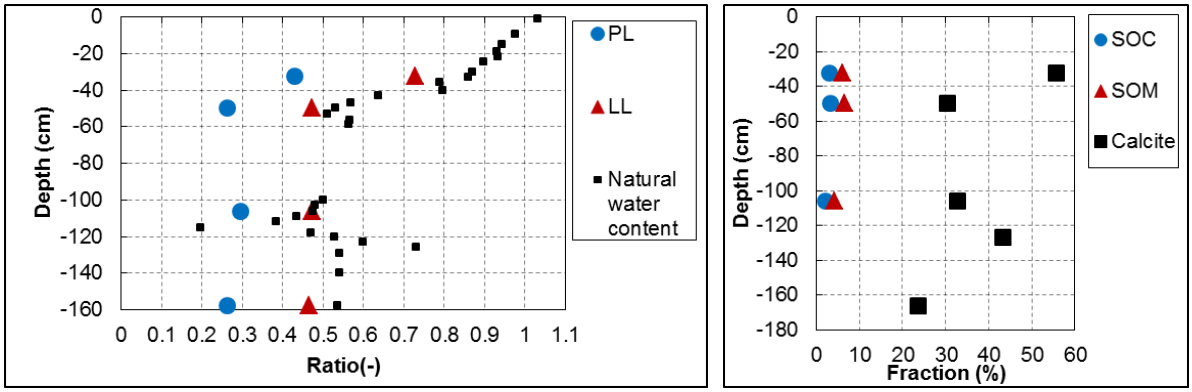

Figure 53: Atterberg limits, SOC contents, SOM content and calcite contents at site 1672.

Table 24 shows the classification of the soil from site 1672. These sediments can be classified as clayey SILT to silty CLAY. Their plasticity is medium to very high. The organic matter content is low to medium and the calcite content is normal to very rich. The soil is inactive.

Table 24: Classification of the sediments at site 1672.

Sample name	Soil type	Plasticity classification	SOM classification	Calcite classification	Activity classification
Core 4 dark (5-15.5)	silty CLAY	medium	medium-organic	highly calcareous	inactive soil
Core 4 light (21-32)	silty CLAY	very high	medium-organic	very highly calcareous	inactive soil
Core 5 beige clay 2 (12-22)	NA	NA	NA	calcareous	NA
Core 5 (22-37)	NA	medium	NA	NA	NA
Core 5 (37-47.5)	NA	NA	NA	NA	NA
Core 5 very light (44-56)	NA	NA	NA	highly calcareous	NA
Core 5 beige (63.5-75)	clayey SILT	medium	low-organic	highly calcareous	inactive soil

4.6.4 Unconsolidated undrained direct shear tests at site 1672

Figure 54 shows the results from the unconsolidated undrained direct shear tests at site 1672. This shows that all the original samples and core 5 beige (88-94.5) remoulded show dilation behaviour during shearing. All the other remoulded samples show contraction during shearing. The reason that core 5 beige (88-94.5) remoulded still shows dilatory behaviour during shearing even though it has been remoulded is because of the high sand content. Undrained shear strengths from 1.6 kPa to 5.8 kPa are found.

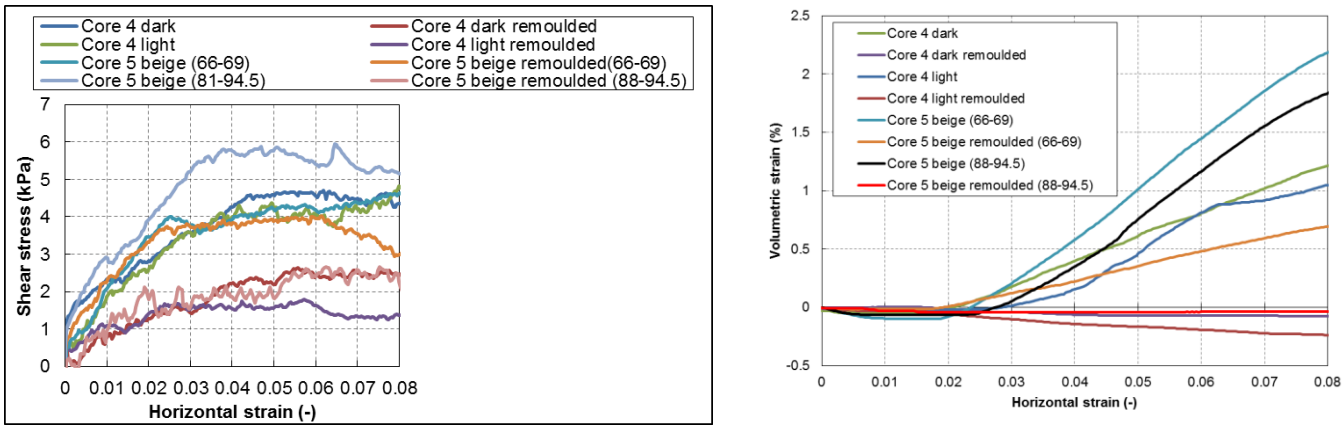

Figure 54: Results from the unconsolidated undrained direct shear tests at site 1672.

Table 25 shows the mandatory reporting value from the unconsolidated undrained tests of site 1672.

Table 25: Results from the unconsolidated undrained direct shear tests at site 1672.

sample name	Ψ(°)	θ_{before} (-)	γ_{bulk}(kN/m^3)	γ_{dry} (kN/m^3)	ρ_{grain}(kg/m^3)	s_u(kPa)	determined at ε_h(%)
Core 4 dark	5.4	0.57	16.1	10.3	2743	4.6	4.4
Core 4 dark remoulded	-0.2	0.54	16.6	10.8	2743	2.2	3.9
Core 4 light	8.1	0.79	15.1	8.4	2753	4.1	3.7
Core 4 light remoulded	-0.9	0.82	15.0	8.3	2753	1.6	2.4
Core 5 (66-69)	10.1	0.50	16.8	11.2	2757	4.0	2.5
Core 5 (66-69) remoulded	3.3	0.47	16.8	11.5	2757	3.7	2.4
Core 5 (81-94.5)	9.7	0.48	16.6	11.2	2757	5.8	3.8
Core 5 (81-94.5) remoulded	0.0	0.50	16.8	11.2	2757	2.1	1.9

4.6.5 Consolidated undrained direct shear test of core 5 (22-37) remoulded at site 1672

Figure 55 shows the consolidated undrained direct shear test of core 5 (22-37) remoulded. In all cases contraction behaviour during shearing is present. The undrained shear strengths range from 8.3 kPa to 19.0 kPa over the normal stress from 15 kPa to 45 kPa. The mandatory reporting information can be found in Table 19.

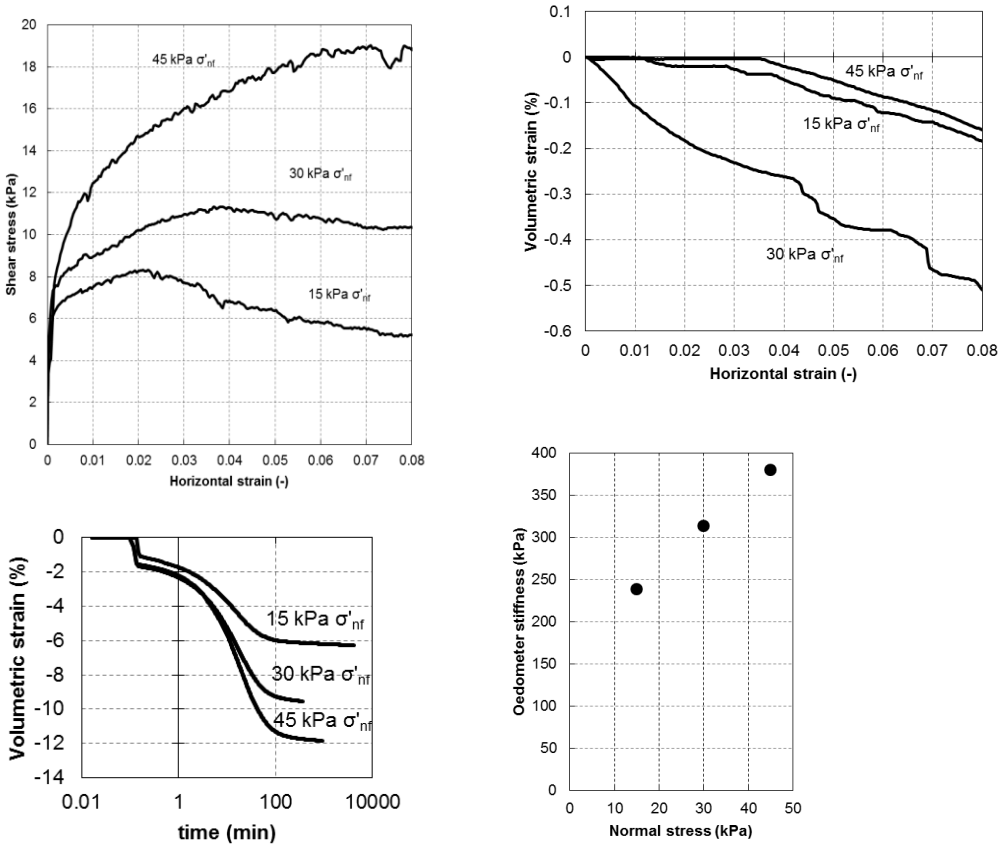

Figure 55: Results from the consolidated undrained direct shear test of core 5 (22-37) remoulded.

Table 26 shows the mandatory reporting values from the remoulded consolidated undrained tests of core 5 (22-37).

Table 26: mandatory reporting results for the consolidated undrained direct shear test of core 5 (22-37) remoulded.

Core name	Ψ(°)	θ_{before} (-)	θ_{after} (-)	γ_{bulk}(kN/m^3)	γ_{dry} (kN/m^3)	ρ_{grain}(kg/m^3)	s_u(kPa)	determined at ε(%)	E_{oed} (kPa)
Core 5 (22-37) remoulded 15 kPa	-1.0	0.49	0.48	16.9	11.4	2757	8.3	1.9	240
Core 5 (22-37) remoulded 30 kPa	-1.7	0.52	0.44	16.7	11.6	2757	11.2	3.7	316
Core 5 (22-37) remoulded 45 kPa	-1.0	0.40	0.37	17.8	13.0	2757	19.0	6.9	382

4.6.6 Consolidated undrained direct sheartest of core 5 (37-47.5) of site 1672

Figure 56 shows the results of the remoulded consolidated undrained direct shear test of core 5 (37-47.5). In all cases the soil shows contraction behaviour and undrained shear strength values ranging from 8.2 kPa to 15.0 kPa over normal stresses of 16 kPa to 15 kPa.

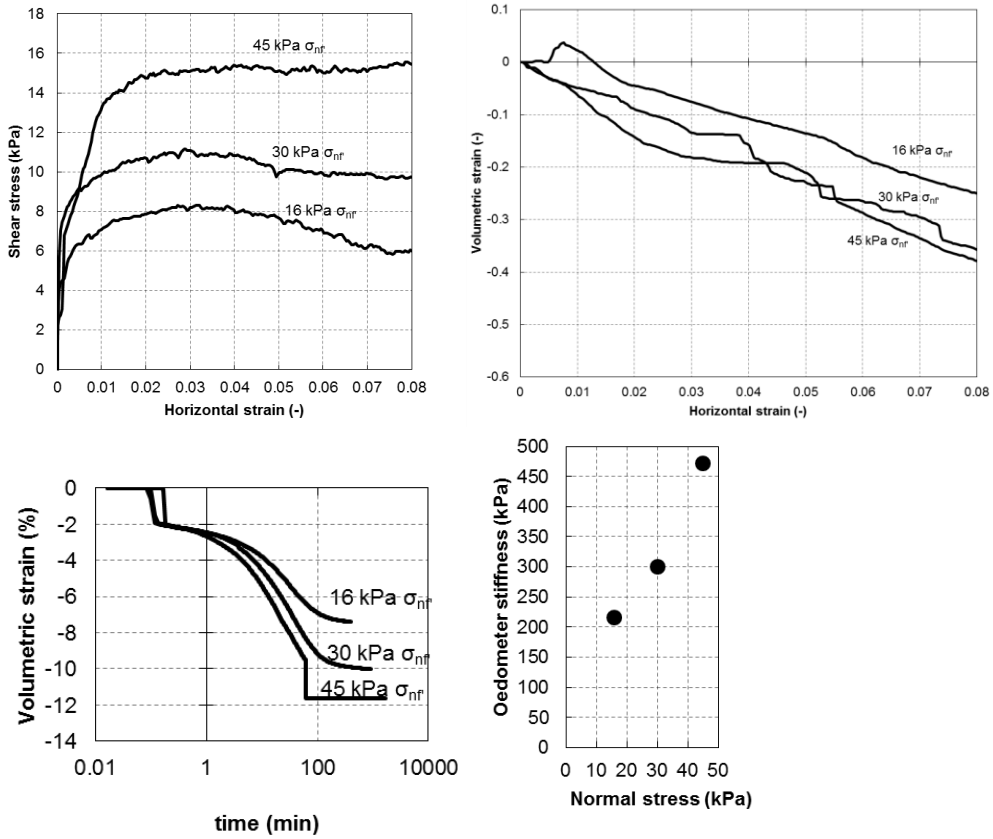

Figure 56: Results from the consolidated undrained direct shear test of core 5 (37-47.5) remoulded.

Table 27 shows all the mandatory reporting from the consolidated undrained direct shear test of core 5 (37.47.5).

Table 27: Mandatory reporting results for the consolidated undrained direct shear test of core 5 (37-47.5) remoulded.

Core name	Ψ(°)	θ_{before} (-)	θ_{after} (-)	γ_{bulk}(kN/m^3)	γ_{dry} (kN/m^3)	ρ_{grain}(kg/m^3)	s_u(kPa)	determined at ε_h(%)	E_{oed} (kPa)
Core 5 (37-47.5) remoulded 16 kPa	-1.3	0.49	0.44	17.0	11.8	2739	8.2	2.6	217
Core 5 (37-47.5) remoulded 30 kPa	-1.0	0.48	0.43	17.0	11.9	2739	11.0	2.6	301
Core 5 (37-47.5) remoulded 45 kPa	-0.9	0.49	0.41	17.0	12.1	2765	15.0	2.3	474

4.6.7 Comparing all undrained shear strengths from original and remoulded fall cone and direct shear tests from site 1672

Figure 57 shows an increase in the undrained shear strength for the direct shear test with decreasing water content. This trend can also be observed for the fall cone tests. Even the pocket vane test shows the same trend. This trend is mainly caused by the increasing sand content with depth. The more sandy parts of the core automatically have a lower void ratio which causes a lower water content. The original direct shear tests shows values between 3.5 kPa to 5 kPa whereas the remoulded direct shear test shows values from 1 kPa to 3kPa. Both original fall cone tests show values from 6kPa to 12 kPa and the remoulded fall cone tests show values from 0.5 kPa to 4 kPa. The original pocket vane test shows values from 6 kPa to 20 kPa. The undrained shear strength here is classified as extremely low to very low.

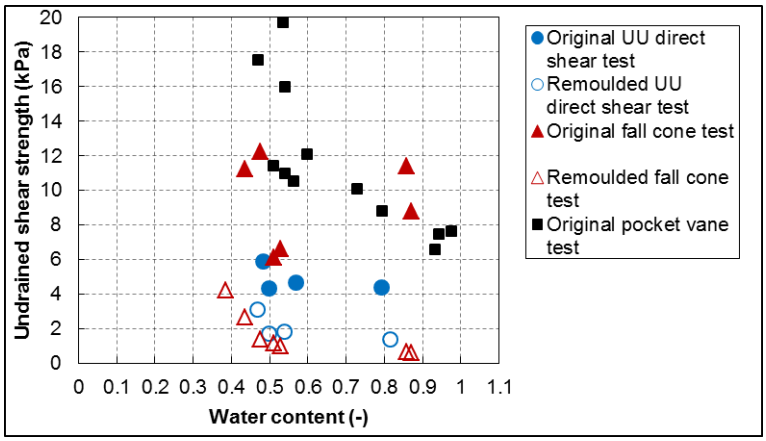

Figure 57: Comparing the undrained shear strenght values from the direct shear test, fall cone test and pocket vane test at site 1672.

4.6.8 Comparing all sensitivity result from the original and remoulded fall cone and direct shear tests from site 1672

Figure 58 shows that the sensitivity values from the direct shear test are between 1 and 3 whereas the sensitivity values for the fall cone tests are between 4 and 18. The sensitivity here is classified as low to average.

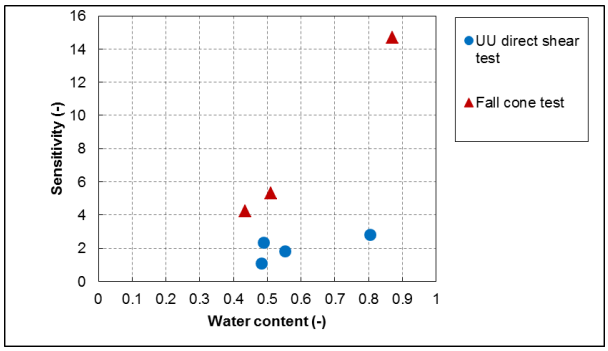

Figure 58: Comparing the sensitivity values from the direct shear test and the two fall cone tests at site 1672.

4.7 All test data from site 688

Here all the test result from site 688 will be presented.

4.7.1 Opening of core 6 at site 688

Figure 59 shows core 6 opened and increasing with depth from right to left. The colour of the core goes from a lighter grey to a darker grey with depth. Some orange iron oxide spots are present.

Figure 59: Core 6 opened.

Tables 28 to 29 give an overview of the amount of cores opened for one site and the total and full core recovery. The total core recovery includes also the broken/disturbed parts of the core whereas the full core recovery includes only parts of the core where the whole diameter is intact.

Table 28: Core 6 core recovery information.

Core 6	
Mass of closed core (kg)	5.066
Mass of empty core (kg)	0.714
Lenght of cylinder (cm)	80
Total core recovery (cm)	80
Full core recovery (cm)	66

Table 29: Site 688 core recovery information

Site 688	
Penetration depth (cm)	NA
Total core recovery (cm)	80
Full core recovery (cm)	66
Recovery ratio (-)	NA
Pull out force (kg)	1000

Figure 60 shows the gravimetric water fluctuating between 0.35 and 0.45. No clear trend is detected, because the top sediments were not fully saturated. This has to do with the storage and the fact that this core is very sandy compared to the more clayey sediments from other cores which have retained their moisture content along the entire length. The volumetric water content shows a increasing trend from 0.52 to 0.55. The bulk volumetric weight increases from 16 kN/m^3 to 18 kN/m^3. The saturation increases from 0.9 to 1 with depth indicating that the top part of the sediments have partially dried out. The void ratio decreases with depth from 1.5 to 1.2 and the liquidity index increases with depth to 0.7 after which a small decrease to 0.43 is noted. The undrained shear strength obtained from the pocket vane test is found to fluctuate between 8 kPa and 22 kPa.

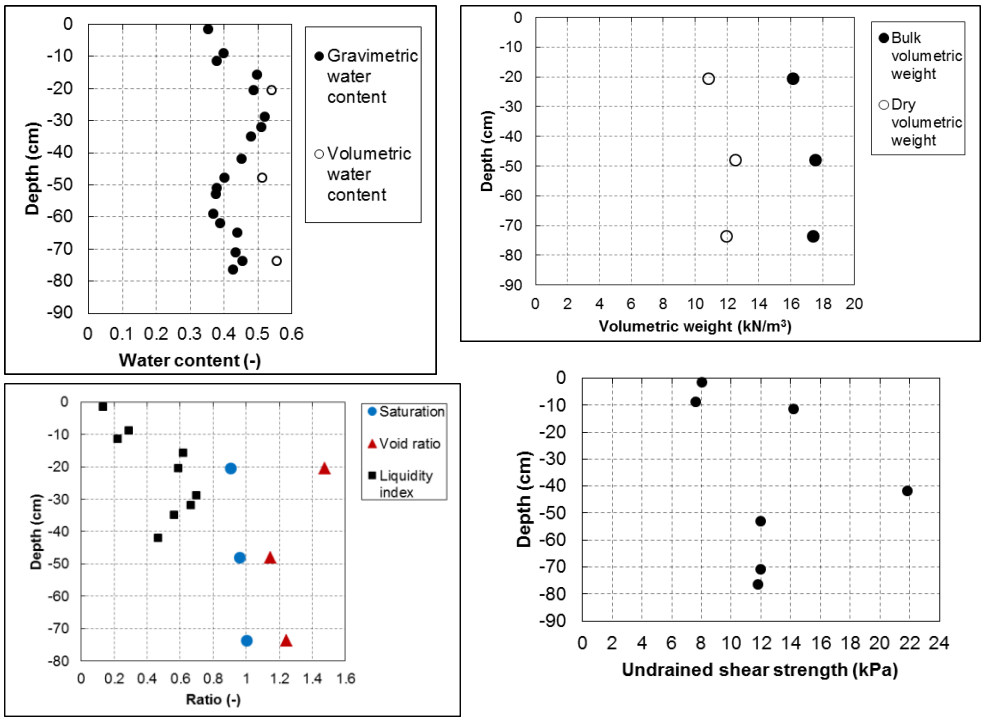

Figure 60: From left to right and top to bottom the water content, volumetric weight, saturation and void ratio and the undrained shear strength from the pocket vane with depth at site 688.

4.7.2 Grain size distribution at site 688

Figure 61 shows the grain size distribution and the soil fractions. The clay content and the silt content both decrease with depth. The sand content increases with depth. A fining-upward sequence is found.

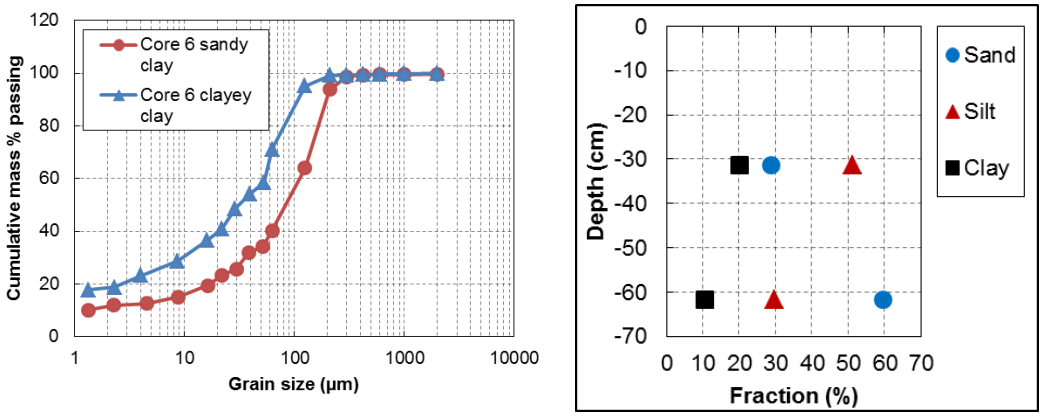

Figure 61: Grain size distribution on the left anf the soil fractions with depth on the right at site 688.

4.7.3 Atterberg limits and derived remoulded undrained shear strength of site 688

Figure 62 shows has only one plastic limit at 0.32 and one liquid limit at 0.61 where the clay content was just high enough to determine both the Atterberg limits. For the more sandy sediment deposit only the liquid limit could be determined. The natural water content is below the liquid limit at 30 cm depth and at the liquid limit at 60 cm depth. Since this is also is very sandy deposit no risk of liquefaction is found here. The calcite content shows only a small

decrease from 33.1% to 32.5% and the organic matter content shows a decrease from 3.4% to 2.6%.

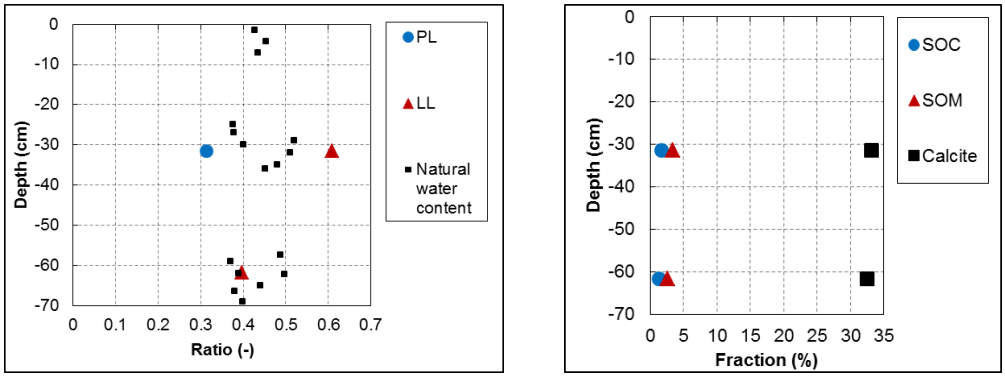

Figure 62: Atterberg limits on the left and SOC content, SOM content and calcie content with depth on the right at site 688.

4.7.4 Organic and inorganic content of site 688

Table 30 shows that the soil at this site can be classified as a silty SAND and a clayey SILT. The organic matter content is low and the sediments are highly calcareous. No plastic limit could be determined due to the high amount of sand present. No activity could be determined since no plastic limit could be determined.

Table 30: Classification of the sediments at site 688.

Sample name	Soil type	Plasticity classification	SOM classification	Calcite classification	Activity classification
Core 6 sandy clay (8.5-24)	silty SAND	NA	low-organic	highly calcareous	NA
Core 6 clayey clay (38-55.5)	clayey SILT	NA	low-organic	highly calcareous	NA

4.7.5 Unconsolidated undrained direct shear tests of site 688

Figure 63 shows the results from the unconsolidated undrained direct shear test. Core 6 clayey clay shows only dilation. The other samples first contract and then dilate. Core 6 clayey clay shows softening behaviour starting around 5% strain. This is due to the large amount of dilation taking place. This softening behaviour stops at 6% strain where the undrained shear strength is at 6%. The soil is still dilating from this point onward. Undrained shear strengths between 4 kPa and 6 kPa are found. The mandatory reporting information can be found in Table.

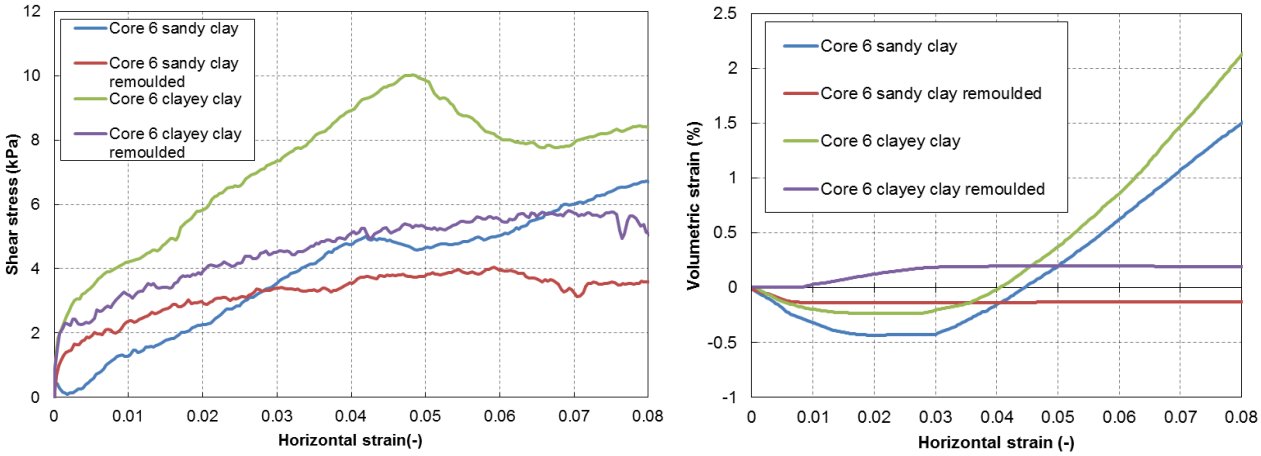

Figure 63: Results from the unconsolidated undrained direct shear test at site 688.

Table 31 shows the mandatory reporting values from the unconsolidated undrained direct shear tests of site 688.

Table 31: All results from the unconsolidated undrained direct shear test from site 688.

Sample name	Ψ(°)	θ_{before} (-)	γ_{bulk}(kN/m^3)	γ_{dry} (kN/m^3)	ρ_{grain}(kg/m^3)	s_u(kPa)	determined at ε_h(%)
Core 6 sandy clay	8.5	0.44	17.3	12.0	2739	5.1	4.1
Core 6 sandy clay remoulded	0.0	0.42	17.5	12.4	2739	3.7	4.1
Core 6 clayey clay	12.8	0.52	16.6	10.9	2739	10.0	4.7
Core 6 clayey clay remoulded	2.3	0.50	16.5	11.0	2739	5.7	6.2

4.7.6 Comparing all undrained shear strengths from original and remoulded fall cone and direct shear tests of site 688

Figure 64 shows a decreasing trend from 8kPa to 4 kPa for the original direct shear test together with the remoulded direct shear test which shows a decreasing trend from 4.5 kPa to 3kPa. Both fall cone tests show values between 2 kPa and 5 kPa with no real trend. The pocket vane test shows a general decreasing trend with decreasing water content from 22 kPa to 7 kPa. These high values are due to the high sand content of the core. The undrained shear strength here is classified as extremely low to very low.

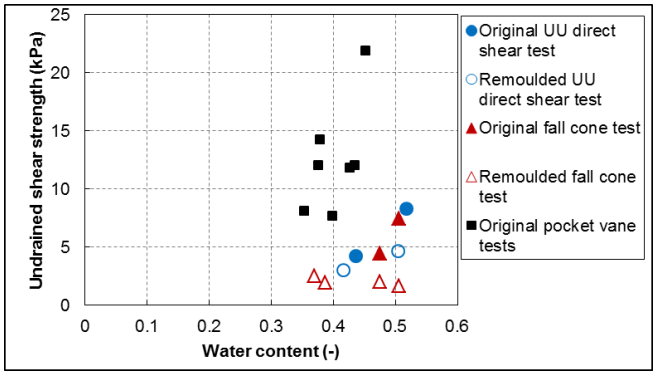

Figure 64: Comparing the undrained shear strenght values from the direct shear test, fall cone test and pocket vane test at site 688.

4.7.7 Comparing all sensitivity result from the original and remoulded fall cone and direct shear tests of site 688

Figure 65 shows sensitivity values between 1 and 2 for the direct shear test and values between 2 and 4.5 for both fall cone tests. Both trends shows an increase in sensitivity with increasing water content. The sensitivity here is classified as low.

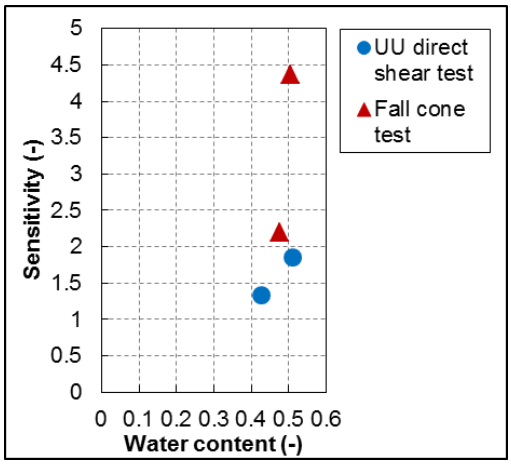

Figure 65: Comparing the sensitivity values from the direct shear test and the two fall cone tests at site 688.

4.8 All test data from site 1988

Here all the test result from site 1988 will be presented.

3.8.1 opening of core 7 at site 1988

Figure 66 shows core 7 opened and increasing with depth from right to left. The colour changes from a light beige colour to a darker beige colour with depth.

Figure 66: Core 7 opened.

Tables 32 and 33 give an overview of the amount of cores opened for one site and the total and full core recovery. The total core recovery includes also the broken/disturbed parts of the core whereas the full core recovery includes only parts of the core where the whole diameter is intact.

Table 32: Core 7 core recovery information.

Core 7	
Mass of closed core (kg)	4.045
Mass of empty core (kg)	0.690
Lenght of cylinder (cm)	95
Total core recovery (cm)	80
Full core recovery (cm)	44

Table 33: Site 1988 core recovery inforamtion

Site 1988	
Penetration depth (cm)	NA
Total core recovery (cm)	80
Full core recovery (cm)	44
Recovery ratio (-)	NA
Pull out force (kg)	2400

Figure 67 shows the gravimetric water content decreasing with depth from 1.18 to 0.7 with depth. The volumetric water content also decrease from 0.75 to 0.67 with depth. The bulk volumetric weight increases with depth from 14 kN/m^3 to 16 kN/m^3 with depth. The saturation remains stable around 1. The void ratio decreases from 2.8 to 2. The liquidity index in the first 15 cm is just above 1, but much lower than the liquidity index of the rest of the core due. From here the liquidity index a very high value of 3 to around 1 at the bottom. The undrained shear strength obtained from the pocket vane tests fluctuates between 8 kPa and 11 kPa.

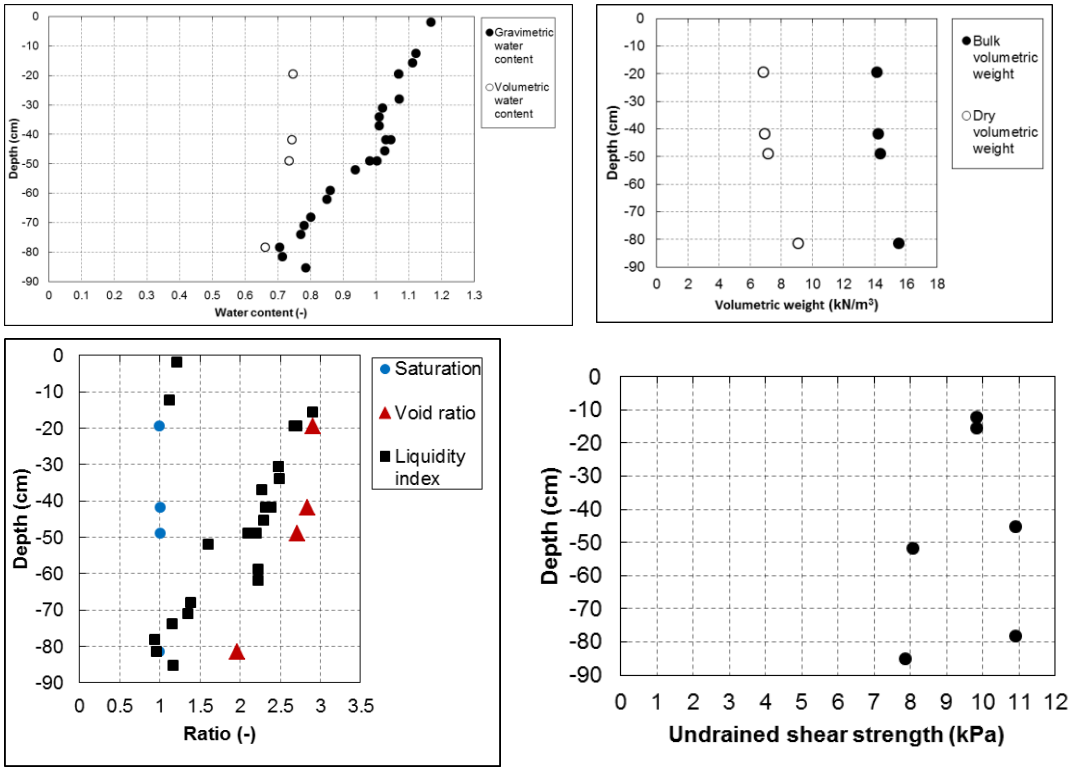

Figure 67: From left to right and top to bottom the water content, volumetric weight, saturation and void ratio and the undrained shear strength from the pocket vane with depth at site 1988.

4.8.2 Grain size distribution at site 1988

Figure 68 shows the grain size distribution and the soil fractions with depth. The clay content decreases with depth. The silt content increases with depth and the sand content remains stable. A fining-upward sequence is found based on the clay content.

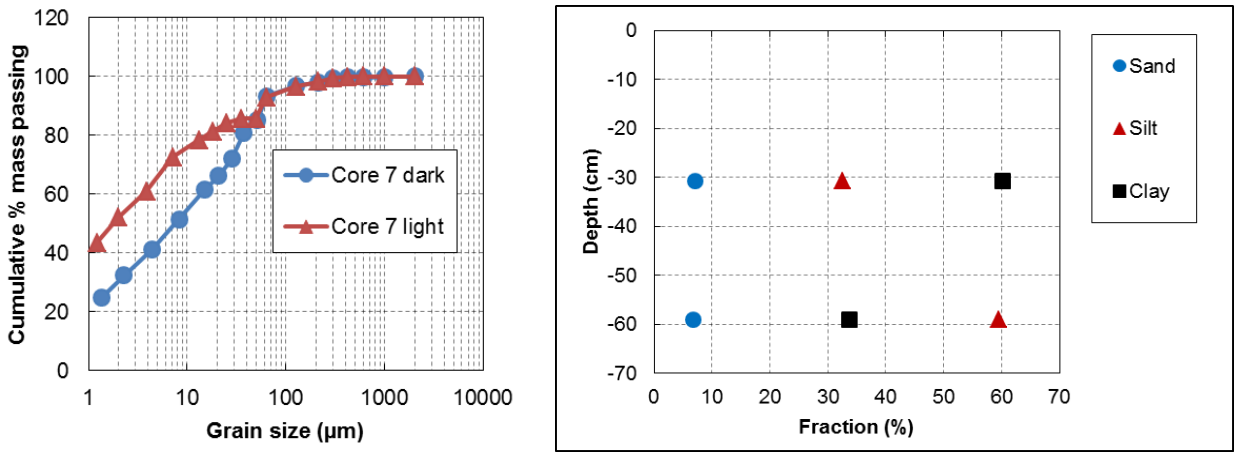

Figure 68: Grain size distribution on the left anf the soil fractions with depth on the right at site 1988.

4.9.3 Atterberg limits and derived remoulded undrained shear strength at site 1988

Figure 69 shows a liquid limit remaining stable around 0.72 whereas the plastic limit decrease from 0.48 to 0.38. In all cases the natural water content is much higher than the liquid limit indicating a danger of liquefaction upon disturbance. The calcite content decreases from 40% to 24%. The organic matter content decreases from 9.0% to 8.4%.

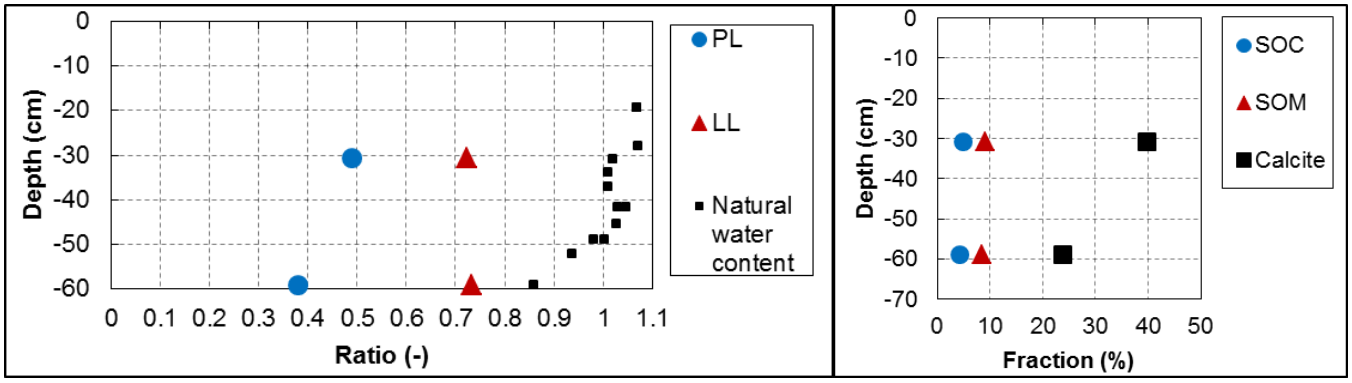

Figure 69: Atterberg limits on the left and SOC content, SOM content and calcie content with depth on the right at site 688.

4.9.4 Organic and inorganic content determined from LOI at 550° and 950° Celsius at site 1988

Table 34 shows the classification for site 1988. The sediments can be classified as silty CLAY or as clayey SILT. The soil has a very high plasticity, is medium-organic and is found to be calcareous to highly calcareous. The soil is found to be inactive to normal.

Table 34: Classification of the sediments at site 1988.

Sample name	Soil type	Plasticity classification	SOM classification	Calcite classification	Activity classification
Core 7 dark (10.5-22.5)	clayey SILT	very high	medium-organic	calcareous	NA
Core 7 dark(22.5-34)	clayey SILT	very high	medium-organic	calcareous	normal
Core 7 light	silty CLAY	very high	medium-organic	highly calcareous	inactive

4.9.5 Unconsolidated undrained direct shear tests at site 1988

Figure 70 shows the unconsolidated undrained direct shear tests of site 1988. All the original soil samples clearly show dilation behaviour while the remoulded samples all show contraction behaviour. The undrained shear strenghts obtained range from about 1.5 kPa to 6 kPa. Further detailed information can be found in Table.

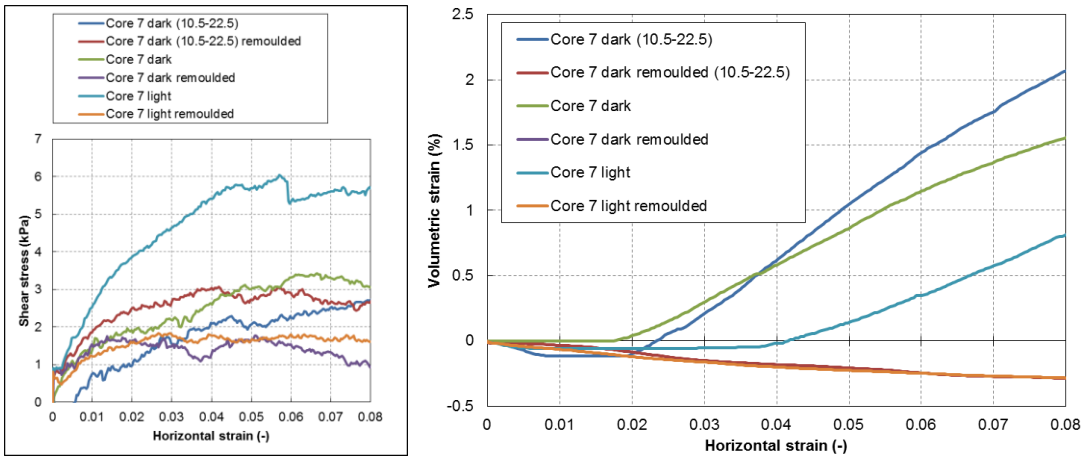

Figure 70: Results from the unconsolidated undrained direct shear tests at site 1988.

Table 35 contains all the mandatory reporting values of the unconsolidated undrained direct shear tests at site 1988.

Table 35: All results from the unconsolidated undrained direct shear tests at site 1988.

Sample name	Ψ(°)	θ_{before} (-)	γ_{bulk}(kN/m^3)	γ_{dry} (kN/m^3)	ρ_{grain}(kg/m^3)	s_u(kPa)	determined at ε_h(%)
Core 7 dark (10.5-22.5)	9.9	0.77	15.4	8.7	2739	2.3	4.4
Core 7 dark (10.5-22.5) remoulded	-0.9	0.76	15.3	8.7	2739	3.0	3.7
Core 7 dark (22.5-34)	7.1	0.86	15.0	8.0	2739	3.1	4.8
Core 7 dark (22.5-34) remoulded	-0.9	0.85	13.3	7.2	2739	1.8	1.4
Core 7 light	5.0	1.01	12.8	6.4	2719	5.8	4.6
Core 7 light remoulded	-0.9	0.95	12.6	6.5	2719	1.8	2.6

4.9.6 Consolidated undrained diect shear test of core 7 light at site 1988

Figure 71 shows the consolidated undrained direct shear test. This shows that under 3 kPa to 6 kPa the soil shows dilation behaviour and at 9 kPa the soil shows contraction behaviour. This test makes it apparent that 3 kPa to 9 kPa normal stress results in similar undrained shear strengths and is not high enough to show a considerable increase. The shear stress starts climbing again after 4% to 5% strain. The oedometer stiffness decreases with increasing normal stress. This is because of the slight differences in water content between the different samples used from the the same 10 cm of soil. The stiffness of the soil here decreases with increasing water content (see Table 21). This is logical since a lower water content results in sample with a lower void ratio that has a higher stiffness.

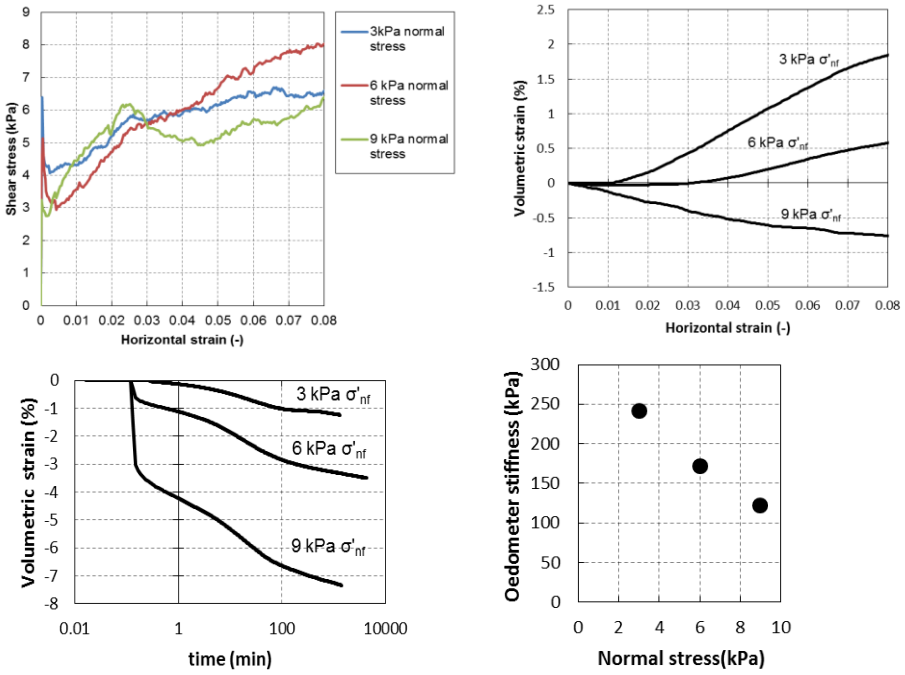

Figure 71: Results from the consolidated undrained direct shear test of core 7 light.

Table 36 contains all the mandatory reporting of the consolidated undrained direct shear test of core 7 light.

Table 36: All results from the consolidated undrained direct shear test at site 1988.

Sample name	Ψ(°)	θ_{before} (-)	θ_{after} (-)	γ_{bulk}(kN/m^3)	γ_{dry} (kN/m^3)	ρ_{grain}(kg/m^3)	s_u(kPa)	determined at ε_h(%)	E_{oed} (kPa)
Core 7 light 3 kPa	7.9	1.02	1.01	14.1	7.0	2719	6.1	2.6	241
Core 7 light 6 kPa	3.9	1.03	1.02	13.8	6.8	2719	5.8	3.4	171
Core 7 light 9 kPa	-1.7	1.07	1.07	11.7	5.7	2719	6.2	2.4	123

4.9.7 Comparing all undrained shear strengths from original and remoulded fall cone and direct shear tests of site 1988

Figure 72 shows values between 2.5 kPa and 5 kPa for the original direct shear test whereas the remoulded direct shear test shows values between 1.5 kPa and 2 kPa. Both the original fall cone tests show values between 6 kPa and 12 kPa whereas the remoulded fall cone test show values around 1 kPa. The pocket vane tests show values between 6 kPa and 11 kPa. The undrained shear strength here is classified as extremely low to very low.

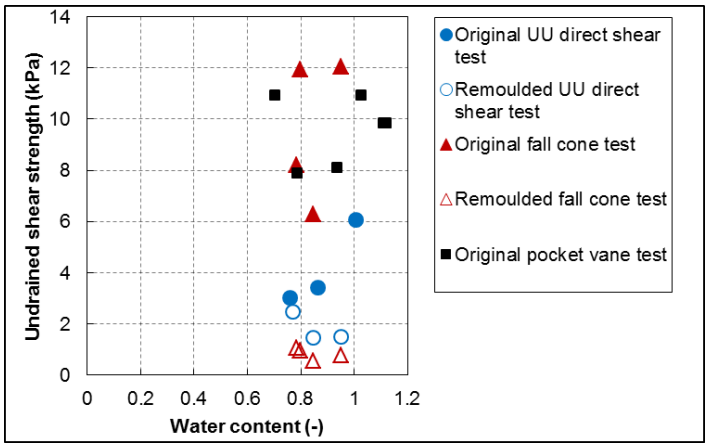

Figure 72: Comparing the undrained shear strenght values from the direct shear test, fall cone test and pocket vane test at site1988.

4.9.8 Comparing all sensitivity result from the original and remoulded fall cone and direct shear tests of site 1988

Figure 73 shows sensitivity values from the direct shear test increasing from 1 to 4 with increasing water content. Both fall cone tests show sensitivity values from 8 to 16 with increasing water content. The sensitivity values here are a lot higher than the sensitivity values from the direct shear test. One reason is that both tests have different failure mechanisms, also the fact that the soil at site 1988 has a higher clay content compared to the more sandy sites could explain why the fall cone sensitivity is so much higher here than at the more sandy sites. The sensitivity here is classified as low to medium.

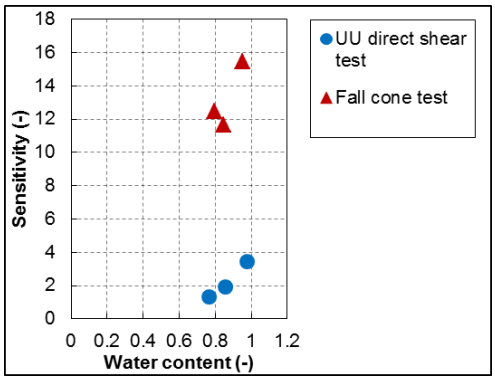

Figure 73: Comparing the sensitivity values from the direct shear test and the two fall cone tests at site 1988.

4.9 All test data from site 1695

Here all the test result from site 1695 will be presented.

4.9.1 Opening of core 8 at site 1695

Figure 74 shows core 8 opened. This core increases with depth left to right. The colour changes with depth from a very light grey to a dark grey with a very sudden border. Orange iron oxide spots are detected with an increasing area covered by these spots towards the deeper part of the very light grey part of the core.

Figure 74: Core 8 from site 1695 opened.

Tables 37 and 38 give an overview of the amount of cores opened for one site and the total and full core recovery. The total core recovery includes also the broken/disturbed parts of the core whereas the full core recovery includes only parts of the core where the whole diameter is intact.

Table 37: Core 8 core recovery information.

Core 8	
Mass of closed core (kg)	1.958
Mass of empty core (kg)	0.312
Lenght of cylinder (cm)	75
Total core recovery (cm)	67
Full core recovery (cm)	64

Table 38: Site 1695 core recovery information.

Site 1695	
Penetration depth (cm)	250
Total core recovery (cm)	67
Full core recovery (cm)	64
Recovery ratio (-)	NA
Pull out force (kg)	2400

Figure 75 shows a decreasing trend in gravimetric water content with depth from 1 to 0.5. The volumetric water content also decreases from 0.7 to 0.6. The bulk volumetric weight decreases from 14 kN/m^3 to 16.5 kN/m^3. The saturation remains stable around 1 with depth. The void ratio decreases from 3 to 1.5 with depth. A general increasing trend is found for the undrained shear strength obtained from the pocket vane test with depth from 6 kPa to 10 kPa at the deepest part of the core.

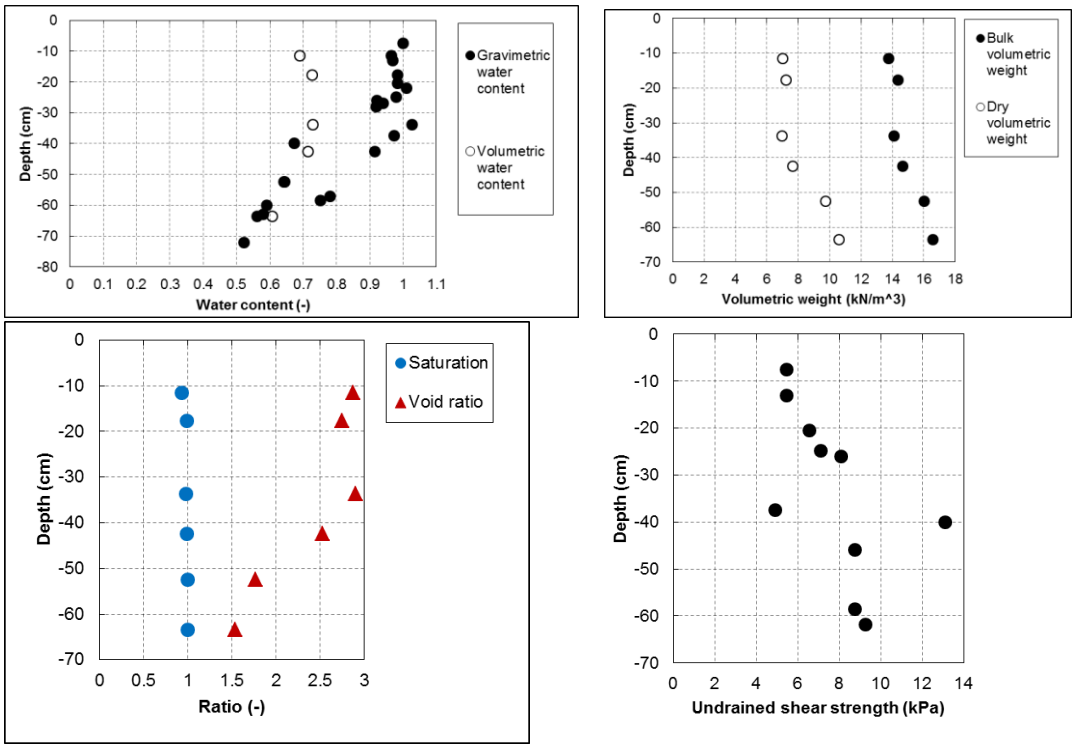

Figure 75: From left to right and top to bottom the water content, volumetric weight, saturation and void ratio and the undrained shear strength from the pocket vane with depth at site 1695.

4.9.2 Grain size distribution ate site 1695

Figure 76 shows the grain size distribution and the soil fractions with depth. This shows that the clay content decreases with depth, the silt content remains stable and the sand content increases with depth. A fining-upward sequence is found based on the clay content.

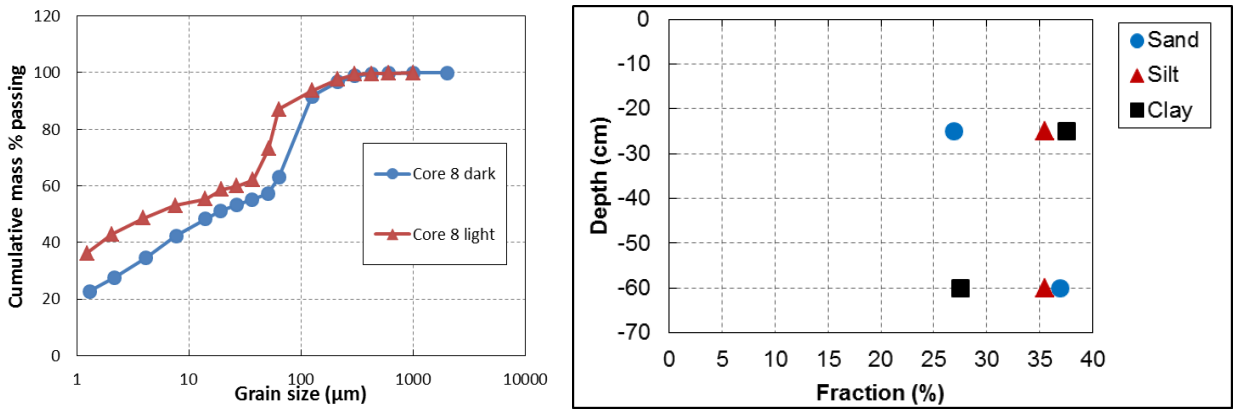

Figure 76: Grain size distribution on the left anf the soil fractions with depth on the right at site 1695.

Figure 77 shows the calcite content decreasing from 53% to 35%. The organic matter content is found to decrease from 5.9% to 5.5%.

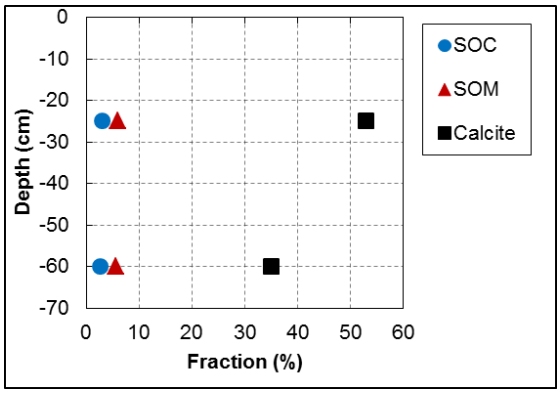

Figure 77: SOC, SOM and calcite content at site 1695.

Table 39 shows the classification of site 1695. The sediments can be classified as clayey SILT and silty CLAY. They are low-organic and are highly to very highly calcareous.

Table 39: Classification of the sediments at site 1695.

Sample name	Soil type	SOM classification	Calcite classification
Core 8 dark	clayey SILT	low-organic	highly calcareous
Core 8 light	silty CLAY	low-organic	very highly calcareous

4.9.3 Consolidated drained test of core 8 dark at 0.024mm/min at site 1695

Figure 78 shows the consolidated drained direct shear test of core 8 dark at site 1695. This test shows that in all cases the soil shows dilation behaviour. Drained peak shear strenght 11.4 kPa to 17.7 kPa over normal stresses of 10 kPa to 30 kPa. In general the oedometer stiffness is increasing with increasing normal stress. Further the mandatory reporting information can be found in Tables 27 and 28.

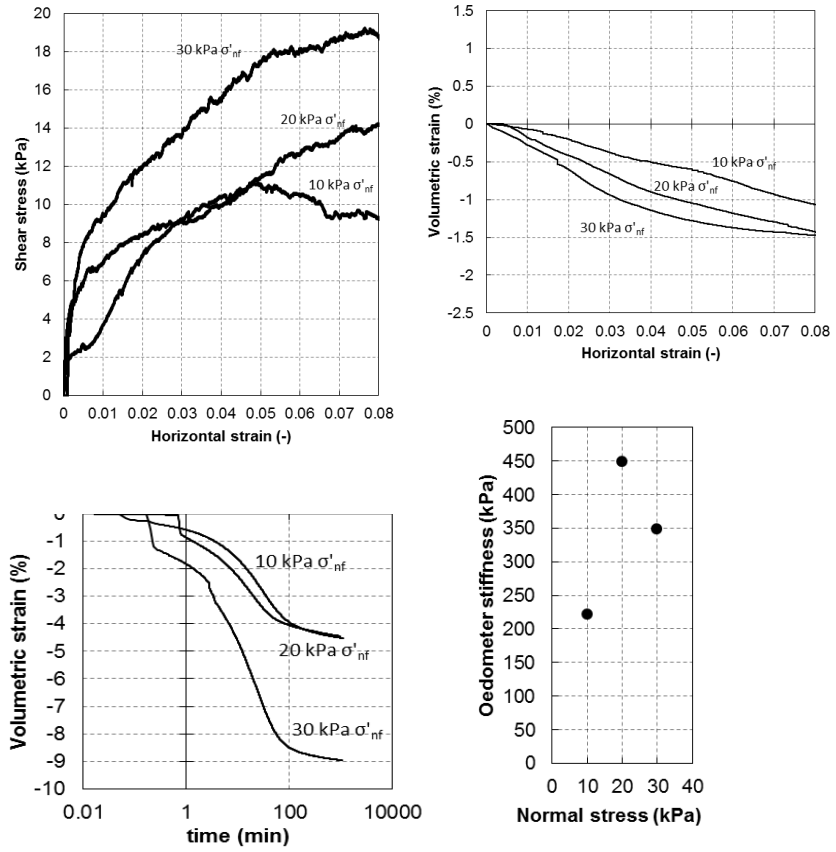

Figure 78: Results from the consolidated drained direct shear test on core 8 dark from site 1695.

Table 40 shows the mandatory reporting results from the consolidated drained direct shear test from core 8 dark at site 1695.

Table 40: All results from the consolidated drained direct shear test of core 8 dark at site 1695.

Sample name	Ψ(°)	θ_{before} (-)	θ_{after} (-)	γ_{bulk}(kN/m^3)	γ_{dry} (kN/m^3)	ρ_{grain}(kg/m^3)	s_u(kPa)	determined at ε_h(%)	E_{oed} (kPa)
Core 8 dark 10 kPa	-1.9	0.78	0.64	15.8	9.6	2750	11.4	4.9	222
Core 8 dark 20 kPa	-4.398	0.59	0.61	15.49	9.60	2750	13.8	7.1	449
Core 8 dark 30 kPa	-9.259	0.58	0.47	17.01	11.59	2750	17.7	5.1	348

Figure 79 shows the comparison between the peak and residual drained shear stress. According to Table 28 the peak shear stress results in a friction angle of 20.8° whereas the residual shear stress results in a friction angle of 25.7°. When calculating these internal friction angles cohesion of zero is assumed. The test strain rate was determined according the ISO standard 17892-10, but it appears that the soil is over consolidated or that the strain rate was too high so that not all of the excess pore water could dissipate. In reality a landslide failure will never be so slow so these test results could still be used and the test could be considered to be partially drained, so not fully drained.

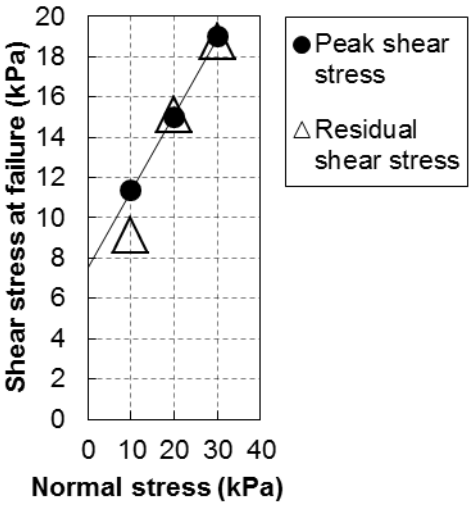

Figure 79: Peak and resual shea stress plotted against normal stress of core 8 dark at site 1695.

Table 41 contains the values of peak and residual shear stress with their peak and resiudual friction angles.

Table 41: Exact values corresponding to Figure 57.

σ'_{nf} (kPa)	$s_{d,peak}$ (kPa)	$s_{d,residual}$ (kPa)	φ_{peak} (°)	$\varphi_{residual}$ (°)
10	11.4	9.1	20.8	25.7
20	15	15.2		
30	19	18.7		

3.9.4 Consoldiated drained direct shear test of core 8 light at 0.0048mm/min at site 1695

Figure 80 shows all the results from the consolidated drained direct shear test at site 1695. The soil contracts in all cases when sheared and the peak shear stresses obtained 9.8 kPa and 20.4 kPa over a normal stress of 10kPa and 30 kPa. The stiffness increases with increase normal stress.

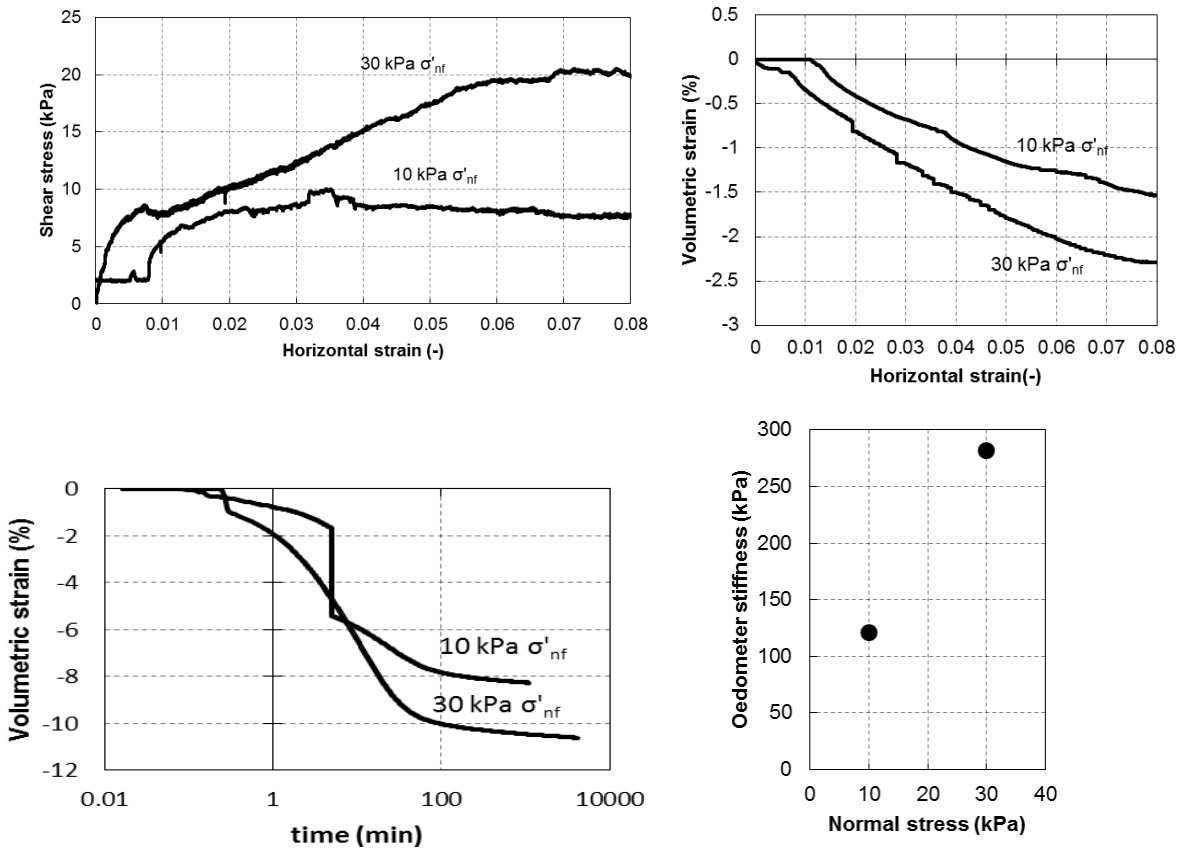

Figure 80: All results from the consolidated drained direct shear test at 0.0048mm/min at site 1695.

Table 42 shows all the mandatory reporting values from the consolidated drained direct shear test of core 8 light at site 1695.

Table 42: All results from the consolidated drained direct shear test of core 8 light at site 1695.

Sample name	Ψ(°)	θ_{before} (-)	θ_{after} (-)	γ_{bulk}(kN/m^3)	γ_{dry} (kN/m^3)	ρ_{grain}(kg/m^3)	$s_{d,peak}$(kPa)	determined at ε_h(%)	E_{oed} (kPa)
Core 8 light 10 kPa	0.0	0.98	0.85	14.4	7.8	2767	9.8	7.0	121
Core 8 light 30 kPa	-0.2	0.92	0.80	14.3	8.0	2767	20.4	3.5	283

Figure 81 shows the peak and residual shear stress with normal stress. This gives peak and residual friction angles of 29° and 31°. This test also shows that the test is not yet fully drained or that the soil is overconsolidated. When calculating the internal friction angle a cohesion of zero is assumed.

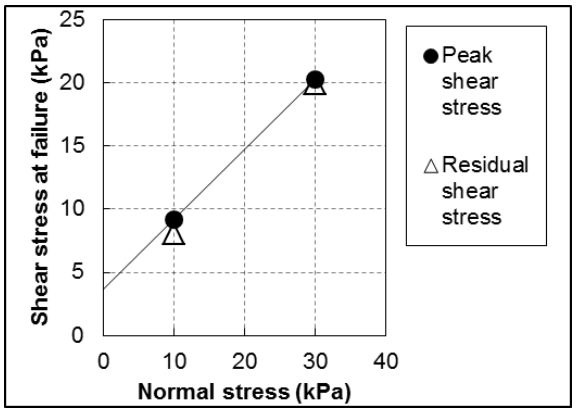

Figure 81: Peak and resual shea stress plotted against normal stress of core 8 dark at site 1695.

Table 43 contains the exact values of peak and residual shear stress with their peak and resiudual friction angles.

Table 43: All excat values corresponding to Figure 59.

Normal stress (kPa)	$s_{d,peak}$(kPa)	$s_{d,residual}$(kPa)	φ_{peak}(°)	$\varphi_{residual}$(°)
10	9.2	8.1	29	31
30	20.3	20.0		

4.9.5 Consolidated undrained direct shear test of core 8 light at 10 kPa at 1.2mm/min at site 1695

Figure 82 shows the consolidated undrained direct shear test of core 8 light. This test shows that the soil has contraction behaviour and an undrained shear strenght of 8.4 kPa is found. Further detailed information can be found in Table 44. When comparing this test to the shear test resulst from core 8 dark at 20 kPa normal stress and core 8 light at 10,30 kPa the undrained shear strenghts are very similar if failure is considered for these drained tests to be at 2% strain or before. This would give an undrained shear strength around 8 kpa to 8.6 kPa which is similar to 8.4 kPa found here in the consolidated undrained test of core 8 light.

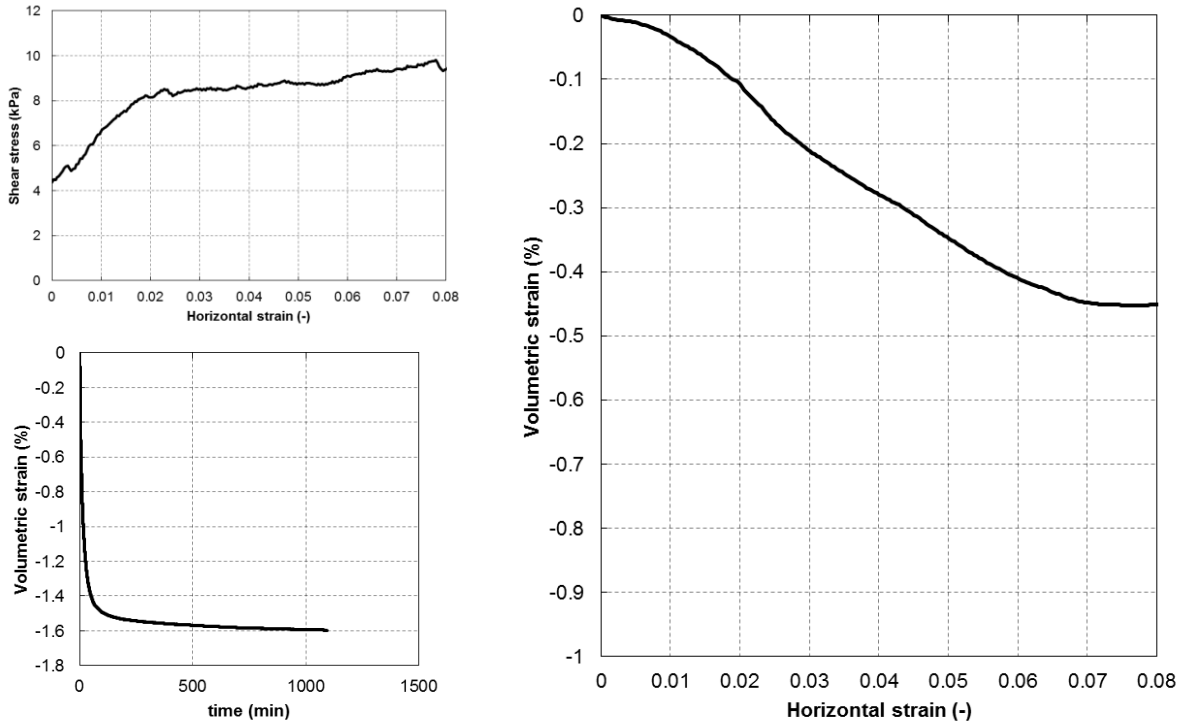

Figure 82: Results from the consolidated undrained direct shear test of core 8 light at 10kPa at 1.2mm/min at site 1695.

Table 44 shows all the mandatory reporting values from the consolidated undrained direct shear test of core 8 light from site 1695.

Table 44: Results from the consolidated undrained direct shear test of core 8 light at 10kPA at 1.2mm/min at site 1695.

Sample name	Ψ(°)	θ_{before} (-)	θ_{after} (-)	γ_{bulk} (kN/m^3)	γ_{dry} (kN/m^3)	ρ_{grain} (kg/m^3)	s_u(kPa)	determined at ε_h(%)	E_{oed} (kPa)
Core 8 light 10 kPa	-2.3	1.01	0.88	14.4	7.7	2767	8.4	2.2	156

4.9.6 Comparing all the undrained shear strengths from the pocket vane tests at site 1695

Figure 83 shows the pocket vane test results. These results show a clear decreasing trend in undrained shear strength from 13 kPa to 5 kPa with increasing water content. The undrained shear strength here is classified as extremely low to very low.

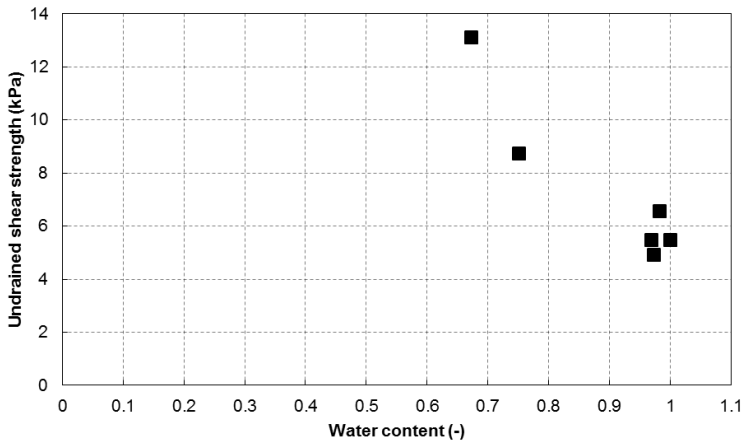

Figure 83: Pocket vane test results from site 1959.

4.10 All test results from site 1959

Here all the test result from site 1959 will be presented.

4.10.1 Opening of core 9 and 10 of site 1959

Figure 84 shows core 9 and core 10 opened. Core 9 is the closest to the seabed and increases with depth from left to right. Core 10 follows core 9 and increases with depth from right to left. A colour change from light grey to a dark grey takes place with increasing depth.

Figure 84: Core 9 above core 10

Tables 45 to 47 give an overview of the amount of cores opened for one site and the total and full core recovery. The total core recovery includes also the broken/disturbed parts of the core whereas the full core recovery includes only parts of the core where the whole diameter is intact.

Table 45: Core 9 core recovery information.

Core 9	
Mass of closed core (kg)	0.973
Mass of empty core (kg)	0.261
Lenght of cylinder section (cm)	25
Total core recovery (cm)	23
Full core recovery (cm)	20

Table 46: Core 10 core recovery information.

Core 10	
Mass of closed core (kg)	4.823
Mass of empty core (kg)	0.714
Lenght of cylinder section (cm)	101
Total core recovery (cm)	91
Full core recovery (cm)	89

Table 47: Site 1959 core recovery information.

Site 1959	
Penetration depth (cm)	600
Total core recovery (cm)	114
Full core recovery (cm)	109
Recovery ratio (-)	0.19
Pull out force (kg)	2700

Figure 85 shows the gravimetric water content decreasing with depth from values between 1 and 1.18 to a value of 0.7. The volumetric water content decreases with depth from 0.75 to 0.64. The bulk volumetric weight increases from 15 kN/m^3 to 16 kN/m^3. The saturation remains stable around 1 along the entire length. The void ratio decreases from 1.3 to 0.75 and the liquidity index is just above 1 for the entire core. Undrained shear strength values from the pocket vane test fluctuate between 6kPa and 12 kPa.

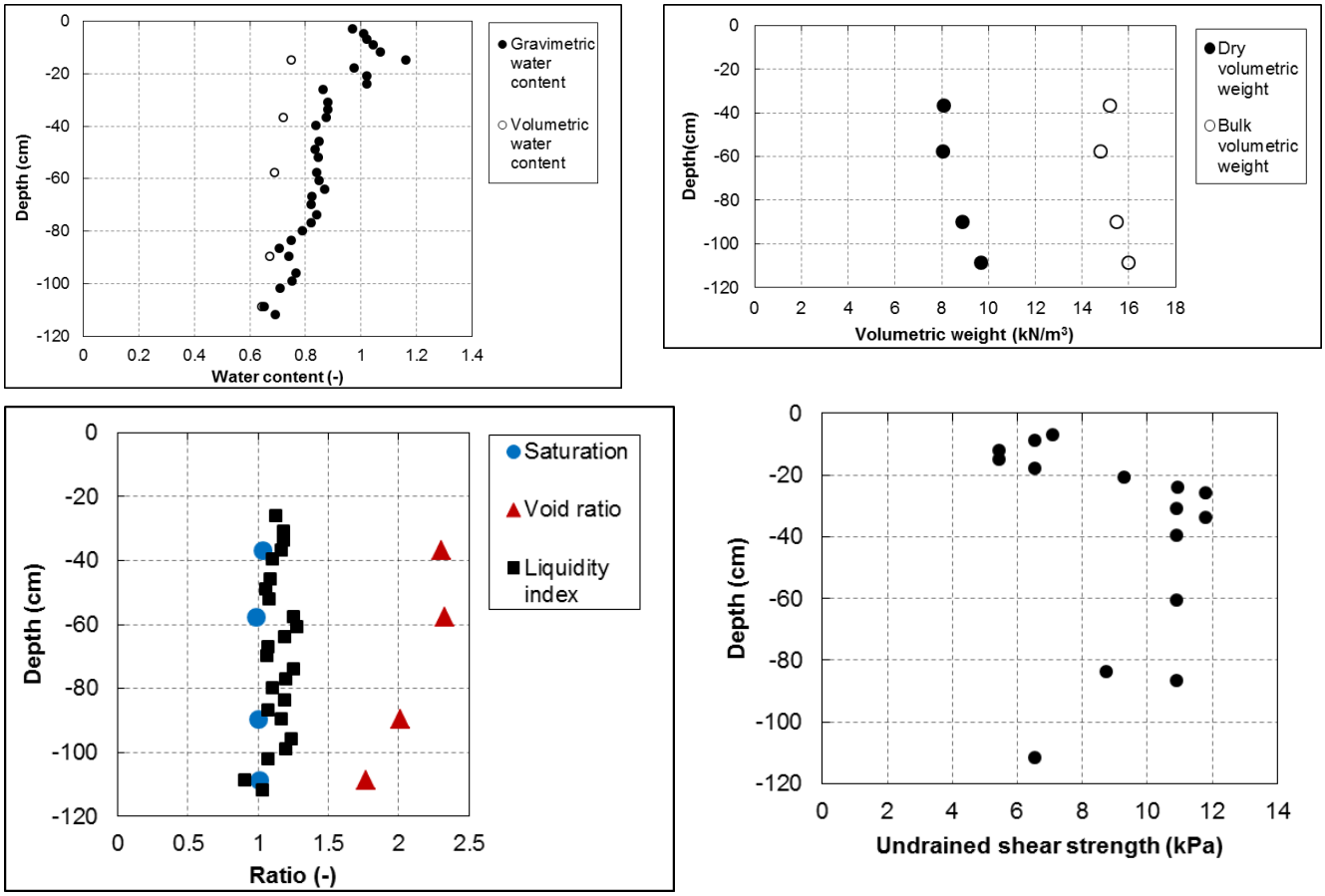

Figure 85: From left to right and top to bottom the water content, volumetric weight, saturation and void ratio and the undrained shear strength from the pocket vane with depth at site 1959.

4.10.2 Grain size distribution at site 1959

Figure 86 shows the grain size distribution and the soil fractions with depth. The clay content and the silt content both fluctuate with depth showing only a fining-upward trend in the lower part of the core based on the clay content. The sand content decreases from 15 to 10% with depth. At this site the clay content is seen increasing and decreasing with depth. Both a fining up-ward and a coarsening-upward sequence is found. This phenomenon of a coarsening-upward sequence on top of a fining-upward sequence will be explained in detail in chapter 5.5.4.

This may be the cause of multiple fining-upward sequences being present. This could not be detected since the resolution of this geotechnical research is less than that of stratigraphic research. One fining-upward sequence is found with one coarsening up-ward sequence on top.

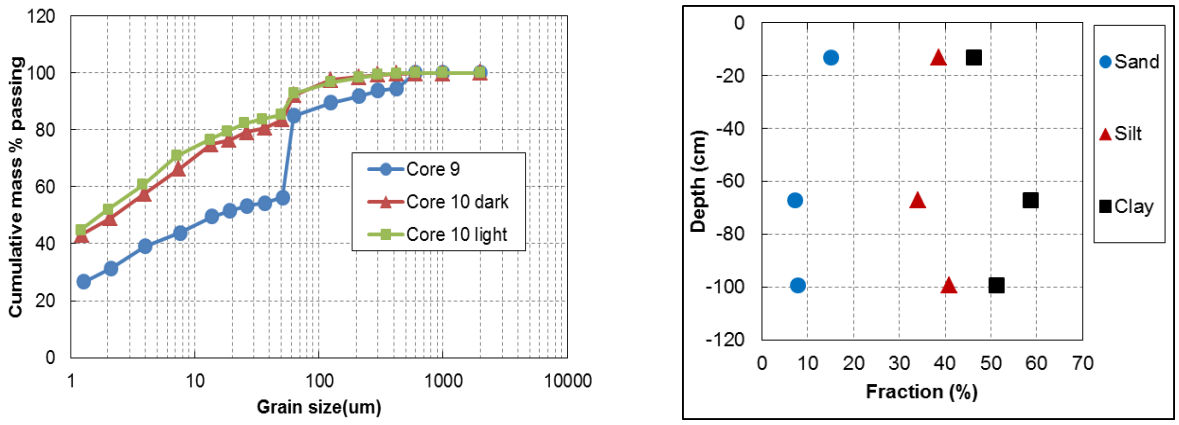

Figure 86: Grain size distribution on the left anf the soil fractions with depth on the right at site 1959.

4.10.3 Atterberg limits and derived remoulded undrained shear strength at site 1959

Figure 87 shows a decrease in plastic limit from 0.48 to 0.4. the liquid limit is decreased from 0.82 to 0.75. In all cases the liquid limit is found to be lower than the natural water content indicating a risk of liquefaction upon disturbance. The calcite content is found to decrease from from 54% to 17% and the organic matter content is found to fluctuate between 6% and 8%.

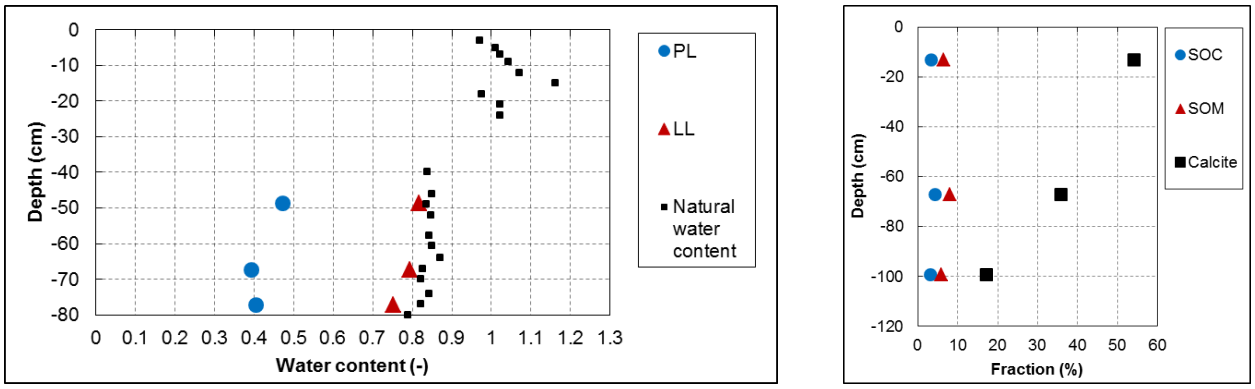

Figure 87: Atterberg limits on the left and SOC content, SOM content and calcie content with depth on the right at site 1959.

Table 48 shows the classification of site 1959. The soil can be classified as silty CLAY. The plasticity is high to very high. The organic matter content is low to medium-organic and the soil the calcareous to very highly calcareous. The soil is inactive.

Table 48: Classification of the sediments from site 1959.

Sample name	Soil type	Plasticity classification	SOM classification	Calcite classification	Activity classification
Core 9	silty CLAY	NA	medium-organic	very highly calcareous	NA
Core 10 dark (6-22)	silty CLAY	high	low-organic	calcareous	inactive
Core 10 light (31-41)	silty CLAY	very high	medium-organic	highly calcareous	inactive
Core 10 light (41-51)	silty CLAY	very high	medium-organic	highly calcareous	inactive
Core 10 light(57-71)	silty CLAY	very high	medium-organic	highly calcareous	inactive

4.10.4 Unconsolidated undrained direct shear tests of site 1959

Figure 88 shows the unconsolidated undrained direct shear test of site 1959. The soil shows clear dilation behaviuor from all the original samples whereas the remoulded samples show no to very little dilation. The undrained shear strengths range from 0 kPa to 6.5 kPa. This very low strenght of 0 kPa is from the remoulded sample of core 10 light (41-43) which

probably liquefied during the remoulding process and proceded to behave as a liquid with not much resistance. The mandatory reporting information can be found in Table 33.

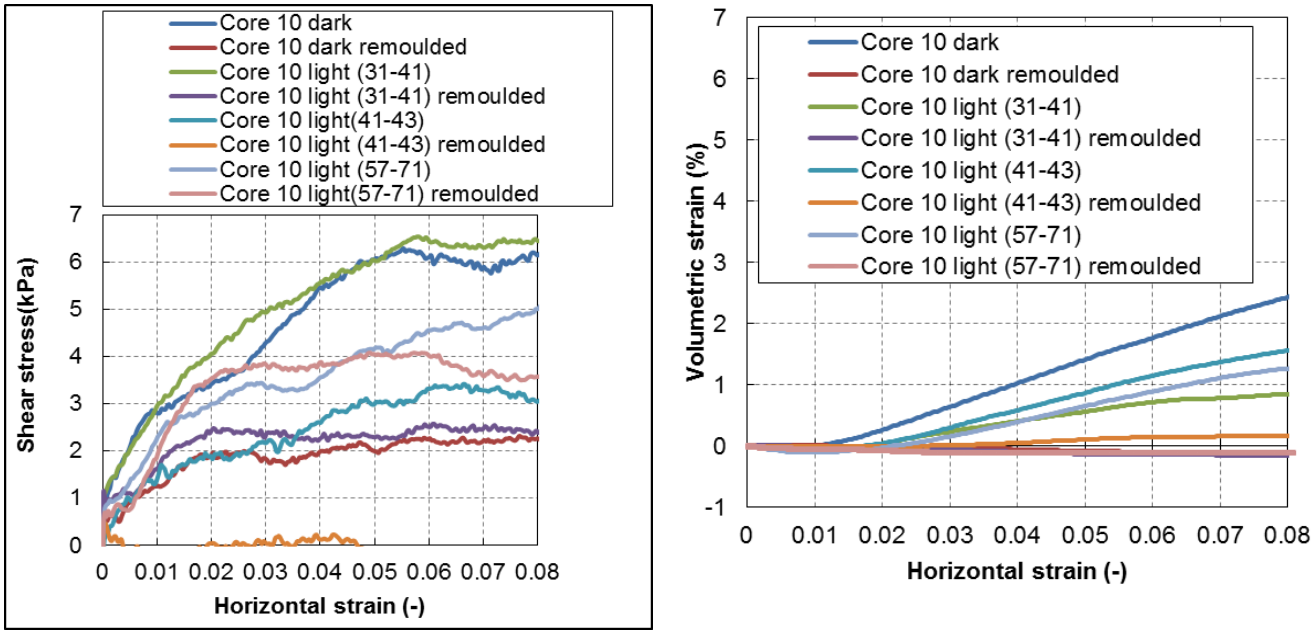

Figure 88: Results from the unconsolidated undrained direct shear tests of site 1959.

Table 49 shows the mandatory reporting values from the unconsolidated undrained direct shear tests of site 1959.

Table 49: All results from the unconsolidated undrained direct shear tests of site 1959.

Sample name	Ψ(°)	θ_{before} (-)	γ_{bulk}(kN/m^3)	γ_{dry} (kN/m^3)	ρ_{grain}(kg/m^3)	s_u(kPa)	determined at ε_h(%)
Core 10 dark	8.7	0.71	15.8	9.2	2736	6.4	5.5
Core 10 dark remoulded	-0.5	0.72	15.5	9.0	2736	2.0	1.9
Core 10 light (31-41)	4.3	0.79	15.1	8.5	2727	6.5	5.7
Core 10 light (31-41) remoulded	-0.6	0.77	15.0	8.5	2727	2.4	2.0
Core 10 light (41-43)	7.1	0.86	14.8	7.9	2727	3.1	4.7
Core 10 light (41-43) remoulded	1.0	0.87	14.9	7.9	2727	0.0	4.3
Core 10 light (57-71)	6.3	0.85	14.8	8.0	2727	3.4	2.6
Core 10 light (57-71) remoulded	-0.1	0.86	14.7	7.9	2727	3.8	2.8

4.10.5 Consolidated undrained direct shear test of core 10 dark at site 1959

Figure 89 shows the consolidated undrained direct shear test of core 10 dark at 6 kPa. This test shows dilation behaviour which is probably because of the low amount of normal stress applied. This normal stress is 1.84 kPa for all UU DS tests and reprsents just the weight of the equipment. No consolidation was initiated so the sample could be sheared without consolidation. The undrained shear strength is determined to be 7.1 kPa. Further mandatory reporting infromation can be found in Table 34.

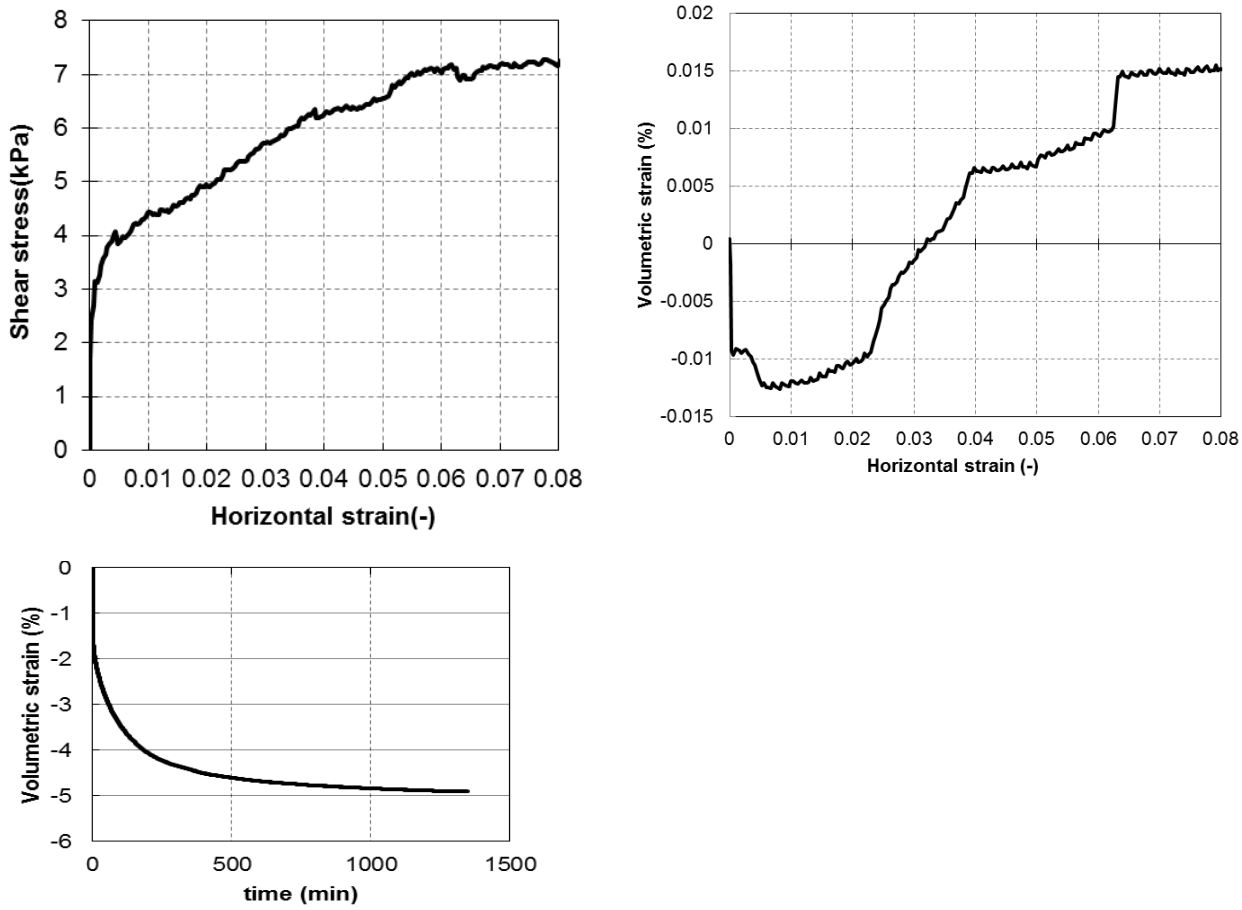

Figure 89: Results from the consolidated undrained direct shear test of core 10 dark of site 1959.

Table 50 shows all the mandatory reporting values from the consolidated undrained direct shear test of site 1959.

Table 50: All results from the consolidated undrained direct shear test of core 10 dark of site 1959.

Sample name	Ψ(°)	θ_{before} (-)	θ_{after} (-)	γ_{bulk}(kN/m^3)	γ_{dry} (kN/m^3)	ρ_{grain}(kg/m^3)	s_u(kPa)	determined at ε_h(%)	E_{oed} (kPa)
Core 10 dark 6 kPa	NA	0.76	0.74	15.4	8.8	2736	7.1	5.9	123

4.10.6 Comparing all undrained shear strengths from original and remoulded fall cone and unconsolidated undrained direct shear tests from site 1959

Figure 90 shows values of the original direct shear test from 5.5 kPa to 3 kPa with an increase in water content whereas the values of the remoulded direct shear test range from 2 kPa to 3.5 kPa with increasing water content. This is not to be expected as the undrained shear strength is expected to be decreasing with increasing water content. This is likely due to samples having different clay content.

Both original fall cone tests show an increase in undrained shear strength with increasing water content. This may be explained by the fact that their water content values are mostly in between 0.8 and 0.9 which is not that different. This can be explained by the soil that will have slightly different clay content.

This can give higher undrained shear strength results with increasing water content. The pocket vane test results are between 6 kPa and 12 kPa. The undrained shear strength here is classified as extremely low to very low.

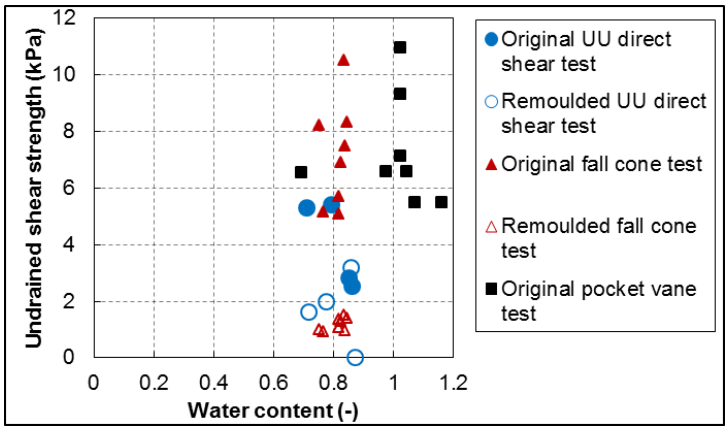

Figure 90: Comparing the undrained shear strenght values from the direct shear test, fall cone test and pocket vane test at site 1959.

4.10.7 Comparing all sensitivity result from the original and remoulded fall cone and unconsolidated undrained direct shear tests from site 1959

Figure 91 shows sensitivity values from 3 to 1 for direct shear tests and values scattered between 4 and 8 for the fall cone tests. The decreasing trend in values for the direct shear test can again be explained by the fact that each soil sample has a slightly different sand, silt and clay content. The sensitivity here is classified as low.

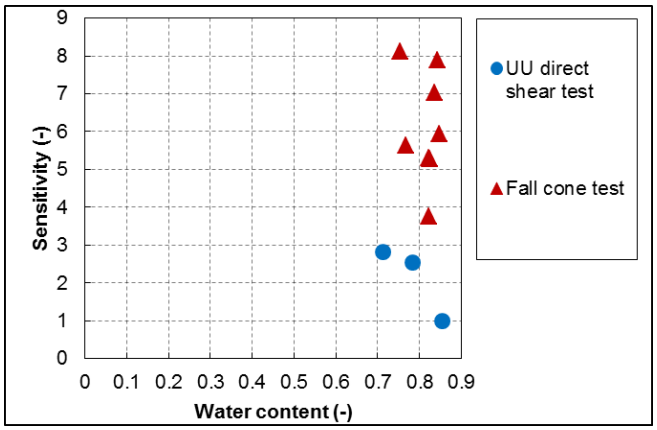

Figure 91: Comparing the sensitivity values from the direct shear test and the two fall cone tests at site 1959.

4.11 All test results from site 1604

4.11.1 Opening core 3 and 11 at site 1604

Figure 92 shows cores 3 and 11 opened. Core 3 is closest to the seabed and increased with depth from right to left. Core 3 is covered in a very thin black oxide layer and the soil below this oxide layer has a light grey colour. Core 11 is increasing with depth from right to left and has orange iron oxide spots across its entire length.

Figure 92: Core 3 above core 111.

Tables 51 to 53 give an overview of the amount of cores opened for one site and the total and full core recovery. The total core recovery includes also the broken/disturbed parts of the core whereas the full core recovery includes only parts of the core where the whole diameter is intact.

Table 51: Core 3 core recovery information.

Core 3	
Mass of closed core (kg)	1.958
Mass of empty core (kg)	0.312
Lenght of cylinder section (cm)	44
Total core recovery (cm)	38.5
Full core recovery (cm)	24

Table 52: Core 11 core recovery information.

Core 11	
Mass of closed core (kg)	6.227
Mass of empty core (kg)	0.774
Lenght of cylinder section (cm)	100
Total core recovery (cm)	98
Full core recovery (cm)	94

Table 53: Site 1604 core recovery information.

Site 1604	
Penetration depth (cm)	300
Total core recovery (cm)	136.5
Full core recovery (cm)	118
Recovery ratio (-)	0.46
Pull out force (kg)	NA

Figure 93 shows the gravimetric water content decreasing with depth from 0.9 to 0.4. The volumetric water content decreases from 0.7 to 0.5 with depth. The bulk volumetric weight increases from 15 kN/m^3 to 18 kN/m^3. The saturation remains stable around 1 until a depth of 130 cm where it fall below 1. This means that the bottom of the core is not fully saturated. The void ratio decreases from 2.5 to 1 with depth and the liquidity index decreases from 2.5 to 1 with depth. The undrained shear strength values obtained from the pocket vane test fluctuate between 10 kPa and 14 kPa.

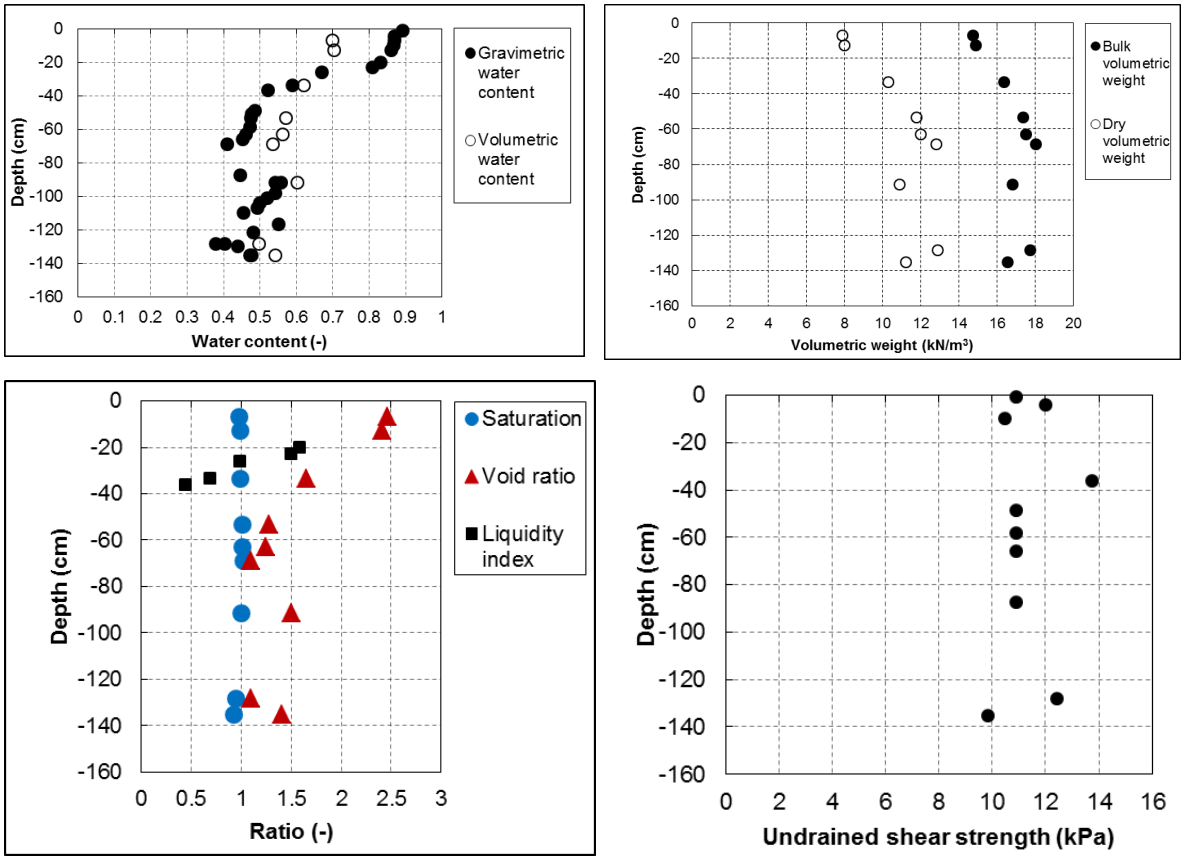

Figure 93: From left to right and top to bottom the water content, volumetric weight, saturation and void ratio and the undrained shear strength from the pocket vane with depth at site 1604.

4.11.2 Grain size distribution at site 1604

Figure 94 shows the grain size distribution and soil fractions with depth at site 1604. This shows the clay content decreasing with depth from 33% to 15% where it remains stable. The sand content also decreases with depth from 70% to 55% and the silt content fluctuates between 15% and 33%. A fining-upward sequence is found based on the clay content.

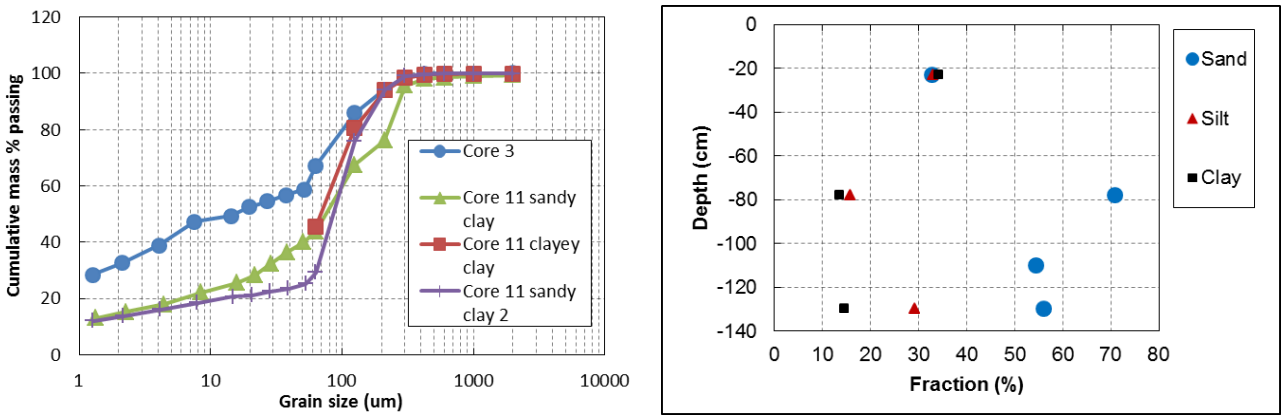

Figure 94: Grain size distribution on the left anf the soil fractions with depth on the right at site 1604.

4.11.3 Atterberg limits and derived remoulded undrained shear strength at site 1604

Figure 95 shows that that only one plastic limit could be determined at a depth of 20 cm. The liquid limit decreases from 0.67 to 0.43 and is in all cases below the natural water content. This indicates risk of liquefaction upon disturbance. The highest risk will be in the top deposits since they contain more clay then the bottom deposits which are more sandy. The calcite content decreases from 57% to 44% and the organic matter content shows a general decrease from 6.7% to 3.1%.

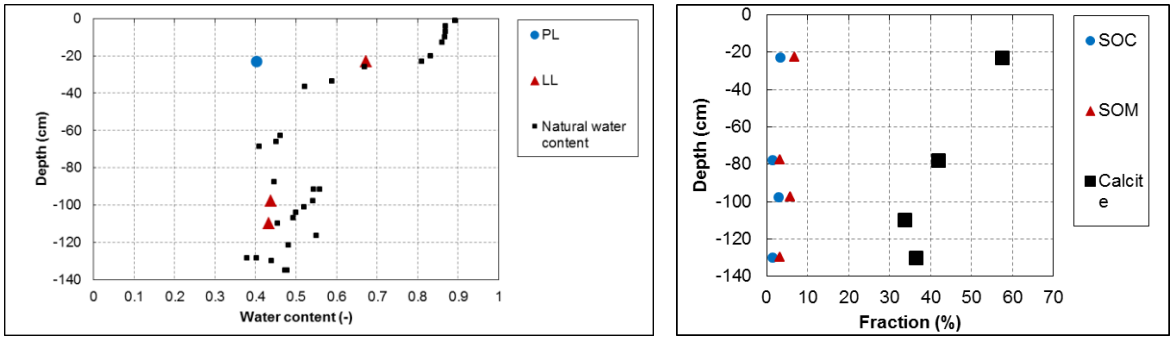

Figure 95: Atterberg limits on the left and SOC content, SOM content and calcie content with depth on the right at site 1604.

Table 54 shows the classification of the soil at site 1604. The soil can be classified as silty CLAY or silty SAND. The plasticity of the soil closes to the seabed is high in plasticity. The bottom part was too sandy to allow for plastic limit determination. The soil is low to medium-organic and highly to very highly calcareous. The soil is classified as inactive.

Table 54: Classification of the sediments present at site 1604.

Sample name	Soil type	Plasticity classification	SOM classification	Calcite classification	Activity classification
Core 3	silty CLAY	high	medium-organic	very highly calcareous	normal soil
Core 11 clayey clay(31-42)	NA	NA	NA	highly calcareous	NA
Core 11 clayey clay(42-52.5)	NA	NA	low-organic	highly calcareous	NA
Core 11 sandy clay	silty SAND	NA	low-organic	highly calcareous	NA
Core 11 sandy clay 2	silty SAND	NA	low-organic	highly calcareous	NA

4.11.4 Unconsolidated undrained direct shear tests at site 1604

Figure 96 shows the results from the unconsolidated undrained direct shear test. The original samples all show dilation behaviour during shearing whereas the remoulded samples all show contraction behaviour during shearing. Undrained shear strength values between 1.9 kPa and 5.8 kPa are found. The mandatory reporting information can be found in Table 35.

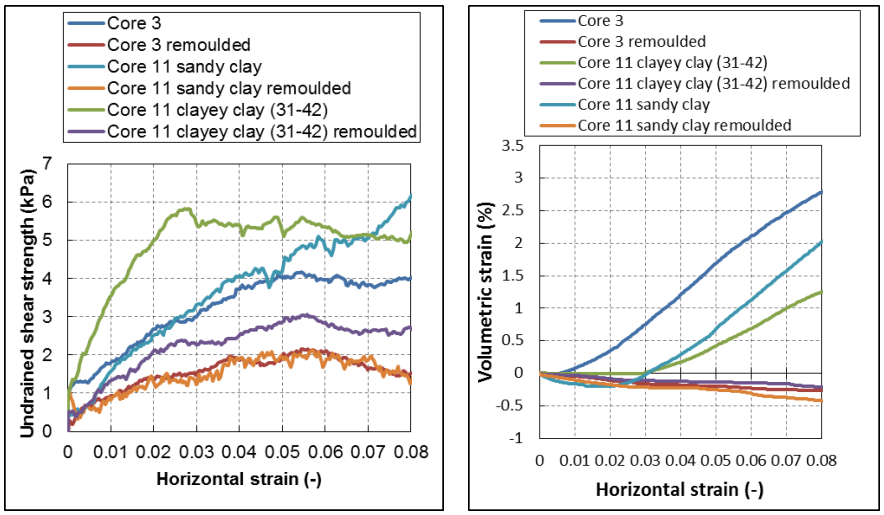

Figure 96: Results from the unconsolidated undrained direct shear tests of site 1604.

Table 55 shows the mandatory reporting values of the unconsolidated undrained direct shear tests of site 1604.

Table 55: All results from the unconsolidated undrained direct shear tests of site 1604.

sample name	Ψ(°)	θ_{before} (-)	γ_{bulk}(kN/m^3)	γ_{dry} (kN/m^3)	ρ_{grain}(kg/m^3)	s_u(kPa)	determined at ε_h(%)
Core 3	10.7	0.67	16.0	9.6	2786	4.2	4.8
Core 3 remoulded	-0.9	0.69	15.6	9.2	2786	1.9	3.8
Core 11 sandy clay	10.5	0.44	18.1	12.6	2756	5.0	6.3
Core 11 sandy clay remoulded	-1.0	0.42	17.3	12.2	2756	1.9	3.8
Core 11 clayey clay	7.1	0.52	15.7	10.4	2785	5.8	2.7
Core 11 clayey claye remoulded	-0.3	0.51	17.3	12.2	2785	2.4	2.5

4.11.5 Comparing all undrained shear strengths from original and remoulded fall cone and direct shear tests from site 1604

Figure 97 shows values from 5.5 kPa to 3.5 kPA with increasing water content for the original direct shear tests whereas the remoulded direct shear test shows values between 1 kPa and 2 kPa with no clear trend. Both original fall cone tests show values from 4 kPa to 13 kPa with increasing water content. Both remoulded fall cone tests shows values increasing from 0.5 kPa to 1.5 kPa with decreasing water content. The pocket vane test results show values between 10 kPa and 14 kPa with no clear trend. The undrained shear strength here is classified as extremely low to very low.

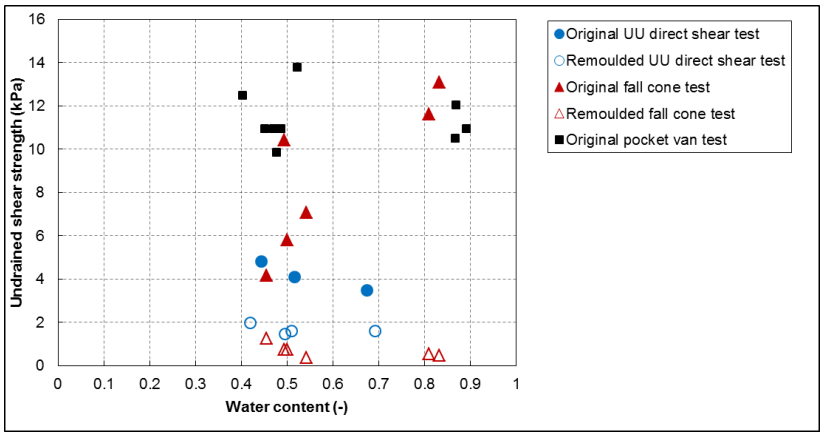

Figure 97: Comparing the undrained shear strenght values from the direct shear test, fall cone test and pocket vane test at site 1604.

4.11.6 Comparing all sensitivity result from the original and remoulded fall cone and direct shear tests from site 1604

Figure 98 shows sensitivity values from the original direct shear test increasing from 1 to 3 with decreasing water content. Both fall cone tests show sensitivity values increasing from 4 to 28 with increasing water content. The sensitivity here is classified as low to medium.

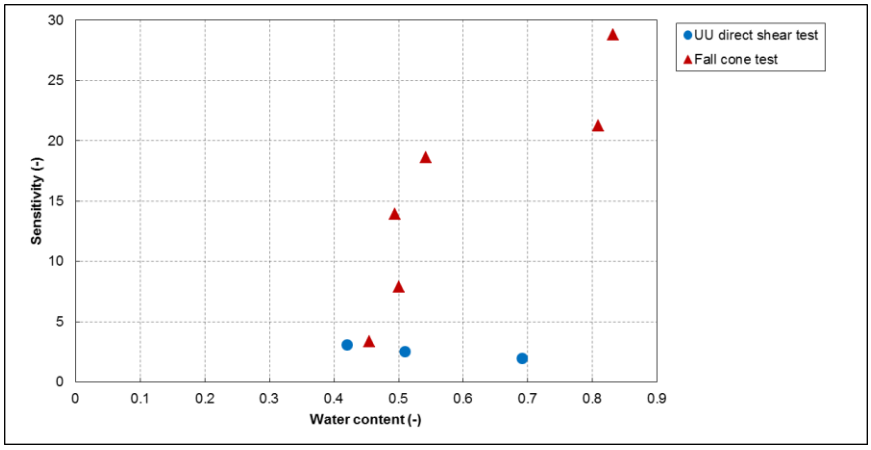

Figure 98: Comparing the sensitivity values from the direct shear test and the two fall cone tests at site 1604.

4.12 Comparison of Atterberg limits, Atterberg classification and Skempton activity classification of the <63µm and <425µm soil fractions of some samples

In this chapter comparisons are made between the soil samples of the <63µm and <425µm fractions that have or have not been dried for 24 hours in the oven at 105° Celcius. This is done so that the effect of the separation of the sand fraction from the soil can be seen.

Table 56 shows the comparison of the Atterberg limits, the Atterberg classification and the activity of the soil based on the Atterberg limits. This comparison is used to see the effect of sand separation out of the soil. The <63µm fractions only have the silt and clay fractions left. The sand fraction was sieved out using wet sieving after which the non-dried samples have not been in the oven and the dried samples have been dried in the oven at 105° Celsius for at least 18 hours. Table 56 shows that when sand is separated out of the soil sample, the liquid limit in all cases except one shows a clear decrease. The one exception is core 4 light (57-71) <63µm where there is no comparable <425µm fraction to compare it with. This reduction in liquid limit seems logical since a lower water content is required to allow the sample to liquefy. This is caused by the relative increase in clay content of the sample which obstructs water flow more than sand and thus could have caused a faster increase in excess pore pressure build up which caused the decrease in liquid limit.

Table 56: Results from all the Atterber determinations of the samples with and without sand fraction.

Sample name	LL (-)	PL (-)	PI (-)	Plasticity classification	Activity classification
Core 2 dark <63 non dried	0.67	0.35	0.32	high	inactive soil
Core 2 dark <63 dried	0.65	0.37	0.28	high	inactive soil
Core 2 dark <425	0.78	0.43	0.34	very high	inactive soil
Core 2 orange <63 non dried	0.69	0.36	0.33	high	inactive soil
Core 2 orange < 425	0.79	0.41	0.37	very high	inactive soil
Core 3 <63 non dried	0.63	0.34	0.29	high	inactive soil
Core 3 <425	0.67	0.40	0.27	high	normal soil
Core 4 light <63 non dried (57-71)	0.74	0.40	0.34	very high	inactive soil
Core 4 light <63 non dried	0.60	0.31	0.29	high	inactive soil
Core 4 light <425	0.73	0.43	0.30	very high	inactive soil
Core 10 light <63 dried	0.68	0.31	0.36	high	inactive soil
Core 10 light (31-41) <425	0.75	0.40	0.35	very high	inactive soil
Core 10 light (41-51) <425	0.79	0.39	0.40	very high	inactive soil
Core 10 light(57-71) <425	0.82	0.47	0.35	very high	inactive soil

The Atterberg classification shows that the soil can mainly be classified as high to very high silty soil. Only in one case it is classified as clay. It has to be said that all the samples are just on the border between the classification as clay or silt and that the organic matter content may have an effect on this classification. The Activity from the soil clearly shows an indication of inactive soil. From this no considerable swelling activity is expected even though smectite minerals were found to be present by doing an x-ray diffraction test on core 10 dark.

5 Comparing all results to each other and to outside literature

In this chapter all the obtained geotechnical properties from all the sites will be compared to each other. These geotechnical properties will then also be compared to geotechnical properties found in other literature.

5.1 An overview of the geotechnical classification of all of the sediments.

Table 57 shows the classification results of all the tests. The soil type ranges from silty SAND to clayey SILT to silty CLAY. The plasticity ranges from medium to very high. The SOM content ranges from low to medium organic. The calcite content ranges from calcareous to very highly calcareous. The activity based on Atterberg limits ranges from inactive soil to normal soil. The undrained shear strength ranges from extremely low to very low and the sensitivity ranges from low to medium.

Table 57: Summary of all the classification of the sediments from each site.

Site	Sample name	Soil type	Plasticity	SOM content	Calcite content	Activity	undrained shear strength	Sensitivity
1736	Core 1 sandy dark	NA	medium	NA	NA	NA	extremely low to very low	low to medium
1736	Core 1 dark	clayey SILT	medium	low-organic	calcareous	inactive soil	extremely low to very low	low to medium
1736	Core 1 grey	silty CLAY	high	medium-organic	highly calcareous	normal soil	extremely low to very low	low to medium
1736	Core 2 orange	silty CLAY	very high	medium-organic	highly calcareous	inactive soil	extremely low to very low	low to medium
1736	Core 2 dark	silty CLAY	very high	medium-organic	highly calcareous	inactive soil	extremely low to very low	low to medium
1672	Core 4 dark (5-15.5)	silty CLAY	medium	medium-organic	highly calcareous	inactive soil	extremely low to very low	low to medium
1672	Core 4 light (21-32)	silty CLAY	very high	medium-organic	very highly calcareous	inactive soil	extremely low to very low	low to medium
1672	Core 5 beige clay 2 (12-22)	NA	NA	NA	calcareous	NA	extremely low to very low	low to medium
1672	Core 5 (22-37)	NA	medium	NA	NA	NA	extremely low to very low	low to medium
1672	Core 5 (37-47.5)	NA	NA	NA	NA	NA	extremely low to very low	low to medium
1672	Core 5 very light (44-56)	NA	NA	NA	highly calcareous	NA	extremely low to very low	low to medium
1672	Core 5 beige (63.5-75)	clayey SILT	medium	low-organic	highly calcareous	inactive soil	extremely low to very low	low to medium
688	Core 6 sandy clay (8.5-24)	silty SAND	NA	low-organic	highly calcareous	NA	very low to low	low
688	Core 6 clayey clay (38-55.5)	clayey SILT	NA	low-organic	highly calcareous	NA	very low to low	low
1988	Core 7 dark (10.5-22.5)	clayey SILT	very high	medium-organic	calcareous	NA	extremely low to very low	low to medium
1988	Core 7 dark(22.5-34)	clayey SILT	very high	medium-organic	calcareous	normal	extremely low to very low	low to medium
1988	Core 7 light	silty CLAY	very high	medium-organic	highly calcareous	inactive	extremely low to very low	low to medium
1695	Core 8 dark	clayey SILT	NA	low-organic	highly calcareous	NA	extremely low to very low	NA
1695	Core 8 light	silty CLAY	NA	low-organic	very highly calcareous	NA	extremely low to very low	NA
1959	Core 9	silty CLAY	NA	medium-organic	very highly calcareous	NA	extremely low to very low	low
1959	Core 10 dark (6-22)	silty CLAY	high	low-organic	calcareous	inactive	extremely low to very low	low
1959	Core 10 light (31-41)	silty CLAY	very high	medium-organic	highly calcareous	inactive	extremely low to very low	low
1959	Core 10 light (41-51)	silty CLAY	very high	medium-organic	highly calcareous	inactive	extremely low to very low	low
1959	Core 10 light(57-71)	silty CLAY	very high	medium-organic	highly calcareous	inactive	extremely low to very low	low
1604	Core 3	silty CLAY	high	medium-organic	very highly calcareous	normal soil	extremely low to very low	low to medium
1604	Core 11 clayey clay(31-42)	NA	NA	NA	highly calcareous	NA	extremely low to very low	low to medium
1604	Core 11 clayey clay(42-52.5)	NA	NA	low-organic	highly calcareous	NA	extremely low to very low	low to medium
1604	Core 11 sandy clay	silty SAND	NA	low-organic	highly calcareous	NA	extremely low to very low	low to medium
1604	Core 11 sandy clay 2	silty SAND	NA	low-organic	highly calcareous	NA	extremely low to very low	low to medium

A quantification of these values is made in Table 58. Here the organic matter content ranges from 2.6% to 9.0 %. The calcite contenten ranges from 17.3% to 55.6%. The undrained shear strength values that are based on the fall cone tests, DS tests and pocket vane tests unless otherwise stated show values between 0.5 kPa and 33.2 kPa. The sensitivty values which are based on the UU DS tests and the fall cone test range from 1.0 to 28.8.

Table 58: A quantification of the classifications at all the intervals from each site.

Site	Sample name	Soil type	Plasticity	SOM content (%)	Calcite content (%)	Activity	undrained shear strength (kPa)	Sensitivity
1736	Core 1 sandy dark	NA	medium	NA	NA	NA	1.0-10.9	1.1-6.2
1736	Core 1 dark	clayey SILT	medium	3.9	22.7	inactive soil	0.8-3.4	1.2-1.6 (based on CU DS tests)
1736	Core 1 grey	silty CLAY	high	6.5	27.2	normal soil	1.5-14.3	9.7-14.3
1736	Core 2 orange	silty CLAY	very high	7.3	33.8	inactive soil	1.4-10.7	3.4-8.3
1736	Core 2 dark	silty CLAY	very high	7.2	48.1	inactive soil	0.6-7.0	3.0-10.0
1672	Core 4 dark (5-15.5)	silty CLAY	medium	6.5	30.4	inactive soil	1.2-6.6	1.8-6.7
1672	Core 4 light (21-32)	silty CLAY	very high	6.2	55.6	inactive soil	0.6-11.4	2.8-17.5
1672	Core 5 beige clay 2 (12-22)	NA	NA	NA	23.6	NA	NA	low to medium
1672	Core 5 (22-37)	NA	medium	NA	NA	NA	NA	low to medium
1672	Core 5 (37-47.5)	NA	NA	NA	NA	NA	NA	low to medium
1672	Core 5 very light (44-56)	NA	NA	NA	43.4	NA	NA	low to medium
1672	Core 5 beige (63.5-75)	clayey SILT	medium	4.3	32.7	inactive soil	2.6-33.2	1.1-8.9
688	Core 6 sandy clay (8.5-24)	silty SAND	NA	2.6	32.5	NA	2.5-4.1	1.3
688	Core 6 clayey clay (38-55.5)	clayey SILT	NA	3.4	33.1	NA	1.1-8.3	1.9-4.4
1988	Core 7 dark (10.5-22.5)	clayey SILT	very high	NA	23.8	NA	1.0-11.9	1.3-12.5
1988	Core 7 dark(22.5-34)	clayey SILT	very high	8.5	23.8	normal	0.5-6.3	1.9-11.6
1988	Core 7 light	silty CLAY	very high	9.0	39.7	inactive	0.8-12.1	3.4-15.5
1695	Core 8 dark	clayey SILT	NA	5.5	35.0	NA	8 to 9 (at 10 kPa normal stress)	NA
1695	Core 8 light	silty CLAY	NA	5.9	52.9	NA	8 to 9 (at 10 kPa normal stress)	NA
1959	Core 9	silty CLAY	NA	6.4	54.2	NA	NA	NA
1959	Core 10 dark (6-22)	silty CLAY	high	5.9	17.3	inactive	0.9-8.2	2.8-8.1
1959	Core 10 light (31-41)	silty CLAY	very high	8.1	35.9	inactive	0.9-7.5	2.5-7.9
1959	Core 10 light (41-51)	silty CLAY	very high	8.1	35.9	inactive	1.3-6.9	3.8-5.3
1959	Core 10 light(57-71)	silty CLAY	very high	8.1	35.9	inactive	1.5-10.5	1.0-7.0
1604	Core 3	silty CLAY	high	6.7	57.4	normal soil	0.5-13.1	1.9-28.8
1604	Core 11 clayey clay(31-42)	NA	NA	NA	33.8	NA	0.7-5.8	2.5-7.9
1604	Core 11 clayey clay(42-52.5)	NA	NA	5.8	33.8	NA	0.7-10.4	13.9-18.6
1604	Core 11 sandy clay	silty SAND	NA	3.2	36.5	NA	1.7-5.3	3.1
1604	Core 11 sandy clay 2	silty SAND	NA	3.3	42.0	NA	NA	NA

5.2 A comparison between all the geotechnical properties obtained from all of the 7 investigated sites

5.2.1 Comparing the gravimetric water contents from all sites

Figure 99 shows the gravimteirc water content fluctuating 0.20 and 1.2. This wide range can be explained by the differences in void ratio caused by the different normal stresses on top of the sediments.

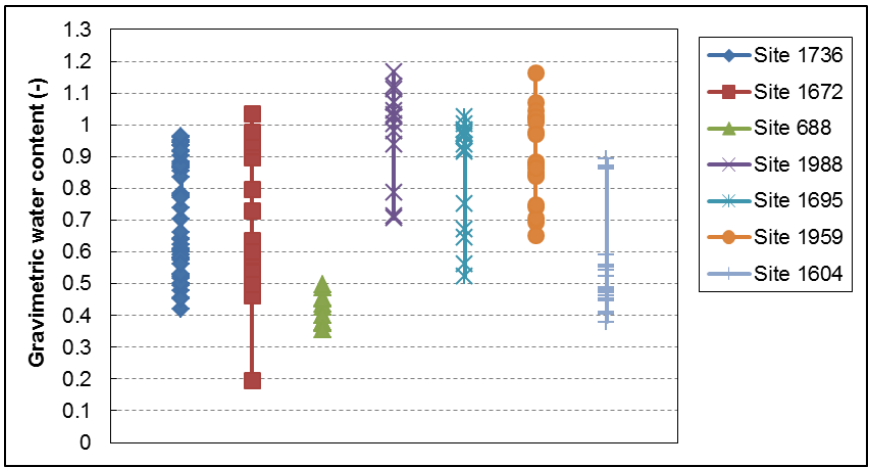

Figure 99: Comparing the gravimetric water content from each site.

5.2.2 Comparing the volumetric water contents from all sites.

Figure 100 shows the volumetric water content. This desribes the volume of water present per bulk volume of soil and ranges from 0.5 to 0.8. This means that the soil volume can conosist of up to 80% water.

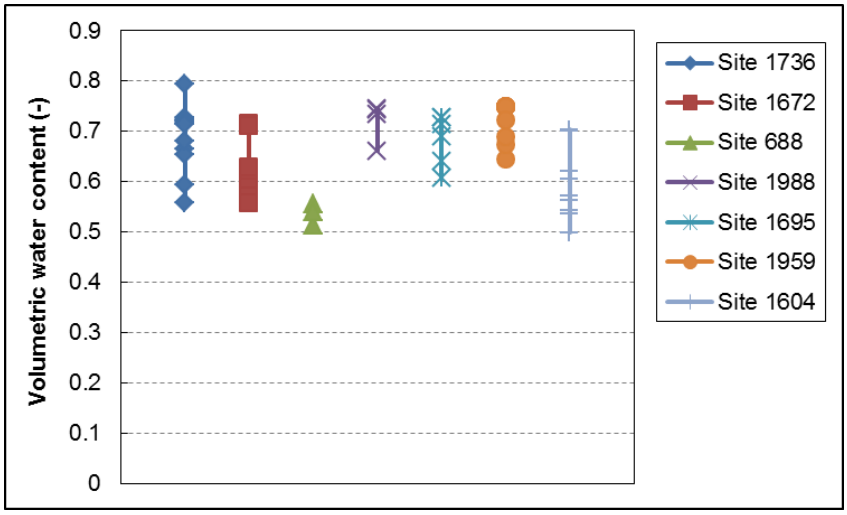

Figure 100: Comparing the volumetric water contents from each site.

5.2.3 Comparing all the liquidity index values from all sites

Figure 101 shows the liquidity index varying from almost 0 to 3. The liquidity index here is determined using the Atterberg limits and the natural water contents of all the tested samples. The samples are prone to a liquefaction if they have a liquidity index over 1 and are

suffuciently disturbed so that their sturcture becomes closer to that of the remoulded samples used for the determination of the Atterberg limits.

It can be concluded that there is a risk for liquefaction at sites 1736, 1672, 1988 and 1959 if a disturbance of the submarine deposits takes place. Site 1604 may have liquidity index values under 1, but all of the lqiuid limits are below the natural water content. This site also has a risk of liquifaction upon disturbance. Site 688 is the only site where no risk of liquifaction upon disturbance is to be expected based on both the liquid limits which are all below the natural water contents and based on the liquidity index which is always below 1.

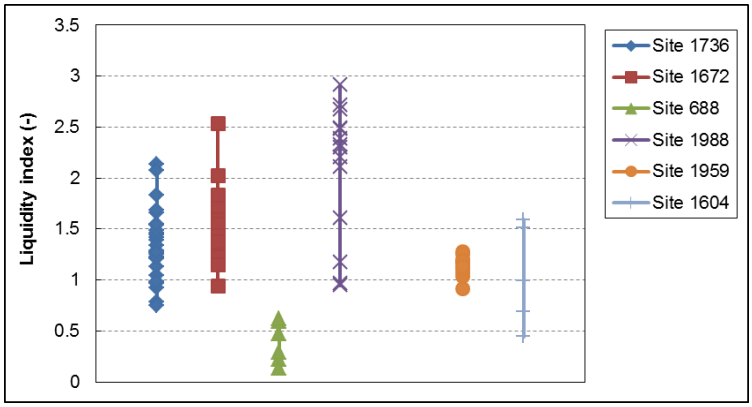

Figure 101: Comparing the liquidity index values for each site.

5.2.4 Comparing all the average particle denisty values from all sites

Figure 102 shows the average particle densities ranging from 2720 kg/m^3 to 2785 kg/m^3 across all of the sites. This corresponds to specific gravity values between 2.72 and 2.79. No siginificant difference in average particles density is found.

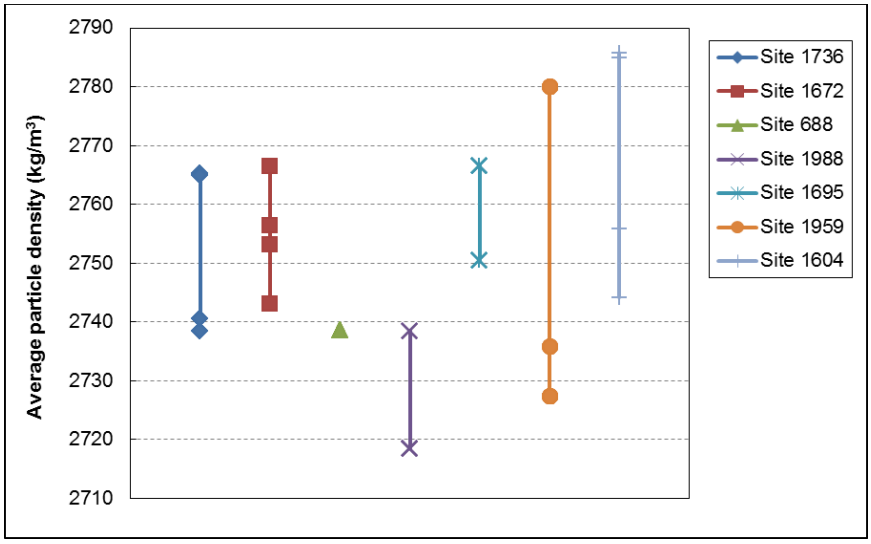

Figure 102: Comparing the average particle denisties for each site.

5.2.5 Comparing all the void ratios from all sites

Figure 103 shows the void ratio of all of the tested samples ranging from 1 to 3. This difference is big and can be explained by the widely varying clay, silt and sand contents and the normal streses that are present in-situ. The more sandy samples have lower void ratios than the more clayey samples. The reason for this may be the fining-upward sequences

which have been found. These show mainly an increase in content towards the seabed where lower normal stresses are occuring.

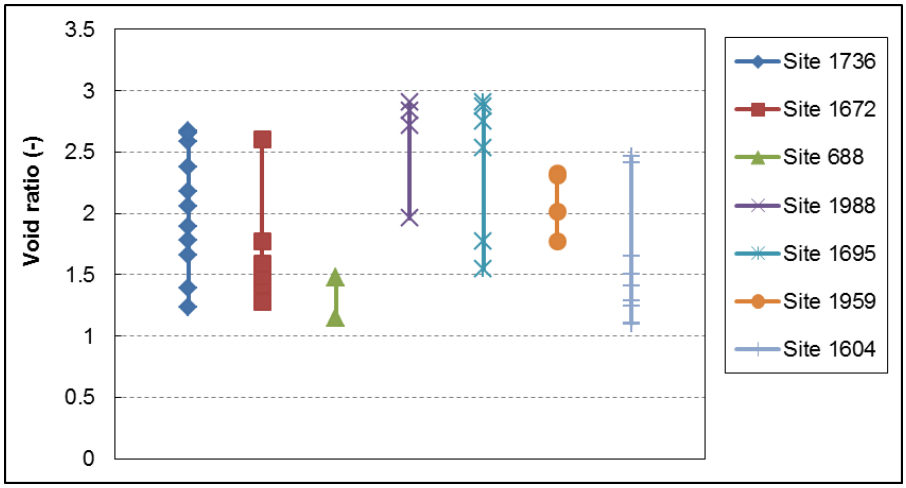

Figure 103: Comparing all the void ratio values for each site.

5.2.6 Comparing all the bulk volumetric weight values obtained from all sites

Figure 104 shows the bulk volumetric weight varying from 14 kN/m^3 to 18 kN/m^3.

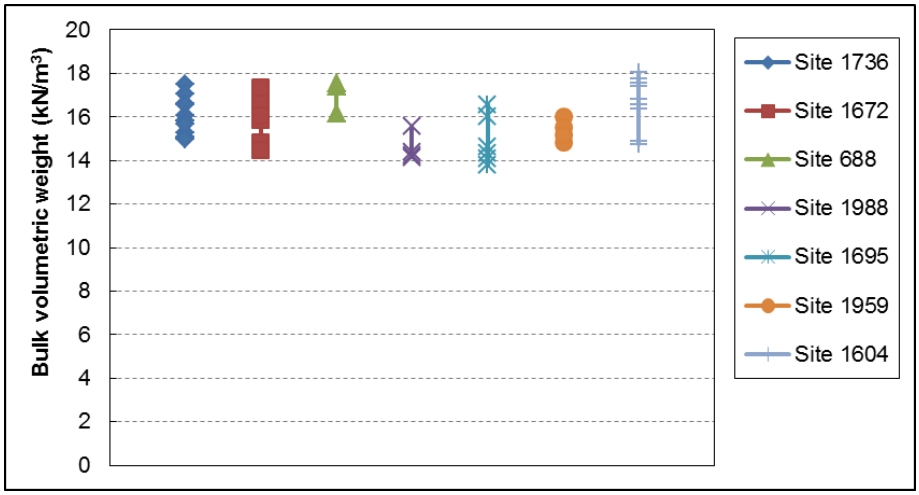

Figure 104: Comparing all the bulk volumetric weight values for each site.

5.2.6 Comparing all the dry volumetric weight values obtained from all sites

Figure 105 shows the dry volumetric weight varying from 7 kN/m^3 to 13 kN/m^3.

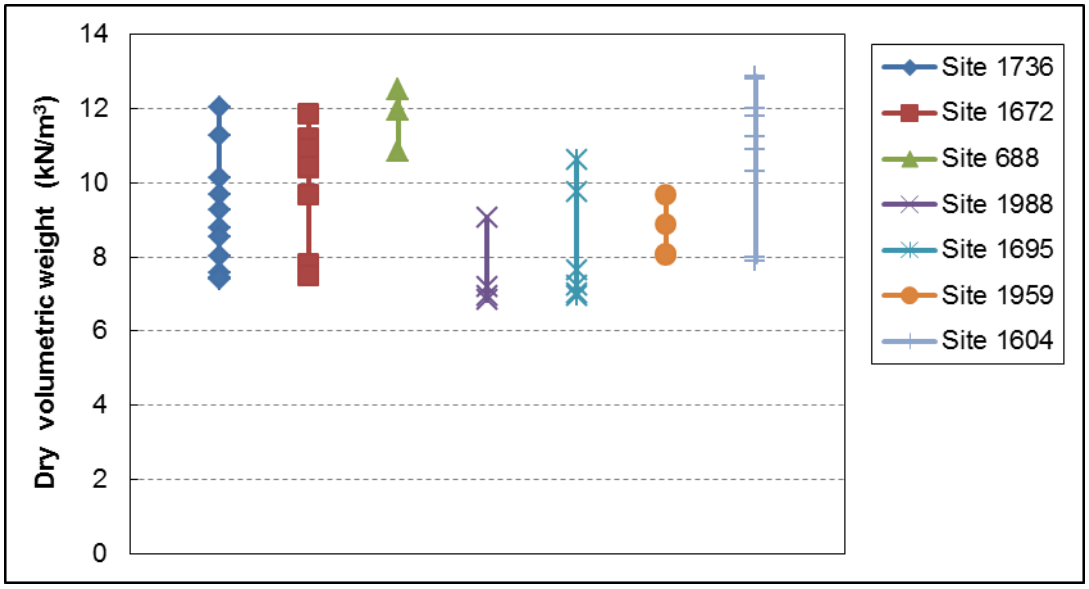

Figure 105: Copmaring all the dry volumetric weights found at each site.

5.2.7 Comparing all the clay content from all sites

The clay contents from all of the sites can be seen varying from 10% to 60% in Figure 106.

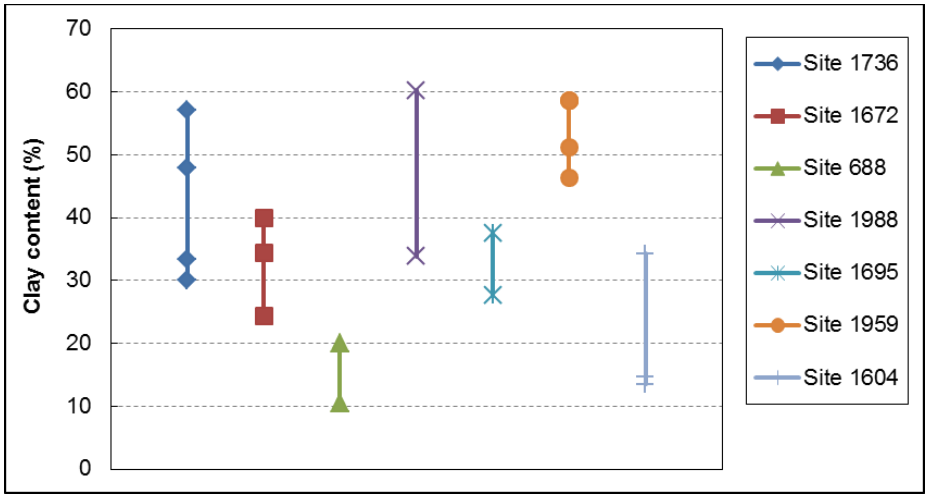

Figure 106: Comparing all the clay contents found at each site.

5.2.8 Comparing all the silt contents from all sites

The silt contents from all of the sites can be seen varying from 15% to 60% in Figure 107.

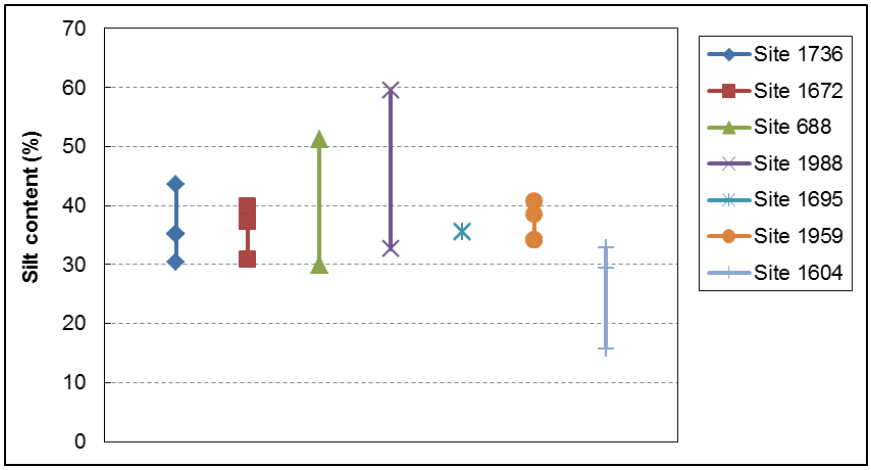

Figure 107: Comparing all the silt contents found at each site.

5.2.9 Comparing all the sand contents from all sites

The sand contents from all of the sites can be seen varying from 8% to 70% in Figure 108.

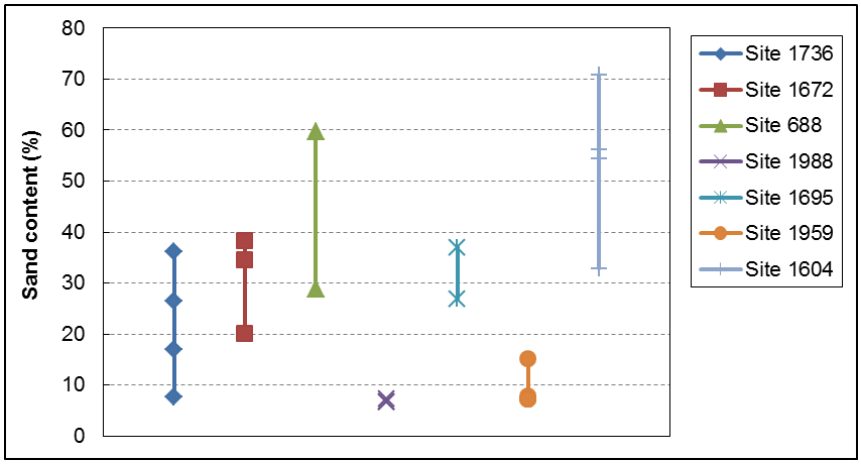

Figure 108: Comparing all the sand contents found at each site.

5.3 Comparing the behaviour and the undrained shear strenghts from all the direct shear tests

5.3.1 Comparing all the original unconsolidated undrained direct shear tests

All of the undrained shear strenght values from all of the original undrained unconsolidated direct shear tests have been compared in Figure 109. This shows that except for 1 sandy sample with a shear strenght of 10 kPa all the other samples have undrained shear strenghts between 3 kPa and 7 kPa. These tests occurred at a normal stress of 1.84 kPa which did not initiate consolidation.

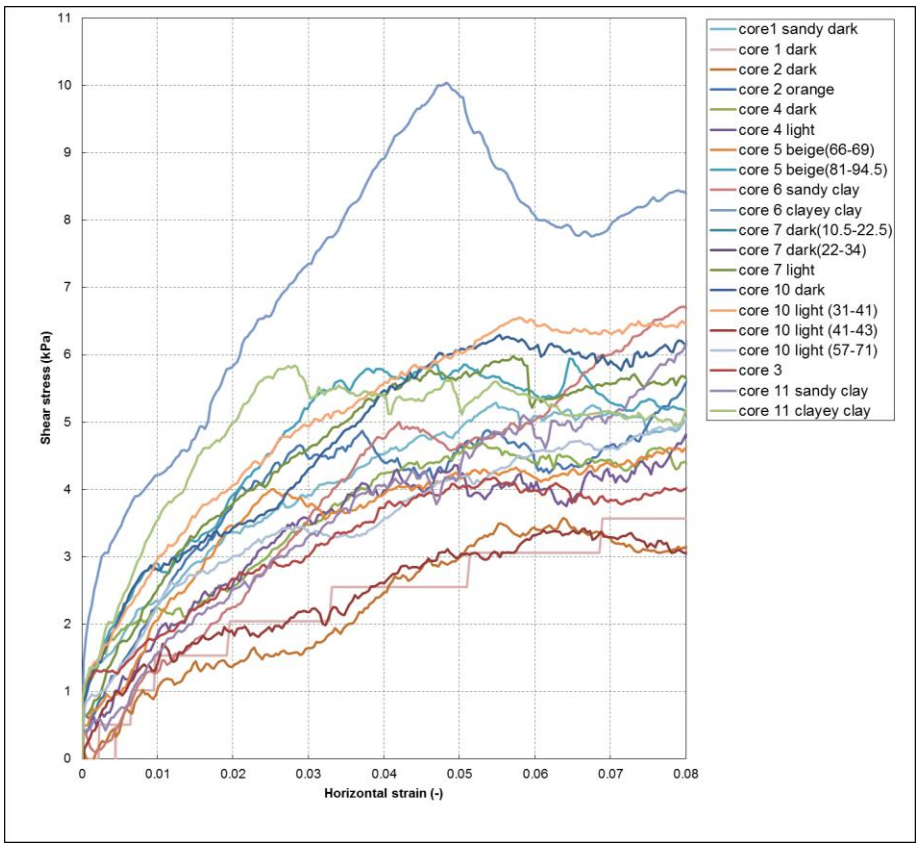

Figure 109: Comparing the strenght results from all the original UU DS tests.

In Figure 110 all of the volumetric strains of the original samples that were recored during the undrained unconsolidated direct shear tests are shown. This shows that most soil show a dilatory behaviour after having some contraction at the start of the test. This dilation behaviour can be explained by the presence of sand and silt. The only samples that don't show dilation are core 2 orange, core 2 dark and core 7 light. The weird anomaly present in the data of core 1 dark is due to equipment failure. This was the only UU DS test to be done in the shearbox in the main laboratory.

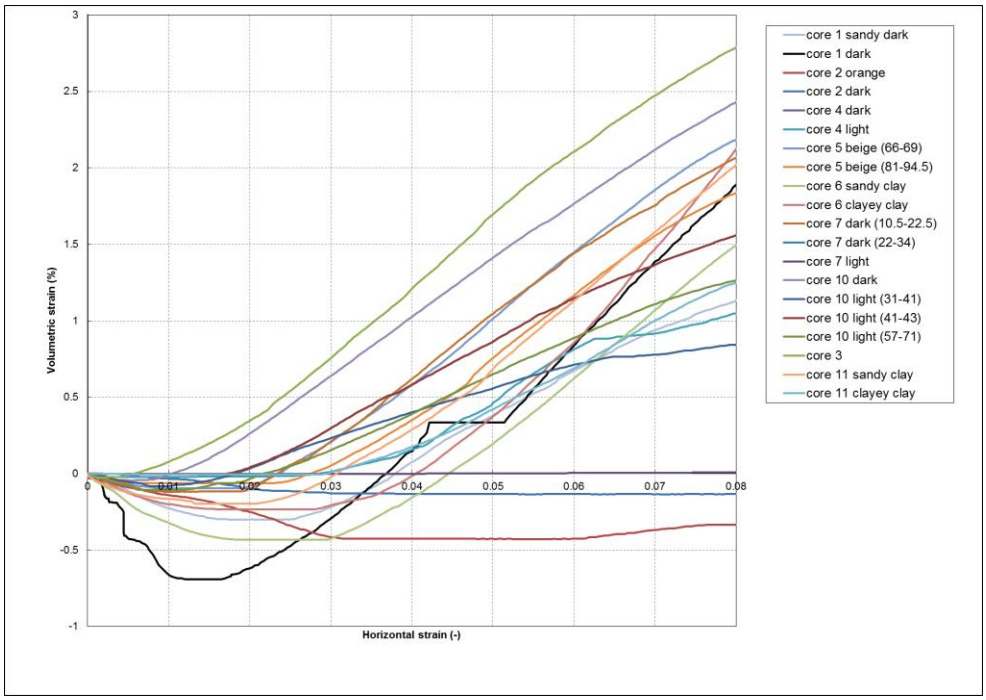

Figure 110: Comparing the soil behaviour from all of the original UU DS tests.

5.3.2 Comparing all the remoulded unconsolidated undrained direct shear tests

In Figure 111 the remoulded undrained shear strengths of the remoulded undrained unconsolidated direct shear tests are shown. The remoulded undrained shear strengths are ranging from 1 kPa to 6 kPa. Core 10 light (41-43) lost almost all of its strength possibly due to liquefaction.

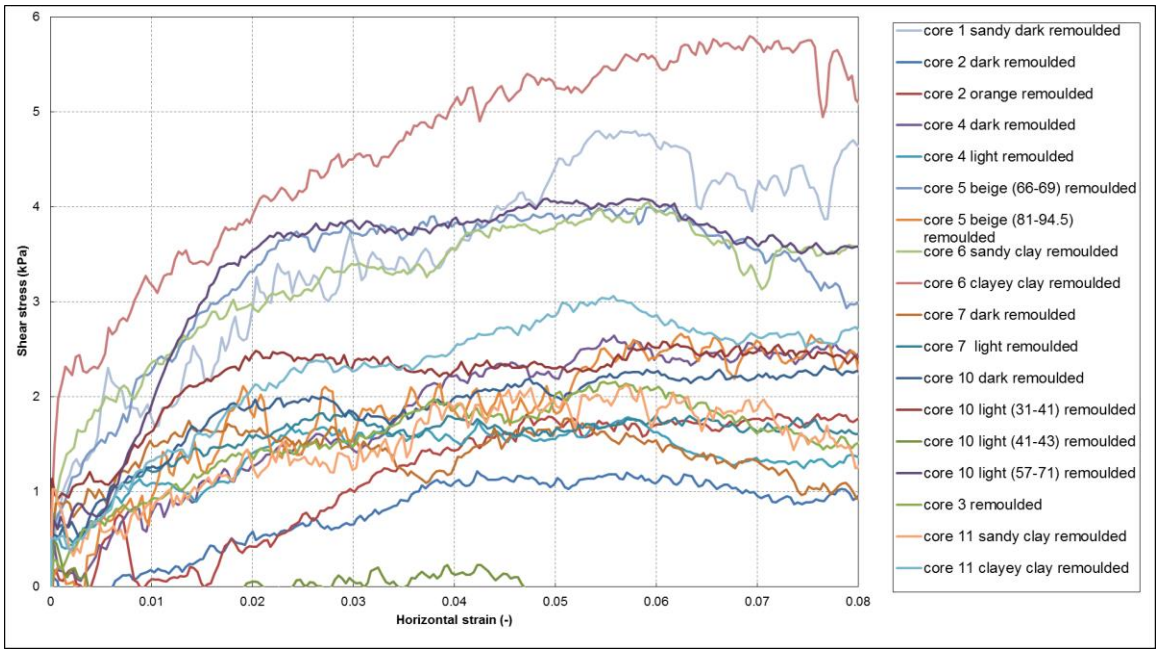

Figure 111: Comparing all the strenght results from all the remoulded UU DS tests.

A comparison of all the volumetric strains obtained is made in Figure 112. This shows that after remoulding most of the samples lose their dilatory behaviour and only show contraction behaviour. Core 5 beige (66-69), core 1 sandy dark, core 6 clayey clay and core 10 light (41-43) do still show dilatory behaviour. Core 10 light (41-43) has liquified in this test so this dilation data is not to be trusted. The other 3 cores all have a relatively higher sand content in common compared to the other samples.

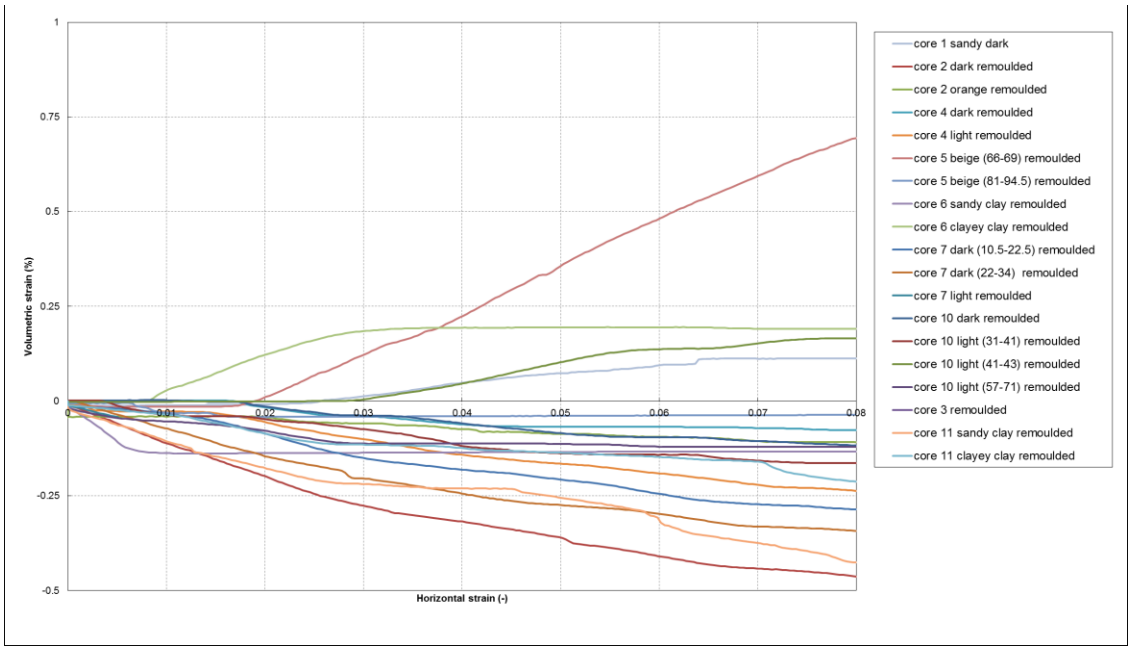

Figure 112: Comparing all the soil behaviours from each remoulded UU DS test.

5.3.3 Comparing all the original consolidated undrained direct shear tests

A comparison between all the undrained shear strengths obtained from the consolidated undrained direct shear tests are shown in Figure 113. This shows that from a normal stress of 30 kPa or higher the soil gains some significant amount of shear strength. Below the normal stress of 30 kPa, so under normal stresses of 3 kPa, 6kPa, 9kPa, 10 kPa, 15 kPa and 20 kPa the shear stress seems to remain at or below 10 kPa.

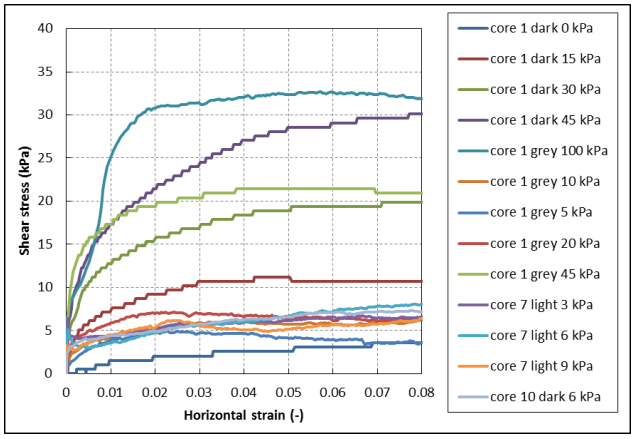

Figure 113: Comparing all the strenght results from all the original consolidated direct shear tests.

A comparison between all the original consolidated undrained direct shear tests is shown in Figure 114. This shows that all of the samples except core 7 light 3 kpa and core 7 light 6 kPa contract during shearing. The reason the two samples showing dilatory behaviour here would be due to the low normal stress applied. From this can be concluded that each sample requires a different level of normal stress before the sample starts contracting during shearing since core 1 grey at a normal stress of 5 kPa and core 10 dark at a normal stress of 6 kPa both show contraction compared to core the dilatory behaviour shown by core 7 light at a similar normal stress of 6 kPa.

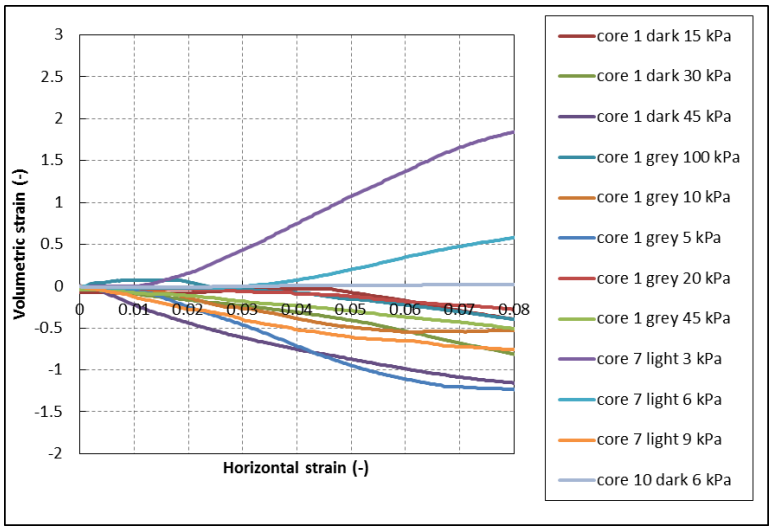

Figure 114: Comparing the soil behaviour from all the original consolidated undrained direct shear tests.

5.3.4 Comparing all the original consolidated draiend direct shear tests

The soil behaviour of these direct shear tests are displayed in Figures 115 and 116 showing mostly contraction behaviour. This is different compared to the unconsolidated direct shear tests which showed mainly dilation behaviour. This is also an important difference to take into account for slope failure since the sediments under low normal stress are likely to show dilation instead of contraction when sheared.

All of the drained direct shear tests results are compared in Figure. These tests were found to be not fully drained even though shear rates were applied according to their respective ISO standards. Their 'drained' shear strengths are between 8 kPa and 20 kPa for normal stresses at 10 kPa, 20 kPa and 30 kPa.

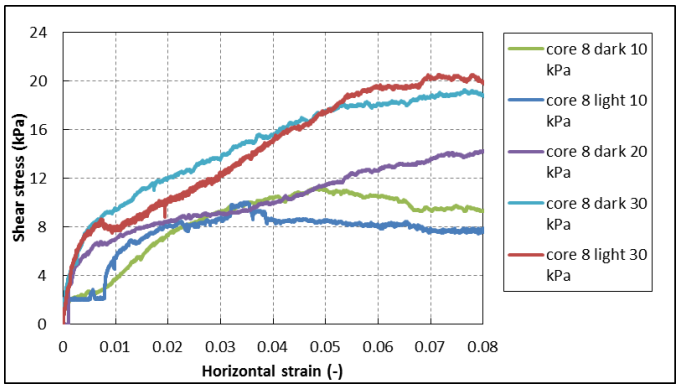

Figure 115: Comparing all the strenght results from all the original consolidated drained direct shear tests.

Figure.. shows that the behaviour of all the sediments present in core 8 under normal stresses from 10 kPa to 30 kPa is contractional.

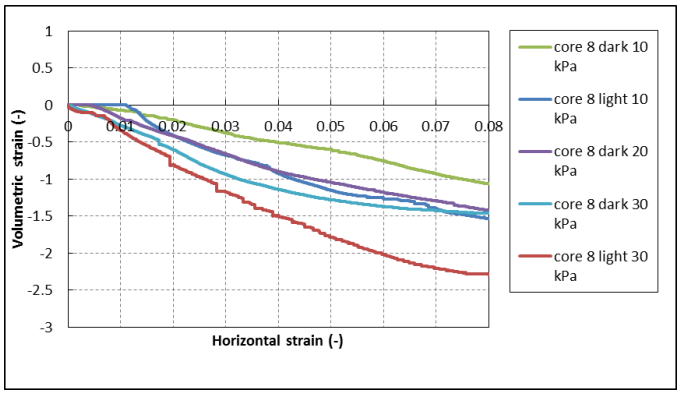

Figure 116: Comparing all the soil behaviours from all the original consolidated drained direct shear tests.

5.3.5 Comparing the remoulded consolidated undrained direct shear tests

A comparison between all the remoulded consolidated undrained direct shear tests is shown in Figure 117. These samples were remoulded from the non-dried original samples and show undrained shear strenghts between 8 kPa and 25 kPA under normal stresses between 15 kPa and 45 kPa.

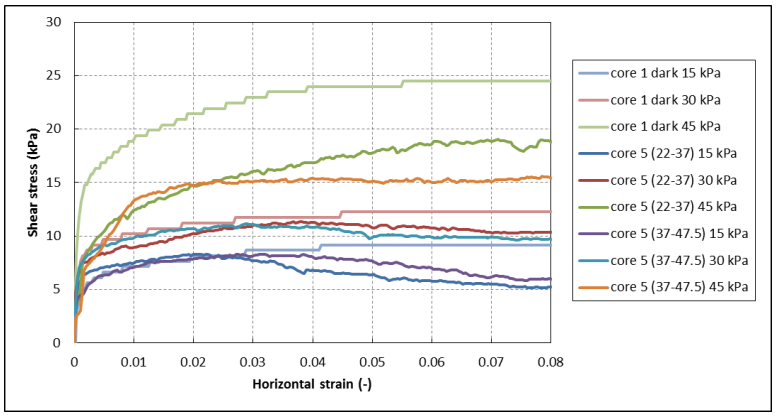

Figure 117: Comparing all the strenght results from all the original consolidated undrained direct shear tests.

The soil behaviour of all the remoulded samples of the remoulded consolidated undrained direct shear tests in Figure 118 all show contraction. Only core 5 (37-47.5) shows some dilation at the start followed by contraction. The samples from core 5 all have a higher sand content compared to the samples from core 1 dark.

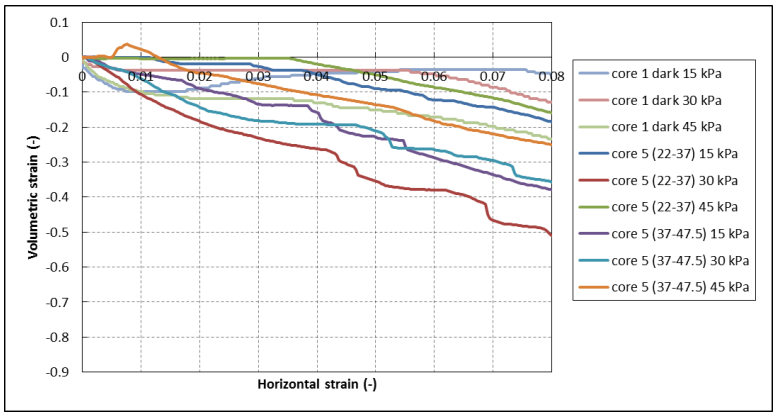

Figure 118: Comparing all the soil behaviours from all the original consolidated undrained direct shear tests.

5.4 Comparing all the undrained shear strenghts and sensitivity values obtained from fall cone testing, pocket vane testing and UU direct shear testing

5.4.1 Comparing the undrained shear strenghts from the UU DS tests, fall cone tests and pocket vane tests

Figure 119 shows all of the obtained undrained shear strenght estimates. These values have been obtained from the original and remoulded soil samples. The original undrained unconsolidated direct shear tests show values for undrained shear strenght between 2 kPa and 8 kPa whereas these same soil specimens show a remoulded undrained shear strength between 0 kPa and 5 kPa. The original fall cone tests show a much wider fluctuation in undrained shear strenght with values from 4 kPa to 33kpa. The remoulded fall cone tests show values of undrained shear strenght between 0 kPa and 4 kPa. The pocket vane tests show undrained shear strenght values between 5kPa and 22 kPa.

The pocket vane test was only done on the original samples. The pocket vane test together with the remoulded fall cone test and the remoulded direct shear test all show a trend of increasing undrained shear strength with decreasing water content. The original fall cone test and direct shear test do not show this trend clearly. There also seems to be a divide in the undrained shear strengths between the more sandy samples with lower water content and the more clayey samples with higher water contents (see Figure 119).

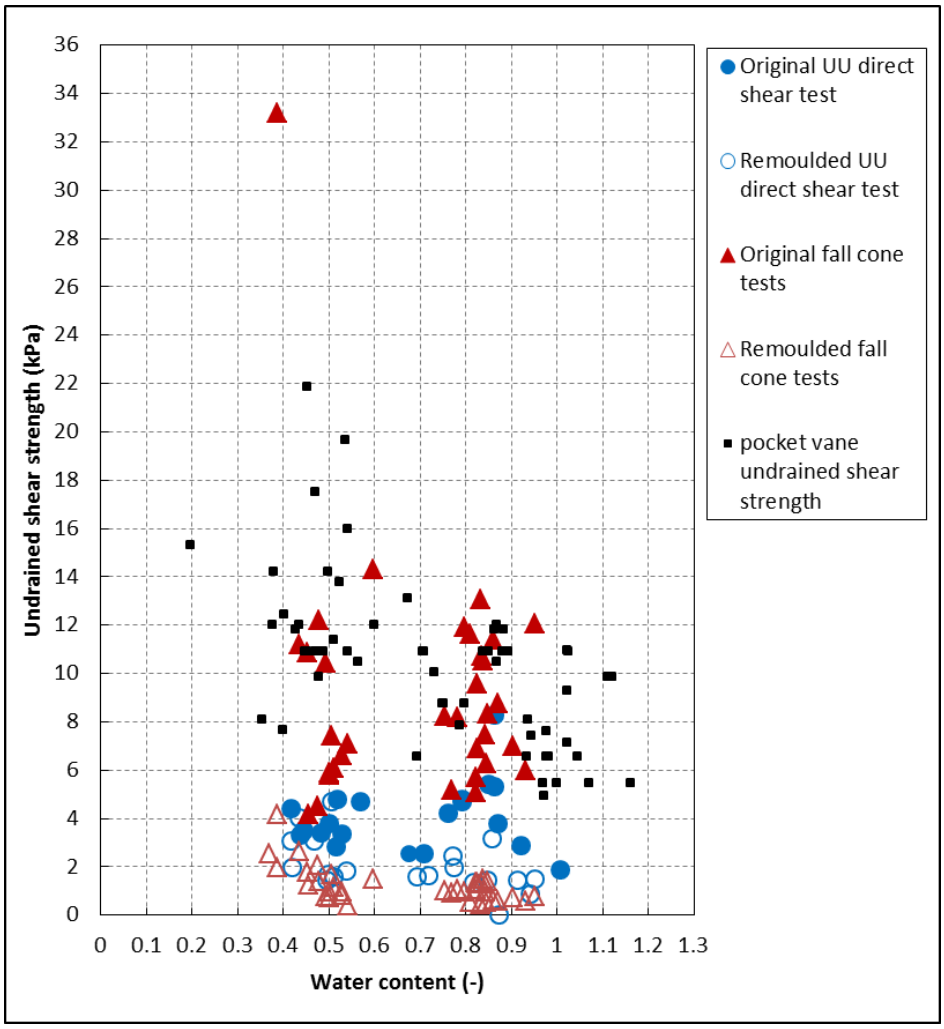

Figure 119: Comparing all the undrained shear strengths obtained from the UU DS tests, fall cone tests and pocket vane tests at all the sites.

The scatter that is present can be explained by the fact that samples from different cores will have a differing amount of clay, silt and sand in their soil fractions. Only in a few cases did show a higher strenght after remoulding.

The original pocket vane tests from Figure 119 show values of undrained shear strenght in the same order of magnitude as that of the oiginal fall cone tests. Both tests have higher values of undrained shear strenght than the undrained shear strengths obtained from the direct shear tests.

So for a slope stability analysis of the undisturbed sediments the values from the direct shear tests should be used since these tests are more precise than the index tests used. The other values can be used for a more general indication of undrained shear strenght.

It could however be argued that the faster failure mechanisms of the index tests represent a more undrained behaviour. This faster failure mechanism could be argued for the remoulded fall cone tests which give the lowest values of undrained shear strenght. In the case of the remoulded sediments the most conservative values are obtained by the results from the remoulded fall cone tests.

5.4.2 Comparing the sensitivity values from the UU DS tests, fall cone tests and pocket vane tests

The sensitivities of these tests will now be compared (see Figure 120). These sensitivties are obtained by comparing the undrained shear strenght of the original and remoulded samples. The remoulding used creates a soil with a different structure. This represents a disturbed soil and could represent the disturbed sediments in a submarine environment if they undergoe the same amount of distrubance. In reality the disturbance of the soil may be less so the obtained sensitivity values are exptected to be on the high side.

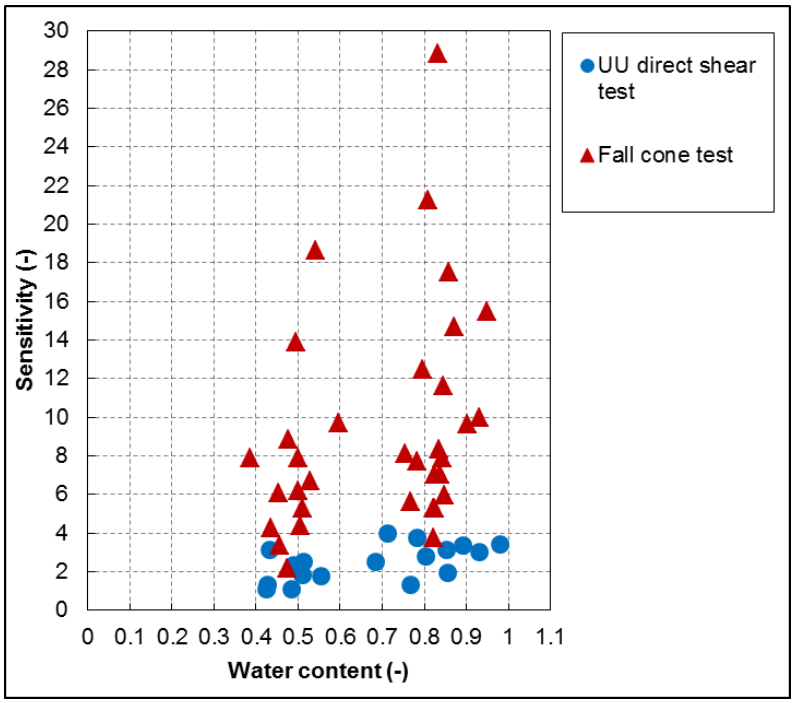

Figure 120: Comparing all the sensititivty values from all the sites obtained from UU DS testing and fall cone testing.

The sensitivities of the fall cone tests seem to be much higher than the sensitivities obtained from the direct shear tests. This is due to the different failure mechanisms occuring in each test, because in both tests the soil specimens were remoulded in the same manner. No sensitivities were obtained from the direct shear tests by looking at the peak and residual shear stress, because for almost all of direct shear tests showed no considerable reduction in shear strength as the strain increased. No clear variation outside of the normal variation of 0.3 kPa was detected in the UU DS tests. The sensitivities displayed are obtained by dividing the original soil strength by the remoulded soil strenght.

From Figure 120 it becomes obvious that the fall cone testing gave a lot of scattered data, so it it recommended to use the sensitivities obtained from the UU DS testing. These sensitivities show a clear trend where the sensitivity increases with water content. This trend is to be expected. However if offshore installations are used with conical shape foundations then it is recommended to also look at the sensitivity values from the fall cone tests, because of the similarities in geometry and the way the load is applied. One also has to keep in mind that Figure 120 is a generalization and at some sites a clear trend between the undrained shear strenghts obtained from the fall cone tests and the water content can be observed.

The sensitivity values obtained from the fall cone tests are between 2 and 28. The sensitivities obtained from the UU DS tests are between 0.5 and 4. The high sensitivity of the fall cone tests are found to be as much as 10 times higher than the field vane test and is attributed to the differences in remoulding method (Tanaka, Hirabayashi, et al., 2012). In the case of this thesis it seems more likley that the big differences in sensitivity and undrained shear strengths arise from the differences in failure mechanisms since the same remoulding methods were used.

5.5 Comparing all the obtained information in this report to outside literature

5.5.1 Correlating the organic matter content to the clay content

All the obtain values for SOM have been plotted against clay content in Figure 121. This shows correlation between increasing organic matter content and clay content. The organic matter that formed due to marine life in the past has clinged onto the clay particles. No such correlation silt and sand content was found. Also no clear correlation between the calcite content and clay, silt and sand content has been found.

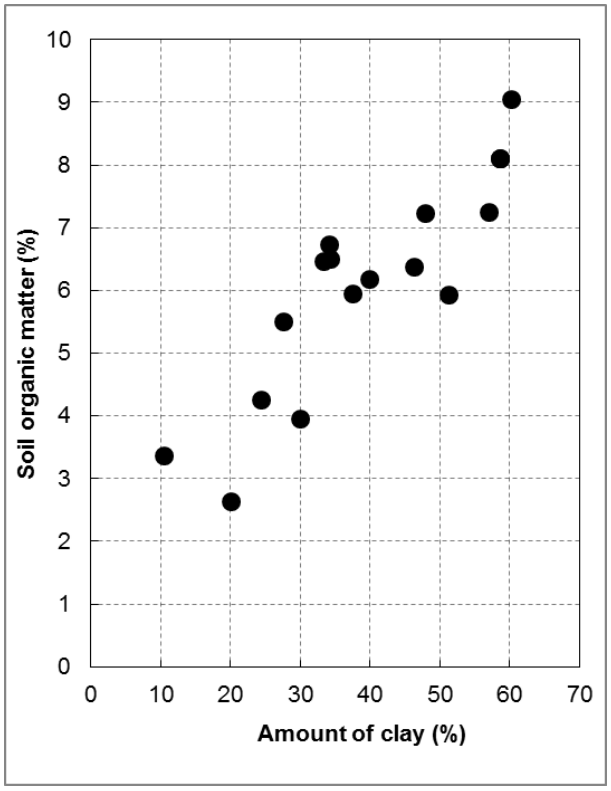

Figure 121: Displaying the correlation between the organic matter content and the clay content.

5.5.2 Information obatined from the description of the cruise report

The information that was provided at each site can be seen in Table 59. Site 1672 seems to have an undisturbed sea floor and at site 688 there is a risk of re-penetration. This means that the sandy intervals obtained from site 688 may be shorter than in reality due to the core having re-penetrated. Also the observation of stiff mud in the core catcher at site 688 is interesting since no dark stiff mud was found here. This may indicate a darker glacial deposit below the sediments found at site 688. The presence of glacial deposits will be explained more further on.

Table 59: Description of all the sites obtained from the CE14011 cruise report.

Site	Cruise report description
1736	stiff silt at the base
1672	southwest of the slide scar on the apparently undishturbed sea floor
688	below intra slide scarp, risk of re-penetration, muddy sand, dark stiff mud in core catcher
1988	-
1695	-
1959	-
1604	-

5.5.3 Comparing the types of sediments found and establishing the presence of glacial sediments below interglacial sediments

Research from (Georgiopoulou, Krastel et al. 2019) found severlal different types of sediments. Sediments such as light-coloured muds with a higher foraminifera content and darker muds with a lower foraminifera content together with fine to medium sand layers were found. Some deformed sediments were also found with deformations that could not be attributed to the disturbance due to gravity coring (Georgiopoulou, Krastel et al. 2019). Only some of these sediments were and could be found in the sediments investigated in this thesis due to the lack of a stratigraphic analysis.

These deposist were mostly found with a fining-upward sequence. Radiocarbon dating was done and it was determined that the light-coloured silty foraminifera-bearing muds were deposited during the current interglacial age and it was also found that the dark-coloured, mottled, foraminifera-poor, clayey mud was deposited during the last glacial age. The lighter and darker colour of these deposits are attributed to the differences in foraminifera content (Georgiopoulou, Krastel et al. 2019).

In this thesis the lighter and darker coloured muds together with layers of fine to medium sand was found. Site 1604 containens only fine to medium sand layers with a low clay content (<20%). This corresponds to what was found in (Georgiopoulou, Krastel et al. 2019), but here also a light-coloured mud layer was found on top. In both cases the sand layers were found in a fining-upward sequence.

Site 1695 has lighter coloured muds on top of darker coloured muds present. This corresponds to what was found in (Georgiopoulou, Krastel et al. 2019), but here also fine to medium sand layers were found together with clast-debrites. These clast-debrites are composed of clasts of multiple lithologies. The presence of the fine to medium sands was not found and the presence of clast-debrites could not be found since no stratigraphic analysis could be done.

Site 1672 has light-coloured muds on top of fine to medium sand. No comparable sediments were found in (Georgiopoulou, Krastel et al. 2019) in an area closeby.

Site 1736 has light coloured muds on top of darker coloured muds. This was also found present in the research from (Georgiopoulou, Krastel et al. 2019) in an area closeby.

No further comparable locations are present in the research of (Georgiopoulou, Krastel et al. 2019), so sites 688, 1988, 1959 and 1604 are not compared to specific locations. These sites

do contains the described ligher and darker coloured muds in sites 1988, 1959 and 1604 together with the fine to medium sand layers in sites 688 and 1604.

Comparing these findings from (Georgiopoulou, Krastel et al. 2019) to the research done in this report comfirm the presence of the darker muds and lighter muds. These lighter muds are found to have a higher calcite content and a higher organic matter content relative to the darker muds. This would indicate that the lighter coloured muds have been deposited during times were more life was present during the formation of the deposits. The calcite content measured is seen here as a representation of the amount of foraminifera shells which used to be life organisms. The organic matter content is seen as a general indicator of marine life, but is not used to distinguish interglacial from glacial deposits as the organic matter content is found to be dependent on the clay content (see Figure 121).

Not all sediments showed a clear difference in colours, so a review will be done for each site based on their calcite content. This together with the colour of the sediments if this colour is clearly visible will give an indication of what sediments have been deposited during the current interglacial age or the last glacial age. No exact borders between the glacial and interglacial deposits will be defined here since the resolution lacks. If in the future an exact border needs to be established then this could be done based on the calcite content coupled with the age of the deposits based on radiocarbon dating.

Interpolation could be done in between the calcite content values in order to obtain the depth at which the calcite content corresponds to the value that represents the glacial/interglacial border. This could only be done if exact values of calcite content can be coupled to exact values of depth instead of only being a relative indicator. The calcite content together with the colour of the deposits will be used as an indicator of the glacal and interglacial deposits.

The following analysis relating to calcite content and organic matter content will be done based on Figuress 122 and 123

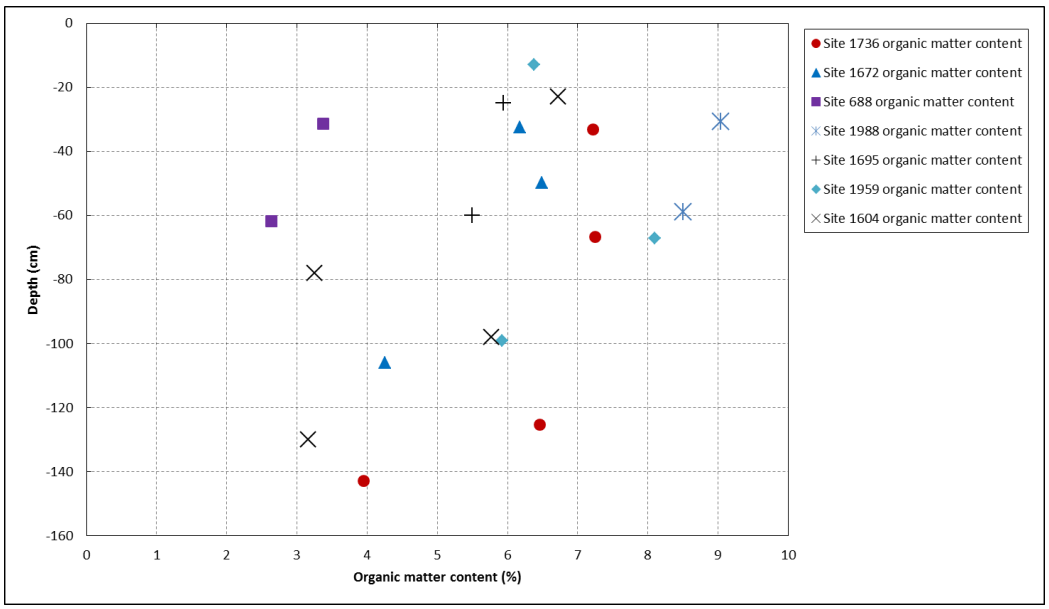

Figure 122: Comparing the organic matter contents from all sites.

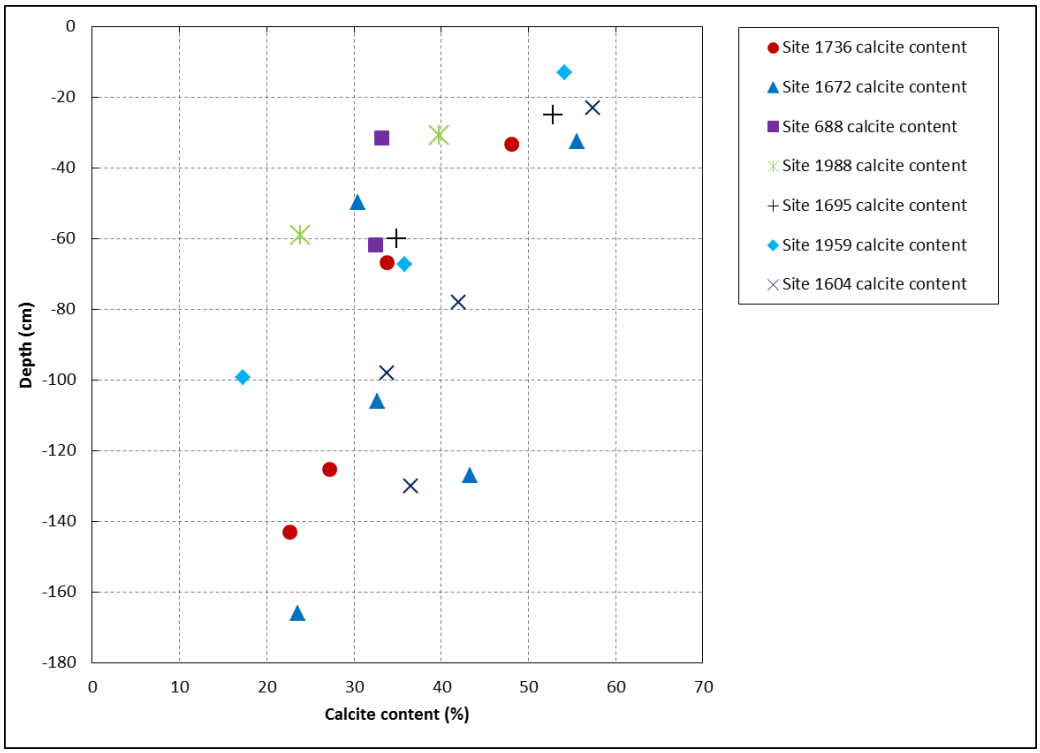

Figure 123: Comparing calcite contents from all sites.

Site 1736 shows a decrease in calcite content of from 48.1% to 22.7% (see Figure 124). the organic matter content decreases from 7.2% to 3.3%. This corresponds to the colour change. The colour of the bottom 97 cm of the deposits are found to have a clearly darker colour than the top 78 cm of the deposits which are light-coloured deposits (see Figur 124). At this site clear evidence is thus found for glacial deposits being present under the interglacial deposits.

Figure 124: Core 1 (lower part) on top and core 2 (upper part) at the bottom from site 1736.

Site 1672 shows a decrease in calcite content from 55.6% to 23.6%. The organic matter content decreases from 6.5% to 1.8%. The ligh grey coloured depoist on top are followed by the slightly darker beige deposits together with dark grey/greenish deposits (see Figure 125). The calcite content indicates a transition from the interglacial deposits towards the glacial deposits. This could be indicating that the bottom 1 m of sediments is partly from glacial deposits.

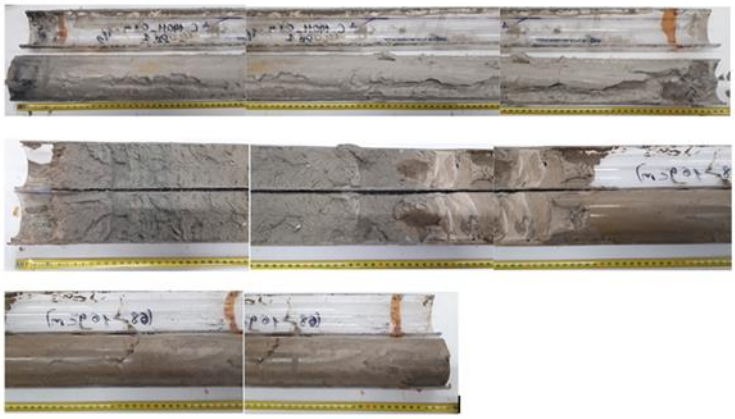

Figure 125: Core 4(upper part) on top and core 5 (lower part) at the bottom from site 1672.

Site 688 shows a decrease in calcite content from 33.1% to 32.5% with depth. The organic matter content decrease from 3.4% to 2.6%. A very slight darkening of the grey colour present is found with depth (see Figure 126). No conclusion can be drawn here about whether glacial or interglacial deposits are indiacted.

Figure 126: Core 6 from site 688.

Site 1988 has a decrease in calcite content from 39.7% to 15.9%. The organic matter content decreases from 9% to 8.5%. A light grey beige colour is found with a slight darkening towards the lower sediments (see Figure 127). An indication of glacials deposist below interglacial deposits is found here.

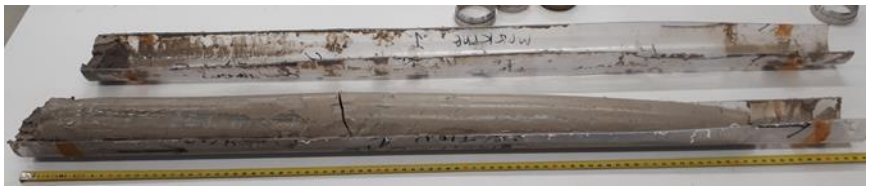

Figure 127: Core 7 from site 1988.

Site 1695 has a decrease in calcite content from 35.0% to 17.9%. The organic matter content decreases from 5.9% to 5.5%. Here 7 cm of darker muds were found on top of 60cm of ligher muds (see Figure 128). An indication of glacial deposist below interglacial deposits is found here.

Figure 128: Core 8 from site 1695.

Site 1959 has a decrease in calcite content from 54.2% to 31.9%. The organic matter content decrease from 35.9% to 17.3%. A clear colour change can be seen from light grey to a very dark grey at the bottom of the core (see Figure 129). In between a beige transition colour is found. An indication of glacial deposist below interglacial deposits is found here. The interglacial sediments are estiated to be 95 cm on top of 20 cm of glacial deposits. An indication of glacial deposist below interglacial deposits is found here.

Figure 129: Core 9 (upper part) on top and core 10 (lower part) at the bottom.

Site 1604 has a decrease in calcite content from 57.4% to 36.5%. The organic matter content decreases from 42.0% to 36.5%. The top 40 cm of sediments are light grey sediments covered in black oxide spots transitioning to darker beige coloured sediments followed by dark grey sands at the bottom where the core split open due to a lack of cohesion (see Figure 130). An indication of glacial deposist below interglacial deposits is found here.

Figure 130: Core 3(upper part) on the top and core 11 (lower part) at the bottom.

From this can be concluded that an indication of intergalcial deposits on top of glacial deposits is found at sites 1736, 1672, 1988, 1695, 1959. At site 688 there is no clear indication for this. No certainty can be given, because no radiocarbon dating was done, but based on the calcite content sediment colour an indication will be given. One should also keep in mind that the resolution of measurements in this research is not as good as that for a straigraphic analysis. This means that some aspects may be missed.

Figure 131 shows core 10 dark and core 10 light in a dried form as a clear example of the lighter grey and darker grey colours found.

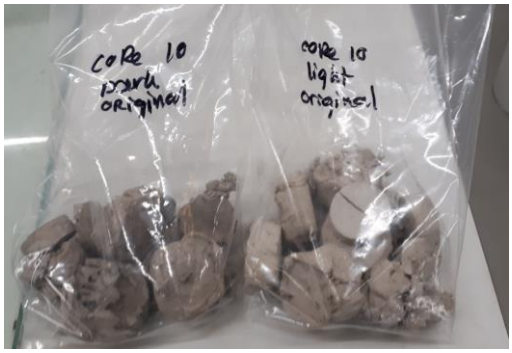

Figure 131: Example of darker and lighter coloured sediments from core 10 dark and core 10 light.

5.5.4 Discussing the possible presence of turbidity deposits

In this chapyer the possible presence of turbidity deposits will be discussed based on the soil the fining-upwards and coarsening-upward sequences found at all sites.

Both site 1736 and site 1959 have a coarsening upward-sequence on top of a fining-upward sequences starting from 70 cm depth and upward to 0 cm depth.

This may be the cause of multiple fining-upward sequences being present. This could not be detected since the resolution of this geotechnical research is less than that of stratigraphic research. One fining-upward sequence is found with one coarsening up-ward sequence on top.

This is more evidence for establishing the presence of multiple fining-upward sequences. If the soil is sampled from the two different fining-upward sequences then it could create a coarsening-upward effect since both deposits have the coarser particles at the bottom. One could for example sample the fine-grained part at the top and continue to sample at the bottom of another fining-upward sequence that is located closer to the seabed. These multiple fining upward sequences could be caused by two things.

The first being turbidity deposits. These deposits have been found to be present in the investigated area (Georgiopoulou, Krastel et al. 2019). Multiple turbidity deposits on top of each other would create the effect of two fining-upward sequences on top of each other. A turbidity deposit itself is defined by the Bouma sequence which has a fining-upward sequence consisting of 5 different types of deposits, but since no stratigraphic analysis was done in this research. The 5 different deposits could not be established. Therefore a fining-upward sequence in which clay content is increasing is chosen here as indication of a turbidity deposit.

The other cause could be sediments that have been reworked by thermohaline currents. Thermohaline currents are found to be present in the investigated area (Elliot, Shannon et al., 2010). These currents can rework the top sediments nearest to the seabed. The reworking of the top sediments could form contourite deposits. Contourite deposits are usually well sorted since they rework material that has already been deposited with for example a fining-upward sequence and thus tend to rework the more fine-grained part at the

top of this sequence. However since in this case the coarsening upward sequence has been found starting from a depth of 70 cm and going up to a depth of 0 cm it is found unlikely that this is the cause of reworking sediments. This does not exclude contourite deposits being present, but it excludes them from having caused this particular coarsening-upward sequence.

It was found by (Shanmugam, 2012) that no evidence is present for turbidity deposits being present exactly as they are described by the Bouma sequence since both the Bouma sequence turbidity deposits as well as the contourite deposits have not been fully replicated in laboratory experiments. Also the models for contourite facies present are fundamentally flawed (Shanmugam, 2012). This reasoning is used to justify for reducing the definition of turbidity deposits to fining-upward deposits. The Bouma sequence could still be present, but this was not analysed.

The most likely of the two will be the deposition of at least two turbidity deposits on top of each other, since all of the sites show a clear or general decrease in calcite content with depth. This calcite content is assumed to be mostly or all from the marine shells. These marine shells indicated the amount of marine life that was present at the time of deposition. These marine shells in the case of turbidity deposits would have been deposited somewhere upslope on the eastern slope of the Rockall Bank. These deposits would have failed, thereby producing a turbidity current with sediment suspended in the seawater. This turbidity current would have travelled to the current location of these deposits where first the sand particles would have been deposited followed by the silt and clay particles. These sand particles are found to contain a lot of marine shells in them by studying the sand fractions at each site location under the microscope, so even though the sediments are re-deposited they can still contain the same amount of marine shells as the original deposits contained.

From this assumption further estimations can be done about the thickness of the turbidity deposits. These thicknesses could be linked back to the volume of sediments that failed during past landslides. These deposits indicate at least two landslides. The first reason being the coarsening-upward sequence found at sites 1736 and 1959 which indicates the presence of at least two turbidity deposits. The second reason being the change in colour from light grey to dark grey which indicates the decrease in the presence of marine shells. The third reason being the calcite content that is found to decrease by 50% or more at some sites. A drastic change in calcite content is an indicator here for the transition from the current interglacial deposits to the last glacial deposits.

Another remark can be made about the velocity of the turbidity currents together with the distance from the actual landslide. Sites 1736 and 1959 which both show a clear indication of at least two turbidity deposits that have different sand contents. The sand content at site 1736 is found to be increasing from 8% to 17% towards the top in the top 70 cm. This corresponds to the sand contents found at site 1959 which also are found to increase from 7% to 15% towards the top in the top 100 cm. However at site 1736 at depths of 120 cm to 160 cm the sand content increases from 26% to 36% towards the top. This difference in the amount of sand present could be an indicator of two different landslides by the following reasoning. A higher velocity turbidity current will transport more coarser particles. This higher velocity turbidity flow could be coupled to distance between the landslide and the turbidity deposit. A greater velocity meaning of course a greater volume of landslide which generated a higher velocity turbidity flow.

If this indeed holds up it leads to the conclusion that the landslide(s) that took place during the last glacial age was either greater in volume than the landslide(s) that have taken place during the current interglacial or the location of the landslide was closer to the location of sites 1736 and 1959.

Evidence was found that a landslide D that occurred after landslide C (see Figure 132) had a very dilute landslide (Georgiopoulou, Krastel et al. 2019). Landslide deposits A and B are found to located much deeper below the surface the deposits C and D (Georgiopoulou, Krastel et al. 2019). From this can be concluded that the deposits found from all the sites are likely from slide C, with maybe a thin deposit from slide D on top. This could explain why the top deposits at site 1736 and 1959 have a lower sand content than the bottom deposits found at site 1736. This could be due to the more dilute turbidity flow from landslide D on top of the turbidity deposits of landslide C, but since landslide D was found to produce a very dilute turbidity flow the more likely explanation is that both turbidity deposits found at site 1736 and site 1959 are from landslide C. Turbidity deposits were found to be present in the deposits from landslide C and D (Georgiopoulou, Krastel et al. 2019). The oldest glacial deposits dated to be >46 years old still fall within the estimated age of 70 thousand years for landslide C (Georgiopoulou, Krastel et al. 2019). This could mean the glacial sediments found in this research are from landslide C.

The fact that multiple landslides took place at the eastern side of the Rockall Bank over a long period of time may indicate that this slope is inherently unstable (Georgiopoulou, Krastel et al. 2019).

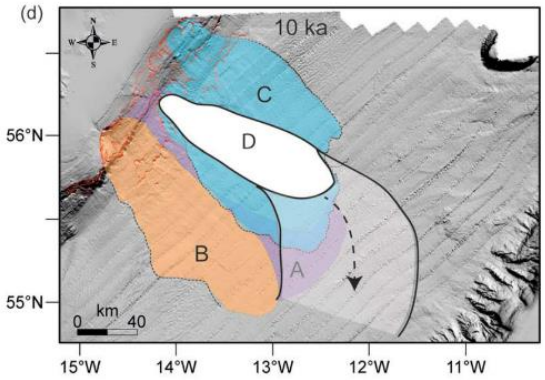

Figure 132: Landslide deposit D on top of the previously discovered landslides A,B and C. The encircled part of area D represents the dpositional area (Georgiopoulou, Krastel et al. 2019)**.**

Sites 1736,1988,1695,1959, 688 and 1604 all show fining-upward sequences (see Table 60).

Table 60: Overview of all the fining-upward and coarsening-upwards sequences found based on clay content.

Site name	Stratigraphy (based on clay content)	Turbidity deposit
1736	coarsening up-ward and fining-upward	Yes, at least 2
1672	fining-upward	Yes
688	fining-upward	Yes
1988	fining-upward	Yes
1695	fining-upward	Yes
1959	coarsening-upward and fining-upward	Yes, at least 2
1604	fining-upward	Yes

Sites 1736 and 1959 (see Table 60) also show a coarsening-upwards sequence on top of that which is assumed to be another fining-upward sequence. This leads to the conclusion that there is an indication of least 1 turbidity deposit present at all sites with site 1736 and site 1959 having an indication of two turbidity deposits present.

This presence of turbidity deposits is determined based on the clay content which increases or decreases with depth. This fining-upward sequence is thought to represent turbidity deposits. This can not be said with certainty, because no stratigraphic analysis was done in this research. The soil was destroyed as part of the determining the geotechnical properties of the soil and so no description of the layering could be made.

5.5.5 Comparing the mineralogy found in this thesis to the available mineralogical data from oustide sources.

The study from (Faugeres, Gauthier et al., 1981) found that the parent material of the Feni drift mainly consists out of basalt and trachyte with some intrusions of gabbro and Aegirine granite intrusions (Faugeres, Gauthier et al., 1981). Minerals indicating granite as parent material are found to be present in chapter 4.1. Therefore the parent material of the RBSC is likely located at the Rockall Bank area.

A high Muscovite to illite ratio was found in the carbonate oozes of the Feni drift (Faugeres, Gauthier et al., 1981). The Feni drift is a sediment transport drift located next to the Rockall Bank. An estimate of the mineralogy at site 1959 indicated that illite and smectite are both present, but the exact ratio was not established. A high muscovite to illite ratio present in carbonate ooze sediments would be an indicator of sediment formation during a period of high sea level rise (Faugeres, Gauthier et al., 1981).

An indication that the eastern slope of the Rockall Bank is inherently instable is given due to the several slope failures that have occurred in the past. Roughly every 10 000 years slope instability occurs (Georgiopoulou, Krastel et al. 2019). Mottled foraminifera-poor bearing clayey mud and magnetic susceptibility was found at the eastern side of the Rockall Bank (Georgiopoulou, Krastel et al. 2019). A mottled pattern on the sediments was also found in this thesis (see Figure) together with magnetic susceptibility that was found to be present in all of the sand fractions of all sites in differing quantities. This was however not quantified. The presence of magnetic particles was found in the dry sand fraction by holding a strong magnet above them. All the sand fraction from all sites seemed have some magnetic particles.

Figure 133: Mottled pattern on the side of core 5 (63mm in inside diameter) at site 1672.

This same mottled pattern as in Figure 133 was also observed at site 1959 on the lighter parts of core 9 and core 10.

5.5.6 Comparing geotechnical properties from sediments at the eastern flank of the Rockall Bank top geotechnical properties found at the eastern flank of the Rockall through

A comparison between the sediments present on the Rockall Bank slide complex and the eastern slope of the Rockall Through will be made by comparing the results from this thesis to the results from the Msc Thesis: A Geotechnical Study of the Eastern Flanks of the Rockall Through from 2004 by Eoin Wyse. This is meant to be a general comparison to see why the sediments on the eastern side of the Rockall through have not undergone multiple big volume landslides.

Eoin Wyse conducted an investigation into the shallow sediments on several locations along the eastern flank of the Rockall Bank. These sediments were obtained using gravity coring. The sediments were found to be carbonate rich sandy silts, sandy silts, silts and foraminifera sandy silts. These sediments had a specific gravity between 2.4 and 2.75, water contents mainly between 20% and 73%. The sediments were found to have medium to high plasticity. All sediments contained less than 13% clay. The sediments could generally be classified as coarse silts and fine sands. The natural water content was found to be close to the liquid limit and he liquidity index showed that when the samples are disturbed, little remoulded shear strength is left which makes a progressive slope failure more likely at least in the shallow sediments (Wyse, 2004).

The results from the sediments obtained from the RBSC located ate the eastern flank of the Rockall Bank are obtained from gravity cores in shallow sediments from 3 to 6 meters which returned around 1 m to 2 m of sediment and are classified as clayey SILT, silty CLAY and silty SAND. All of the samples tested contained a majority of silt and clay with the exception of samples from the lower half of the gravity cores from sites 688 and 1604 which contained more than 50% fine and medium sand. Foraminifera shells in the sand fraction were also found to be present in all cores. The gravimetric water contents ranged from 0.20 to 1.20. The specific gravities ranged from 2.72 to 2.79 and plasticity values were found to be medium to very high. Also remoulded undrained shear strengths determined by the fall cone test were found to be very low. This data comes from Table 61.

Table 61: Summarizing several properties of all the investigated sites from this research.

-	all sites
Gravimetric water content (-)	0.20 to 1.20
Volumetric water content (-)	0.5 to 0.8
Liquidity index (-)	0 to 3.0
Specific gravity (-)	2.72-2.79
Void ratio (-)	1.0 to 3.0
Bulk volumetric weight (kN/m^3)	14.0-18.0
Clay content (%)	10 to 60
Silt content (%)	15 to 60
Sand content (%)	8 to 70

When comparing these results to the results from this thesis it becomes clear that the sediments at the eastern flank of the Rockall through have generally lower water contents, less clay, more sand, specific gravities that are lower and a lower plasticity. The remoulded shear strengths were found to be on the low side on both side of the Rockall through.

These differences may explain why landslide(s) occurred on the eastern side of the Rockall Bank which formed the RBSC. Compared to the deposits along the eastern flank of the Rockall through the sediments on the eastern flank of the Rockall Bank have higher clay contents and higher water contents. Also the plasticity is higher and values of specific gravity of the particles are higher and have a more narrow range. A clear factor here seems to be the big difference in clay content and the higher water contents.

From this can be concluded that the more sandy sites present on the RBSC are less likely to fail. Sites 1736, 1672, 1988, 1695 and 1959 are thus more likely to fail than sites 688 and 1604 which contain more sand.

6 Effects of the obtained geotechnical properties on the strength parameters of sediments from the RBSC

6.1 Effect of the void ratio and Oedometer stiffness on the strength parameters

The void ratio varies from about 1 of the more sandy soils to about 3 from the more clayey and silty soils. The void ratio depends mainly on the grain size distribution and is found to decrease with depth. Figure 134 shows that at the same normal stress a difference in stiffness of about 100 kPa to 250 kPa is found. This difference is not big enough to prove the theory of slope failure due to differential compaction across the scarps from (Georgiopoulou et al. 2013).

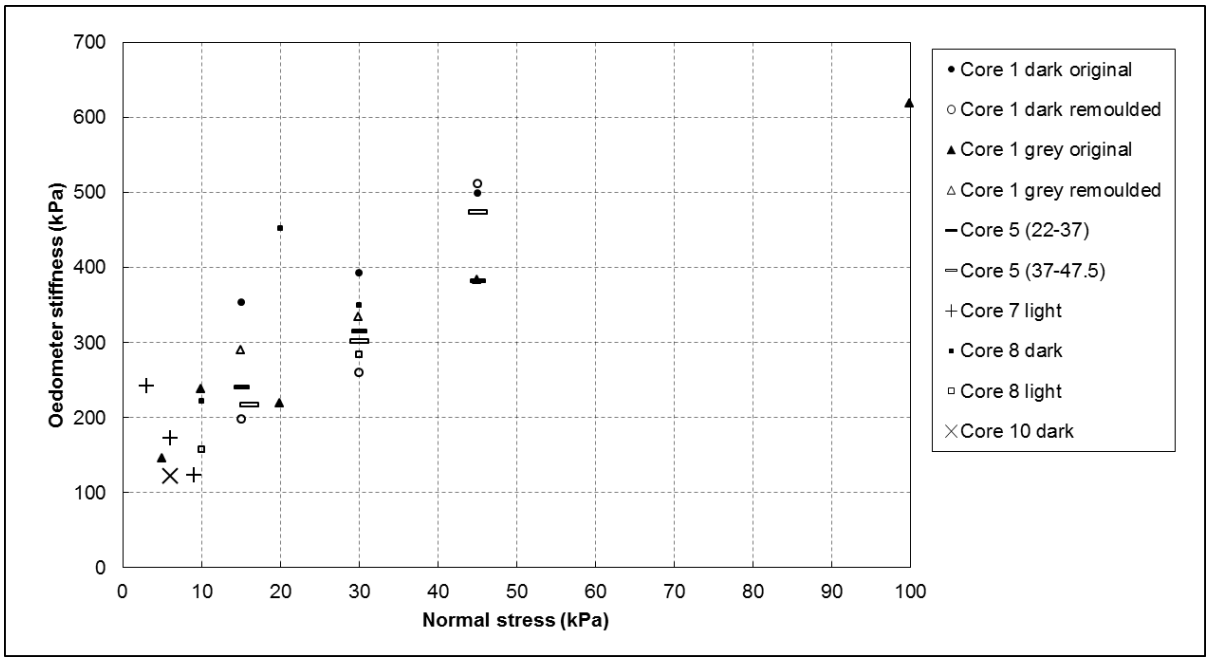

Figure 134: Comparing oedometer stiffnesses based normal stress.

6.2 Effect of the mineralogy on the strength parameters

The mineralogy that is present indicates that the soil is still in a weathering process in which the main process is the Illitization of the Smectite minerals. This is a slow process and will eventually change all the Smectite minerals into Illite minerals or Kaolinite minerals. This has an effect on the liquid limit which will decrease if all the Smectite have transforms into Illite and Kaolinite. This lower liquid limit causes an increased risk of liquefaction due to the high water content and lowered liquid limit which was found to be already below the natural water content in most cases.

This is a concern if the high water content sediments that are present do not consolidate and expel the pore water. This consolidation may not happen at all since the Rockall through is found to be sediment starved (Georgiopoulou, Shannon, 2013).

Insights into weathering rates under submarine conditions with high pH around 9.5 would need to be studied in order to couple a time scale to this process.

6.3 Effect of the grain size distribution on the strength parameters

Sediments from silty SAND, to clayey SILT and silty CLAY are found to be present on the RBSC. This creates possibilities for different failure mechanisms. The more sandy soils in general also show higher estimated undrained shear strengths. This is possibly because of the excess pore pressure that can escape faster than with the more silty and clayey soils. The more clayey and silty sediments will have a faster increase in excess pore pressure if a sudden load is applied due to a decreased hydraulic conductivity. These clayey and silty soils may thus be more prone to failure than the sandy soils if rapid sedimentation takes place, because this could create a sudden increase in pore pressure build-up. Also it is found that the more upslope sites 688 and 1604 have considerably more sand in their sediments than the more downslope sediments at sites 1736, 1672, 1988, 1695, 1959.

Erodability is also a factor influence by grain size distribution. The sediments with a low amount of clay have less cohesion. This may cause the more sandy deposits that have a low amount of clay them to be eroded faster than the sediments with higher clay contents. This erosion could take place by bottom currents or by focused fluid flow along basement-bounding faults (Georgiopoulou, Shannon, 2013).

There is a case here to say that if the more sandy sediments are present downslope together with more clayey sediments upslope the erosion could increase the slope stability. It could however also be the case that regardless of the grain size distribution erosion could take place due to a focused fluid flow in a specific area downslope. This focused fluid-flow is considered to have an important role in slope instability (Georgiopoulou, Shannon, 2013). In the case of rapid sedimentation the more clayey sediments are more unstable than the more sandy sediments.

This leads to the conclusion that erosion by bottom currents could erode certain parts of the slope faster than others and could thereby lead to slope instability. However it was found that downslope the sediments become higher in sand content. This would mean that erosion likely takes place higher up on the slope near seabed levels of around 688m to 1604m below sea level. Clays and silts have been found to be present in increased presence on the parts of the slope with seabed levels from 1736m to 1988m below sea level on the RBSC. These sediments are prone to liquefaction due to an increased sediment supply. This is not a major concern since the Rockall though is found to be sediment starved (Georgiopoulou, Shannon, 2013).

6.4 Effect of the fossil fraction on the strength parameters

A lot of Foraminifera fossils were found to be present. These consist mainly out of planktonic foraminifera. An increased presence of these marine shells present in the soil could increase the shear strength of the sediments. Also the possible dissolution and re-precipitation of the marine shells could strengthen the sediments. If this occurs then the already present

particles could be cemented to each other. The difference angularity of the marine shells themselves may become a factor. Figure 135 shows the two most occurring marine shells. These show a clear difference in angularity. The marine shell on the left is more rounded than the one on the right. If the percentage of marine shells present is high and it contains more rounded shells than sub-angular shells then it could cause a decrease in internal friction angle.

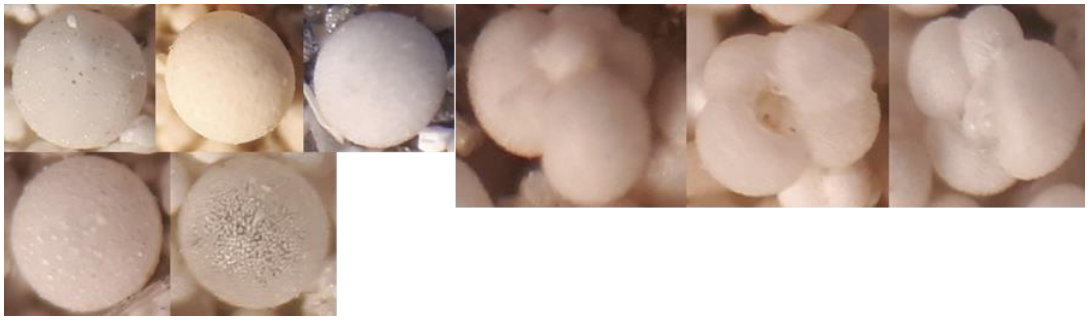

Figure 135: Images of the most occuring fossils in the fossil fraction (100µm to 300µm).

6.5 Effect of the organic matter content on the slope stability

The organic matter content (SOM) is thought to mainly come from the foraminifera shells or preserved faecal matter from organisms. This organic matter content is thus thought to not be present in the form of fibres which could increase the shear strength of the soil. Thus the organic matter content is thought to not influence the slope stability in any significant manner. Also no significant change in organic matter content was present to justify increasing strength even if the organic matter is present in fibre form.

7 Conclusion

7.1 What are the geotechnical properties of the landslide deposits on the Eastern slope of the Rockall Bank and what is their full geotechnical classification?

Geotechnical properties such as gravimetric water content, volumetric water content, bulk and dry volumetric weight, average particle density, saturation, void ratio, undrained shear strengths, sensitivities, dilation angles, oedometer stiffness, Atterberg limits, mineralogy, grain size distributions, SOC content, SOM content, calcite content, sand content, silt content, clay content and activity have been obtained. These values vary depending on the tested samples. They vary from location to location and from interval to interval.

The full geotechnical classification of the sediments present is from inactive to normal soil, from calcareous to very highly calcareous soil, from low to medium organic soil, from silty SAND to clayey SILT and silty CLAY, from medium to very high plasticity, from extremely low undrained shear strength to very low undrained shear strength, from low to medium sensitivity, gap-graded and well graded grain size distributions are also found.

The gravimetric water contents are found to range from 0.20 to 1.18, the volumetric water contents range from 0.50 to 0.80, a liquidity index from 0 to 3, specific gravities from 2.72 to 2.79, void ratios from 1 to 3, bulk volumetric weights from 14 kN/m^3 to 18 kN/m^3, dry volumetric weights from 7 kN/m^3 to 13 kN/m^3, clay contents from 10% to 60%, a silt content of 15% to 60%, a sand content from 8% to 70%, calcite contents from 17.3% to 57.4%, organic matter contents from 2.6% to 9.0%, liquid limits from 0.40 to 0.82 and plastic limits from 0.23 to 0.49.

The undrained shear strength for the original and remoulded sediments from the UU DS tests at a normal stress of 1.84 kPa is found to range from 2 kPa to 8 kPa and from 0 kPa to 4 kPa. The undrained shear strengths from original and remoulded sediments from the fall cone test range from 4 kPa to 33 kPa and from 0 kPa to 4 kPa. The undrained shear strengths from the original pocket vane tests range from 5 kPa to 22 kPa. The sensitivities of the sediments measured by the fall cone tests are found to range from 2 to 28 and the sensitivities obtained by direct shear testing is found to range from 0.5 to 4.

From these undrained shear strength values the conclusion can be drawn that undisturbed sediments are more likely to fail in a direct shear test failure mechanism whereas the disturbed remoulded sediments are found to fail more likely in a failure mechanism representing that of a fall cone test.

7.2 What are the mineralogical properties of the sediments present and what could be their parent material?

The non-phyllosilicate minerals that are present are Smectite, Illite, Muscovite, Chlorite and Kaolinite. The phyllosilicate minerals that are present are Quartz, Alakali feldspar, Plagioclase, Calcite, Ankerite, Siderite, Anatase, Rutile, Hematite, Pyrite, Halite and Apatite. This mineral composition can be logically explained by their possible weathering paths and indicates that the possible parent material is Monzogranite type 2 also called Muscovite-metagranite. Magnetic particles are found to be present. The Smectite minerals are the only clay minerals present that are swelling minerals. The calcite that is present is assumed to all come from the marine foraminifera shells that are found to be present by a microscope study.

7.3 How do these geotechnical properties compare to geotechnical properties from the same or similar areas obtained in previous research?

The lighter coloured and darker coloured silty CLAYS and clayey SILTS and fine to medium silty SANDS that are found to be present on the RBSC have also been found in the research of (Georgiopoulou, Krastel et al. 2019) withing a 1 km radius. The darker sediments and the lighter sediments are found to be glacial and interglacial sediments (Georgiopoulou, Krastel et al. 2019). These colour difference are attributed to the low and high amount of foraminifera shells present. Magnetic particles are found to be present in the sediments studied in this thesis as well as in the sediments studied in (Georgiopoulou, Krastel et al. 2019). At sites 1736, 1672, 1988, 1695, 1959, 1604 interglacial sediments were found on top of glacial sediments. At site 688 no evidence was found of glacial deposits being present, but interglacial sediments were found to be present.

At all sites fining-upward sequences and at sites 1736 and 1959 also a coarsening-upward was found to be present. This is taken as an indication that at all sites turbidity deposits are present and at sites 1736 and 1959 at least two turbidity deposits are present. Contourite deposits could also be present, this could however not be confirmed since no stratigraphic analysis was done.

A comparison of the geotechnical properties of the sediments obtained in this thesis from the eastern side of the Rockall Bank with the geotechnical properties obtained from the eastern side of the Rockall through from the research of (Wyse, 2004) is as follows. It was found that the most important differences between the sediments are the differences in water content and clay content both of which are much higher on th eastern side of the Rockall Bank. This leads to the conclusion that sediments present at sites 1736,1988, 1695, 1959 and the top 1m of sediments from site 1672 are more likley to fail than the sediments with much higher sand contents and much lower water contents at sites 688, 1604 and the sediments from a depth of 1m to 2m depth from site 1672.

The possibility of liquifaction upon disturbance is found at sites 1736, 1988, 1695, 1959, 1672 and 1604. Only site 688 has no risk of liquifaction upon disturbance.

7.4 How could all of these properties affect the strength parameters of the shallow marine sediments deposited on the eastern slope of the Rockall Bank?

A long term instability due to the weathering of Smectite minerals to Illite and Kaolinite minerals is proposed. This reduces the liquid limit and thereby increases the risk of liquefaction if the sediments retain their water contents. This is found to be possible since there is a low amount of sediment supply for the Rockall through (Georgiopoulou, Shannon, 2013).

The erosion erosional resistance is found to be lower of the upper slope sediments with seabeds located at 688m and 1604m below sea level due to the increased amount of sand and decreased amount of clay present. This reduces the overall cohesion of the sediments and makes it easier particles to be eroded way. The lower sediments found with seabeds located at 1736m, 1674m, 1988m, 1695m and 1959m below sea level are found to be more prone to liquifaction due to excess pore pressure generation due to the lowered hydraulic conductivty due to the increased clay contents.
The cause of this liquefaction due to excess pore pressure generation could be due to a supply of sediments, but this is unlikely since the Rockall thourgh is found to be sediment starved (Georgiopoulou, Shannon, 2013).

The presence of the foraminifera shells is considered to cause an inccrease in the shear strength and the internal friction angle. An increased presence of these shells would cause a greater internal friction angle of the sediments since these shells are of the sand fraction. Dissolution and re-precipitation of these shells can also take place. This would create a cementation effect by cementing the already present particles in a calcite cement. Also an increased amount of the rounded foraminifera shells realtive to the less rounded foraminifora shells could cause a decrease in internal friction angle.

The organic matter content is considered to not have an influence on the strenght paramers of the sediments since the organic matter considered to not be present in fibre form and in any significant quantitiy to become governing in the soil behaviour. This organic matter content likley comes from preserved feacal matter from organisms or from the foraminifera shells.

The failure mechanims that are considered to be a probable or improbable cause of future landslide faliures based on the geotechnical properties obtained from the sediments from the eastern side of the Rockall Bank are as follows.

Possible slope failures in the future due to bottom currents eroding parts of the lower slope and contuorite deposits found to be present by (Elliot, Shannon et al., 2010) are found to be probable, because sediments containing widely ranging clay and sand contents are found to be present in this thesis. This creates a difference in erodability of the sediments. Also high water content sediments are found to be present which could be partly contourite deposits. These high water sediments are found to have high void ratios of up to 3 which causes these sediments to have an increased danger of liquefaction since the liquid limit is below the natural water contents.

Possible slope failure in the future due to only the differential compaction suggested by (Georgiopoulou, Shannon et al., 2013) is not found to be probable to cause slope failure based on the oedometer stiffnesses of the sediments present at the eastern slope of the Rockall Bank. These differences in stiffnesses found of the sediments at sites 1736, 1672,

1988 and 1959 are found to be 100 kPa to 250 kPa. In geotechnical terms these sediments do not vary drastically in stiffness.

It is also suggested by (Georgiopoulou, Krastel et al., 2019) that the two most recent landslides could have been from seismicity from isostatic rebound. This is found to be a probable failure mechanism due to very high water content and high clay content sediments being present.

7.5 Summary

The geotechnical investigation of the sediments from each of the 7 locations located at the eastern flank of the Rockall Bank proved useful and allowed for answering what geotechnical properties of the sediments are present and how these sediments could be classified. Also the mineralogical properties of the sediments became known together with an indication of the possible parent material and with possible weathering paths for all the minerals found present. Also comparable sediments are found closeby together with the indication of turbidty deposits being present. The connection between the soil properties and the strenght parameters is also made. All this is then used to confirm or deny some of the proposed failure mechanisms in outside literature.

8 Recommendations

- A further more detailed study of counting and identifying the marine shells present in the sand fraction. This should be done in a quantitative manner in order to obtain better estimates of the depth of sediment deposition. The marine shells could be separated from the crystals in the sand fraction based on density, but this is not necessary. The marine shells can be seen using a microscope which illuminates the shells from the top. The sampling method of these shells should also be taken into account since the sediments are found to have turbidity deposits in them. It would be good to take into account the different types of deposits present when sampling.

- Visual microscope spectometry could be done on the rock fragments, crystalline sand particles and marine shells present in the sand fraction in order to obtain the mineralogy. Thin glass plates with certain sand fratcions in between would have to be preapred for this. The marine shells could be excluded from the sand fraction using sulphuric acid, but this is a time consuming task and may dissolve some of the minerals present so it is recommended to keep the marine shells in the sand fraction for the microscope spectometry. Further X-ray diffraction testing is recommended to see what clay minerals are present. So at least one X-ray diffraction test should be done on only the < 63µm fraction in order to find the specific clay minerals present of each mineral group. It is recommended to take at least one sample from the light-coloured muds and one sample from the dark-coloured muds since these two types of deposits represent the interglacial and glacial deposits. In thesis the results of an X-ray diffraction test are already present from core 10 dark which is a dark-coloured mud.

  The interest here would be to dermine if the same types of minerals are present in all sediments together with the source of these minerals. Think of parent material

- A full slope stability analysis could be done based on the data from this report. A study could be made about what failure mechanisms are more likely to occur at a certain site with keeping the local geometry in mind together with the shear strength and likely failure mechanisms described in this report. Fitting soil behaviour models could be picked based on the geotechnical characterization of the sediments in this thesis.

Bibliography

Here a list of all the used literature is published.

Georgiopoulo, A., Krastel, S., Finch, N., Zehn, K., McCarron, S., Huvenne, V.A.I., Haughton, P.D.W., Shannon, P.M., 2019. On the timing and Nature of the Multiple Phases of Slope Instability on Eastern Rockall Bank, Northeast Atlantic. Geochemistry, Geophysics, Geosystems, 20. https://agupubs.onlinelibrary.wiley.com/doi/abs/10.1029/2018GC007674

Jensen, J.L., Christensen, B.T., Schjønning, P.S., Watts, C.W., Munkholm, L.J., 2018. Converting loss-on-ignition to organic carbon content in arable topsoil: pitfalls and proposed procedure. European Journal of Soil Science, 69, 604–612. https://doi.org/10.1111/ejss.12558.

Elliot, G.M., Shannon, P.M., Haughton, P.D.W., Øvrebø, L.K., 2010. The Rockall Bank Mass Flow: Collapse of a moated contourite drift onlapping the eastern flank of Rockall Bank, west of Ireland. Marine and Petroleum Geology 27, 92-107.

Evans, D., Harrison, Z. Shannon, P.M., Laberg, J.S., Nielsen, T., Ayers, S., Holmes, R. Hoult, R.J., Lindberg, B., Haflidason, H., Long, D., Kuijpers, A., Anderson, E.S., Bryn, P., 2005. Palaeoslides and other mass failures of Pliocene to Pleistocene age along the Atlantic continental margin of NW Europe. Marine and Petroleum Geology 22, 1131–1148.

Faugeres, J.C., Gonthier, E., Grousset, F., Poutiers, J., 1981. THE FENI DRIFT: THE IMPORTANCE AND MEANING OF SLUMP DEPOSITS ON THE EASTERN SLOPE OF THE ROCKALL BANK. Marine Geology, 40, M49--M57

Flood, R.D., Hollister, C.D., Lonsdale, P., 1979. Disruption of the Feni drift by debris flows from Rockall Bank. Marine Geology, 32: 311-334.

Georgiopoulou, A., Shannon, P.M., Sachetti, F., Haughton, P.D.W., Benetti, S., 2013. Basement-controlled multiple slope collapses, Rockall Bank Slide Complex, NE Atlantic. Marine Geology 336, 198–214.

Van Gorsel, J.T., 2018. Bibliography of the geology of Indonesia and surrounding areas. http://www.vangorselslist.com/

Hinsbergen, D.J.J., Kouwenhoven, T.J., van der Zwaan, G.J., 2005. Paleobathymetry in the backstripping procedure: Correction for oxygenation effects on depth estimates. Palaeogeography, Palaeoclimatology, Palaeoecology 221, 245–265

Jenssen, J.L., Schjønning, P., Watts, C.W., Christensen, B.T., Munkholm, L.J., 2017. Soil texture analysis revisited: Removal of organic matter matters more than ever. PLoS ONE 12(5): e0178039, 1-10.

Kulhawy, F.H., Mayne, P.W., 1990. Manual on estimating soil properties for foundation design. Cornell University Ithaca, New York, 4-49.

Lanson, B., Sakharov, B.A., Claret, F., Drifts, V.A., 2009. Diagenetic Smectite-to-Illite Transition in Clay-Rich Sediments: A Reappraisal of X-Ray Diffraction Results Using the Multi- Specimen Method. American Journal of Science, vol. 309, 476-516. https://www.researchgate.net/publication/223692410

Roberts, D.G., 1975. Sediment distribution on the Rockall Bank, Rockall Plateau. Marine Geology, 19, 239-257.

Salmanidou, D.M., Georgiopoulou, A., Guillas, S., Dias, F., 2018. Rheological considerations for the modelling of submarine sliding at Rockall Bank, NE Atlantic Ocean. Physics of Fluids 30, 030705. https://aip.scitation.org/doi/10.1063/1.5009552

Salmanidou, D.M., Guillas, S., Georgiopoulou, A., Dias, F., 2017. Statistical emulation of landslide-induced tsunamis at the Rockall Bank, NE Atlantic. Proc.R.Soc.A 473: 20170026. http://dx.doi.org/10.1098/rspa.2017.0026

Shanmugam, 2012. New perspectives on deep-water sandstones: Origin, recognition and reservoir quality. Handbook of petroleum exploration and production, vol. 9, 1-488.

Skempton, A.W., 1953. The colloidal “Activity” of Clays. The international society for soil mechanics and geotechnical engineering, 58.

Tanaka, H., Hirabayashi, H., Matsuoka, T., Kaneko, H., 2012. Use of fall cone test as measurement of shear strength for soft clay materials. Soils and Foundations, 52(4): 590-599.

Wyse, E., 2004. A geotechnical study of the eastern flanks of the Rockall through. University College Dublin, 37-76.

CE14011 cruise report from the Marine institute Foras na Mara

A Results from direct testing op opened core

The (F) in the sample names indicates the intervals of the core that have been stored in the fridge for further testing.

Table 62: Results from testing on opened cores at site 1736.

Sample name	Depth (cm)	θ_g (-)	Liquidity index(-)	θ_v (-)	ρ_{grain} (kg/m^3)	S (-)	e (-)	γ_{bulk} (kN/m^3)	γ_{dry} (kN/m^3)	$s_{u,pocket}$ (kPa)
Core 1 dark	-178	NA	NA	NA	2739	NA	NA	NA	NA	NA
Core 1 dark	-174	0.48	1.05	NA	2739	NA	NA	NA	NA	11.8
Core 1 dark	-172	0.45	0.92	0.56	2739	1.01	1.23	17.5	12.0	NA
Core 1 sandy dark(F)	-164	NA	NA	NA	2739	NA	NA	NA	NA	NA
Core 1 sandy dark	-156	0.50	1.22	NA	2739	NA	NA	NA	NA	7.2
Core 1 dark	-154	0.61	1.66	NA	2739	NA	NA	NA	NA	10.9
Core 1 dark	-151	0.70	2.13	0.67	2739	1.02	1.89	15.8	9.3	NA
Core 1 dark(F)	-143	NA	NA	NA	2739	NA	NA	NA	NA	NA
Core 1 dark	-135	0.64	1.83	NA	2739	NA	NA	NA	NA	8.7
Core 1 grey	-133	0.64	1.20	NA	2741	1.06	1.66	16.6	10.1	NA
Core 1 grey(F)	-125	NA	NA	NA	2741	NA	NA	NA	NA	NA
Core 1 grey	-118	0.52	0.78	NA	2741	NA	NA	NA	NA	10.9
Core 1 grey	-114	0.52	0.75	0.59	2741	1.02	1.39	17.1	11.3	NA
Core 1 grey(F)	-106	NA	NA	NA	2741	NA	NA	NA	NA	NA
Core 1 grey	-98	0.58	0.97	NA	2741	NA	NA	NA	NA	9.8
Core 1 grey	-95	0.88	2.08	0.79	2741	1.18	2.06	16.6	8.8	NA
Core 1 grey	-91	0.62	1.13	NA	2741	NA	NA	NA	NA	10.9
Core 1 grey	-88	0.66	1.27	0.65	2741	1.02	1.78	16.1	9.7	NA
Core 1 grey	-86	0.74	1.55	NA	2741	NA	NA	NA	NA	8.7
Core 1 grey	-82	0.78	1.69	NA	2741	NA	NA	NA	NA	10.9
Core 2 orange	-78	0.78	0.97	NA	2765	NA	NA	NA	NA	10.5
Core 2 orange	-76	0.78	0.99	0.68	2765	0.99	2.18	15.8	8.5	NA
Core 2 orange(F)	-67	NA	NA	NA	2765	NA	NA	NA	NA	NA
Core 2 orange	-58	0.94	1.39	NA	2765	NA	NA	NA	NA	7.7
Core 2 orange	-55	0.94	1.42	0.73	2765	1.01	2.59	15.3	7.6	NA
Core 2 orange	-52	0.91	1.34	NA	2765	NA	NA	NA	NA	10.9
Core 2 orange	-49	0.95	1.44	0.72	2765	0.99	2.65	15.1	7.4	NA
Core 2 black	-46	0.93	1.46	NA	2765	NA	NA	NA	NA	7.2
Core 2 black	-43	0.96	1.53	0.72	2765	0.99	2.67	15.0	7.4	NA
Core 2 black(F)	-33	NA	NA	NA	2765	NA	NA	NA	NA	NA
Core 2 black	-24	0.86	1.25	NA	2765	NA	NA	NA	NA	12.1
Core 2 black	-20	0.88	1.29	0.72	2765	1.02	2.38	15.7	8.0	NA
Core 2 black	-16	0.85	1.23	NA	2765	NA	NA	NA	NA	14.2
Core 2 black	-12	0.87	1.27	NA	2765	NA	NA	NA	NA	14.2
Core 2 black	-8	0.94	1.49	0.71	2765	0.98	2.66	15.0	7.4	NA
Core 2 black	-3	0.96	1.55	NA	2765	NA	NA	NA	NA	10.1

Table 63: Results from testing on opened cores at site 1672.

Sample name	Depth (cm)	θ_g (-)	Liquidity index (-)	θ_v (-)	$_{in}$ (kg/	S (-)	e (-)	γ_{bulk} (kN/m^3)	γ_{dry} (kN/m^3)	$s_{u,pocket}$ (kPa)
Core 4 dark	-59	0.56	1.43	NA	2743	NA	NA	NA	NA	10.5
Core 4 dark	-56	0.57	1.44	0.60	2743	0.98	1.58	16.3	10.4	NA
Core 4 dark(F)	-50	NA	NA	NA	2743	NA	NA	NA	NA	NA
Core 4 dark	-43	0.64	1.78	0.63	2743	0.99	1.78	15.9	9.7	NA
Core 4 dark	-40	0.80	2.53	NA	2743	NA	NA	NA	NA	8.7
Core 4 light(F)	-33	NA	NA	NA	2753	NA	NA	NA	NA	NA
Core 4 light	-25	0.90	1.57	0.72	2753	NA	NA	14.8	7.8	NA
Core 4 light	-22	0.93	1.69	NA	2753	NA	NA	NA	NA	6.6
Core 4 light	-19	0.93	1.68	0.71	2753	0.99	2.61	14.5	7.5	NA
Core 4 light	-15	0.94	1.72	NA	2753	NA	NA	NA	NA	7.4
Core 4 light	-10	0.98	1.83	NA	2753	NA	NA	NA	NA	7.6
Core 4 light	-1	1.03	2.02	NA	2753	NA	NA	NA	NA	NA
Core 5 (22-37)	-168	0.51	1.23	NA	2757	NA	NA	NA	NA	NA
Core 5 (22-37)	-165	0.51	1.23	0.58	2757	1.00	1.41	16.9	11.2	11.4
Core 5 (22-37)	-158	0.54	1.36	0.59	2757	0.99	1.50	16.6	10.8	19.7
Core 5 (22-37)	-140	0.54	1.38	0.58	2757	0.95	1.56	16.3	10.6	16.0
Core 5 very light (F)	-129	0.54	NA	0.60	2767	0.99	1.51	16.7	10.8	10.9
Core5 very light (F)	-126	0.73	NA	NA	2767	NA	NA	NA	NA	10.1
Core 5 very light	-123	0.60	NA	NA	2767	NA	NA	NA	NA	12.0
Core 5 very light	-120	0.53	NA	0.59	2767	0.99	1.49	16.7	10.9	NA
Core 5 beige heavy clay	-118	0.47	NA	NA	2757	NA	NA	NA	NA	17.5
Core 5 beige heavy clay	-115	0.20	NA	NA	2757	NA	NA	NA	NA	15.3
Core5 beige heavy clay	-113	NA	NA	NA	2757	NA	NA	NA	NA	NA
Core 5 beige(F)	-106	NA	NA	NA	2757	NA	NA	NA	NA	NA
Core5 beige sand	-98	0.54	NA	0.57	2757	0.93	1.59	16.1	10.4	NA
Core5 beige sand	-95	0.47	NA	NA	2757	NA	NA	NA	NA	10.9
Core5 beige(F)	-87	NA	NA	NA	2757	NA	NA	NA	NA	NA
Core 5 beige	-79	0.46	0.94	0.56	2757	1.00	1.28	17.4	11.9	NA
Core 5 beige	-77	0.50	1.15	NA	2757	NA	NA	NA	NA	14.2

Table 64: Results from testing on opened core at site 688

Sample name	Depth (cm)	θ_g (-)	Liquidity index (-)	θ_v (-)	ρ_{grain} (kg/m^3)	S (-)	e (-)	γ_{bulk} (kN/m^3)	γ_{dry} (kN/m^3)	$s_{u,pocket}$ (kPa)
Core 6 sandy clay	-77	0.43	NA	NA	2739	-1.17	NA	NA	NA	11.8
Core 6 sandy clay	-74	0.45	NA	0.56	2739	1	1.25	17.4	12.0	NA
Core 6 sandy clay	-71	0.44	NA	NA	2739	-1.2	NA	NA	NA	12.0
Core 6 sandy clay(F)	-62	NA	NA	NA	2739	NA	NA	NA	NA	NA
Core 6 sandy clay	-53	0.38	NA	NA	2739	-1.03	NA	NA	NA	12.0
Core 6 sandy clay	-51	0.38	NA	NA	2739	-1.04	NA	NA	NA	NA
Core 6 sandy clay	-48	0.40	NA	0.51	2739	0.96	1.15	17.5	12.5	NA
Core 6 clayey clay	-42	0.45	0.47	NA	2739	-1.24	NA	NA	NA	21.9
Core 6 clayey clay(F)	-32	NA	NA	NA	2739	NA	NA	NA	NA	NA
Core 6 clayey clay	-21	0.49	0.59	0.54	2739	0.91	1.48	16.1	10.8	NA
Core 6 clayey clay	-16	0.50	0.62	NA	2739	-1.36	NA	NA	NA	NA
Core 6 clayey clay	-12	0.38	0.22	NA	2739	-1.04	NA	NA	NA	14.2
Core 6 clayey clay	-9	0.40	0.29	NA	2739	-1.1	NA	NA	NA	7.7
Core 6 clayey clay	-2	0.35	0.14	NA	2739	-0.97	NA	NA	NA	8.1

Table 65: Results from testing on opened core at site 1988.

Sample name	Depth (cm)	θ_g (-)	Liquidity index (-)	θ_v (-)	ρ_{grain} (kg/m^3)	S (-)	e (-)	γ_{bulk} (kN/m^3)	γ_{dry} (kN/m^3)	$s_{u,pocket}$ (kPa)
Core 7 dark	-85	0.79	1.17	NA	2738.5	NA	NA	NA	NA	7.9
Core 7 dark	-82	0.71	0.97	0.66	2738.5	1.00	1.96	15.6	9.1	NA
Core 7 dark	-78	0.71	0.95	NA	2738.5	NA	NA	NA	NA	10.9
Core 7 dark(F)	-71	NA	NA	NA	2738.5	NA	NA	NA	NA	NA
Core 7 dark(F)	-59	NA	NA	NA	2738.5	NA	NA	NA	NA	NA
Core 7 dark	-52	0.94	1.61	NA	2738.5	NA	NA	NA	NA	8.1
Core 7 light	-49	0.98	2.11	NA	2718.5	NA	NA	NA	NA	NA
Core 7 light	-49	1.00	2.20	0.73	2718.5	1.01	2.72	14.4	7.2	NA
Core 7 light	-46	1.03	2.30	NA	2718.5	NA	NA	NA	NA	10.9
Core 7 light	-42	1.05	2.39	0.74	2718.5	1.00	2.83	14.2	7.0	NA
Core 7 light	-42	1.03	2.32	NA	2718.5	NA	NA	NA	NA	NA
Core 7 light(F)	-31	NA	NA	NA	2718.5	NA	NA	NA	NA	NA
Core 7 light	-20	1.07	2.49	0.75	2718.5	1.00	2.90	14.1	6.8	NA
Core 7 light	-20	1.07	2.49	NA	2718.5	NA	NA	NA	NA	NA
Core 7 light	-16	1.11	2.67	NA	2718.5	NA	NA	NA	NA	9.8
Core 7 light	-13	1.12	2.71	NA	2718.5	NA	NA	NA	NA	9.8
Core 7 light	-2	1.17	2.91	NA	2718.5	NA	NA	NA	NA	NA

Table 66: Results from testing on opened core at site 1695.

Sample name	Depth (cm)	θ_g (-)	θ_v (-)	ρ_{grain} (kg/m^3)	S (-)	e (-)	γ_{bulk} (kN/m^3)	γ_{dry} (kN/m^3)	$s_{u,pocket}$ (kPa)
Core 8 dark	-72	0.52	NA	2750	NA	-1	NA	NA	NA
Core 8 dark	-64	0.56	0.61	2750	1.00	1.54	16.6	10.6	NA
Core 8 dark	-62	NA	NA	2750	NA	NA	NA	NA	9.3
Core 8 dark(F)	-60	NA	NA	2750	NA	NA	NA	NA	NA
Core 8 dark	-59	0.75	NA	2750	NA	NA	NA	NA	8.7
Core 8 dark	-53	0.64	0.64	2750	1.00	1.77	16.0	9.7	NA
Core 8 dark	-46	NA	NA	2750	NA	NA	NA	NA	8.7
Core 8 dark	-43	0.92	0.71	2750	1.00	2.53	14.6	7.6	NA
Core 8 dark	-40	0.67	NA	2750	NA	NA	NA	NA	13.1
Core 8 light	-38	0.97	NA	2767	NA	NA	NA	NA	4.9
Core 8 light	-34	1.03	0.73	2767	0.98	2.91	14.1	7.0	NA
Core 8 light	-27	0.94	NA	2767	NA	NA	NA	NA	NA
Core 8 light	-26	0.92	NA	2767	NA	NA	NA	NA	8.1
Core 8 light	-25	NA	NA	2767	NA	NA	NA	NA	7.1
Core 8 light(F)	-25	NA	NA	2767	NA	NA	NA	NA	NA
Core 8 light	-21	0.98	NA	2767	NA	NA	NA	NA	6.6
Core 8 light	-18	0.98	0.73	2767	0.99	2.75	14.3	7.2	NA
Core 8 light	-13	0.97	NA	2767	NA	NA	NA	NA	5.5
Core 8 light	-12	0.97	0.69	2767	0.93	2.87	13.8	7.0	NA
Core 8 light	-8	1.00	NA	2767	NA	NA	NA	NA	5.5

Table 67: Results from testing on opened core at site 1959.

Sample name	Depth (cm)	θ_g (-)	Liquidity index (-)	θ_v (-)	ρ_{grain} (kg/m^3)	S (-)	e (-)	γ_{bulk} (kN/m^3)	γ_{dry} (kN/m^3)	$s_{u,pocket}$ (kPa)
Core 9 light grey	-24	1.02	NA	0.75	2780	NA	NA	NA	NA	10.9
Core 9 light grey	-21	1.02	NA	0.75	2780	NA	NA	NA	NA	9.3
Core 9 light grey	-18	0.98	NA	0.75	2780	NA	NA	NA	NA	6.6
Core 9 light grey	-15	1.16	NA	0.75	2780	NA	NA	NA	NA	5.5
Core 9 light grey	-12	1.07	NA	0.75	2780	NA	NA	NA	NA	5.5
Core 9 light grey	-9	1.04	NA	0.75	2780	NA	NA	NA	NA	6.6
Core 9 light grey	-7	1.02	NA	0.75	2780	NA	NA	NA	NA	7.1
Core 9 light grey	-5	1.01	NA	0.75	2780	NA	NA	NA	NA	NA
Core 9 light grey	-3	0.97	NA	0.75	2780	NA	NA	NA	NA	NA
Core 10 dark	-112	0.69	1.03	NA	2736	NA	NA	NA	NA	6.6
Core 10 dark	-109	0.65	0.91	0.64	2736	1.01	1.77	16.0	9.7	NA
Core 10 dark(F)	-99	NA	NA	NA	2736	NA	NA	NA	NA	NA
Core 10 dark	-90	0.74	1.17	0.67	2736	1.01	2.02	15.5	8.9	NA
Core 10 dark	-87	0.71	1.07	NA	2736	NA	NA	NA	NA	10.9
Core 10 dark	-84	0.75	1.19	NA	2736	NA	NA	NA	NA	8.7
Core 10 light(F)	-77	NA	NA	NA	2727	NA	NA	NA	NA	NA
Core 10 light(F)	-67	NA	NA	NA	2727	NA	NA	NA	NA	NA
Core 10 light	-61	0.85	1.28	NA	2727	NA	NA	NA	NA	10.9
Core 10 light	-58	0.84	1.26	0.69	2727	0.99	2.33	14.8	8.0	NA
Core 10 light(F)	-49	NA	NA	NA	2727	NA	NA	NA	NA	NA
Core 10 light	-40	0.84	1.11	NA	2727	NA	NA	NA	NA	10.9
Core 10 light	-37	0.87	1.17	0.72	2727	1.04	2.31	15.2	8.1	NA
Core 10 light	-34	0.88	1.19	NA	2727	NA	NA	NA	NA	11.8
Core 10 light	-31	0.88	1.18	NA	2727	NA	NA	NA	NA	10.9
Core 10 light	-26	0.86	1.13	NA	2727	NA	NA	NA	NA	11.8

Table 68: Results from testing on opened core at site 1604.

Sample name	Depth (cm)	θ_g (-)	Liquidity index (-)	θ_v (-)	ρ_{grain} (kg/m^3)	S (-)	e (-)	γ_{bulk} (kN/m^3)	γ_{dry} (kN/m^3)	$s_{u,pocket}$ (kPa)
Core 3 dark grey	-37	0.52	0.45	NA	2786	NA	NA	NA	NA	13.8
Core 3 dark grey	-34	0.59	0.69	0.62	2786	1.00	1.65	16.4	10.3	NA
Core 3 dark grey(F)	-23	NA	NA	NA	2786	NA	NA	NA	NA	NA
Core 3 light grey	-13	0.86	NA	0.70	2786	0.99	2.41	14.9	8.0	NA
Core 3 light grey	-10	0.87	NA	NA	2786	NA	NA	NA	NA	10.5
Core 3 light grey	-7	0.87	NA	0.70	2786	0.98	2.47	14.7	7.9	NA
Core 3 light grey	-4	0.87	NA	NA	2786	NA	NA	NA	NA	12.0
Core 3 light grey/dark	-1	0.89	NA	NA	2786	NA	NA	NA	NA	10.9
Core 11 sandy clay	-142	NA	NA	NA	2756	NA	NA	NA	NA	NA
Core 11 sandy clay	-135	0.47	NA	0.54	2756	0.93	1.41	16.5	11.2	NA
Core 11 sandy clay	-135	0.48	NA	NA	2756	NA	NA	NA	NA	9.8
Core 11 sandy clay	-129	0.38	NA	0.50	2756	0.95	1.10	17.8	12.9	NA
Core 11 sandy clay	-129	0.40	NA	NA	2756	NA	NA	NA	NA	12.5
Core 11 sandy clay	-122	0.48	NA	NA	2756	NA	NA	NA	NA	NA
Core 11 sandy clay	-117	0.55	NA	NA	2756	NA	NA	NA	NA	NA
Core 11 clayey clay(F)	-104	NA	NA	NA	2785	NA	NA	NA	NA	NA
Core 11 clayey clay	-92	0.54	NA	0.60	2785	1.00	1.51	16.8	10.9	NA
Core 11 clayey clay	-92	0.56	NA	NA	2785	NA	NA	NA	NA	NA
Core 11 clayey clay	-88	0.45	NA	NA	2785	NA	NA	NA	NA	10.9
Core 11 sandy clay 2(F)	-78	NA	NA	NA	2744	NA	NA	NA	NA	NA
Core 11 sandy clay 2	-69	0.41	NA	0.54	2744	1.02	1.10	18.1	12.8	NA
Core 11 sandy clay 2	-66	0.45	NA	NA	2744	NA	NA	NA	NA	10.9
Core 11 sandy clay 2	-63	0.46	NA	0.56	2744	1.02	1.24	17.5	12.0	NA
Core 11 sandy clay 2	-59	0.47	NA	NA	2744	NA	NA	NA	NA	10.9
Core 11 sandy clay 2	-51	0.48	NA	NA	2744	NA	NA	NA	NA	NA
Core 11 sandy clay 2	-53	0.48	NA	0.57	2744	1.02	1.28	17.4	11.8	0.0
Core 11 sandy clay 2	-49	0.49	NA	NA	2744	NA	NA	NA	NA	10.9

B Atterberg limits, soil fractions, LOI, activity, SOM, SOC and calcite values of all samples

Table 69: Atterberg limits, soil fractions, LOI values, activity values, SOM values, SOC values and calcite values of all samples.

Sample name	LL (-)	PL (-)	PI (-)	Sand (%)	Silt (%)	Cay (%)	LOI(%) at 550° C	LOI (%) at 950° C	Acivity (-)	SOM (%)	SOC (%)	Calcite (%)
Core 1 grey	0.58	0.31	0.28	36	30	33	8.8	12.0	0.84	6.5	3.3	27
Core 1 dark	0.47	0.26	0.21	26	44	30	6.0	10.0	0.68	3.9	2.7	23
Core 1 sandy dark	0.46	0.28	0.18	NA	NA	NA	NA	NA	NA	NA	NA	NA
Core 2 dark (37.5-54)	0.78	0.43	0.34	17	35	48	10.6	21.2	0.71	7.2	5.8	48
Core 2 orange (4.5-20.5)	0.79	0.41	0.37	8	35	57	11.2	14.9	0.66	7.3	4.1	34
Core 3	0.67	0.40	0.27	33	33	34	9.1	25.3	0.79	6.7	6.9	57
Core 4 dark (5-15.5)	0.47	0.26	0.21	35	31	34	8.9	13.4	0.61	6.5	3.7	30
Core 4 light (21-32)	0.73	0.43	0.30	20	40	40	9.0	24.5	0.75	6.2	6.7	56
Core 5 beige clay 2 (12-22)	NA	NA	NA	NA	NA	NA	8.0	10.4	NA	NA	2.8	24
Core 5 very light(44-56)	NA	NA	NA	NA	NA	NA	8.3	19.1	NA	NA	5.2	43
Core 5 beige(63.5-75)	0.47	0.30	0.18	38	37	24	6.0	14.4	0.73	4.3	3.9	33
Core 5 (22-37)	0.46	0.26	0.20	NA	NA	NA	NA	NA	NA	NA	NA	NA
Core 5 (37-47.5)	NA	NA	NA	NA	NA	NA	NA	NA	NA	NA	NA	NA
Core 6 sandy clay (8.5-24)	0.40	NA	NA	60	30	10	4.0	14.3	NA	2.6	3.9	32
Core 6 clayey clay (38-55.5)*	0.61	0.31	0.29	29	51	20	4.1	14.6	NA	3.4	4.0	33
Core 7 dark (10.5-22.5)	0.72	0.37	0.35	7	NA	NA	10.9	10.5	NA	NA	2.9	24
Core 7 dark(22.5-34)	0.73	0.38	0.35	7	59	34	10.9	10.5	1.04	8.5	2.9	24
Core 7 light	0.72	0.49	0.23	7	33	60	13.3	17.5	0.39	9.0	4.8	40
Core 8 dark	0.41	0.23	0.17	37	35	28	7.4	15.4	0.63	5.5	4.2	35
Core 8 light	0.54	0.34	0.20	27	36	38	8.6	23.3	0.53	5.9	6.3	53
Core 9	NA	NA	NA	15	39	46	9.6	23.9	NA	6.4	6.5	54
Core 10 dark (6-22)	0.68	0.33	0.35	8	41	51	9.5	7.6	0.68	5.9	2.1	17
Core 10 light (31-41)	0.75	0.40	0.35	7	34	59	12.2	15.8	0.59	8.1	4.3	36
Core 10 light (41-51)	0.79	0.39	0.40	7	34	59	12.2	15.8	0.68	8.1	4.3	36
Core 10 light(57-71)	0.82	0.47	0.35	7	34	59	12.2	15.8	0.59	8.1	4.3	36
Core 11 clayey clay(31-42)	0.43	NA	NA	54	NA	NA	5.8	14.9	NA	NA	4.1	34
Core 11 clayey clay(42-52.5)	0.44	NA	NA	54	NA	NA	5.8	14.9	NA	5.8	4.1	34
Core 11 sandy clay	NA	NA	NA	56	29	15	4.2	16.1	NA	3.2	4.4	37
Core 11 sandy clay 2	NA	NA	NA	71	16	13	4.2	18.5	NA	3.3	5.0	42
*not sure about plastic limit determination since soil was very sandy												

C Results from fall cone tests

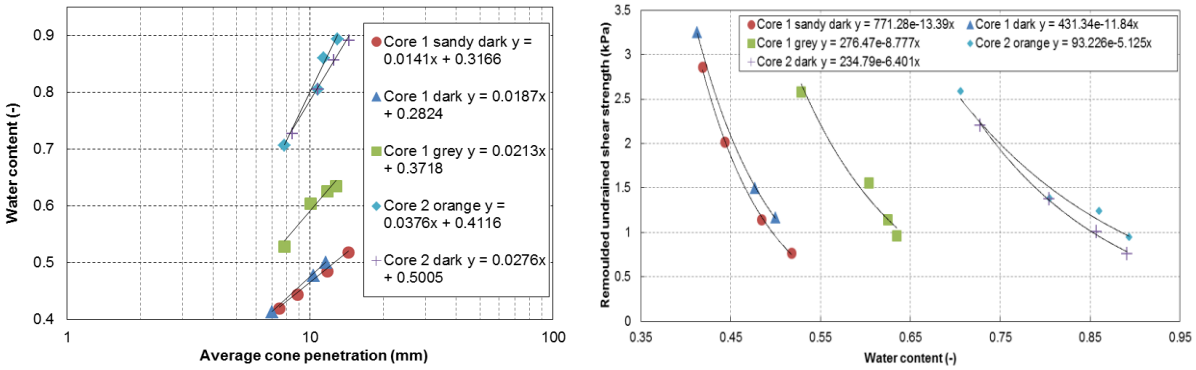

Figure 136: Fall cone tests results on the left and the derived remoulded undrained shear strenght on the right of site 1736.

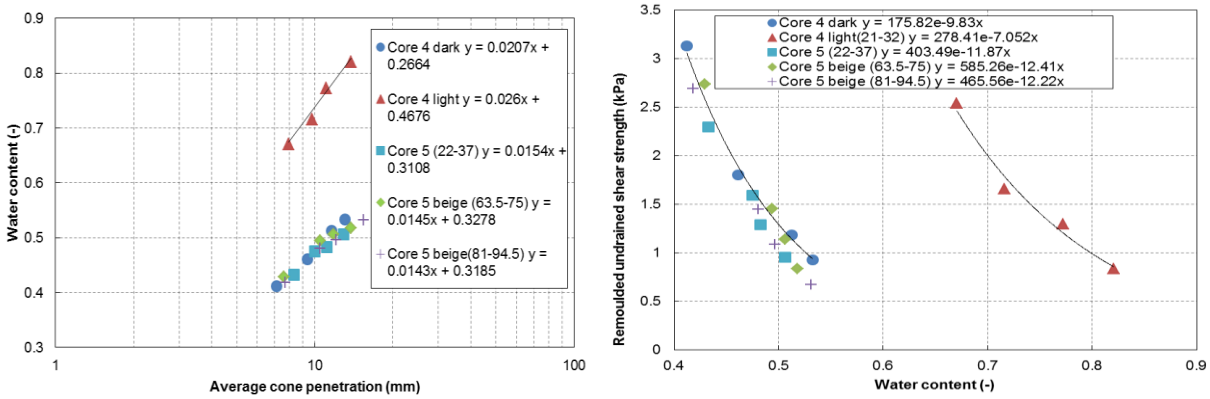

Figure 137: Fall cone tests results on the left and the derived remoulded undrained shear strenght on the right of site 1672.

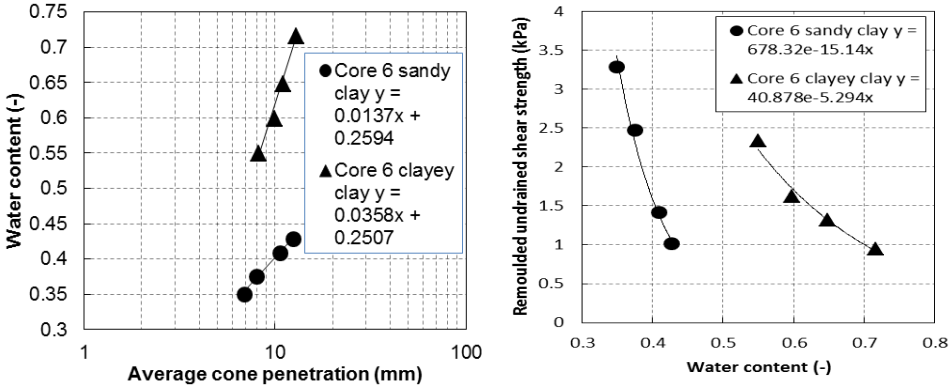

Figure 138: Fall cone tests results on the left and the derived remoulded undrained shear strenght on the right of site 688.

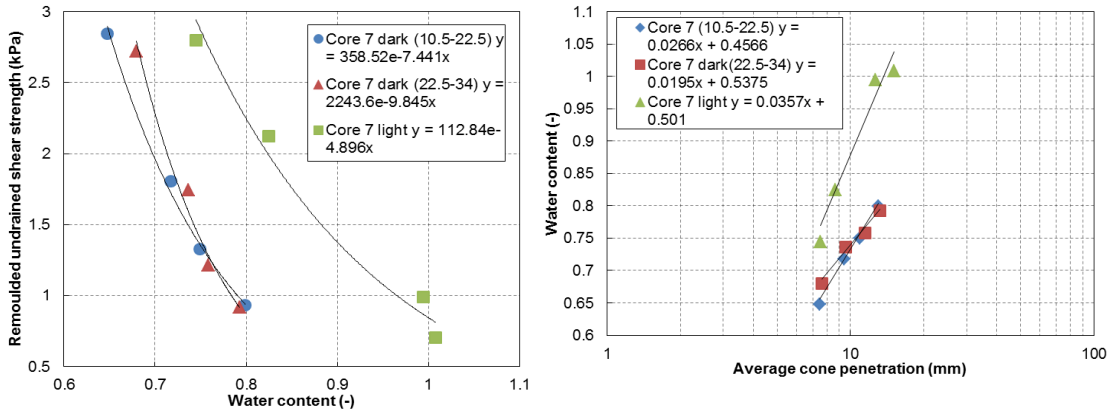

Figure 139: Fall cone tests results on the left and the derived remoulded undrained shear strenght on the right of site 1988.

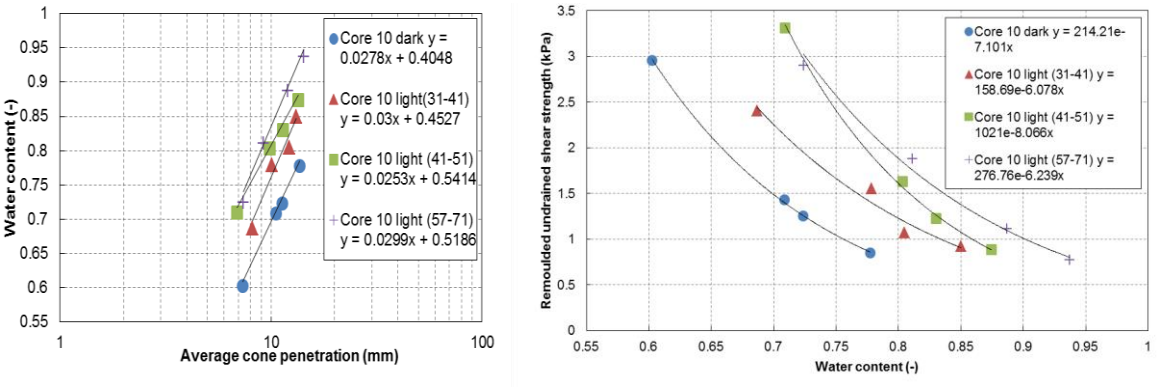

Figure 140: Fall cone tests results on the left and the derived remoulded undrained shear strengths on the right of site 1959.

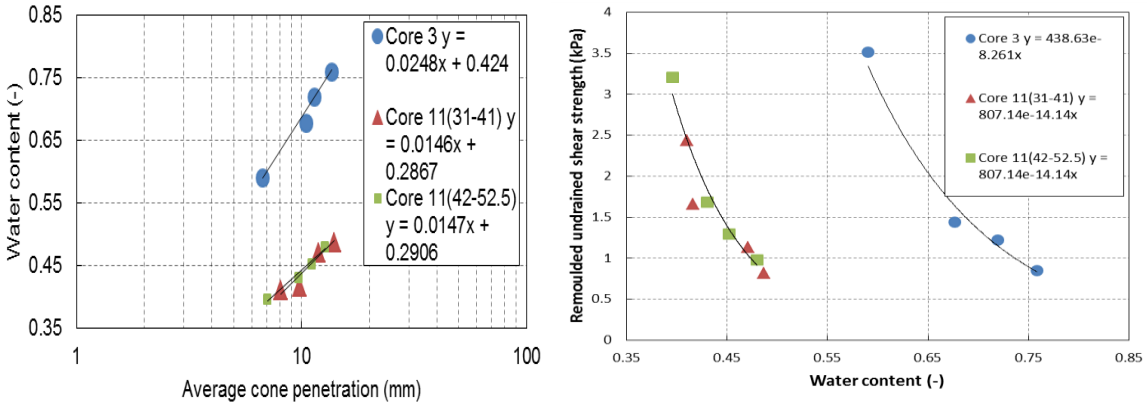

Figure 141: Fall cone tests results on the left and the derived remoulded undrained shear strenghts on the right of site 1604.

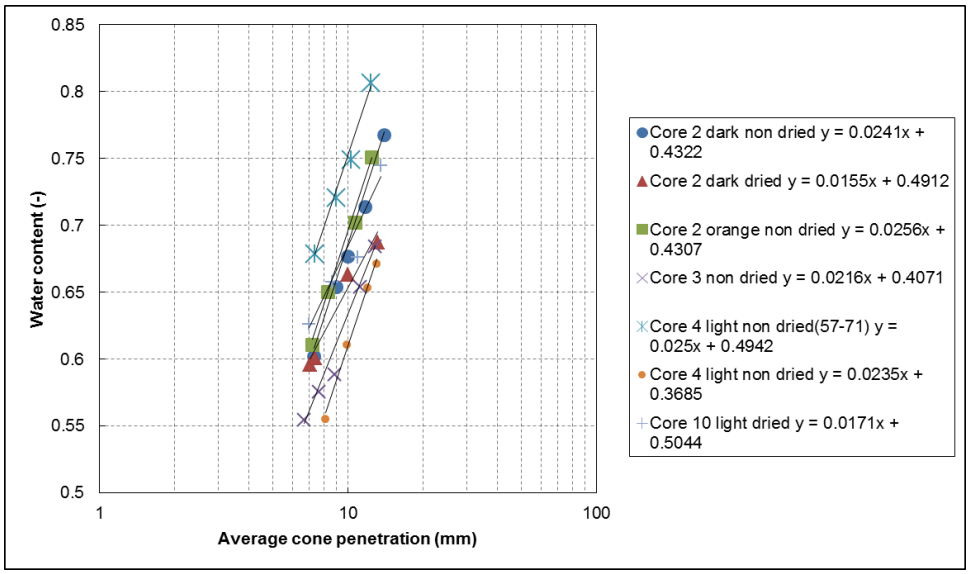

Figure 142: Fall cone test results of some soil samples without the sand fraction.

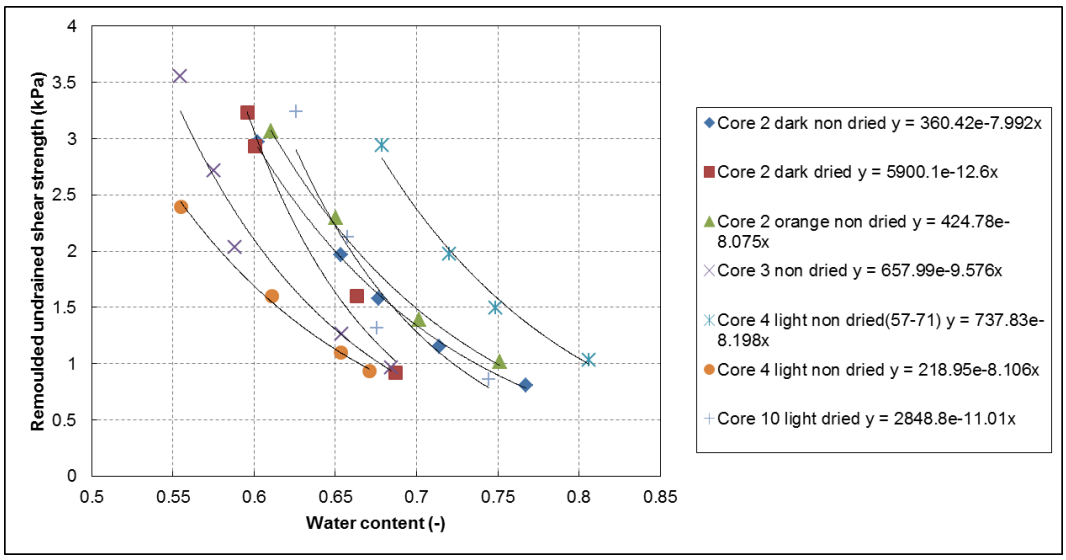

Figure 143: Remoulded undrained shear strength results of some soil samples derived from fall cone test without the sand fraction.

D Results from grain size distribution

In this appendix the grain size distribution values with their classifications are displayed per site and per samples interval of that site. Note that the <63µm fraction has different grain size particles displayed for each sample. This done as to replicate the exact results obtained from the hydrometer test.

Table 70: Grain size distribution values of site 1736.

Core 1 dark grain size (µm)	Core 1 dark mass % passing	Core 1 grey grain size (µm)	Core 1 grey mass % passing	Core 2 orange grain size (µm)	Core 2 orange mass % passing	Core 2 dark grain size (µm)	Core 2 dark mass % passing
2000	99	2000	100	2000	100	2000	100
1000	99	1000	100	1000	100	1000	100
600	99	600	100	600	100	600	100
425	99	425	100	425	100	425	100
300	98	300	100	300	99	300	100
210	96	210	99	210	96	210	99
125	90	125	93	125	92	125	97
63	74	63	64	63	83	63	92
52	66	52	57	53	73	51	91
38	61	37	55	38	71	37	88
29	54	28	51	27	71	26	86
21	50	20	49	19	68	19	83
15	46	14	47	14	66	14	80
8	42	8	43	7	62	7	74
4	36	4	37	4	52	4	66
2	31	2	32	2	45	2	56
1	25	1	27	1	38	1	49

Table 71: Grain size distribution values of site 1672.

Core 4 dark grain size (µm)	Core 4 dark mass % passing	Core 4 light grain size (µm)	Core 4 light mass % passing	Core 5 grain size (µm)	Core 5 mass % passing
2000	100	2000	100	2000	100
1000	100	1000	100	1000	100
600	100	600	100	600	100
425	100	425	100	425	100
300	99	300	98	300	97
210	96	212	93	210	91
125	90	125	85	125	81
63	65	63	80	63	62
55	52	51	71	53	53
40	51	37	68	39	49
28	50	27	66	29	46
20	49	19	62	21	42
15	46	14	59	15	39
8	43	7	56	8	34
4	38	4	46	4	29
2	33	2	38	2	25
1	29	1	33	1	21

Table 72: Grain size distribution values of site 688.

Core 6 sandy clay grain size (µm)	Core 6 sandy clay mass % passing	Core 6 clayey clay grain size (µm)	Core 6 clayey clay mass % passing
2000	100	2000	100
1000	100	1000	100
600	99	600	100
425	99	425	100
300	99	300	99
210	94	210	99
125	64	125	95
63	40	63	71
52	34	53	58
38	32	39	54
30	26	29	49
22	23	22	41
16	19	16	36
9	15	9	29
5	12	4	23
2	12	2	19
1	10	1	18

Table 73: Grain size distribution values of site 1988.

Core 7 dark grain size (µm)	Core 7 dark mass % passing	Core 7 light grain size (µm)	Core 7 light mass % passing
2000	100	2000	100
1000	100	1000	100
600	100	600	100
425	100	425	100
300	99	300	100
210	98	210	98
125	97	125	97
63	93	63	93
51	85	50	86
37	81	35	86
28	72	25	84
21	66	18	81
15	62	13	78
8	51	7	73
4	41	4	61
2	32	2	52
1	25	1	44

Table 74: Grain size distribution values of site 1695.

Core 8 dark grain size (µm)	Core 8 dark mass % passing	Core 8 light grain size (µm)	Core 8 light mass % passing
2000	100	2000	100
1000	100	1000	100
600	100	600	100
425	100	425	99
300	99	300	98
210	97	210	94
125	92	125	87
63	63	63	73
50	57	51	62
36	55	37	60
26	53	27	59
19	51	19	55
14	48	14	53
8	42	8	49
4	34	4	43
2	28	2	36
1	23	1	32

Table 75: Grain size distribution values of site 1959.

Core 9 grain size (µm)	Core 9 mass % passing	Core 10 dark grain size (µm)	Core 10 dark mass % passing	Core 10 light grain size (µm)	Core 10 light mass % passing
2000	100	2000	100	2000	100
1000	100	1000	100	1000	100
600	100	600	100	600	100
425	95	425	100	425	100
300	94	300	99	300	99
210	92	210	98	210	98
125	90	125	97	125	97
63	85	63	92	63	93
51	56	51	84	49	85
37	54	37	81	35	84
26	53	26	79	25	82
19	51	19	76	18	79
14	50	14	75	13	77
8	44	7	66	7	71
4	39	4	58	4	61
2	31	2	49	2	52
1	27	1	43	1	45

Table 76: Grain size distribution values of site 1604.

Core 3 grain size (µm)	Core 3 mass % passing	Core 11 sandy clay grain size (µm)	Core 11 sandy clay mass % passing	Core 11 sandy clay 2 grain size (µm)	Core 11 sandy clay 2 mass % passing
2000	100	2000	99	2000	100
1000	100	1000	99	1000	100
600	100	600	99	600	100
425	100	425	98	425	100
300	99	300	96	300	99
210	94	210	76	212	94
125	86	125	68	125	76
63	67	63	44	63	29
52	59	51	40	53	25
38	57	38	37	39	23
27	55	29	32	28	23
20	52	22	28	21	21
14	49	16	26	15	21
8	47	8	22	8	18
4	39	4	18	4	16
2	33	2	15	2	14
1	28	1	13	1	12

Table 77: Grain size distribution properties from site 1736.

Sample name	D_{10}(µm)	D_{30}(µm)	D_{50}(µm)	D_{60}(µm)	C_u(-)	C_c(-)	M_z(%)
Core 1 dark	0.3	2.0	21.6	44.2	133	0.3	86
Core 1 grey	0.1	1.7	22.6	56.1	412	0.4	82
Core 2 orange	0.0	0.2	1.3	0.5	15	2.3	96
Core 2 dark	0.1	0.4	3.3	40.8	813	0.1	91

Table 78: Classification of the grain size distribution at site 1736.

Sample name	Shape of grain size curve
Core 1 dark	Gap graded
Core 1 grey	Gap graded
Core 2 orange	Well graded
Core 2 dark	Gap graded

Table 79: Results from grain size distribution at site 1672.

Sample name	D_{10}(µm)	D_{30}(µm)	D_{50}(µm)	D_{60}(µm)	C_u(-)	C_c(-)	M_z(%)
Core 4 dark	0.1	1.5	24.6	59.7	1073	0.6	83
Core 4 light	0.1	0.8	5.2	39.4	339	0.1	90
Core 5	0.4	4.9	41.0	60.9	151	1.0	81

Table 80: Classification of grain size distribution curve at site 1672.

Sample name	Shape of grain size curve
Core 4 dark	not classifiable
Core 4 light	Gap graded
Core 5	Well graded

Table 81: Results from grain size distribution at site 688.

Sample name	D_{10}(µm)	D_{30}(µm)	D_{50}(µm)	D_{60}(µm)	C_u(-)	C_c(-)	M_z(%)
Core 6 clayey clay	0.4	9.7	31.3	53.9	151	4.9	86
Core 6 sandy clay	1.3	35.5	83.5	122.5	92	7.7	70

Table 82: Classification of grain size distribution curve at site 688.

Sample name	Shape of grain size curve
Core 6 clayey clay	not classifiable
Core 6 sandy clay	not classifiable

Table 83: Results from grain size distribution at site 1988.

Sample name	D_{10}(µm)	D_{30}(µm)	D_{50}(µm)	D_{60}(µm)	C_u(-)	C_c(-)	M_z(%)
Core 7 dark	0.6	1.9	7.6	26.5	43	0.2	97
Core 7 light	0.1	0.3	1.8	3.6	67	0.4	96

Table 84: Classification of grain size distribution curve at site 1988.

Sample name	Shape of grain size curve
Core 7 dark	Gap graded
Core 7 light	Gap graded

Table 85: Grain size distribution properties from site 1695.

Sample name	D_{10}(µm)	D_{30}(µm)	D_{50}(µm)	D_{60}(µm)	C_u(-)	C_c(-)	M_z(%)
Core 8 dark	0.3	2.7	16.7	56.1	172	0.4	81
Core 8 light	0.1	0.9	9.2	49.3	618	0.2	87

Table 86: Classification of grain size distribution curve at site 1695.

Sample name	Shape of grain size distribution
Core 8 dark	Gap graded
Core 8 light	Gap graded

Table 87: Grain size distribution properties from site 1959.

Sample name	D_{10}(µm)	D_{30}(µm)	D_{50}(µm)	D_{60}(µm)	C_u(-)	C_c(-)	M_z(%)
Core 9	0.1	1.8	15.0	52.4	389	0.47	92.4
Core 10 light	0.0	0.3	1.8	3.6	83	0.42	96.4
Core 10 dark	0.1	0.3	2.2	4.7	83	0.43	96.1

Table 88: Classification of grain size distribution curve at site 1604.

Sample name	Shape of grain size curve
Core 9	Gap graded
Core 10 light	Gap graded
Core 10 dark	Gap graded

Table 89: Grain size distribution properties from site 1604.

Sample name	D_{10}(µm)	D_{30}(µm)	D_{50}(µm)	D_{60}(µm)	C_u(-)	C_c(-)	M_z(%)
Core 3	0.1	1.5	15.3	53.3	430.7	0.4	84
Core 11 sandy clay	1.2	24.3	75.2	100.5	82.0	4.8	72
Core 11 sandy clay 2	0.7	63.7	85.5	99.0	137.2	56.9	65

Table 90: Classification of grain size distribution curve at site 1604.

Sample name	Shape of grain size curve
Core 3	Gap graded
Core 11 sandy clay	not classifiable
Core 11 sandy clay 2	not classifiable

E Results from comparing undrained shear strength values of unconsolidated undrained direct shear tests and fall cone tests.

Table 91: Undrained shear strength and sensitivity results from the direct shear tests and the fall cone tests.

Sample name	UU DS test s_u (kPa)	UU DS test remoulded s_u (kPa)	$\theta_{g,original}$ (-)	$\theta_{g,remoulded}$ (-)	$\theta_{g,average}$ (-)	S_t (-) of UU DS test
Core 1 grey	NA	NA	NA	NA	NA	NA
Core 1 dark	3.4	NA	NA	0.53	0.53	NA
Core 1 sandy dark	4.4	4.0	0.43	0.42	0.43	1.1
Core 2 dark (37.5-54)	2.9	1.0	0.94	0.92	0.93	3.0
Core 2 orange (4.5-20.5)	4.0	1.2	0.91	0.87	0.89	3.4
Core 3	3.5	1.8	0.69	0.67	0.68	1.9
Core 4 dark (5-15.5)	3.9	2.2	0.54	0.57	0.55	1.8
Core 4 light (21-32)	3.6	1.3	0.82	0.79	0.80	2.8
Core 5 beige clay 2 (12-22)	NA	NA	NA	NA	NA	NA
Core 5 very light(44-56)	NA	NA	NA	NA	NA	NA
Core 5 beige(63.5-75)	3.6	3.3	0.47	0.50	0.48	1.1
Core 5 beige (81-94.5)	4.8	2.1	0.50	0.48	0.49	2.3
Core 5 (22-37)	NA	NA	NA	NA	NA	NA
Core 5 (37-47.5)	NA	NA	NA	NA	NA	NA
Core 6 sandy clay (8.5-24)	4.1	3.1	0.42	0.44	0.43	1.3
Core 6 clayey clay (38-55.5)	8.3	4.5	0.50	0.52	0.51	1.9
Core 7 dark (10.5-22.5)	2.5	1.9	0.77	0.76	0.77	1.3
Core 7 dark(22.5-34)	2.8	1.5	0.85	0.86	0.86	1.9
Core 7 light	5.0	1.5	0.95	1.01	0.98	3.4
Core 8 dark	NA	NA	NA	NA	NA	NA
Core 8 light	NA	NA	NA	NA	NA	NA
Core 9	NA	NA	NA	NA	NA	NA
Core 10 dark (6-22)	5.2	1.9	0.72	0.71	0.71	2.8
Core 10 light (31-41)	5.4	2.1	0.77	0.79	0.78	2.5
Core 10 light (41-51)	2.8	0.2	0.87	0.86	0.87	13.7
Core 10 light(57-71)	3.3	3.3	0.86	0.85	0.85	1.0
Core 11 clayey clay(31-42)	4.8	1.9	0.51	0.52	0.51	2.5
Core 11 clayey clay(42-52.5)	NA	1.5	0.49	NA	0.49	NA
Core 11 sandy clay	5.3	1.7	0.42	0.44	0.43	3.1
Core 11 sandy clay 2	NA	NA	NA	NA	NA	NA

Table 92: Undrained shear strenght and sensititivy values from fall cone 1 testing.

Sample name	Fall cone 1 S_u (kPa)	Remoulded fall cone 1 S_u (kPa)	θ_g(-)	S_t(-)
Core 1 grey	14.3	1.5	0.60	9.7
Core 1 dark	NA	0.8	0.53	NA
Core 1 sandy dark	10.9	1.8	0.45	6.1
Core 2 dark (37.5-54)	6.0	0.6	0.93	10.0
Core 2 orange (4.5-20.5)	9.6	1.4	0.83	7.1
Core 3	11.6	0.5	0.81	21.3
Core 4 dark (5-15.5)	6.1	1.2	0.51	5.3
Core 4 light (21-32)	8.8	0.6	0.87	14.7
Core 5 beige clay 2 (12-22)	NA	NA	NA	NA
Core 5 very light(44-56)	NA	NA	NA	NA
Core 5 beige(63.5-75)	11.2	2.6	0.44	4.2
Core 5 beige (81-94.5)	12.2	1.4	0.48	8.9
Core 5 (22-37)	NA	NA	NA	NA
Core 5 (37-47.5)	NA	NA	NA	NA
Core 6 sandy clay (8.5-24)	102.1	2.5	0.37	40.3
Core 6 clayey clay (38-55.5)	7.4	1.7	0.51	4.4
Core 7 dark (10.5-22.5)	11.9	1.0	0.80	12.5
Core 7 dark(22.5-34)	6.3	0.5	0.85	11.6
Core 7 light	12.1	0.8	0.95	15.5
Core 8 dark	NA	NA	NA	NA
Core 8 light	NA	NA	NA	NA
Core 9	NA	NA	NA	NA
Core 10 dark (6-22)	5.2	0.9	0.77	5.6
Core 10 light (31-41)	5.7	1.1	0.82	5.3
Core 10 light (41-51)	6.9	1.3	0.83	5.3
Core 10 light(57-71)	10.5	1.5	0.84	7.0
Core 11 clayey clay(31-42)	5.8	0.7	0.50	7.9
Core 11 clayey clay(42-52.5)	10.4	0.7	0.49	13.9
Core 11 sandy clay	NA	NA	NA	NA
Core 11 sandy clay 2	NA	NA	NA	NA

Table 93: Undrained shear strength and sensitivity values from fall cone 2 testing.

Sample name	Fall cone 2 S_u (kPa)	Remoulded fall cone 2 S_u (kPa)	θ_g(-)	S_t(-)
Core 1 grey	NA	NA	NA	NA
Core 1 dark	NA	NA	NA	NA
Core 1 sandy dark	5.9	1.0	0.50	6.2
Core 2 dark (37.5-54)	7.0	0.7	0.90	9.7
Core 2 orange (4.5-20.5)	10.7	1.3	0.84	8.3
Core 3	13.1	0.5	0.83	28.8
Core 4 dark (5-15.5)	6.6	1.0	0.53	6.7
Core 4 light (21-32)	11.4	0.7	0.86	17.5
Core 5 beige clay 2 (12-22)	NA	NA	NA	NA
Core 5 very light(44-56)	NA	NA	NA	NA
Core 5 beige(63.5-75)	NA	NA	NA	NA
Core 5 beige (81-94.5)	33.2	4.2	0.39	7.9
Core 5 (22-37)	NA	NA	NA	NA
Core 5 (37-47.5)	NA	NA	NA	NA
Core 6 sandy clay (8.5-24)	85.8	1.9	0.39	44.0
Core 6 clayey clay (38-55.5)	4.5	2.1	0.48	2.2
Core 7 dark (10.5-22.5)	8.2	1.1	0.78	7.7
Core 7 dark(22.5-34)	NA	NA	NA	NA
Core 7 light	NA	NA	NA	NA
Core 8 dark	NA	NA	NA	NA
Core 8 light	NA	NA	NA	NA
Core 9	NA	NA	NA	NA
Core 10 dark (6-22)	8.2	1.0	0.75	8.1
Core 10 light (31-41)	7.5	0.9	0.84	7.9
Core 10 light (41-51)	5.1	1.4	0.82	3.8
Core 10 light(57-71)	8.3	1.4	0.85	5.9
Core 11 clayey clay(31-42)	4.2	1.2	0.45	3.3
Core 11 clayey clay(42-52.5)	7.1	0.4	0.54	18.6
Core 11 sandy clay	NA	NA	NA	NA
Core 11 sandy clay 2	NA	NA	NA	NA

F Results from comparing Oedometer stiffnesses

Table 94: Comparing oedometer stiffnesses of all samples at various normal stresses.

Sample name	Normal stress (kPa)	Oedometer stiffness (kPa)
Core 1 dark original	0	NA
Core 1 dark original	15	353
Core 1 dark original	30	392
Core 1 dark original	45	498
Core 1 dark remoulded	15	197
Core 1 dark remoulded	30	260
Core 1 dark remoulded	45	511
Core 1 grey original	5	146
Core 1 grey original	10	238
Core 1 grey original	20	219
Core 1 grey original	45	383
Core 1 grey original	100	619
Core 1 grey remoulded	15	290
Core 1 grey remoulded	30	334
Core 5 (22-37)	15	240
Core 5 (22-37)	30	316
Core 5 (22-37)	45	382
Core 5 (37-47.5)	16	217
Core 5 (37-47.5)	30	301
Core 5 (37-47.5)	45	474
Core 7 light	3	242
Core 7 light	6	172
Core 7 light	9	123
Core 8 dark	10	222
Core 8 dark	20	451
Core 8 dark	30	350
Core 8 light	10	157
Core 8 light	30	283
Core 10 dark	6	122

G Fossils identified from microscopy study

The images presented are all ranging from 63µm to 425µm with most of the fossils estimated to be ranging from 100µm to 300µm. All these photos were taken with a Samsung A7(2017) camera of 16 MP, however the shown pictures are of a lower unkown resultion since they needed to be compressed in order to fit into this word document.

Figure 144: Images of Ostracodes.

Figure 145: Images of Eubuliminella exilis or Fursenkoina pauciloculata of the benthic foraminifera.

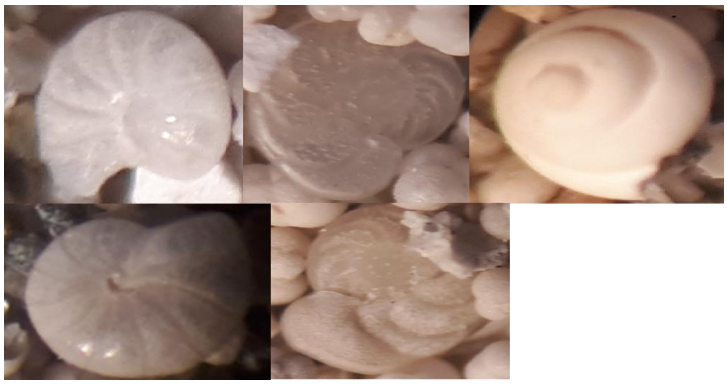

Figure 146: Discorbus, planktonic or Cibicides wuellerstorfi of the benthic foraminifera.

Figure 147: Image of a Quinqueloculina.

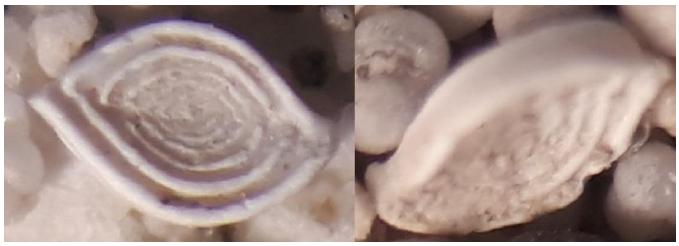

Figure 148: Image of Nummulites fossils.

Figure 149: Image of Lagena sulcata.

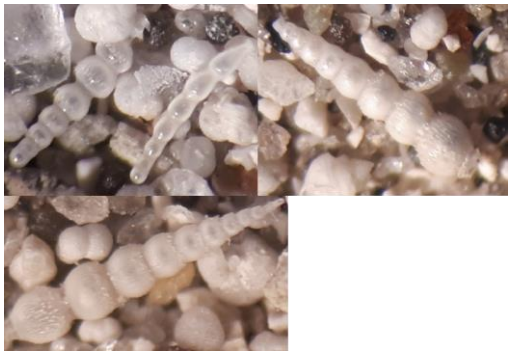

Figure 150: Images of Elipsonodosaria.

Figure 151: Infilling of fossil fragments with mud, sand and crystals.

Figure 152: Some unidentified fossils with possibly coral on the right.

Figure 153: A type of sea urchin spine.

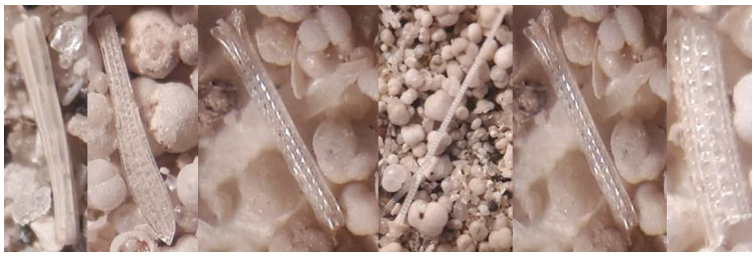

Figure 154: Sponge needles.

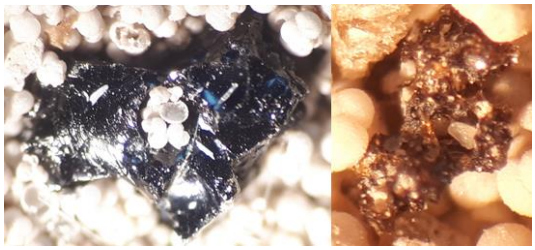

Figure 155: A volcanic piece of glass on the left and a piece of rock with crystals attached to each other on the right.

H All results from microscope study

The images presented are all ranging from 63µm to 425µm with most of the fossils estimated to be ranging from 100µm to 300µm and most the crystals from 63µm to 100µm.

Figure 156: Core 1 dark sand fraction

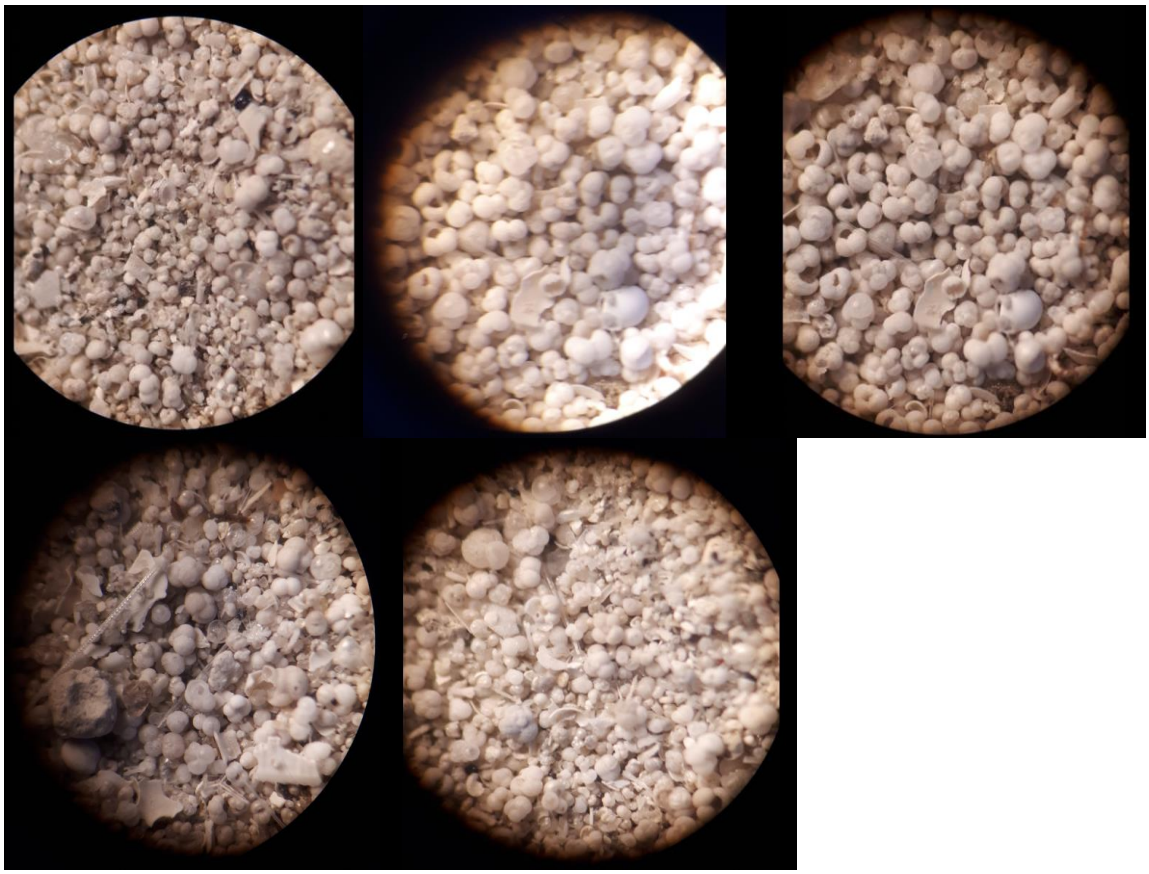

Figure 157: Core 1 grey sand fraction

Figure 158: Core 2 dark sand fraction

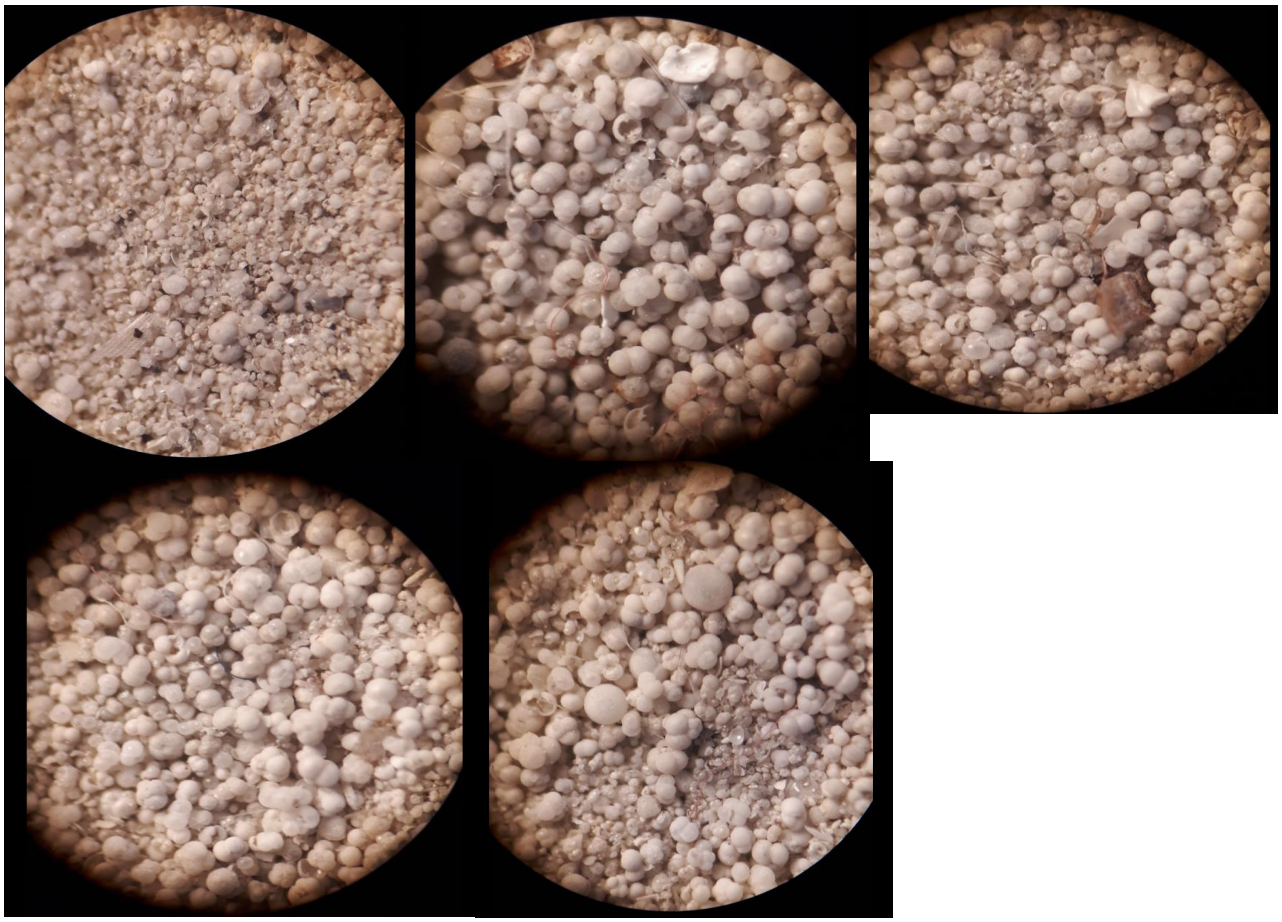

Figure 159: Core 2 orange sand fraction

Figure 160: Core 3 sand fraction

Figure 161: Core 3 sand fraction

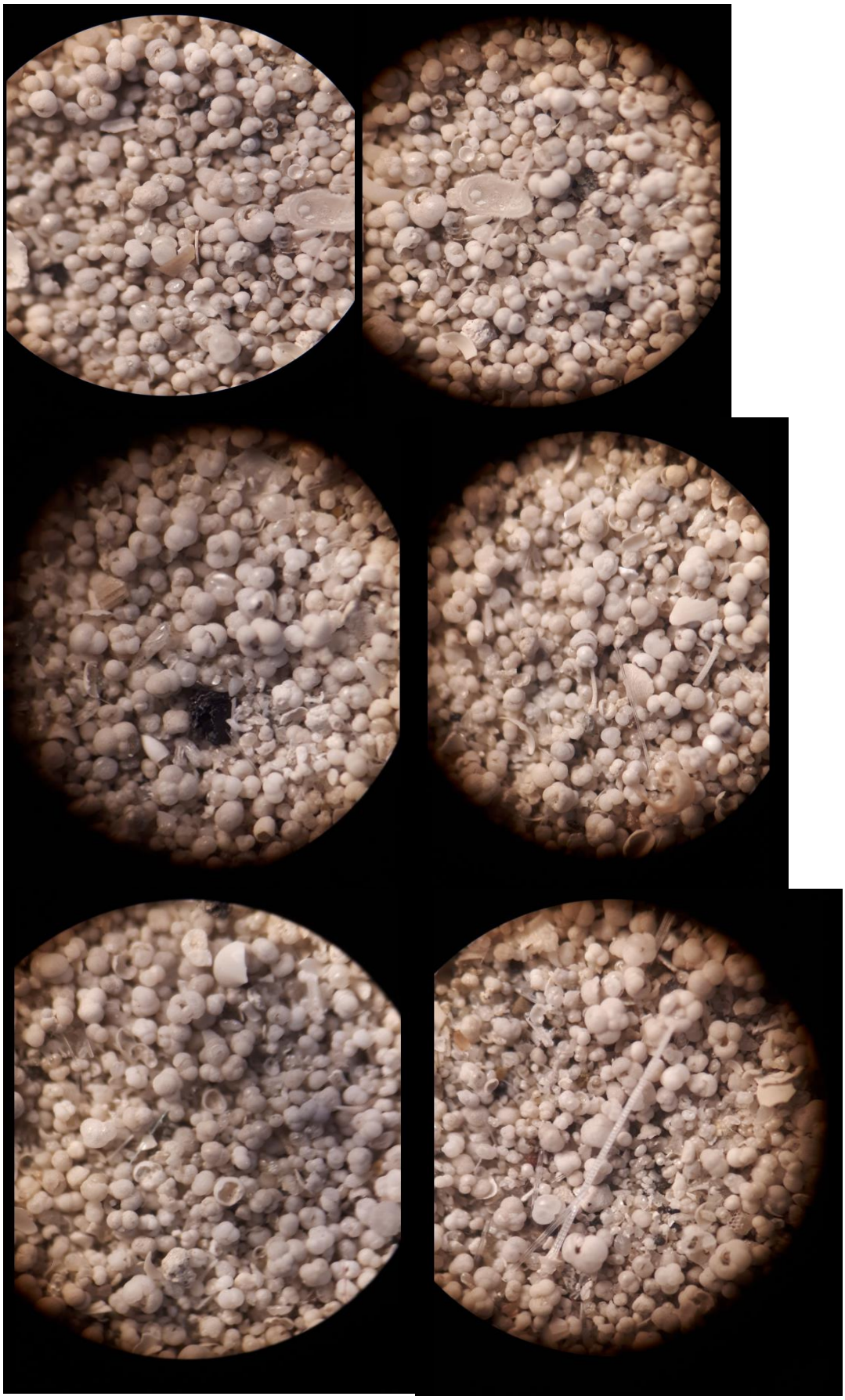

Figure 162: Core 4 dark sand fraction

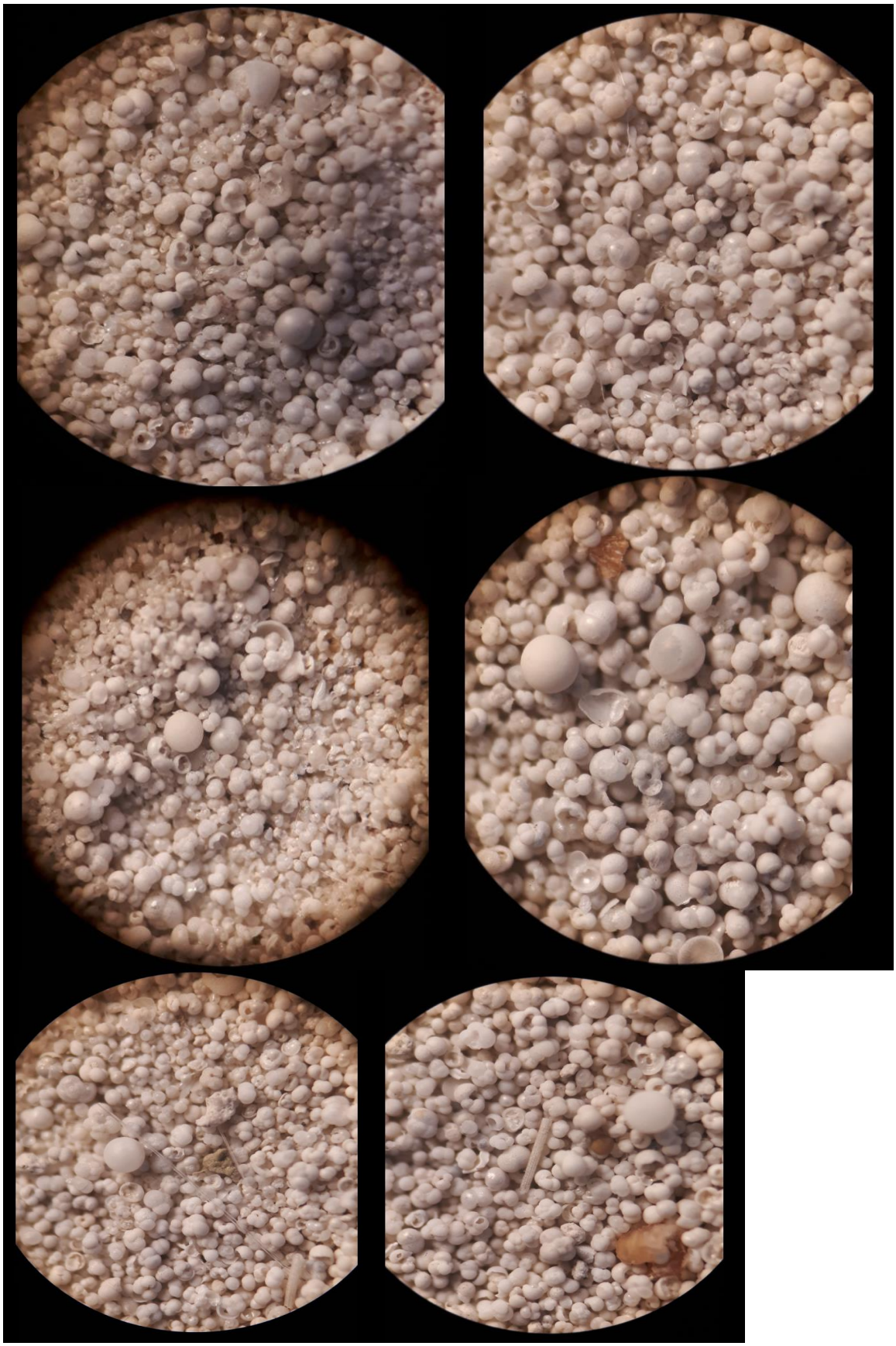

Figure 163: Core 5 beige sand fraction

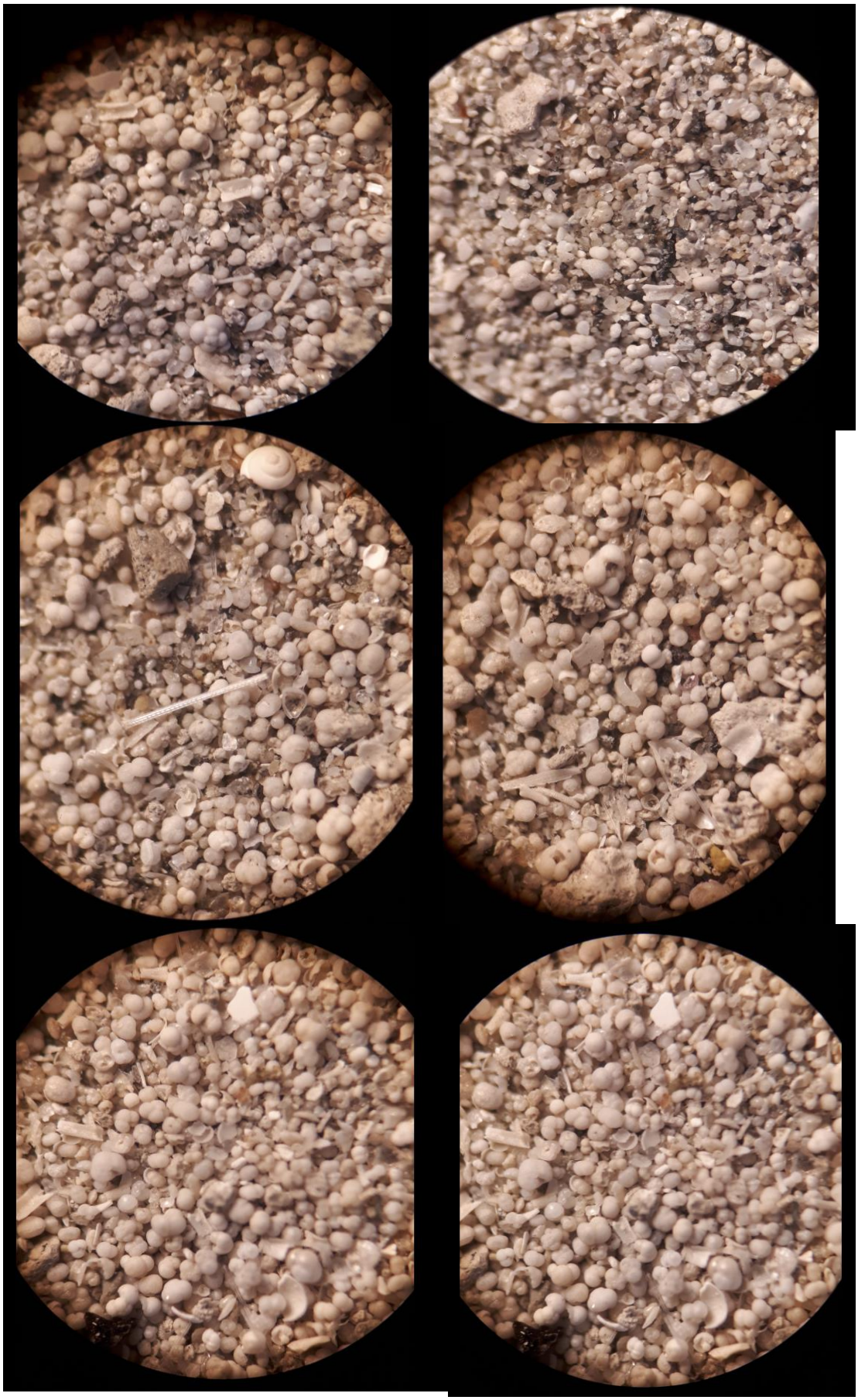

Figure 164: Core 5 beige sand fraction

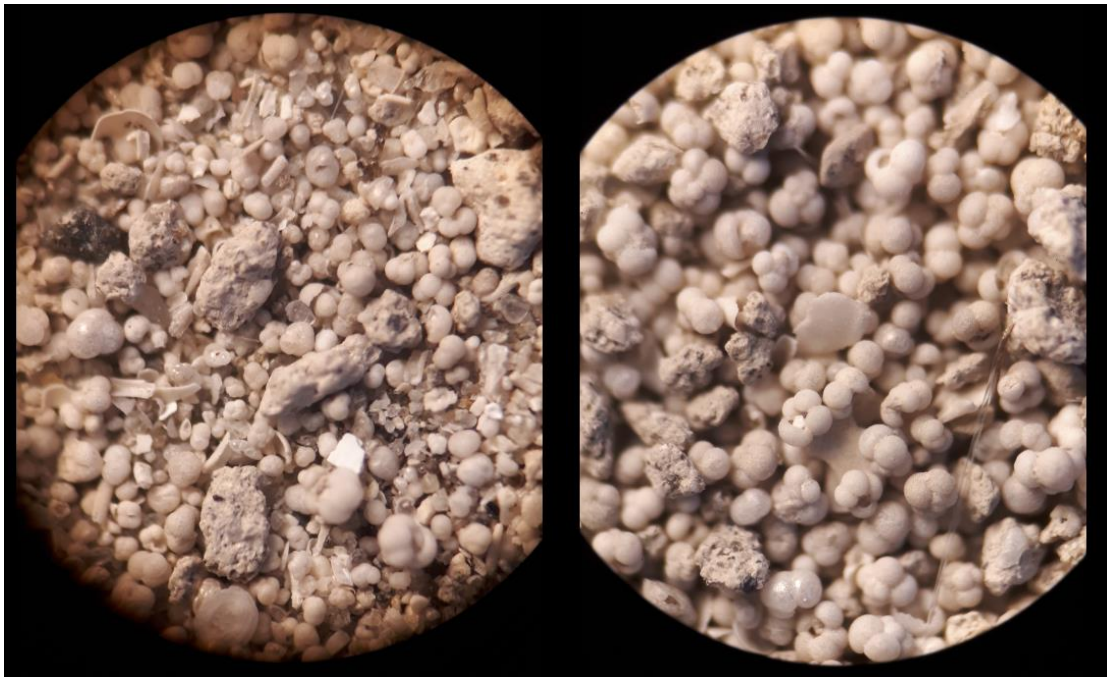

Figure 165: Core 5 beige sand fraction

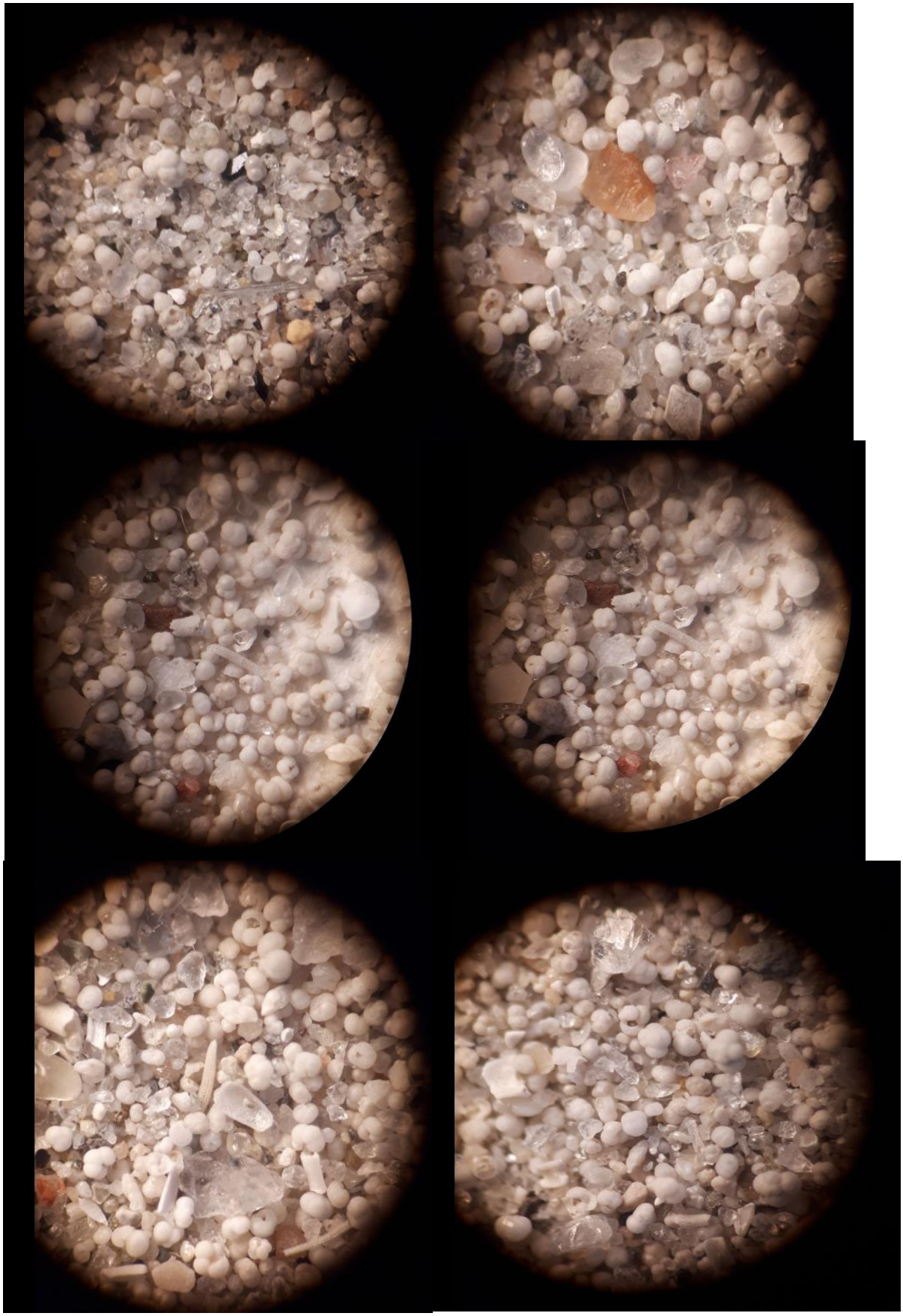

Figure 166: Core 5 beige clay (12-22) sand fractio

V

Figure 167: Core 5 very light sand fraction

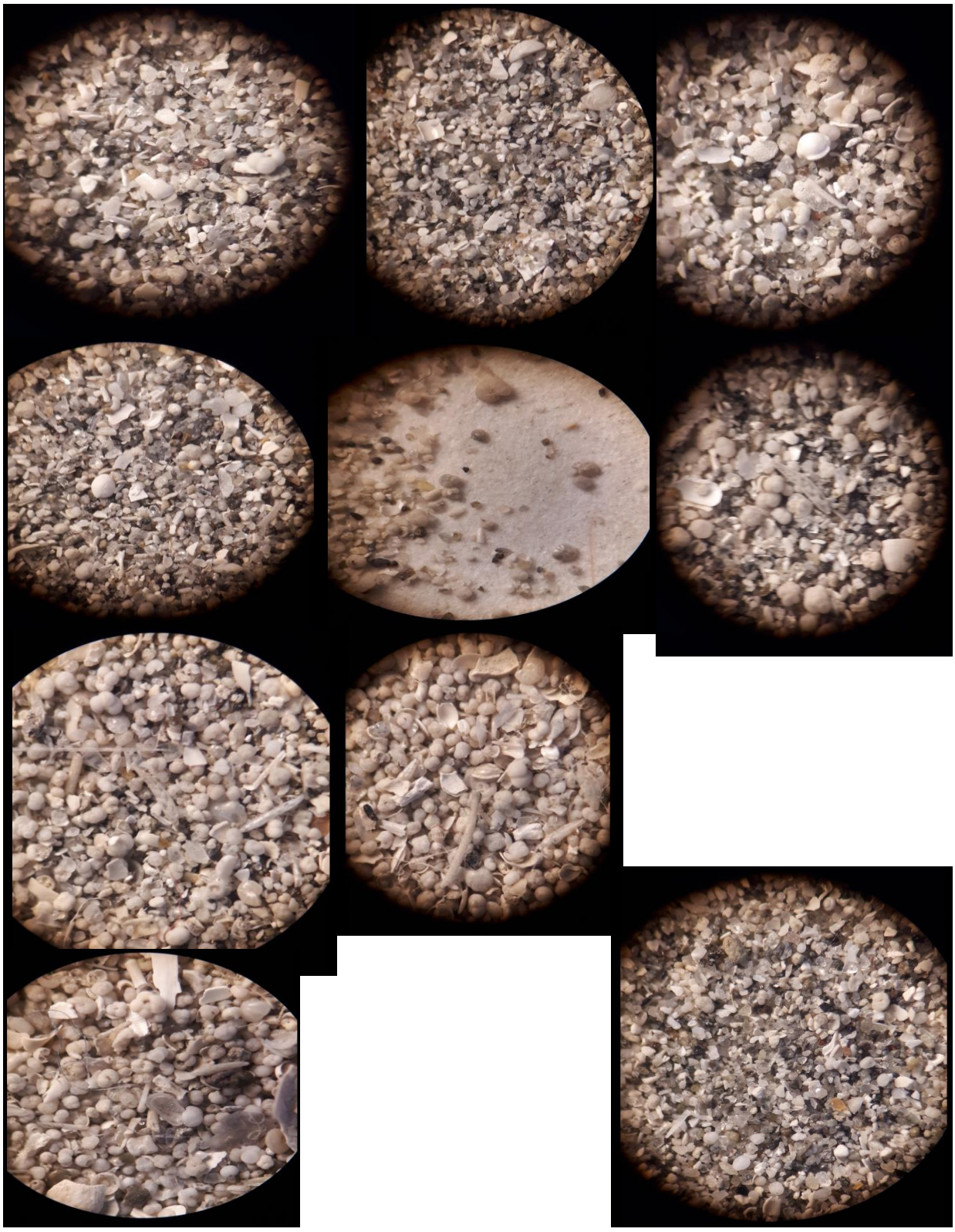

Figure 168: Core 6 clayey clay sand fraction

Figure 169: Core 6 sandy clay sand fraction

Figure 170: Core 6 sandy clay sand fraction

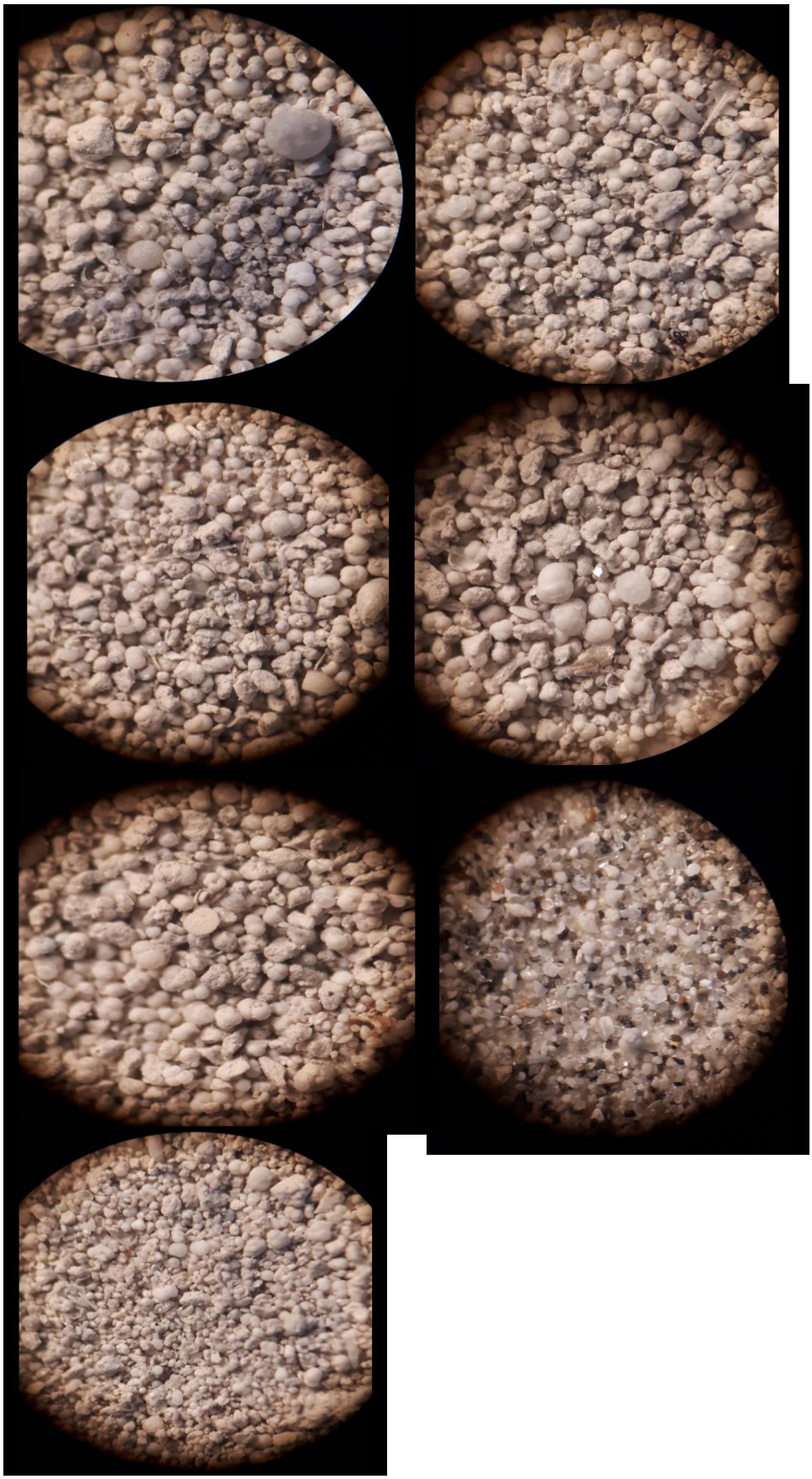

Figure 171: Core 7 dark sand fraction

Figure 172: Core 8 dark sand fraction

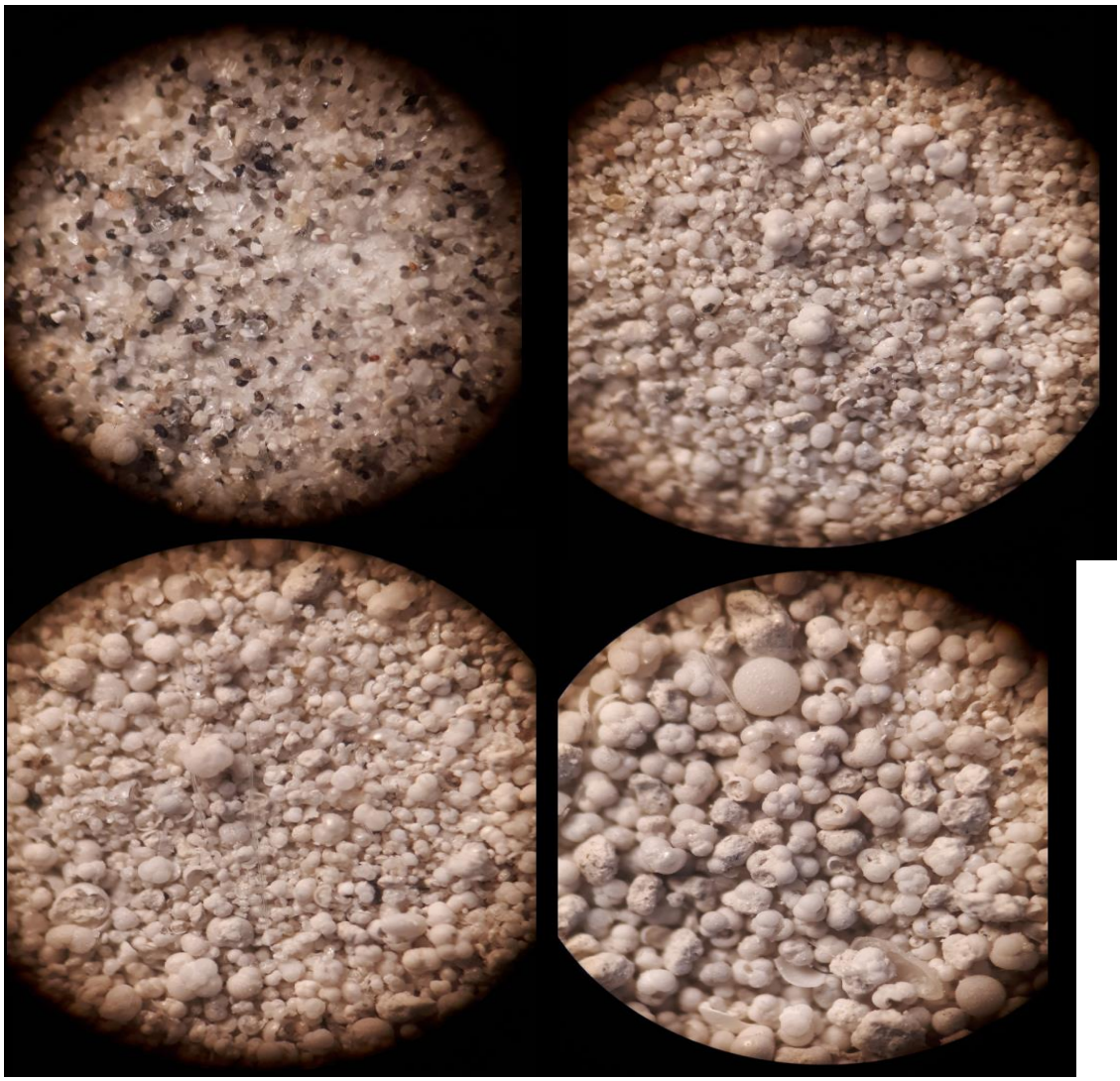

Figure 173: Core 8 light sand fraction

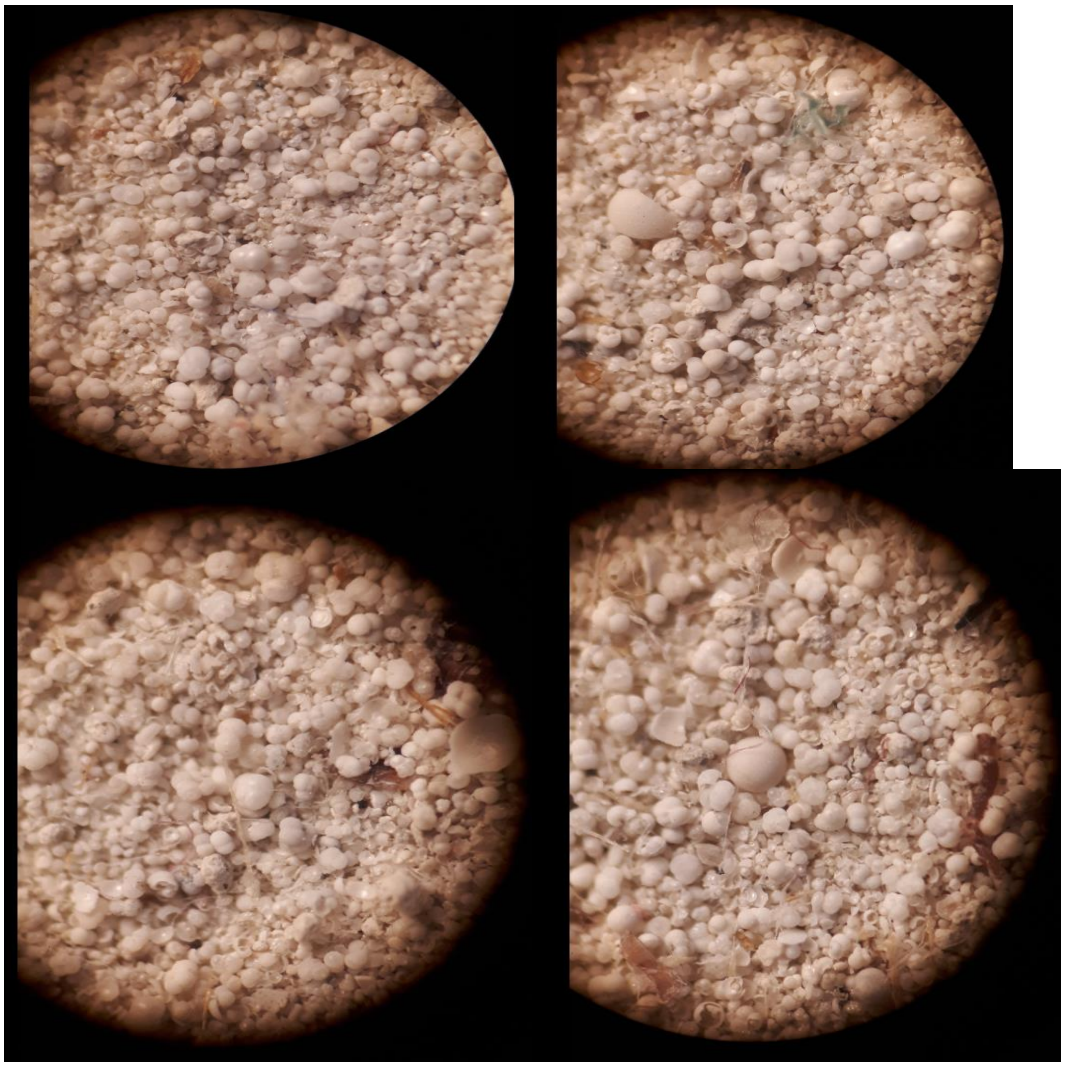

Figure 174: Core 9 sand fraction

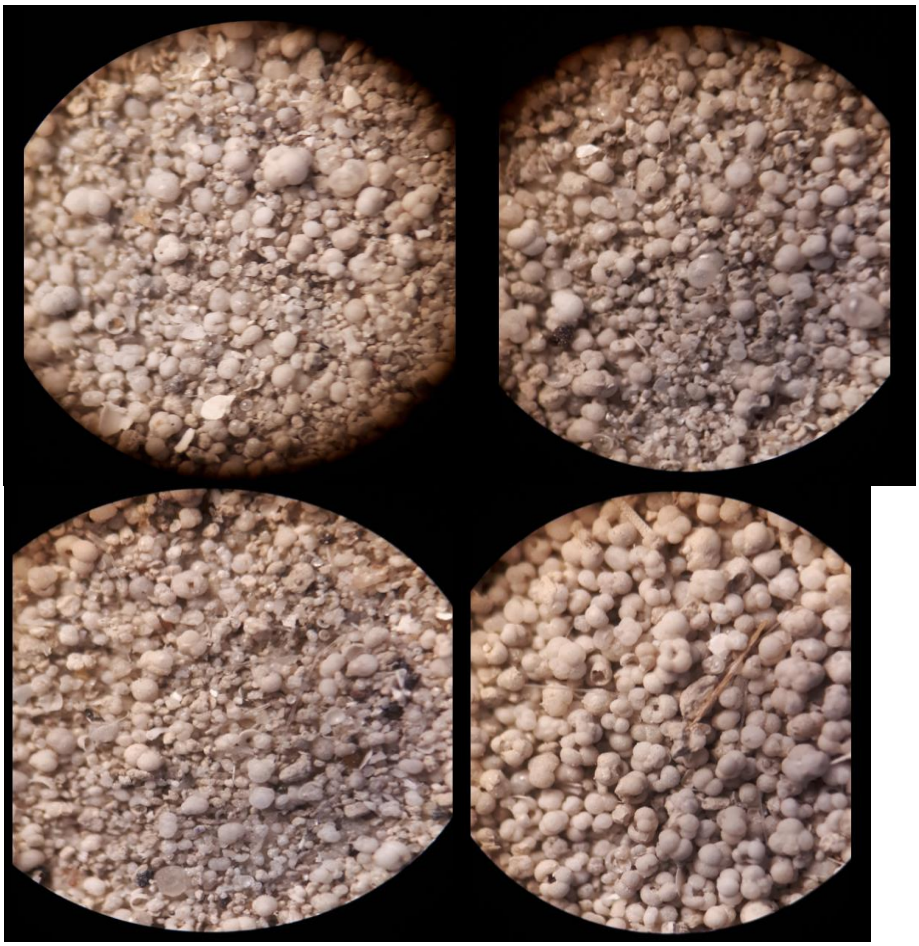

Figure 175: Core 10 dark sand fraction

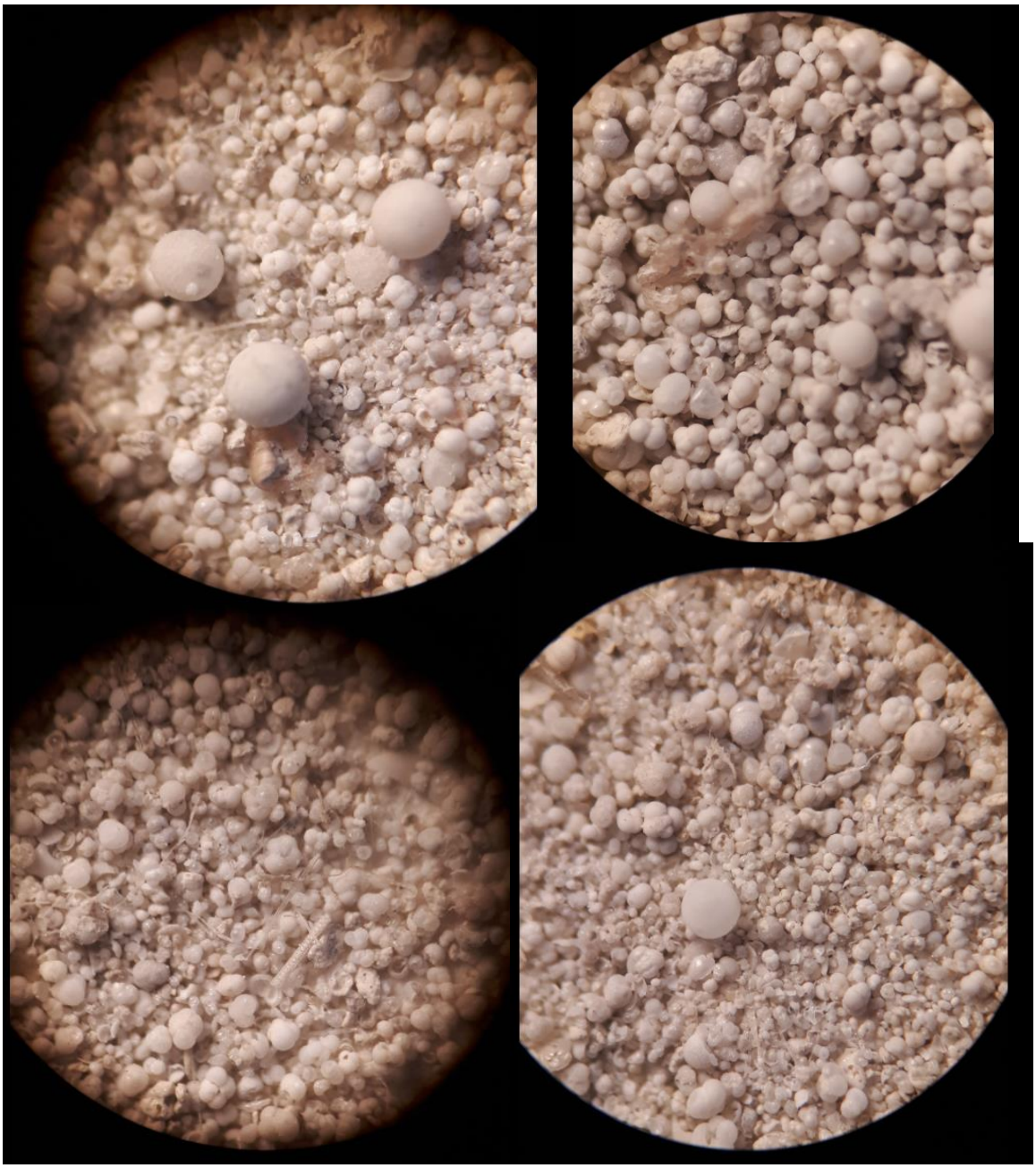

Figure 176: Core 10 light sand fraction

Figure 177: Core 11 clayey clay sand fraction

Figure 178: Core 11 sandy clay sand fraction

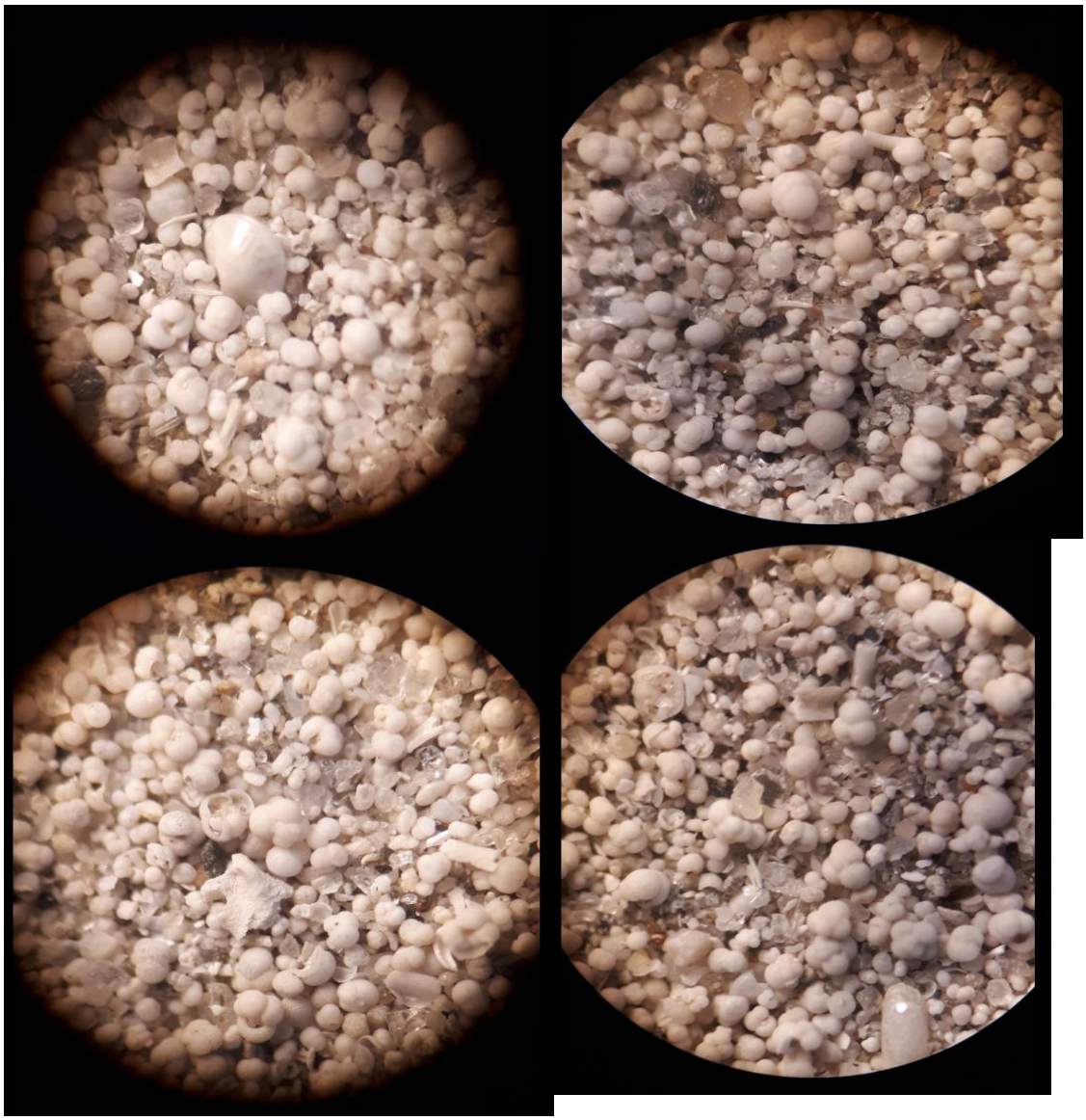

Figure 179: Core 11 sandy clay sand fraction